Dynamics of Loschmidt echoes and fidelity decay

Thomas Gorin [a], Tomaž Prosen [b,*], Thomas H. Seligman [c,d], and Marko Žnidarič [b]

[a] *Max-Planck-Institut für Physik komplexer Systeme, Nöthnitzer Str. 38, D-01187 Dresden, Germany*

[b] *Physics Department, Faculty of Mathematics and Physics, University of Ljubljana, Jadranska 19, SI-1000 Ljubljana, Slovenia*

[c] *Centro Internacional de Ciencias, Apartado postal 6-101, C.P.62132 Cuernavaca, Morelos, Mexico*

[d] *Centro de Ciencias Físicas, University of Mexico (UNAM), C.P.62132 Cuernavaca, Morelos, Mexico*

Abstract

Fidelity serves as a benchmark for the relieability in quantum information processes, and has recently atracted much interest as a measure of the susceptibility of dynamics to perturbations. A rich variety of regimes for fidelity decay have emerged. The purpose of the present review is to describe these regimes, to give the theory that supports them, and to show some important applications and experiments. While we mention several approaches we use time correlation functions as a backbone for the discussion. Vanicek's uniform approach to semiclassics and random matrix theory provides an important alternative or complementary aspects. Other methods will be mentioned as we go along. Recent experiments in micro-wave cavities and in elastodynamic systems as well as suggestions for experiments in quantum optics shall be discussed.

Key words: Loschmidt echo, Fidelity
PACS: 03.65.Nk, 03.65.Sq, 03.65.Ud, 03.65.Yz, 03.67.Lx, 03.67.Pb, 05.45.Mt, 05.45.Pq, 43.20.Gp, 76.60.Lz

Contents

* Corresponding author
Email addresses: gorin@mpipks-dresden.mpg.de (Thomas Gorin), tomaz.prosen@fmf.uni-lj.si (Tomaž Prosen), seligman@fis.unam.mx (Thomas H. Seligman), marko.znidaric@fmf.uni-lj.si (Marko Žnidarič).

1. Introduction

Irreversibility of macroscopic behavior has attracted attention ever since Boltzmann introduced his H-theorem in a seminal paper in 1872 [1] (for English translation of some of Boltzmann's papers see book [2]), together with the equation bearing his name. The problem of irreversibility is how to reconcile the apparent "arrow of time" with the underlying *reversible* microscopic laws. How come that macroscopic systems always seem to develop in one direction whether the underlying dynamics is symmetric in time? This so called reversibility paradox is usually attributed to Josef Loschmidt. He mentioned it briefly at the end of a paper published in 1876 [3] discussing the thermal equilibrium of a gas subjected to a gravitational field, in an attempt to refute Maxwell's distribution of velocities for a gas at constant temperature. He also questioned Boltzmann's monotonic approach towards the equilibrium. Discussing that, if one would reverse all the velocities, one would go from equilibrium towards the initial non equilibrium state, he concludes with : *"... Das berühmte Problem, Geschehenes ungeschehen zu machen, hat damit zwar keine Lösung ... "*. Bolzmann was quick to answer Loschmidt's objections in a paper from 1877 [4], pointing out the crucial

importance of the initial conditions and of the probabilistic interpretation of the second law. The story goes that Boltzmann's reply to Loschmidt's question regarding velocity reversal was: "Then try to do it!". It is obvious that such velocity reversal is for all practical purposes impossible due to large number of particles involved and also due to high sensitivity to small errors made in the reversal.

The first written account of the reversibility paradox is actually not due to Loschmidt but due to William Thompson (later Lord Kelvin), although it is possible that Loschmidt mentioned the paradox privately to Boltzmann before. Boltzmann and Loschmidt became good friends while working at the Institute of Physics in Vienna around 1867, for a detailed biography of Boltzmann see book [5]. In a vivid paper [6] from 1874 Thompson gave a very modern account of irreversibility. When discussing the heat conduction and the equalization of temperature he says: *"... If we allowed this equalization to proceed for a certain time, and then reversed the motions of all the molecules, we would observe a disequalization. However, if the number of molecules is very large, as it is in a gas, any slight deviation from absolute precision in the reversal will greatly shorten the time during which disequalization occurs... Furthermore, if we take account of the fact that no physical system can be completely isolated from its surroundings but is in principle interacting with all other molecules in the universe, and if we believe that the number of these latter molecules is infinite, then we may conclude that it is impossible for temperature-differences to arise spontaneously ... "*. The interesting question is then, how short is this *short disequalization time*?

An analysis of the disequalization time is very near to the modern concept of echo dynamics. From discussions of Boltzmann, Loschmidt and Thompson it is clear that this disequalization time will depend on the imperfections made in the reversal, *i.e.* the change in the initial condition for the backward evolution, and on the *perturbations* to this backward evolution, *i.e.* on how much the backward evolution after the reversal differs from the forward evolution. The quantity measuring sensitivity to perturbations of the backward evolution is nowadays known as the Loschmidt echo after Ref. [7], or the fidelity (we will interchangingly use both terms, Loschmidt echo and fidelity). It is the overlap of the initial state with the state obtained after the forward unperturbed evolution followed by the backward perturbed evolution (Loschmidt echo) or equivalently as the overlap of state obtained after the forward unperturbed evolution and the state after the forward perturbed evolution (fidelity). It can be considered in classical mechanics as well as in quantum mechanics. If unperturbed and perturbed evolutions are the same the Loschmidt echo is obviously equal to one while for unequal evolutions it generally decreases with time. The decay time of the Loschmidt echo will then be the time of disequalization in question. Surprisingly, despite its importance for statistical mechanics and irreversibility it was not considered until some years ago, even though various "problems" regarding irreversibility appear again and again. Echo dynamics and with it connected the Loschmidt echo is the subject of the present report.

Echo dynamics has its applications beyond statistical mechanics. Performing echo evolution is a standard experimental technique in NMR where also the earliest measurements of the Loschmidt echo were performed [8–11]. It can also be related to other situations like such as the seismic response in volcanos [12]. The quantum information community has adopted the autocorrelation function of echo dynamics, known as fidelity, as a standard benchmark for the quality of any implementation of a quantum information device [13]. Quantum information theory enables one to do things not possible by classical means, e.g. perform quantum computation. The main obstacle in producing quantum devices that manipulate individual quanta are errors in the evolution, either due to unwanted coupling with the environment or due to internal imperfections. Therefore, the goal is to build a device that is resistant to such perturbations. For this one ought to understand the behavior of fidelity in different situations to know hot to maximize it. The theoretical framework for decreasing the unwanted evolution in quantum information devices, called dynamical decoupling [14,15], is intimately connected to the fidelity theory, especially to the interesting phenomenon of quantum freeze [16–18]. But the ultimate motivation for theoretical study of fidelity neither came from quantum information theory nor from statistical mechanics but from the field of quantum chaos [19,20]. The exponential instability of classical systems is a well known and much studied subject. As the underlying laws of nature are quantum mechanical the obvious question arises how this "chaoticity" manifests itself in quantum systems whose classical limit is chaotic. The field of quantum chaos mainly dealt with stationary properties of classically chaotic systems, like spectral and eigenvector statistics. Despite classical chaos being defined in a dynamical way it was easier to pinpoint the "signatures" of classical chaos in stationary

properties. There were not that many studies of the dynamical aspects of quantum evolution in chaotic systems, some examples being studies of the reversibility of quantum evolution [21,22], the dynamical localization [23,24], energy spreading [25,26] or wave-packet evolution [27,28]. Classical instability is usually defined as an exponential separation of two nearby trajectories in time. In quantum mechanics one could be tempted to look at the sensitivity of quantum mechanics to variations of the initial wave function. But quantum evolution is unitary and therefore preserves the dot product (*i.e.* the distance) between two states and so there is no exponential sensitivity with respect to the variation of the initial state. The sensitivity to perturbations as measured by the Loschmidt echo on the other hand naturally lends to the comparison between quantum and classical situation. For classical systems Loschmidt echo gives the same exponential sensitivity to perturbations of the evolution as to perturbations of initial conditions. The quantum fidelity though can behave in a very different way, displaying a rich variety of regimes. Some other theoretical questions like quantization ambiguity, *i.e.* the difference between different quantizations having the same classical limit, can also be connected to the fidelity decay [29]. Considering that the fidelity lies at the crossroad of three very basic areas of physics: statistical mechanics, quantum information theory and quantum chaos, and that its understanding is crucial for building successful quantum devices it is not surprising that it received a lot of attention in recent years. Let us give a brief historical overview, listing the most important discoveries. The list of references is by no means complete, for detailed references see the later sections of the paper.

1.1. *Historical overview*

Fidelity has been first used as a measure of stability by Peres in 1984 [30], see also his book [31]. Peres reached the conclusion that the decay of fidelity is faster for chaotic than for regular classical dynamics. As we will see the general situation can be exactly the opposite. Non decay of the fidelity for regular dynamics in Peres's work was due to a very special choice of the initial condition, namely that a coherent wave packet was placed in the center of a stable island. Such a choice is special in two ways, first the center of an island is a stationary point and second the number of constituent eigenstates of the initial state is very small. After Peres's work the subject lay untouched for about a decade. In 1996 Ballentine and Zibin [32] numerically studied a quantity similar to fidelity. Instead of perturbing the backward evolution, they took the same backward evolution but instead perturbed the state after forward evolution by some instantaneous perturbation, like shifting the whole state by some δx. They also looked at the corresponding classical quantity. The conclusion they reached was that for chaotic dynamics quantum stability was much higher than the classical one, while for regular dynamics the two agreed. All these results were left mainly unexplained. Gardiner et al. [33,34] proposed an experimental scheme for measuring the fidelity in an ion trap. In a related work, Schack and Caves [35–37] studied how much information about the environment is needed to prevent the entropy of the system to increase. Fidelity studies received fresh impetus from a series of NMR experiments carried out by the group of Levstein and Pastawski.

In NMR echo experiments are a standard tool. The so called spin echo experiment of Hahn [8] refocuses free induction decay in liquids due to dephasing of the individual spins caused by slightly different Larmor frequencies experienced due to magnetic field inhomogeneities. By an appropriate electromagnetic pulse the Zeeman term is reversed and thus the dynamics of *non-interacting* spins is reversed. The first *interacting* many-body echo experiment was done in solids by Rhim et al. [9]. Time reversal, *i.e.* changing the sign of the interaction, is achieved for a dipolar interaction whose angular dependence can change sign for a certain "magic" angle, that causes the method to be called magic echo. Still, the magic echo showed strong irreversibility. Much later a sequence of pulses has been devised enabling a *local* detection of polarization [10] (*i.e.* magnetic moment). They used a molecular crystal, ferrocene $Fe(C_5H_5)_2$, in which the naturally abundant isotope ^{13}C is used as an "injection" point and a probe, while a ring of protons ^1H constitutes a many-body spin system interacting by dipole forces. The experiment proceeds in several steps: first the ^{13}C is magnetized, then this magnetization is transferred to the neighboring ^1H. We thus have a single polarized spin, while others are in "equilibrium". The system of spins then evolves freely, *i.e.* spin diffusion takes place, until at time t the dipolar interaction is reversed and by this also spin diffusion. After time $2t$ the echo is

formed and we transfer the magnetization back to our probe ^{13}C enabling the detection of the *polarization echo*. Note that in the polarization echo experiments the total polarization is conserved as the dipole interaction has only "flip-flop" terms like $S_+^j S_-^{j+1}$, which conserve the total spin. To detect the spin diffusion one therefore needs a local probe. With the increase of the reversal time t the polarization echo – the fidelity – decreases in approximately exponential way. The nature of this decay has been further investigated by Pastawski et al. [38]. The group of Pastawski performed a series of NMR experiments where they studied in more detail the dependence of the polarization echo on various parameters [11,39,40]. They were able to control the strength of the residual part of the Hamiltonian, which was not reversed in the experiment and is assumed to be responsible for the polarization echo decay. By diminishing the residual interactions they obtained a Gaussian decay with a decay rate, saturated and independent of the perturbation strength, *i.e.* the strength of the residual interaction. That would imply the existence of a perturbation independent regime. While there is still no complete consensus on the interpretation of these experimental results they triggered a number of theoretical and even more numerical investigations. We will briefly list just the most important ones, first regarding quantum fidelity.

Using the semiclassical expansion of the quantum propagator Jalabert and Pastawski [7] derived a *perturbation independent* quantum fidelity decay for localized initial states and chaotic dynamics, also called "Lyapunov decay" due to its dependence on the Lyapunov exponent. This regime has been numerically observed for the first time in Ref. [41]. Studying fidelity turned out to be particularly fruitful in terms of the *correlation function* [42], see also Ref. [43], which is also the approach we use in the present review. Perturbation dependent exponential decay of quantum fidelity observed in Ref. [42,44–46], also called the Fermi golden rule decay, has been derived in Refs. [44] using random matrix theory and in Ref.[45] using semiclassical methods, and independently in Refs. [42,46] using Born expansion in terms of correlation functions. Perhaps the most interesting result of this approach is that one can, by *increasing* chaoticity of the corresponding classical system, *increase* quantum fidelity, *i.e.* improve the *stability* of the quantum dynamics. Note that classical correlators already appeared in Ref. [7], and also later in Ref. [45]. For sufficiently small perturbations fidelity decays as a Gaussian, which is the so-called perturbative decay [44–46]. Refs. [44,45] were the first which presented a unified theoretical treatment of all main regimes of fidelity decay, and identified the scales of perturbation strength which controlled the transitions among them.

Decoherence, as characterized by the decay of off-diagonal matrix elements of the reduced density matrix, has been connected to the fidelity in Ref. [47,48]. Echo purity, which is a generalization of purity to echo dynamics, has been introduced in Refs. [49] and the so-called reduced fidelity, measuring the stability on a subsystem, in Ref. [50]. A rigorous inequality between fidelity, reduced fidelity and echo purity has been proved in Refs. [50,51]. It is well known that the quantization of classical system is not unique. Kaplan [29] compared the quantization ambiguity in chaotic and regular systems, reaching the conclusion that in chaotic systems the quantization ambiguity is *suppressed* as compared with regular ones. A detailed random matrix (RMT) formulation of fidelity has been presented in Ref. [52], although random matrix theory for describing fidelity decay has been used before[44,53,54]. A supersymmetric method has been used to derive an analytic expression for fidelity decay in RMT models [55,56]. Quantum fidelity decay in regular systems has been discussed in Ref. [46]. An interesting phenomenon of prolonged stability for certain type of perturbations, called quantum freeze, has been discovered in Refs. [16–18]. Using a semiclassical propagator fidelity has been expressed as a Wigner function average of phases due to action differences [57,58], the so-called dephasing representation, which is particularly handy for numerical evaluation of quantum fidelity in terms of classical orbits.

Classical fidelity as compared to the quantum one received much less attention. It has been first defined and linear response derived in Ref. [46]. Numerical results on the classical fidelity and its correspondence with the quantum fidelity in chaotic systems and in systems exhibiting diffusion have been presented in Ref. [59]. Classical fidelity in regular and chaotic systems has also been theoretically discussed [60]. A detailed explanation of the asymptotic decay in chaotic systems has been given in Ref. [61]. Short time Lyapunov decay of classical fidelity has been obtained in Ref. [62], showing that the Lyapunov decay of quantum fidelity is a consequence of quantum-classical correspondence. Classically regular systems on the other hand have been worked out in Ref. [63].

1.2. *Outline of the paper*

A wide variety of methods have been used to treat echo dynamics, and shall be discussed in this report, yet a linear response treatment, which relates fidelity decay to the decay of the correlation function of the perturbation in the interaction picture, is sufficient to understand most of the results. The method is based on writing the so-called echo propagator in the interaction picture, thereby focusing attention only on the perturbation that actually causes fidelity to decay. By employing the Baker-Campbell-Hausdorff formula or a linear response expansion, one is then able to obtain approximations in a perfectly controllable way as. In this review we shall therefore use this method as skeleton and discuss other methods as they are needed or have been used in the literature. All the theoretical work has been accompanied by extensive numerical experiments. Finally we shall see, that a random matrix model represents real and numerical experiments under chaotic conditions quite well.

Throughout this review we shall pay special attention to the role of the initial state (localized packets versus random states) and the type of dynamics (integrable versus chaotic dynamics). Furthermore, we shall discuss random matrix models.

We shall now describe the organization of this review. In the process we shall point out a hierarchical structure, that will allow the reader interested in some particular aspect, to read only the next section and a few subsections to obtain the information he needs.

Thus Section 2 contains the basic definitions of echo dynamics and fidelity, which will be indispensable throughout the paper. Also we shall see, that the interaction picture provides the ideal representation to understand echo dynamics, because it isolates the effect of the perturbation on the wave function from that of the unperturbed dynamics. To get a first understanding we shall in Section 2.1 see how dynamical correlations of the perturbation control the basic behavior of fidelity decay, in a linear response analysis. This subsection is essential for the entire paper, because we shall use it as a skeleton for most considerations, and all new results will be based on its contents. The section will give definitions of other measures corresponding to different experimental and theoretical situations, such as scattering, polarization echo, or the evolution of entanglement as measured by purity under echo dynamics. The analysis of the precision of different quantization schemes is also connected to fidelity decay.

Section 3 deals with dynamical chaotic systems, and we shall explicitely see the effects of correlations of the perturbation on the fidelity decay. Special attention will be given to perturbations with zero diagonal, which result in the so-called quantum freeze. We will discuss echo measures for composite systems.

In Section 4 random matrix theory of echo dynamics will be developed, and we shall discuss when we expect the results found by RMT to represent a chaotic system well. The quantum freeze will be analyzed in the context of RMT. New results on quantum freeze and decoherence will be presented.

Section 5 will deal with integrable systems and has similar internal structure as the one on chaotic dynamics. Though, due to the lack of universality the behavior is richer. In this context the difference between coherent states and radom states will play a significant role. Some previously unpublished results are presented in this section. These includes Section 5.2.3 describing decay of fidelity averaged over position of initial packets and Section 5.3.2 describing freeze in a harmonic oscillator.

The following Section 6 deals with the decay of classical fidelity. First linear response is derived already showing marked difference between classical and quantum fidelity. Then long time Lyapunov decay is discussed as well as the decay in regular systems. The section concludes with the discussion of classical fidelity decay in many-body systems.

Section 7 on time scales is an overview of various decays derived for chaotic and regular systems. It can serve as a brief summary of results obtained in Sections 3 and 5. The scaling of decay time scales on different parameters is given and the decay is compared between chaotic and regular dynamics. In certain situations quantum regular systems can be more sensitive to perturbations than chaotic ones and additionally, increasing the chaoticity can improve the stability. The decay of fidelity is also illustrated in terms of Wigner functions. Unpublished material consists of some figures illustrating and comparing decay time scales in chaotic and regular systems.

Application of fidelity to quantum information is described in Section 8. First we give an incomplete list

of various studies of the influence of errors on quantum computation and point out how different results obtained in previous sections can be employed to understand results obtained in the literature. We give an illustrative example of how more randomness can improve stability of quantum computation. A connection between dynamical decoupling and fidelity freeze is also pointed out.

Finally in Section 9 we shall describe experiments measuring fidelity. We shall discuss NMR experiments, microwave experiments and elasticity experiments, for which fidelity measurements have already been performed as well as possible atom optics experiment.

Although our exposition is intended as a unified and self-contained review of the results which have mainly been published before in the quoted literature, there is however a substantial body of new results which have never been published. Let us here pin down the main original results presented in this report: (i) The results about quantum freeze of fidelity in the random matrix framework (Section 4.3), (ii) The extension of the results on scattering fidelity to the weak coupling regime (Appendix C), (iii) Random matrix treatment of purity decay in composite systems, both in the framework of echo dynamics and of forward dynamics of a central system weakly coupled to an environment, (iv) Treatment of the quantum freeze of fidelity for quadratic Hamiltonians (Section 5.3.2).

2. General theoretical framework

2.1. *Fidelity*

We consider a general quantum Hamilton operator $H_\varepsilon(t)$ which may depend explicitly on time t, as well as on some external parameter ε, like magnetic field, interaction strength, shape of potential well, etc. Without essential loss of generality we shall assume that the parameter dependence is linear, namely

$$H_\varepsilon(t) = H_0(t) + \varepsilon V(t). \tag{1}$$

Let $U_\varepsilon(t)$ be the propagator

$$U_\varepsilon(t) = \hat{T} \exp\left(-\frac{\mathrm{i}}{\hbar}\int_0^t \mathrm{d}t' H_\varepsilon(t')\right) \tag{2}$$

where $\hat{T}$ designates the time ordering. If $|\Psi\rangle$ is some arbitrary initial state, then the time evolution, depending on the time variable t as well on the perturbation parameter ε of the Hamiltonian, is given by

$$|\Psi_\varepsilon(t)\rangle = U_\varepsilon(t)|\Psi\rangle. \tag{3}$$

Having the tools defined above, *the fidelity amplitude*, with respect to the unperturbed evolution $U_0(\varepsilon)$, is defined as the overlap of the perturbed and unperturbed time-evolving states as

$$f_\varepsilon(t) = \langle\Psi_0(t)|\Psi_\varepsilon(t)\rangle = \langle\Psi|U_0(-t)U_\varepsilon(t)|\Psi\rangle. \tag{4}$$

The square of its modulus is *fidelity*

$$F_\varepsilon(t) = |f_\varepsilon(t)|^2. \tag{5}$$

At this point we wish to stress the dual interpretation of fidelity, which is the central characteristic of echo dynamics often called 'Loschmidt echo': on one hand $F_\varepsilon(t)$ is the probability that the states of unperturbed and perturbed time evolution are the same, but on the other hand, due to unitarity of time evolutions, $F_\varepsilon(t)$ is also the probability that after an echo - composition of forward perturbed and backward unperturbed dynamics - we arrive back to the initial state.

In the following we shall write the expectation value in a given initial state simply as $\langle A\rangle = \langle\Psi|A|\Psi\rangle$. The fidelity amplitude may now be compactly written in terms of the *expectation value* of the so-called *echo-operator*

$$M_\varepsilon(t) = U_0(-t)U_\varepsilon(t), \tag{6}$$

as

$$f_\varepsilon(t) = \langle M_\varepsilon(t)\rangle. \tag{7}$$

One may also use a non-pure initial state, namely a statistical mixture described by a density matrix ρ, with $\langle A\rangle = \mathrm{tr}\,\rho A = \sum_k p_k\langle\phi_k|A|\phi_k\rangle$, where p_k and $|\phi_k\rangle$ are, respectively, the eigenvalues and eigenvectors of the

density matrix ρ. One might be lead to an intuitive belief that incoherent superpositions of fidelity amplitude, such as the above for non-pure initial states, would not have a clear physical significance. Nevertheless, it turns out that this is not the case and that such a generalized object may be experimentally observable [64] and exhibit certain interesting theoretical features [65].

Writing the perturbation operator in the interaction picture

$$\tilde{V}(t) = U_0(-t)V(t)U_0(t) \tag{8}$$

one can straightforwardly check by differentiating Eq. (6) that the echo-operator solves the evolution equation

$$\frac{\mathrm{d}}{\mathrm{d}t}M_\varepsilon(t) = -\frac{\mathrm{i}}{\hbar}\varepsilon\tilde{V}(t)M_\varepsilon(t) \tag{9}$$

with the (effective) Hamiltonian $\varepsilon\tilde{V}$. The echo-operator is nothing but the propagator in the interaction picture, which can be written in terms of a formal solution of Eq. (9)

$$M_\varepsilon(t) = \hat{T}\exp\left(-\frac{\mathrm{i}}{\hbar}\varepsilon\int_0^t \mathrm{d}t'\tilde{V}(t')\right). \tag{10}$$

Again, a time-ordered product has to be used since $\tilde{V}(t)$ for different times does not in general commute. The computation of fidelity becomes rather straightforward if one plugs the expression for the echo-operator (10) into the definition (7).

In particular, this approach is ideally suited for a perturbative treatment when the perturbation strength ε can be considered as a small parameter. One can write explicitely the Born series for the echo operator, which has an infinite radius of convergence provided that the perturbation $V(t)$ is an operator, uniformly bounded for all t:

$$M_\varepsilon(t) = \mathbf{1} + \sum_{m=1}^{\infty}\frac{(-\mathrm{i}\varepsilon)^m}{\hbar^m m!}\int_0^t \mathrm{d}t_1\mathrm{d}t_2\cdots\mathrm{d}t_m\hat{T}\tilde{V}(t_1)\tilde{V}(t_2)\cdots\tilde{V}(t_m). \tag{11}$$

If we truncate the above series at the second order, $m = 2$, and insert the expression into Eq. (7), we obtain

$$f_\varepsilon(t) = 1 - \frac{\mathrm{i}\varepsilon}{\hbar}\int_0^t \mathrm{d}t'\langle\tilde{V}(t')\rangle - \frac{\varepsilon^2}{\hbar^2}\int_0^t \mathrm{d}t'\int_{t'}^t \mathrm{d}t''\langle\tilde{V}(t')\tilde{V}(t'')\rangle + O(\varepsilon^3). \tag{12}$$

Taking the square modulus we obtain the fidelity

$$F_\varepsilon(t) = 1 - \frac{\varepsilon^2}{\hbar^2}\int_0^t \mathrm{d}t'\int_0^t \mathrm{d}t''C(t',t'') + O(\varepsilon^4) \tag{13}$$

where

$$C(t',t'') = \langle\tilde{V}(t')\tilde{V}(t'')\rangle - \langle\tilde{V}(t')\rangle\langle\tilde{V}(t'')\rangle, \tag{14}$$

is the 2-point time-correlation function of the perturbation. This high-fidelity approximation (13) shall be called *linear response* expression for fidelity. We stress that the validity of the linear response formula (13) is by no means restricted to short times. The only condition is to have high-fidelity, namely $\eta := 1 - F_\varepsilon(t)$ has to be small. The error of the linear approximation is typically of order $O(\varepsilon^4)$. However, using the same technique one can go beyond the linear response approximation for certain particular cases of dynamics, for example we shall derive Fermi golden rule decay for strongly mixing dynamics (Subsect. 3.1) and various non-universal decays for integrable dynamics (e.g. Subsect. 5.2).

Note that the linear-response formula (13) already establishes a very important physical property of quantum echo-dynamics. One observes an intimate connection between fidelity decay and temporal-correlation decay, namely faster decay of the correlation function $C(t',t'')$, as $|t'-t''|$ grows, implies slower decay of fidelity and vice versa. For example, for quantum systems in the semiclassical regime, whose classical limit is chaotic and fast mixing, such that $C(t',t'')$ decays faster than $\mathrm{const}/|t'-t''|$, fidelity is expected to decay as a linear function of time $F_\varepsilon(t) = 1 - \mathrm{const}\,\varepsilon^2 t$, whereas for regular systems, with integrable classical limit, $C(t',t'')$ is expected to have oscillating behavior with generally *nonvanishing* time average, hence fidelity is expected to decay as a quadratic function of time $F_\varepsilon(t) = 1 - \mathrm{const}\,\varepsilon^2 t^2$. This implies the seemingly

paradoxical conclusion that the fidelity of regular dynamics may decay faster than the fidelity of chaotic ones. Detailed discussion and comparision between chaotic and regular dynamics is given in Sect. 7.

The linear response formula (13) can be cast into another intuitively useful form. Let us define an *integrated perturbation operator* $\Sigma(t)$

$$\Sigma(t) = \int_0^t \mathrm{d}t' \tilde{V}(t'). \tag{15}$$

Then, the RHS of Eq. (13) rewrites in terms of an *uncertainty* of operator $\Sigma(t)$:

$$F_\varepsilon(t) = 1 - \frac{\varepsilon^2}{\hbar^2} \left\{ \langle \Sigma^2(t) \rangle - \langle \Sigma(t) \rangle^2 \right\} + O(\varepsilon^4) \tag{16}$$

Now, another interpretation of the quantum fidelity decay in the quantum chaotic - or stochastic - versus regular regime can be given. For quantum chaotic dynamics, one expects to have *diffusive* [1] behavior of typical observables, like V, hence $\langle \Sigma^2 \rangle - \langle \Sigma \rangle^2 \propto t$, whereas for regular dynamics one expects *ballistic* behavior, $\langle \Sigma^2 \rangle - \langle \Sigma \rangle^2 \propto t^2$.

Another point has to be stressed: The fidelity amplitude is in general a c-number whose phase can be shifted by a perturbation which is a a multiple of an identity operator. So, adding a constant to the perturbation, e.g. forcing it to have a vanishing expectation value $V' = V - \langle V \rangle \mathbf{1}$, rotates the fidelity amplitude by a unimodular factor $f'_\varepsilon(t) = \exp(\mathrm{i}\varepsilon t \langle V \rangle / \hbar) f_\varepsilon(t)$ while it leaves the fidelity $F_\varepsilon(t)$ unchanged. This follows trivially from the representation of fidelity amplitude (7) in terms of the echo operator (10).

2.1.1. *Quantum Zeno regime*

Note, however, that for very short times, below a certain time scale t_Z, namely before the correlation function starts to decay, $|t'|, |t''| < t_\mathrm{Z}$, $C(t', t'') \approx C(0,0) = \langle V^2 \rangle$, the fidelity always exhibits (universal) quadratic decay

$$F(t) = 1 - \frac{\varepsilon^2}{\hbar^2} \langle V^2 \rangle t^2, \quad \text{for } |t| < t_\mathrm{Z} = \left(\frac{C(0,0)}{\mathrm{d}^2 C(0,t)/\mathrm{d}t^2} \right)^{1/2} = \hbar \left(\frac{\langle V^2 \rangle}{\langle [H_0, V]^2 \rangle} \right)^{1/2} \tag{17}$$

This short-time regime (also discussed in [30]) may be identified with the quantum Zeno effect [66,67], and the time scale t_Z referred to as the Zeno time.

2.1.2. *Temporally stochastic perturbations*

It is instructive to explain what happens in the case when the perturbation $V(t)$ is explicitly time dependent and stochastic, *i.e.* being a Gaussian delta correlated white noise, with variance

$$\overline{V(t')V(t'')} = v^2 \delta(t' - t'') \mathbf{1}. \tag{18}$$

$\overline{\bullet}$ here denotes an average over an ensemble of stochastic perturbation operators. The dynamical correlation $C(t', t'')$ is obviously insensitive to the nature of unperturbed dynamics; hence the correlation function is again a delta function $C(t', t'') = v^2 \delta(t' - t'')$. Furthermore, due to the Gaussian nature of the noise, higher-order correlation functions, say of order $2n$, in the expression for the echo operator (11) factorize with the multiplicity $(2n-1)!!$ due to the Wick theorem, yielding a simple exponential decay

$$F(t) = \exp\left(-\frac{\varepsilon^2}{\hbar^2} v^2 t \right). \tag{19}$$

For stochastic uncorrelated perturbations fidelity thus decays exponentially with the rate which depends on the magnitude of perturbation only and not on dynamics of the unperturbed system.

[1] Of course, for a finite quantum system, diffusive behavior can only be observed on finite time scales, typically below the Heisenberg time. The issue of time scales is discussed extensively in later sections, in particular in Section 7.

2.1.3. *Effect of conservation laws*

One should note that the correlation integral

$$C_{\rm i}(t) = \int_0^t {\rm d}t' \int_0^t {\rm d}t'' C(t',t'') = \langle \Sigma^2(t) \rangle - \langle \Sigma(t) \rangle^2 \tag{20}$$

always increases quadratically, even in the case of chaotic quantum dynamics, if the perturbation has a nonvanishing component in the direction of some *(trivial) conserved quantities* such as the energy, the Hamilton operator H_0 (if time-independent) or the angular momentum, *etc.* For example, let $\{Q_n, n = 1, 2 \ldots M\}$ be an orthonormalized set of conserved quantities with respect to the initial state $|\Psi\rangle$, such that $\langle Q_n Q_m \rangle = \delta_{nm}$. [2] Then any time-independent perturbation can be decomposed uniquely as

$$V = \sum_{m=1}^{M} c_m Q_m + V' \tag{21}$$

with coefficients $c_m = \langle V Q_m \rangle$ and V' being the remaining non-trivial part of the perturbation, by construction orthogonal to *all* trivial conservation laws,

$$\langle Q_m V' \rangle = 0, \quad \text{for all } m. \tag{22}$$

In such a case the correlation integral will always grow asymptotically as a quadratic function

$$C_{\rm i}(t) \to \left(\sum_{m=1}^{M} c_m^2 \right) t^2; \tag{23}$$

hence fidelity will decay quadratically. Therefore it is desirable to subtract this trivial effect by always choosing perturbations which are orthogonal to all known trivial conservation laws.

For example, if H_0 is time-independent, then it is a trivial invariantbe . The fact that a general perturbation V may not be orthogonal to H_0, $\langle H_0 V \rangle \neq 0$ is equivalent to the fact that V will change the density of states (in the first order in ε) in the region of eigenstates of H_0 populated by the initial state Ψ. This means that the Heisenberg time will be different for forward (perturbed) and backward (unperturbed) dynamics, so fidelity will decay quadratically due to this trivial effect. This effect is simply removed by replacing the perturbation by $V' = V - \langle H_0 V \rangle H_0 / \langle H_0^2 \rangle$, or equivalently by measuring forward and backward time evolution in units of their respective Heisenberg times. We note that this effect has actually been discussed and taken care of in beautiful experimental studies of fidelity by Lobkis and Weaver [68] and Stöckmann et al. [69,70] (see Section 9.2). Nevertheless it is important to add that such "trivial" perturbations are non-trivial in the framework of quantum information applications, and indeed this shows, that the control of such perturbations is particularly important.

There is another consequence of conservation laws, namely they divide the Hilbert space of unperturbed evolution $U_0(t)$ into blocks specified by eigenvalues of the conserved operators, or quantum numbers. As a result the effective Heisenberg time - which will be one of the key time scales in later discussions - is reduced due to a reduced average density of states with *fixed* quantum numbers.

2.1.4. *Baker-Campbell-Hausdorff expansion of the echo operator*

For the purposes of semi-classical analysis in subsequent sections it will be useful to perform another formal manipulation on the echo operator (10), namely we may want to rewrite it approximately in terms of a single exponential. For this aim, we apply the well known Baker-Campbell-Hausdorff expansion $e^A e^B = \exp(A + B + (1/2)[A, B] + \ldots)$, to the infinite product (10) yielding

[2] Any set of physical conservation laws Q'_m can be orthogonalized using a standard Gram-Schmidt procedure. In order to prevent degeneracy of the scalar product we only have to assume *independence of conservation laws* in the sense that all the M states $Q'_m|\Psi\rangle$ should be linearly independent.

$$M_\varepsilon(t) = \exp\left\{-\mathrm{i}\frac{\varepsilon}{\hbar}\int_0^t \mathrm{d}t'\tilde{V}(t') + \frac{\varepsilon^2}{2\hbar^2}\int_0^t \mathrm{d}t'\int_{t'}^t \mathrm{d}t''[\tilde{V}(t'),\tilde{V}(t'')] + \ldots\right\}$$
$$= \exp\left\{-\frac{\mathrm{i}}{\hbar}\left(\Sigma(t)\varepsilon + \frac{1}{2}\Gamma(t)\varepsilon^2 + \ldots\right)\right\} \tag{24}$$

where

$$\Gamma(t) = \frac{\mathrm{i}}{\hbar}\int_0^t \mathrm{d}t'\int_{t'}^t \mathrm{d}t''[\tilde{V}(t'),\tilde{V}(t'')]. \tag{25}$$

Similar algebraic manipulations are well known in quantum field theory and are sometimes known as the Magnus expansions, see for example Ref. [71]. Two general remarks concerning the above asymptotic BCH expansion (24) are in order. First, the double integral of the commutator, which defines the operator $\Gamma(t)$, does in general grow only linearly in time, namely one can show that for arbitrary pair of states $|\psi\rangle$ and $|\phi\rangle$,

$$|\langle\psi|\Gamma(t)|\phi\rangle| < C_{\psi\phi}t. \tag{26}$$

where $C_{\psi\phi}$ is some constant, which may depend on the choice of the states $|\psi\rangle$ and $|\phi\rangle$.

Second, the matrix elements of the *third* and *fourth* order terms of the BCH expansion (24) can be estimated by $\mathrm{const}\,\varepsilon^3 t$ and $\mathrm{const}\,\varepsilon^4 t^2$, respectively. Therefore, Eq. (24) provides in general a good approximation of the echo operator up to times $t < \mathrm{const}\,\varepsilon^{-1}$, which can be made arbitrary long for sufficiently weak perturbations.

2.2. *Perturbation with vanishing time average*

Let us define the *time average* of the perturbation operator

$$\bar{V} = \lim_{t\to\infty}\frac{\Sigma(t)}{t} = \lim_{t\to\infty}\frac{1}{t}\int_0^t \mathrm{d}t'\tilde{V}(t'). \tag{27}$$

Generally, an arbitrary perturbation V can be decomposed into its time average $\bar{V}$ and the rest, denoted by V_{res} and called the *residual part*,

$$V = \bar{V} + V_{\mathrm{res}}. \tag{28}$$

Let us, for the rest of this discussion, assume for simplicity that the unperturbed Hamiltonian H_0 and the perturbation V are time-independent operators. Let E_k and $|E_k\rangle$ denote, respectively, eigenenergies and eigenvectors of the unperturbed Hamiltonian H_0 and assume that the spectrum $\{E_k\}$ is non-degenerate, which is typical for non-integrable and often true even for integrable systems. In this case the time average is the *diagonal part* of the perturbation $\bar{V} = \mathrm{diag}V$, and the residual part V_{res} is the *off-diagonal part*. The operator $\Sigma(t)$ can be asymptotically written as $\Sigma(t) = \bar{V}t + \mathcal{O}(t^0)$, where the second term has off-diagonal matrix elements only, if expressed in the eigenbasis of H_0. A further important condition is that V_{res} does not grow asymptotically with time. Therefore, the second order correlation integral $C_{\mathrm{i}}(t)$ when expressed as (20) does not grow with time either and remains bounded for all times if $\bar{V} = 0$ or, more precisely, if and only if $\langle\bar{V}^2\rangle - \langle\bar{V}\rangle^2 = 0$.

Even though one may argue that the case of vanishing time-averaged perturbation $\bar{V} = 0$ may be rather special and non-generic, it deserves to be studied separately as it exhibits very unusual and perhaps surprisingly stable behavior of echo-dynamics. Furthermore, it can be realized in several important physical situations:

– When the perturbation V can be written as time-derivative of another observable or equivalently as a commutator with the Hamiltonian then obviously, by construction the diagonal part $\bar{V}$ vanishes.
– When the unperturbed system is invariant under a certain unitary symmetry operation P, say parity, $PH_0 = H_0P$, whereas the symmetry changes sign of the perturbation $PV = -VP$. This means that the perturbation breaks the unitary symmetry in a maximal way and matrix elements of V are nonvanishing only between the states of opposite parity.
– When the unperturbed system is invariant under a certain anti-unitary symmetry operation T, say time-reversal, $TH_0 = H_0T$, whereas the symmetry changes sign of the perturbation $TV = -VT$. This means

that the perturbation breaks the antiunitary symmetry in an optimal way and the matrix of V in the eigenbasis of H_0 can be generally written as $V_{mn} = \mathrm{i}A_{mn}$ where A is a *real antisymmetric* matrix.

– Sometimes diagonal elements of the perturbation can be taken out *by hand* and treated as a trivial first order perturbation of the unperturbed part. In few-body and many-body physics this approach is commonly known as the mean-field approximation. One may be generally interested in the effect of residual perturbations and analyze it through echo-dynamics.

In the present subsection we discuss some general properties of echodynamics for perturbations with $\bar{V} = 0$, also called *residual* perturbations because $V = V_{\mathrm{res}}$. As we shall see, the short time fidelity will still be given by the operator $\Sigma(t)$. Because its norm does not grow with time, the fidelity will *freeze* at a constant value for the time of validity of the linear response approximation. After a sufficiently long time it will again start to decay due to the operator $\Gamma(t)$. We claim that this behavior is rather insensitive to the nature of unperturbed dynamics, for example whether it is regular or chaotic.

Provided that the spectrum of H_0 is non-degenerate, any residual perturbation can be defined in terms of another operator W by the following prescription [3]

$$V = (d/dt)W(t) = \frac{\mathrm{i}}{\hbar}[H_0, W], \qquad W(t) = U_0(-t)WU_0(t). \tag{29}$$

Indeed, given a residual perturbation one easily determines the matrix elements of W as

$$W_{jk} := -\mathrm{i}\hbar\frac{V_{jk}}{E_i - E_j}, \tag{30}$$

where E_i are eigenenergies of H_0. For the corresponding definition in a discrete-time case, e.g. for kicked systems, see [16,17]. From the definition of W in Eq. (30) we can see that the matrix elements W_{jk} are large for near degeneracies. For W to be well behaved the matrix elements V_{jk} of the perturbation must decrease smoothly approaching the diagonal. Setting diagonal elements of V to zero will typically [e.g. in classically chaotic systems (Section 3.2) or in models of random matrices (Section 4.3)] produce singular behavior and reduce the effect of fidelity freeze. However, for regular unperturbed systems the effect of quantum freeze is even more robust due to abundance of selection rules, namely the matrix V_{jk} is typically sparse so singularities due to near degeneracies may not occur even if we take out the diagonal part by hand. With this newly defined operator W, the expression for the integrated perturbation $\Sigma(t)$ is extremely simple,

$$\Sigma(t) = W(t) - W(0). \tag{31}$$

Similarly, the expression for $\Gamma(t)$ (25) is considerably simplified to

$$\Gamma(t) = \Sigma_R(t) - \frac{\mathrm{i}}{\hbar}[W(0), W(t)], \qquad R = \frac{\mathrm{i}}{\hbar}[W, (d/dt)W(t)], \tag{32}$$

where

$$\Sigma_R(t) = \int_0^t R(t')dt', \qquad R(t) = U_0(-t)RU_0(t). \tag{33}$$

Apart from the "boundary term" $\frac{\mathrm{i}}{\hbar}[W, W(t)]$, the operator $\Gamma(t)$ has, similarly to $\Sigma(t)$, the structure of a time integral of another operator R. From this representation it follows that any matrix element or the norm of operator $\Gamma(t)$ grows at most linearly with time. The aforementioned boundary term can be used to factorize the expression for the echo operator which will be the form most useful for applications in the following sections. Namely, to order $O(t\varepsilon^3)$ it can be written as

$$M_\varepsilon(t) = \exp\left(-\frac{\mathrm{i}}{\hbar}W(t)\varepsilon\right)\exp\left(-\frac{\mathrm{i}}{\hbar}\Sigma_R(t)\frac{\varepsilon^2}{2}\right)\exp\left(\frac{\mathrm{i}}{\hbar}W(0)\varepsilon\right). \tag{34}$$

From the expression (34) we see that, since $||W(t)|| = ||W(0)||$, a time scale $t_2 = O(1/\varepsilon)$ should exist such that for times $t < t_2$, the term in the second exponential $\Sigma_R(t)\varepsilon^2$ can be neglected as compared to the one in the first and the third, $W(t)\varepsilon, W(0)\varepsilon$. Therefore, for $t < t_2$ we can write

$$F(t) = \left|\langle\exp\left(-\mathrm{i}\frac{\varepsilon}{\hbar}W(t)\right)\exp\left(\mathrm{i}\frac{\varepsilon}{\hbar}W(0)\right)\rangle\right|^2. \tag{35}$$

[3] Note that in the classical limit one can replace the commutator with a Poisson bracket, $(1/\mathrm{i}\hbar)[A, B] \to \{A, B\}$.

As we shall see later, the RHS of the above equation will typically not depend on time, beyond some timescale t_1, much shorter than t_2, namely for $t_1 < t < t_2$, but we can claim quite generally that RHS of Eq. (35) has a strict lower bound. Expanding the formula (35) to the second order in ε one can show [17] that the fidelity has a lower bound irrespective on the nature of dynamics, given by

$$F(t) \geq 1 - 4\frac{\varepsilon^2}{\hbar^2} r^2, \qquad t < t_2, \tag{36}$$

where

$$r^2 = \sup_t \left[\langle W(t)^2 \rangle - \langle W(t) \rangle^2 \right]. \tag{37}$$

For a residual perturbation the fidelity therefore stays high up to a classically long time $t_2 \sim 1/\varepsilon$ and only then starts to decay again. We call this phenomena fidelity freeze. The freeze happens for *arbitrary* quantum dynamics, irrespective of the existence and the nature of the classical limit. After t_2 the term $\Gamma(t) \sim t\bar{R}$ in the second exponential of (34) will become important and eventually this will cause the fidelity to decay. In the regime $t > t_2$ the expression of the echo operator is formally similar to the original form (10) where the perturbation εV has to be replaced by an effective perturbation operator $\frac{1}{2}\varepsilon^2 R$. This point shall be discussed in more detail later. We have to stress that the freeze of fidelity is of purely quantum origin. The classical fidelity discussed in Section 6 does not exhibit a freeze.

2.3. *Average fidelity*

2.3.1. *Time averaged fidelity*

In a finite Hilbert space the fidelity will not decay to zero but fluctuate around some small plateau value, which is equal to the time averaged fidelity. For ergodic systems this time averaged value is in turn equal to the phase space averaged one. For a finite Hilbert space of size N, fidelity will start to fluctuate for long times due to the discreteness of the spectrum of the evolution operator. The size of this fluctuations can be calculated by evaluating time averaged fidelity $\bar{F}$

$$\bar{F} = \lim_{t\to\infty} \frac{1}{t} \int_0^t \mathrm{d}t' F(t'). \tag{38}$$

We expand the initial state in the eigenstates $|E_n\rangle$ of the unperturbed Hamiltonian H_0, write the eigenenergies and eigenstates of the perturbed Hamiltonian as E_n^ε and $|E_n^\varepsilon\rangle$, and denote the matrix elements between unperturbed and perturbed eigenstates by

$$O_{kl} = \langle E_k | E_l^\varepsilon \rangle. \tag{39}$$

The transition matrix O is unitary, and if both eigenvectors can be chosen real it is orthogonal. This happens if H_0 and H_ε commute with an antiunitary operator T whose square is identity. The fidelity amplitude can now be written

$$f(t) = \sum_{lm} (O^\dagger \rho)_{lm} O_{ml} \exp\left(-\mathrm{i}(E_l^\varepsilon - E_m)t/\hbar\right), \tag{40}$$

with $\rho_{lm} = \langle E_l | \rho(0) | E_m \rangle$ being the matrix elements of the initial density matrix in the unperturbed eigenbasis. To calculate the average fidelity $\bar{F}$ we have to take the absolute value square of $f(t)$. Averaging over time t we will assume that the phases are non-degenerate and find

$$\overline{\exp\left(\mathrm{i}(E_l^\varepsilon - E_{l'}^\varepsilon + E_m - E_{m'})t/\hbar\right)} = \delta_{m\,m'}\delta_{l\,l'}. \tag{41}$$

This results in the average fidelity

$$\bar{F} = \sum_{ml} |(\rho O)_{ml}|^2 |O_{ml}|^2. \tag{42}$$

The time averaged fidelity therefore understandably depends on the initial state ρ as well as on the "overlap" matrix O.

For *small perturbation* strengths, say ε smaller than some critical $\varepsilon_{\rm rm}$, the unitary matrix O will be close to identity. Using $O \to \mathbb{1}$ for $\varepsilon \ll \varepsilon_{\rm rm}$ (42) gives us

$$\bar{F}_{\rm weak} = \sum_l (\rho_{ll})^2 \tag{43}$$

One should keep in mind that for the above result $\bar{F}_{\rm weak}$ we needed the eigenenergies to be non-degenerate, $E_l^\varepsilon \neq E_m$ (41), and at the same time $O \to \mathbb{1}$. This approximation is justified in lowest order in ε, if the offdiagonal matrix elements are $|O_{ml}|^2 \propto \varepsilon^2$. For pure initial states $\sum_l \rho_{ll}^2 = \sum_l |\langle E_l|\Psi\rangle|^4$ is just the inverse participation ratio of the initial state expressed in terms of the unperturbed eigenstates. Note that these expressions should be symmetric with respect to the interchange of the unperturbed and perturbed basis. On the other hand, for sufficiently *large* perturbation strength ε and complex perturbations V, such that the two bases – the perturbed one and the unperturbed one – become practically unrelated, one might assume O to be close to a random matrix, unitary or orthogonal. In the limit $N \to \infty$, the matrix elements O_{ml} can be treated as independent complex or real Gaussian random numbers. Then we can average the expression (42) over a Gaussian distribution $\propto \exp\left(-\beta N |O_{ml}|^2/2\right)$ of matrix elements O_{ml}, where we have $\beta = 1$ for orthogonal O and $\beta = 2$ for unitary O. This averaging gives $\langle |O_{ml}|^4\rangle = (4-\beta)/N^2$ and $\langle |O_{ml}|^2\rangle = 1/N$ for the variance of O_{ml} (brackets $\langle\bullet\rangle$ denote here averaging over the distribution of matrix elements and not over the initial state). The average fidelity for strong perturbation can therefore be expressed as

$$\bar{F}_{\rm strong} = \frac{4-\beta}{N} \sum_l \rho_{ll}^2 + \frac{1}{N} \sum_{l,n}^{l\neq m} |\rho_{lm}|^2. \tag{44}$$

More details on various cases of initial states as well as on crossover of the average fidelity from the case of weak to the case of strong perturbations can be found in Appendix A.

2.3.2. *State averaged fidelity*

Sometimes the average fidelity is of interest, *i.e.* the fidelity averaged over some ensemble of initial states. Such an average fidelity is also more amenable to theoretical treatment. Easier to calculate is the average fidelity amplitude $f(t)$ which is of second order in the initial state $|\Psi\rangle$ while fidelity $F(t)$ is of fourth order in $|\Psi\rangle$. We will show that the difference between the absolute value squared of the average fidelity amplitude and the average fidelity is small for large Hilbert space dimensions N.

Let us look only at the simplest case of averaging over random initial states, denoted by $\langle\!\langle\bullet\rangle\!\rangle$. In the asymptotic limit of large Hilbert space size $N \to \infty$ the averaging is simplified by the fact that the expansion coefficients c_m of a random initial state in an arbitrary basis become independent Gaussian variables, with variance $1/N$. Quantities bilinear in the initial state, like the fidelity amplitude or the correlation function, result in the following expression

$$\langle\!\langle \Psi|A|\Psi\rangle\!\rangle =: \langle\!\langle A\rangle\!\rangle = \langle\!\langle \sum_{ml} c_m^* A_{ml} c_l\rangle\!\rangle = \frac{1}{N} \operatorname{tr} A, \tag{45}$$

where A is an arbitrary operator. The averaging is done simply by means of a trace over the whole Hilbert space. For the fidelity $F(t)$ which is of fourth order in $|\Psi\rangle$ we get after some analysis

$$\langle\!\langle F(t)\rangle\!\rangle = \sum_{mlpr} \langle\!\langle c_m^* [M_\varepsilon(t)]_{ml} c_l c_p [M_\varepsilon(t)]_{pr}^* c_r^*\rangle\!\rangle = \frac{|\langle\!\langle f(t)\rangle\!\rangle|^2 + 1/N}{1+1/N}. \tag{46}$$

The difference between the average fidelity and the average fidelity amplitude is therefore of order $1/N$ [72]. Note that the random state average (46) is in fact exact for any N.

There are two reasons why averaging over random initial states is of interest. First, in the field of quantum information processing these are the most interesting states as they have the least structure, *i.e.* can accommodate the largest amount of information. Second, for ergodic dynamics and sufficiently long times, one can replace expectation values in a specific generic state $|\Psi\rangle$ by an ergodic average.

Assuming ergodicity for sufficiently large Hilbert spaces there should be no difference between averaging the fidelity amplitude or the fidelity or taking a typical single random initial state. For mixing dynamics

the long time fidelity decay is independent of the initial state even if it is non-random, whereas in the regular regime it is state dependent. For instance, the long time Gaussian decay (Section 5) depends on the position of the initial coherent state. The fidelity averaged over this position of the initial coherent state might be of interest and will not be equal to the fidelity averaged over random initial states. In the special case of very strong perturbation, $\varepsilon > \hbar$, the average fidelity depends on the way we average even for mixing dynamics. This happens due to large fluctuations of fidelity for different initial coherent states, see Ref. [73] and also [74]. Systematic study of fluctuation of fidelity with respect to an ensemble of initial coherent states has been performed in Ref. [75] and showed that variance of fidelity is a non-monotonous function of time with a well defined maximum, where the standard deviation of fidelity can dominate its average value.

2.4. *Estimating fidelity*

For relatively short times or sufficiently weak perturbations, there exists an inequality giving a lower bound on fidelity in terms of the quantum uncertainty of the time-evolving perturbation operator. This is a time dependent version of Mandelstam-Tamm inequality [76] (sometimes also called Fleming's bound [77]) which is usually used to derive bounds on the time necessary for a given state to evolve into an orthogonal state [78]. In the context of fidelity it was used by Peres [30], see also Ref. [47]. In order to derive the inequality one starts with an observation that the time derivative of fidelity can be written as

$$\frac{\mathrm{d}}{\mathrm{d}t}F(t) = -\frac{\mathrm{i}\varepsilon}{\hbar}\langle\Psi_0(t)|[P_\varepsilon, V]|\Psi_0(t)\rangle \tag{47}$$

where $P_\varepsilon = |\Psi_\varepsilon(t)\rangle\langle\Psi_\varepsilon(t)|$ is the projector onto the time-evolving state of the perturbed evolution. Using the Heisenberg uncertainty relation for the operators P_ε and V,

$$\delta V(t)\delta P_\varepsilon(t) \leq \frac{1}{2}\,|\langle\Psi_0(t)|[P_\varepsilon, V]|\Psi_0(t)\rangle| \tag{48}$$

with the time-evolving quantum uncertainty of operator A defined as

$$\delta A(t) = \left(\langle\Psi_0(t)|A^2|\Psi_0(t)\rangle - \langle\Psi_0(t)|A|\Psi_0(t)\rangle^2\right)^{1/2}, \tag{49}$$

we can estimate the time-derivative of fidelity as

$$-\frac{\mathrm{d}}{\mathrm{d}t}F(t) \leq \left|\frac{\mathrm{d}}{\mathrm{d}t}F(t)\right| \leq \frac{2\varepsilon}{\hbar}\delta V(t)\delta P_\varepsilon(t) = \frac{2\varepsilon}{\hbar}\delta V(t)F(t)(1-F(t)). \tag{50}$$

Separating the variables and integrating we arrive at the final inequality

$$F(t) \geq \cos^2(\phi(t)), \quad \phi(t) = \frac{\varepsilon}{\hbar}\int_0^t \mathrm{d}t'\delta V(t') \tag{51}$$

We should note, however, that the inequality (51) can be used only in the first of $\cos^2$, namely for $|\phi| \leq \pi/2$.

2.5. *Errors in approximate quantization schemes*

Let us sidetrack our discussion for a moment by mentioning a closely related subject.

An early and very fundamental application of fidelity decay was given by L. Kaplan, who analyzed extensively the discrepancy between semi-classical quantization and the exact one [79,29,80,81]. While most research concentrates directly on the behavior of the spectra, here the temporal deviation between the exact and the approximate solution are discussed. Considering the deviation at Heisenberg time will then yield information about the correctness of the level sequence and also shed light on the question whether localization can be explained in the framework of semi-classics.

Iterating Bogomolny's semi-classical solution for a quantum Poincaré map [82] provides a crude approximation. The fidelity taken between this approximation and the real quantum time evolution will show a significant decay of fidelity long before the Heisenberg time. On the other hand it is by no means practical to pursue semi-classical evolution up to Heisenberg time, because the exponential growth in the number of

classical orbits, which we have to consider, precludes such a task. What Kaplan shows, is that semi-classics can be performed for times long compared to the return time T of a simple Poincaré map, but short compared to Heisenberg time T_H *i.e.* for a time T_K such that $T \ll T_K \ll T_H$. Iterating this map we can then reach Heisenberg time with a good semi-classical approximation. With other words this iterated dynamics is an arbitrarily good approximation to the true semiclassics, the difference falling off exponentially as $\exp(-\text{const}\, T_K/T)$. Therefore the fidelity decay between true quantum evolution and exact semiclassics is essentially the same as between quantum evolution and iterated semiclassics as long as $T_K \gg T$.

The upshot of these investigations is in agreement with our general findings. Fidelity decay of even the best semi-classical approximation will go as $1 - \text{const}t^2$ for integrable systems and as $1 - \text{const}t$ for chaotic ones. Thus semi-classical approximations are found to be more stable for chaotic systems than for integrable ones. In particular the level sequence becomes marginally correct in two dimensions for integrable systems, while for chaotic ones three dimensions seem to be just about the limit. Note that this does not imply that semi-classics cannot be usefully applied for some purposes in higher dimensional cases. Yet if we use a correct level sequence as the criterion, then this limitation exists for sure.

2.6. *Echo measures beyond the fidelity*

The quantum state overlap - the fidelity amplitude - is only one of the measures of quality of the echo, or of the deviation between two quantum time evolutions. For example in real experiments, there is often different information at our disposal to make the comparison between two quantum states. The information about the system's state is based on the measurements of certain observables whose outcomes, in turn, only partially determine the state in question. It is thus relevant to define other measures of echo-dynamics based on the partial informations between two quantum states.

2.6.1. *Scattering fidelity*

Fidelity, as it is usually defined, also applies to scattering systems. A wave packet can be evolved with two slightly different scattering Hamiltonians. This would be the standard fidelity of a scattering system. In contrast, "scattering fidelity" stands for a quantity which can be obtained from simple scattering data, though under certain conditions it agrees with the standard fidelity [69,70,83].

Typically scattering theory is developed around the scattering or S-matrix, and in this context it is only logical to inquire on the stability of S-matrix elements under perturbations. If we take into account that the S-matrix is due to some Hamiltonian that now describes an open system, we can again consider an unperturbed Hamiltonian and its perturbation, which define the S-matrices S and S'. Usually the S-matrix is given in the energy domain, *i.e.* an S-matrix element is written as $S_{ab}(E)$, where a and b denote the scattering channels. By taking the Fourier transform

$$\hat{S}_{ab}(t) = \int \mathrm{d}E \ \mathrm{e}^{-2\pi \mathrm{i}\, Et} \ S_{ab}(E) \,, \tag{52}$$

of any S-matrix element, we obtain the S-matrix $\hat{S}$ in the time domain.

It now seems natural to consider the correlation function in the time domain

$$\hat{C}[{S_{ab}}^*, S'_{ab}](t) \propto \hat{S}_{ab}(t)^* \ \hat{S}'_{ab}(t) \tag{53}$$

as an appropriate measure of scattering fidelity. Yet this is not the case, because this quantity is dominated by the behavior of the autocorrelation functions. This can be amended by normalizing with the autocorrelation functions to obtain the scattering fidelity amplitude

$$f^s_{ab}(t) = \hat{C}[{S_{ab}}^*, S'_{ab}](t) \ \big[\, \hat{C}[{S_{ab}}^*, S_{ab}](t) \ \hat{C}[{S'_{ab}}^*, S'_{ab}](t) \,\big]^{-1/2} \,. \tag{54}$$

While we formally started out in the energy domain, to conform with the usual language of scattering theory, it must be noted, that Lobkis and Weaver [68] reach essentially the same definition when analyzing scattering data taken in the time domain. The connection with fidelity was established in [83].

We may ask how the scattering fidelity amplitude is related to the usual concept of fidelity. In principle, we could do this by considering the scattering process in terms of wave packet dynamics, where fidelity can

be defined in the usual sense, *i.e.* as the overlap between two forward evolutions. Yet, the relation between the scattering matrix and the scattering of wave packets is somewhat involved and not very practical, even if it is standard textbook knowledge (see [84]).

We shall therefore ask a question which looks more practical: Under what circumstances scattering fidelity will be equivalent to fidelity or maybe state averaged fidelity in the bound system used to describe the interaction region? For such a concept to be well defined we need a fairly weak coupling to the asymptotic channels. We shall analyze this question below, but it is important to note, that the interest of scattering fidelity is by no means limited to such a situation, because a perturbation of ideal couplings to the continuum is very relevant, and then no simple analogy to standard fidelity exists.

Scattering theory usually distinguishes between short time signals usually referred to as direct reactions and long time signals which are termed very fittingly *coda* in elasticity. It is the latter, that tends to be universal and associated to some form of equilibration in the system. It is thus for this part, that we expect a close analogy with standard fidelity decay. This is fortunate, because the theory of fidelity decay that is available is also restricted to this part. This becomes clear, in the formulation of correlations of the perturbation in the interaction picture. The particular shape of this decay is usually not considered, and will give very specific properties that may be strongly system dependent. It will also depend on the initial state even if we consider chaotic or mixing systems. On the other hand we expect the signal of scattering fidelity to become independent of the channels for the coda.

To investigate the analogy of scattering fidelity with standard fidelity we shall use the simplest and most common model for scattering with a resonant part, which we present in the following subsection exclusively for the discussion of this analogy [69,70].

The effective Hamiltonian approach

In the effective Hamiltonian approach to scattering [85,86], the S-matrix reads

$$S_{ab}(E) = \delta_{ab} - V^{(a)\dagger}\,\frac{1}{E - H_{\rm eff}}\,V^{(b)} \qquad H_{\rm eff} = H_0 - {\rm i}\Gamma/2 \qquad \Gamma = V\,V^\dagger + \gamma_W\;, \tag{55}$$

where $V^{(a)}$ is the column vector of V corresponding to the scattering channel a. For later use, we introduce the absorption width γ_W, which is simply a scalar in the present context. This is equivalent to model absorption with infinitely many very weakly coupled channels, whose partial widths add up to γ_W [87]. The Fourier transform of $S_{ab}(E)$ reads (for $t \neq 0$)

$$\hat{S}_{ab}(t) = \int {\rm d}E\;\, {\rm e}^{-2\pi{\rm i}\,Et}\;\, S_{ab}(E) = -2\pi{\rm i}\;\theta(t)\;V^{(a)\dagger}\;\, {\rm e}^{-2\pi{\rm i}\,H_{\rm eff}t}\;\, V^{(b)}\;. \tag{56}$$

Assume, H_0 and $H_0' = H_0 + \epsilon\,W$ are two slightly different Hamiltonians. According to Eq. (55) these define two effective Hamiltonians $H_{\rm eff}$ and $H'_{\rm eff}$, as well as two scattering matrices $S_{ab}(E)$ and $S'_{ab}(E)$. We consider the cross-correlation function

$$\hat{S}_{ab}(t)^*\,\hat{S}'_{ab}(t) = 4\pi^2\;\theta(t)\;V^{(b)\dagger}\;\, {\rm e}^{2\pi{\rm i}\,H^\dagger_{\rm eff}t}\;\, V^{(a)}\;V^{(a)\dagger}\;\, {\rm e}^{-2\pi{\rm i}\,H'_{\rm eff}t}\;\, V^{(b)}\;. \tag{57}$$

The singular value decomposition of V provides an orthogonal (unitary) transformation of the $S(E)$ and $S'(E)$ where the channel vectors are orthogonal to each other (Engelbrecht-Weidenmüller transformation [88]). Thus, we may restrict ourselves to the case of orthogonal channel vectors; this implies that all direct or fast processes will happen in the elastic channels. We then have

$$\hat{S}_{ab}(t)^*\,\hat{S}'_{ab}(t) = 4\pi^2\;w_a\,w_b\;\theta(t)\;\langle v_b|\;{\rm e}^{2\pi{\rm i}\,H^\dagger_{\rm eff}t}\;|v_a\rangle\;\langle v_a|\;{\rm e}^{-2\pi{\rm i}\,H'_{\rm eff}t}\;|v_b\rangle\;. \tag{58}$$

$V^{(a)} = \sqrt{w_a}\;|v_a\rangle$ with normalized vectors $|v_a\rangle$. The general idea of what follows is to assume the state vectors $|v_a\rangle$ and $|v_b\rangle$ to be random and independent. This equation looks very suggestive to obtain the desired relation with the standard fidelity for a random state $|v_b\rangle$

$$f(t) = \langle v_b|\;{\rm e}^{2\pi{\rm i}\,H_0\,t}\;\, {\rm e}^{-2\pi{\rm i}(H_0+\epsilon W)\,t}\;\, |v_b\rangle\;. \tag{59}$$

In the eigenbasis of H_0 we have

$$f(t) = \sum_j \langle |v_{jb}|^2\rangle\;\, {\rm e}^{2\pi{\rm i}\,E_j\,t}\;\, U_{jj}(t) = \frac{1}{N}\sum_j {\rm e}^{2\pi{\rm i}\,E_j\,t}\;\, U_{jj}(t) = \frac{1}{N}\sum_{jk} O^2_{jk}\;\, {\rm e}^{2\pi{\rm i}\,(E_j - E'_k)\,t}\;, \tag{60}$$

where

$$U_{jj}(t) = \sum_k \langle j|o_k\rangle \, \mathrm{e}^{-2\pi \mathrm{i}\, E'_k\, t} \, \langle o_k|j\rangle = \sum_k O_{jk}^2 \;\; \mathrm{e}^{-2\pi \mathrm{i}\, E'_k\, t} \;\; . \tag{61}$$

Comparing with Eq. (58) we see that the only remaining problem resides in the fact, that we have the effective Hamiltonian in the exponent, which includes the coupling term. This can be handled for weak and intermediate coupling. While the former will be presented in what follows, more involved cases of intermediate coupling are presented in appendix C, still leading to the same result.

We assume that all coupling parameters w_a go to zero. Then the anti-Hermitian part of $H_{\rm eff}$ becomes a scalar and we are essentially left with transition amplitudes of Hermitian Hamiltonians.

$$\begin{aligned} \hat{S}_{ab}(t)^* \, \hat{S}'_{ab}(t) &\sim 4\pi^2 \; w_a \, w_b \; \theta(t) \;\; \mathrm{e}^{-\gamma_W \, t} \;\; \langle v_b| \;\; \mathrm{e}^{2\pi \mathrm{i}\, H_0 \, t} \;\; |v_a\rangle \;\; \langle v_a| \;\; \mathrm{e}^{-2\pi \mathrm{i}\, (H_0 + \epsilon W)\, t} \;\; |v_b\rangle \\ &= 4\pi^2 \; w_a \, w_b \; \theta(t) \;\; \mathrm{e}^{-\gamma_W \, t} \;\; \sum_{j,klm} v^*_{jb} \;\; \mathrm{e}^{2\pi \mathrm{i}\, E_j \, t} \;\; v_{ja} \;\; v^*_{ka} \;\; \langle k|o_l\rangle \;\; \mathrm{e}^{-2\pi \mathrm{i}\, E'_l \, t} \;\; \langle o_l|m\rangle \;\; v_{mb} \; . \end{aligned} \tag{62}$$

For $a \neq b$, we find by averaging over the initial states:

$$\begin{aligned} \langle \hat{S}_{ab}(t)^* \, \hat{S}'_{ab}(t)\rangle &\sim 4\pi^2 \; w_a \, w_b \; \theta(t) \;\; \mathrm{e}^{-\gamma_W \, t} \;\; \sum_{j,l} \langle |v_{jb}|^2\rangle \;\; \langle |v_{ja}|^2\rangle \;\; \mathrm{e}^{2\pi \mathrm{i}\, E_j \, t} \;\; \langle j|o_l\rangle \;\; \mathrm{e}^{-2\pi \mathrm{i}\, E'_l \, t} \;\; \langle o_l|j\rangle \\ &= 4\pi^2 \; \frac{w_a \, w_b}{N} \; \theta(t) \;\; \mathrm{e}^{-\gamma_W \, t} \;\; \frac{1}{N} \sum_{jl} O_{jl}^2 \;\; \mathrm{e}^{2\pi \mathrm{i} (E_j - E'_l) t} = 4\pi^2 \; \frac{w_a \, w_b}{N} \; \theta(t) \;\; \mathrm{e}^{-\gamma_W \, t} \;\; f(t) \; . \end{aligned} \tag{63}$$

The prefactor, which decays exponentially in time, is exactly the normalization by the two autocorrelation functions, which we postulated at the beginning, as the two agree in this approximation up to the factor w_a or w_b, respectively.

An average over initial states will often be impractical. However, for chaotic (ergodic) systems it may not be necessary. We may use a spectral average and/or average over different samples, instead. Indeed the results obtained for stronger coupling in the appendix assume chaotic behavior of the long time dynamics in the interaction region more explicitly, and probably the relation to standard fidelity is of practical importance only in such a situation. Yet it must be emphasized, that scattering fidelity is a relevant concept in its own right, if we take into account the fundamental role played by the S-matrix in many approaches to quantum systems.

2.6.2. *Polarization echo*

In NMR experiments the quantity that can naturally be measured is the echo in the polarization of the local nuclear spin. One prepares the initial state $|\Psi_0\rangle$ of a many-spin system in an eigenstate of a projection of the spin (1/2) of a specific nucleus, say $s_0^{\rm z}$

$$s_0^{\rm z}|\Psi_0\rangle = m_0|\Psi_0\rangle, \tag{64}$$

where $m_0 = \pm 1/2$. Next one performs the echo experiment, *i.e.* we apply the echo operator and then measures local polarization of the same nucleus. It has the expectation value

$$m_\varepsilon(t) = \langle M_\varepsilon^\dagger(t) s_0^{\rm z} M_\varepsilon(t)\rangle. \tag{65}$$

The *polarization echo* $P_\varepsilon(t)$ is defined as the probability that the local polarization of the spin is restored after the echo dynamics

$$P_\varepsilon(t) = \frac{1}{2} + 2 m_0 m_\varepsilon(t) = \frac{1}{2} + 2\langle s_0^{\rm z} M_\varepsilon^\dagger(t) s_0^{\rm z} M_\varepsilon(t)\rangle \tag{66}$$

This quantity has been extensively measured in a series of NMR experiments performed by the group of Levstein and Pastawski [38,40]

One can try to generalize this quantity to an echo with respect to some arbitrary quantum observable A. Again, in order that the quantity makes sense as the echo of a observable A, the system has to be prepared in the initial state which is an eigenstate $|\Psi\rangle$, or eventually a statistical mixture ρ of eigenstates, of observable

A. Due to this properties, the averages have the property $\langle AB\rangle = \langle BA\rangle$ for any other observable B. Then we define the echo of an observable A as its correlation function with respect to echo-dynamics

$$P_\varepsilon^A(t) = \frac{\langle AM_\varepsilon^\dagger(t)AM_\varepsilon(t)\rangle}{\langle A^2\rangle}. \tag{67}$$

One can write a general linear response expression for this quantity. Inserting into the previous expression the echo operator to second order

$$M_\varepsilon(t) = \mathbf{1} - \mathrm{i}\frac{\varepsilon}{\hbar}\Sigma(t) - \frac{\varepsilon^2}{2\hbar^2}\hat{T}\Sigma^2(t) + O(\varepsilon^3) \tag{68}$$

and retaining terms to second order, we obtain a simple expression to order$O(\varepsilon^4)$

$$P_\varepsilon^A(t) = 1 - \frac{\varepsilon^2}{\hbar^2}\frac{\langle A^2\Sigma^2(t)\rangle - \langle A\Sigma(t)A\Sigma(t)\rangle}{\langle A^2\rangle}. \tag{69}$$

This can for example be used for the polarization echo.

2.6.3. *Composite systems, entanglement and purity*

In various studies of decoherence and effects of external degrees of freedom to the system's dynamics one studies composite systems. Coupling with the environment is usually unavoidable so that the evolution of our system is no longer Hamiltonian. To preserve the Hamiltonian formulation we have to include the environment in our description. We therefore have a "central system", denoted by a subscript "c", and an environment, denoted by subscript "e". The names *central system* and *environment* will be used just to denote two pieces of a composite system, without any connotation on their properties, dimensionality etc. The central system will be that part which is of actual interest. The Hilbert space is a tensor product $\mathcal{H} = \mathcal{H}_\mathrm{c}\otimes\mathcal{H}_\mathrm{e}$ and the evolution of a whole system is determined by a Hamiltonian or a unitary propagator on the whole Hilbert space $\mathcal{H}$ of dimension $\mathcal{N} = \mathcal{N}_\mathrm{c}\mathcal{N}_\mathrm{e}$. The unperturbed state $|\psi(t)\rangle$ and the perturbed one $|\psi_\varepsilon(t)\rangle$ are obtained with propagators $U(t)$ and $U_\varepsilon(t)$. Fidelity would in this case be the overlap of two wave functions on the *whole space* $\mathcal{H}$. But if we are not interested in the environment, this is clearly not the relevant quantity. Namely, the fidelity will be low even if the two wave functions are the same on the subspace of the central system and differ only on the environment.

We can define a quantity analogous to the fidelity, but which will measure the overlap just on the subspace of interest *i.e.* on the subspace of the central system. Let us define the reduced density matrix of the central subsystem

$$\rho_\mathrm{c}(t) := \mathrm{tr}_\mathrm{e}[\rho(t)], \qquad \rho_\mathrm{c}^\mathrm{M}(t) := \mathrm{tr}_\mathrm{e}[\rho^\mathrm{M}(t)], \tag{70}$$

where $\mathrm{tr}_\mathrm{e}[\bullet]$ denotes a trace over the environment and $\rho^\mathrm{M}(t) = M_\lambda(t)\rho(0)M_\lambda(t)^\dagger$ is the so-called echo density matrix. Throughout this chapter we will assume that the initial state is a pure product state *i.e.* a direct product,

$$|\psi(0)\rangle = |\psi_\mathrm{c}(0)\rangle\otimes|\psi_\mathrm{e}(0)\rangle =: |\psi_\mathrm{c}(0);\psi_\mathrm{e}(0)\rangle, \tag{71}$$

where we also introduced a short notation $|\psi_\mathrm{c};\psi_\mathrm{e}\rangle$ for pure product states. The resulting initial density matrix $\rho(0) = |\psi(0)\rangle\langle\psi(0)|$ is of course also pure. Fidelity can be written as $F(t) = \mathrm{tr}\,[\rho(0)\rho^\mathrm{M}(t)]$ and in a similar fashion we will define a *reduced fidelity* [50] denoted by $F_\mathrm{R}(t)$,

$$F_\mathrm{R}(t) := \mathrm{tr}_\mathrm{c}[\rho_\mathrm{c}(0)\rho_\mathrm{c}^\mathrm{M}(t)]. \tag{72}$$

The reduced fidelity measures the distance between the initial reduced density matrix and the reduced density matrix after the echo. Note that our definition of the reduced fidelity agrees with the information-theoretic fidelity [89,90,13] on a central subspace $\mathcal{H}_\mathrm{c}$ only if the initial state is a pure product state, so that $\rho_\mathrm{c}(0)$ is also a pure state.

One of the most distinctive features of quantum mechanics is entanglement. Due to the coupling between the central system and the environment the initial product state will evolve after an echo into the pure entangled state $M_\lambda(t)|\psi(0)\rangle$ and therefore the reduced density matrix $\rho_\mathrm{c}^\mathrm{M}(t)$ will be a mixed one. For a pure state $|\psi(t)\rangle$ there is a simple criterion for entanglement. It is quantified by *purity* $I(t)$, defined as

$$I(t) := \mathrm{tr}_\mathrm{c}[\rho_\mathrm{c}^2(t)], \qquad \rho_\mathrm{c}(t) := \mathrm{tr}_\mathrm{e}[|\psi(t)\rangle\langle\psi(t)|]. \tag{73}$$

Purity, or equivalently von Neumann entropy $\mathrm{tr}\,(\rho_\mathrm{c}\ln\rho_\mathrm{c})$, is a standard quantity used in decoherence studies [91]. If the purity is less than one, $I<1$, then the state $|\psi\rangle$ is entangled (between the environment and the central system), otherwise it is a product state. Similarly, one can define a purity after an echo, called *purity fidelity* in [49] by

$$F_\mathrm{P}(t) := \mathrm{tr}_\mathrm{c}[\{\rho_\mathrm{c}^\mathrm{M}(t)\}^2]. \tag{74}$$

We shall rename this quantity more appropriately *echo purity*. All three quantities, the fidelity $F(t)$, the reduced fidelity $F_\mathrm{R}(t)$ and the echo purity $F_\mathrm{P}(t)$ measure stability with respect to perturbations of the dynamics. If the perturbed evolution is the same as the unperturbed one, they are all equal to one, otherwise they are less than one. Fidelity $F(t)$ measures the stability of a whole state, the reduced fidelity gives the stability on the subspace $\mathcal{H}_\mathrm{c}$ and the purity fidelity measures separability of $\rho^\mathrm{M}(t)$. One expects that fidelity is the most restrictive quantity of the three - $\rho(0)$ and $\rho^\mathrm{M}(t)$ must be similar for $F(t)$ to be high. For $F_\mathrm{R}(t)$ to be high, only the reduced density matrices $\rho_\mathrm{c}(0)$ and $\rho_\mathrm{c}^\mathrm{M}(t)$ must be similar, and finally, the purity fidelity $F_\mathrm{P}(t)$ is high if only $\rho^\mathrm{M}(t)$ factorizes. Fidelity is the strongest criterion for stability.

2.6.4. *Inequality between fidelity, reduced fidelity and echo purity*

Actually, one can prove the following inequality for an arbitrary *pure* state $|\psi\rangle$ and an arbitrary *pure product* state $|\phi_\mathrm{c};\phi_\mathrm{e}\rangle$ [50,51],

$$|\langle\phi_\mathrm{c};\phi_\mathrm{e}|\psi\rangle|^4 \le |\langle\phi_\mathrm{c}|\rho_\mathrm{c}|\phi_\mathrm{c}\rangle|^2 \le \mathrm{tr}_\mathrm{c}[\rho_\mathrm{c}^2], \tag{75}$$

where $\rho_\mathrm{c} := \mathrm{tr}_\mathrm{e}[|\psi\rangle\langle\psi|]$.

Proof. Uhlmann's theorem [89], *i.e.* noncontractivity of the fidelity, states that tracing over an arbitrary subsystem can not decrease the fidelity,

$$\mathrm{tr}\,[|\phi_\mathrm{c};\phi_\mathrm{e}\rangle\langle\phi_\mathrm{c};\phi_\mathrm{e}||\psi\rangle\langle\psi|] \le \mathrm{tr}\,[|\phi_\mathrm{c}\rangle\langle\phi_\mathrm{c}|\rho_\mathrm{c}]. \tag{76}$$

Then, squaring and applying the Cauchy-Schwartz inequality $|\,\mathrm{tr}\,[A^\dagger B]|^2 \le \mathrm{tr}\,[AA^\dagger]\,\mathrm{tr}\,[BB^\dagger]$ we immediately obtain the wanted inequality (75).

The rightmost quantity in the inequality $I = \mathrm{tr}\,[\rho_\mathrm{c}^2]$ is nothing but the purity of state $|\psi\rangle$ and so does not depend on $|\phi_\mathrm{c};\phi_\mathrm{e}\rangle$. One can think of inequality (75) as giving us a *lower bound* on purity. An interesting question for instance is, which state $|\phi_\mathrm{c};\phi_\mathrm{e}\rangle$ optimizes this bound for a given $|\psi\rangle$, *i.e.* what is the maximal attainable overlap $|\langle\phi_\mathrm{c};\phi_\mathrm{e}|\psi\rangle|^4$ (fidelity) for a given purity. The rightmost inequality is optimized if we choose $|\phi_\mathrm{c}\rangle$ to be the eigenstate of the reduced density matrix ρ_c corresponding to its largest eigenvalue λ_1, $\rho_\mathrm{c}|\phi_\mathrm{c}\rangle = \lambda_1|\phi_\mathrm{c}\rangle$. To optimize the left part of the inequality, we have to choose $|\phi_\mathrm{e}\rangle$ to be the eigenstate of $\rho_\mathrm{e} := \mathrm{tr}_\mathrm{c}[\rho]$ corresponding to the same largest eigenvalue λ_1, $\rho_\mathrm{e}|\phi_\mathrm{e}\rangle = \lambda_1|\phi_\mathrm{e}\rangle$. The two reduced matrices ρ_e and ρ_c have the same eigenvalues [92], $\lambda_1 \ge \lambda_2 \ge \ldots \ge \lambda_{\mathcal{N}_\mathrm{c}}$. For such choice of $|\phi_\mathrm{c};\phi_\mathrm{e}\rangle$ the left inequality is actually an equality, $|\langle\phi_\mathrm{c};\phi_\mathrm{e}|\psi\rangle|^4 = |\langle\phi_\mathrm{c}|\rho_\mathrm{c}|\phi_\mathrm{c}\rangle|^2 = \lambda_1^2$ and the right inequality is

$$\lambda_1^2 \le \mathrm{tr}\,[\rho_\mathrm{c}^2] = \sum_{j=1}^{\mathcal{N}_\mathrm{c}} \lambda_j^2, \tag{77}$$

with equality iff $\lambda_1 = 1$. If the largest eigenvalue is close to one, $\lambda_1 = 1-\varepsilon$, the purity will be $I = (1-\varepsilon)^2 + \mathcal{O}(\varepsilon^2) \sim 1-2\varepsilon$ and the difference between the purity and the overlap will be of the *second order* in ε, $I - |\langle\phi_\mathrm{c};\phi_\mathrm{e}|\psi\rangle|^4 \sim \varepsilon^2$. Therefore, for high purity the optimal choice of $|\phi_\mathrm{c};\psi_\mathrm{s}\rangle$ gives a sharp lower bound, *i.e.* its deviation from I is of second order in the deviation of I from unity.

For our purpose of studying stability to perturbations, a special case of the general inequality (75) is especially interesting. Namely, taking for $|\psi\rangle$ the state after the echo evolution $M_\lambda(t)|\psi(0)\rangle$ and for a product state $|\phi_\mathrm{c};\phi_\mathrm{e}\rangle$ the initial state $|\psi(0)\rangle$ (71), we obtain

$$F^2(t) \le F_\mathrm{R}^2(t) \le F_\mathrm{P}(t). \tag{78}$$

As a consequence of this inequality we find: If fidelity is high, reduced fidelity and the echo purity are also high. In the case of perturbations with zero time average, the fidelity freezes and from the inequality we can conclude that the reduced fidelity and the echo purity will display a similar behavior.

2.6.5. *Uncoupled Unperturbed Dynamics*

A special, but very important, case arrises if the unperturbed dynamics U_0 represents two uncoupled systems, so we have

$$U_0 = U_\mathrm{c} \otimes U_\mathrm{e}. \tag{79}$$

This is a frequent situation if the coupling with the environment is "unwanted", so that our ideal evolution U_0 is uncoupled. Under these circumstances the reduced fidelity $F_\mathrm{R}(t)$ and the echo purity $F_\mathrm{P}(t)$ have especially nice forms.

The reduced fidelity (72) can be rewritten as

$$F_\mathrm{R}(t) = \mathrm{tr}_\mathrm{c}[\rho_\mathrm{c}(0)\rho_\mathrm{c}^\mathrm{M}(t)] = \mathrm{tr}_\mathrm{c}[\rho_\mathrm{c}(t)\rho_\mathrm{c}^\varepsilon(t)], \tag{80}$$

where $\rho_\mathrm{c}(t)$ is the unperturbed state of the central system and $\rho_\mathrm{c}^\varepsilon(t) := \mathrm{tr}_\mathrm{e}[U_\varepsilon(t)\rho(0)U_\varepsilon^\dagger(t)]$ the corresponding state obtained by perturbed evolution. Whereas for a general unperturbed evolution the reduced fidelity was an overlap of the initial state with an echo state, for a factorized unperturbed evolution it can also be interpreted as the overlap of the (reduced) unperturbed state at time t with a perturbed state at time t, similarly as for fidelity.

Echo purity can also be simplified for uncoupled unperturbed evolution. As U_0 it factorizes we can bring it out of the innermost trace in the definition of echo purity and use the cyclic property of the trace, finally arriving at

$$F_\mathrm{P}(t) = \mathrm{tr}_\mathrm{c}[\{\rho_\mathrm{c}^\mathrm{M}(t)\}^2] = \mathrm{tr}_\mathrm{c}[\{\rho_\mathrm{c}^\varepsilon(t)\}^2] = I(t). \tag{81}$$

Echo purity is therefore equal to the purity of the forward evolution. The general inequality gives in this case

$$F^2(t) \leq F_\mathrm{R}^2(t) \leq I(t), \tag{82}$$

and so the fidelity and the reduced fidelity give a lower bound on the decay of purity. Because the purity is frequently used in studies of decoherence this connection is especially appealing.

In most of our theoretical derivations regarding the purity fidelity we will assume a general unperturbed evolution, but one should keep in mind that the results immediately carry over to purity in the case of uncoupled unperturbed dynamics. Also a large part of our numerical demonstration in next two sections will be done on systems with an uncoupled unperturbed dynamics as this is usually the more interesting case.

2.6.6. *Linear Response Expansion*

We proceed with the linear response expansion of reduced fidelity (72) and echo purity (74). We use the notation $\rho_\mathrm{c} := |\psi_\mathrm{c}(0)\rangle\langle\psi_\mathrm{c}(0)|$ for a pure initial density matrix for the central system and $\rho_\mathrm{e} := |\psi_\mathrm{e}(0)\rangle\langle\psi_\mathrm{e}(0)|$ for the environment. For explicit calculations it is convenient to use an orthogonal basis $|j;\nu\rangle$, $j = 1,\ldots,\mathcal{N}_\mathrm{c}$, $\nu = 1,\ldots,\mathcal{N}_\mathrm{e}$, with the convention that the first basis state $|1;1\rangle := |\psi_\mathrm{c};\psi_\mathrm{e}\rangle$ is the initial state. Then, inserting the second order approximation to the echo operator (68) into the definitions, and keeping only quantities to second order in ε, we have up to $\mathcal{O}(\varepsilon^4)$ (since third orders exactly vanish)

$$\begin{aligned}
1 - F(t) &= \left(\frac{\varepsilon}{\hbar}\right)^2 \left\{\langle 1;1|\Sigma^2(t)|1;1\rangle - \langle 1;1|\Sigma(t)|1;1\rangle^2\right\} \\
1 - F_\mathrm{R}(t) &= \left(\frac{\varepsilon}{\hbar}\right)^2 \left\{\langle 1;1|\Sigma^2(t)|1;1\rangle - \sum_{\nu=1}^{\mathcal{N}_\mathrm{e}} |\langle 1;\nu|\Sigma(t)|1;1\rangle|^2\right\} \\
1 - F_\mathrm{P}(t) &= 2\left(\frac{\varepsilon}{\hbar}\right)^2 \left\{\langle 1;1|\Sigma^2(t)|1;1\rangle - \sum_{\nu=1}^{\mathcal{N}_\mathrm{e}} |\langle 1;\nu|\Sigma(t)|1;1\rangle|^2 - \sum_{j=2}^{\mathcal{N}_\mathrm{c}} |\langle j;1|\Sigma(t)|1;1\rangle|^2\right\}.
\end{aligned} \tag{83}$$

Writing the expectation value in the initial product state as usual, $\langle\bullet\rangle = \mathrm{tr}\,[(\rho_\mathrm{c}\otimes\rho_\mathrm{e})\bullet]$, we can rewrite the linear response result in basis free form

$$1 - F(t) = \left(\frac{\varepsilon}{\hbar}\right)^2 \langle \Sigma(t)(\mathbb{1}\otimes\mathbb{1} - \rho_{\rm c}\otimes\rho_{\rm e})\Sigma(t)\rangle$$
$$1 - F_{\rm R}(t) = \left(\frac{\varepsilon}{\hbar}\right)^2 \langle \Sigma(t)(\mathbb{1} - \rho_{\rm c})\otimes\mathbb{1}\Sigma(t)\rangle$$
$$1 - F_{\rm P}(t) = 2\left(\frac{\varepsilon}{\hbar}\right)^2 \langle \Sigma(t)(\mathbb{1} - \rho_{\rm c})\otimes(\mathbb{1} - \rho_{\rm e})\Sigma(t)\rangle. \quad (84)$$

The linear response expansion of course also satisfies the general inequality (78). The difference between $F_{\rm R}(t)$ and $F(t)$ as well as between $F_{\rm P}(t)$ and $F(t)$ results from *off-diagonal* matrix elements of operator $\Sigma(t)$. One may compare these results to time-independent perturbative expansions valid up to quantum Zeno time $t_{\rm Z}$ [93,94]. Depending on the growth of the linear response terms with time we will again have two general categories, that of mixing dynamics and that of regular dynamics.

In the general linear response expressions above we have not assumed anything on the particular form of perturbation V and unperturbed system H_0. It may be however, interesting to study separately the special case where the unperturbed system in uncoupled and the perturbation is the coupling. This we shall do for different situations in later sections.

3. Quantum echo-dynamics: Non-integrable (chaotic) case

3.1. *Fidelity and dynamical correlations*

In the previous section we have elaborated in detail on different general properties of echo dynamics. At this point we specialize our interest to the case of systems which produce maximal possible dynamical disorder. For systems which possess a well defined classical limit this means that the latter should be non-integrable and fully chaotic. For other systems, we assume that the system's stationary properties are well described by Gaussian or circular ensembles of random matrices and hence fall into the general category of quantum chaos. Yet, we postpone the discussion of the random matrix formulation of echo dynamics to the next section and here concentrate on individual physical dynamical systems which possess the property of dynamical mixing, either in the semiclassical or the thermodynamic limit. Again, we use the Born expansion (11) and express fidelity in terms of dynamical correlations.

At first we assume that a well defined classical limit exists and that the classical system has the strong ergodic property of *mixing* such that the correlation function of the perturbation V decays sufficiently fast; this typically (but not necessarily) corresponds to globally chaotic classical motion. However, reference to underlying classical dynamics is not strictly necessary as the corresponding quantum mixing can sometimes be established in thermodynamic limit without taking the classical limit. For the application of echo-dynamics in such a situation see Refs. [42,49].

Due to ergodicity and mixing we can assume that averages of any dynamical observables over a specific initial state can be replaced by a full Hilbert space average, $\langle\langle\bullet\rangle\rangle = {\rm tr}\,(\bullet)/N$, at least after times longer than a certain relaxation time-scale $t_{\rm E}$

$$\langle\Psi_0(t)|A|\Psi_0(t)\rangle \approx \langle\langle A\rangle\rangle, \quad \text{for} \quad |t| \geq t_{\rm E}. \quad (85)$$

For minimal-uncertainty wave packet initial state with typical phase space diameter $\sqrt{\hbar}$ and exponentially unstable classical dynamics with characteristic exponent λ, the time scale $t_{\rm E}$ can be estimated as $t_{\rm E} \sim \log(1/\hbar)/\lambda$ and is sometimes known as the *Ehrenfest time*. This is the time needed for an initially localized wavepacket to spread effectively over the accessible phase space [95]. For other types of initial states this time is in general even shorter. For example, for a *random* initial state, Eq. (85) is satisfied for *any* t, by definition of a random state (45).

Therefore, for any initial state (e.g. in the worst case for a minimal-uncertainty wave packet) one obtains identical results for $F(t)$ for sufficiently long times [4], *i.e.* longer than $t_{\rm E}$. The state averaged quantum

[4] The exception might be systems with non-ergodic quantum behavior, for example exhibiting dynamical localization.

correlation function is homogeneous in time, *i.e.* $C(t,t') = C(t-t')$, so we simplify the second order linear response formula (13) for fidelity

$$F(t) = 1 - \frac{\varepsilon^2}{\hbar^2}\left\{tC(0) + 2\int_0^t \mathrm{d}t'(t-t')C(t')\right\} + O(\varepsilon^4). \tag{86}$$

If the decay of the correlation function $C(t)$ is sufficiently fast, namely if its integral converges on a certain characteristic *mixing time* scale $t_{\rm mix}$, meaning that $C(t)$ should in general decay faster than $O(t^{-2})$, then the above formula can be further simplified. For times $t \gg t_{\rm mix}$ we can neglect the second term under the summation in (86) and obtain a linear fidelity decay in time t (in the linear response)

$$F(t) = 1 - 2(\varepsilon/\hbar)^2\sigma t, \tag{87}$$

with the transport coefficient σ being

$$\sigma = \int_0^\infty \mathrm{d}t C(t) = \lim_{t\to\infty} \frac{\langle\Sigma^2(t)\rangle - \langle\Sigma(t)\rangle^2}{2t}. \tag{88}$$

Note that σ has a well defined classical limit obtained from the classical correlation function and in the semiclassical limit this classical $\sigma_{\rm cl}$ will agree with the quantum one.

We can make a stronger statement in a non-linear-response regime if we make an additional assumption on the factorization of higher order time-correlations, namely assuming $n-$point mixing [96]. This implies that $2m$-point correlation $\langle V(t_1)\cdots V(t_{2m})\rangle$ is appreciably different from zero for $t_{2m} - t_1 \to \infty$ only if all (ordered) time indices $\{t_k, k = 1\ldots 2m\}$ are *paired* with the time differences within each pair, $t_{2k} - t_{2k-1}$, being of the order or less than $t_{\rm mix}$. Then we can make a further reduction, namely if $t \gg mt_{\rm mix}$ the terms in the expansion of the fidelity amplitude $f(t)$ (7,11) are

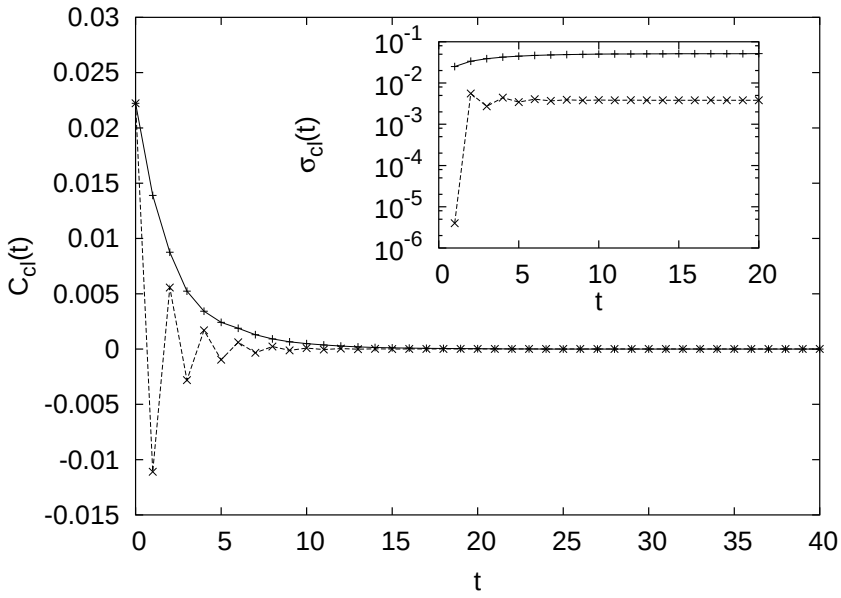

Fig. 1. The classical correlation function of perturbation V (91) for chaotic kicked top and $\gamma = \pi/6$ (top solid curve) and $\gamma = \pi/2$ (bottom broken curve). The finite time integrated correlation function is shown in the inset.

$$\hat{T}\int_0^t \mathrm{d}t_1\mathrm{d}t_2\cdots\mathrm{d}t_{2m}\langle V(t_1)V(t_2)\cdots V(t_{2m})\rangle \to$$
$$\to \hat{T}\int_0^t \mathrm{d}t_1\mathrm{d}t_2\cdots\mathrm{d}t_{2m}\langle V(t_1)V(t_2)\rangle\cdots\langle V(t_{2m-1})V(t_{2m})\rangle \to \frac{(2m)!}{m!2^m}(2\sigma t)^m. \tag{89}$$

The fidelity amplitude is therefore $f(t) = \exp(-\varepsilon^2\sigma t/\hbar^2)$ and the fidelity is

$$F(t) = \exp(-t/\tau_{\rm m}), \qquad \tau_{\rm m} = \frac{\hbar^2}{2\varepsilon^2\sigma_{\rm cl}}, \tag{90}$$

where $\tau_{\rm m} = O(\varepsilon^{-2})$ is the time scale for decay and the subscript "m" stands for mixing dynamics. If the system has a classical limit, one may take also a classical limit of the transport coefficient $\sigma_{\rm cl}$, so the decay time-scale $\tau_{\rm m}$ can be computed from classical mechanics. We should stress again that the above result (90) has been derived under the assumption of true quantum mixing which can be justified only in the limit $N \to \infty$, e.g. either in the semiclassical or the thermodynamic limit. Thus for the true quantum-mixing dynamics the fidelity will decay exponentially.

The same result can also be derived using the standard Fermi golden rule interpreting fidelity as the transition probability and estimating the square of perturbation matrix elements in terms of classical correlation functions [44,45]. This regime of exponential fidelity decay is often refereed to as a *Fermi golden rule regime*. It is consistent with the effective treatment of fidelity as a Fourier transform of the local density of states of the eigenstates of H_ε expressed in the eigenbasis of H_0, or vice versa. Within the standard random matrix assumptions corresponding to classical chaos, the local density of states has a Lorentzian form and this corresponds to an exponential decay (90).

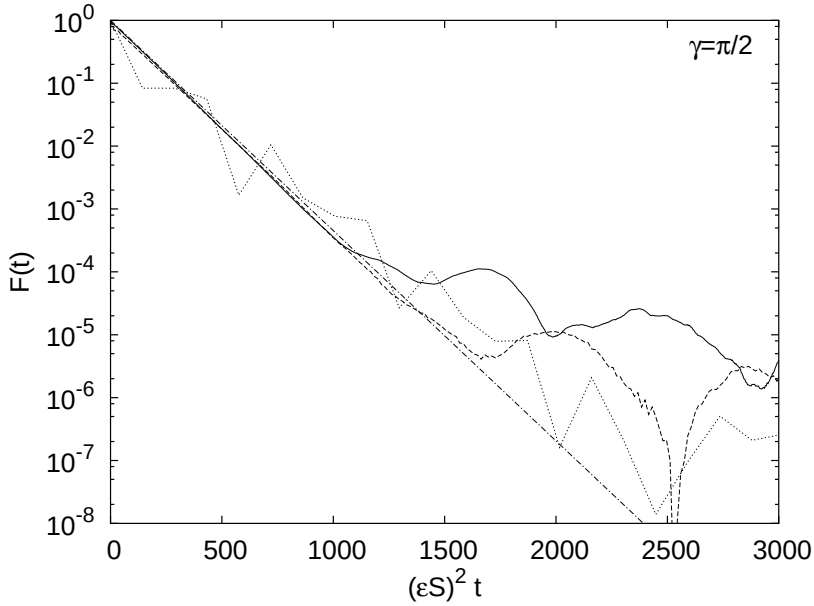

Fig. 2. Quantum fidelity decay in the chaotic regime for $\gamma = \pi/2$ and three different perturbation strengths $\varepsilon = 5 \times 10^{-4}$, 1×10^{-3} and 3×10^{-3} (solid, dashed and dotted curves, respectively) is shown. The chain line gives theoretical decay (90) with the classically calculated σ seen in Fig. 1.

To numerically check the above exponential decay, we will use the kicked top (B.1) with parameter $\alpha = 30$, giving totally chaotic classical dynamics. As argued before, one can calculate the transport coefficient σ (88) by using the classical correlation function of the perturbation (B.3),

$$V_{\rm cl} = v = \frac{1}{2}z^2. \tag{91}$$

We consider two different values of kicked top parameter γ, namely $\gamma = \pi/2$ and $\gamma = \pi/6$. The classical correlation functions is shown in Fig. 1. The correlation function (obtained by averaging over 10^5 initial conditions on a sphere) is shown in the main frame. The correlation functions have qualitatively different decay towards zero for the two chosen γ's. In the inset the convergence of the classical σ (88) is shown. One can see that the mixing time is $t_{\rm mix} \approx 5$. The values of $\sigma_{\rm cl}$ are $\sigma_{\rm cl} = 0.00385$ for $\gamma = \pi/2$ and $\sigma_{\rm cl} = 0.0515$ for $\gamma = \pi/6$. These values are used to calculate the theoretical decay of fidelity $F(t) = \exp(-\varepsilon^2 S^2 2\sigma_{\rm cl} t)$

according to Eq. (90) which is compared with numerical simulations in the Figs. 2 and 3. We used averaging over the whole Hilbert space, and checked that due to ergodicity there was no difference for large S if we choose a fixed initial state, say a coherent state. As fidelity will decay only until it reaches its finite size fluctuating value $\bar{F}$ (A.3) we choose a large $S = 4000$ in order to be able to check the exponential decay over as many orders of magnitude as possible. In Fig. 2 the decay of quantum fidelity is shown for $\gamma = \pi/2$. The agreement with theory is excellent. Note that the largest ε shown corresponds to $\tau_{\rm m} \approx 1$ so that the condition for $n-$point mixing $t \gg t_{\rm mix}$ is no longer strictly satisfied, hence we observe some oscillations around the theoretical curve. However, overall agreement with the theory is still good due to the oscillatory nature of the correlation decay (see Fig. 1) fulfilling the factorization assumption (89) on average.

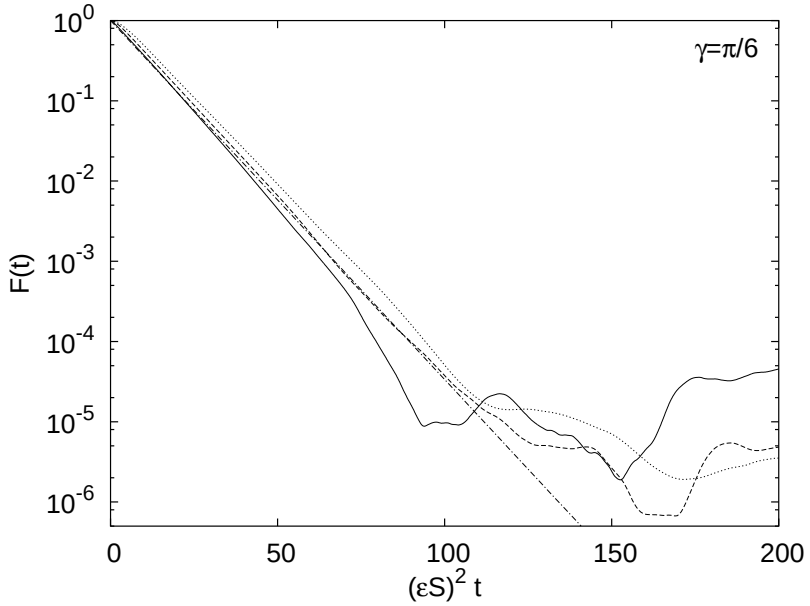

Fig. 3. Similar figure as 2, only for $\gamma = \pi/6$ and perturbation strengths $\varepsilon = 1 \times 10^{-4}$, 2×10^{-4} and 3×10^{-4} (solid, dashed and dotted curves, respectively).

In Fig. 3 for $\gamma = \pi/6$ a similar decay can be seen. In both cases fidelity starts to fluctuate around $\bar{F}$ calculated in the Section 2.3.1 for sufficiently long times t_∞ (see appendix A).

3.1.1. *Long time behavior*

So far, we have assumed that the quantum correlation function $C(t)$ decays to zero and its integral (or sum, for discrete-time dynamical systems) converges to σ. However, for a system with a Hilbert space of finite dimension N, the correlation function asymptotically does not decay but has a non-vanishing plateau $\bar{C}$, similar to the finite asymptotic value of fidelity $\bar{F}$. This will cause the double correlation integral to grow, asymptotically, quadratically with time. Because this plateau $\bar{C}$ is small, the quadratic growth will overtake linear growth $2\sigma_{\rm cl}t$ only for large times. The time averaged correlation function $C(t,t')$ (14) can be calculated assuming a nondegenerate unperturbed spectrum E_k as

$$\bar{C} = \lim_{t\to\infty} \frac{1}{t^2} \int_0^t {\rm d}t' \int_0^t {\rm d}t'' C(t',t'') = \sum_k \rho_{kk} (V_{kk})^2 - \left(\sum_k \rho_{kk} V_{kk} \right)^2 , \tag{92}$$

where ρ_{kk} are diagonal matrix elements of the initial density matrix $\rho(0)$ and V_{kk} are diagonal matrix elements of the perturbation V in the eigenbasis of the unperturbed propagator U_0. One can see that $\bar{C}$ depends only on the diagonal matrix elements, in fact it is equal to the variance of the diagonal matrix elements. Since the classical system is ergodic and mixing, we will use a version of the *quantum chaos conjecture* [97–101] saying that V_{mn} are independent Gaussian random variables with a variance given by

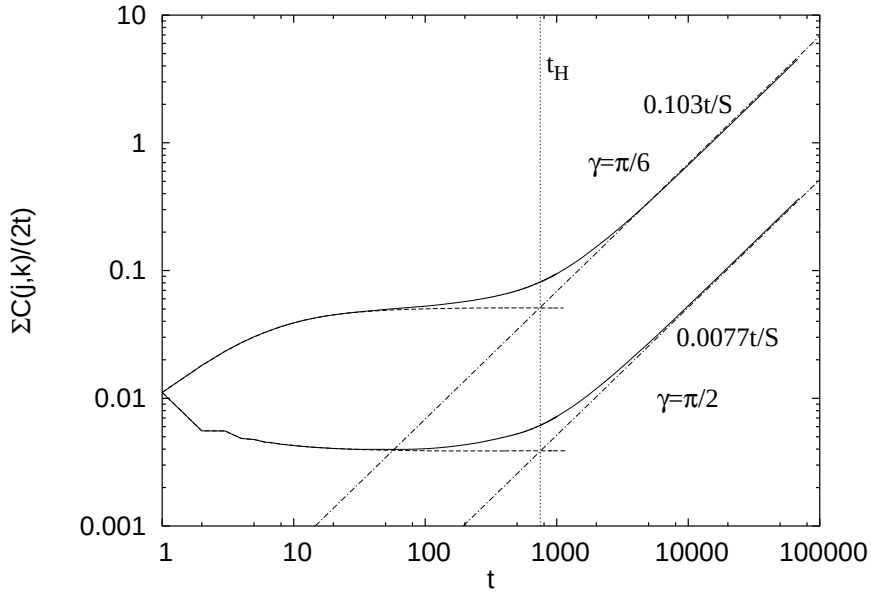

Fig. 4. The finite time quantum correlation sum $\sigma(t) = \sum_{j,k=0}^{t-1} C(j,k)/2t$ (solid curves) together with the corresponding classical sum $\sigma_{\rm cl}(t) = \sum_{j,k=0}^{t-1} C_{\rm cl}(j,k)/2t$ (dashed curves saturating at $\sigma_{\rm cl}$ and ending at $t \sim 1000$) is shown for the chaotic kicked top. Quantum data are for a full trace $\rho = \mathbb{1}/N$ with $S = 1500$. Upper curves are for $\gamma = \pi/6$ while lower curves are for $\gamma = \pi/2$. Chain lines are best fits for asymptotic linear functions corresponding to $\bar{C}t/2 = 0.0077t/S$ for $\gamma = \pi/2$ and $0.103t/S$ for $\gamma = \pi/6$.

the Fourier transformation $S(\omega)$ (divided by N) of the corresponding classical correlation function $C_{\rm cl}(t)$ at frequency $\omega = (E_m - E_n)/\hbar$. On the diagonal we have $\omega = 0$ and an additional factor of 2 due to the random matrix measure of the diagonal elements. Using $2\sigma_{\rm cl}t = \int_0^t {\rm d}t' \int_0^t {\rm d}t'' C(t',t'') = S(0)t$ we can write

$$\bar{C} = \frac{2S(0)}{N} = \frac{4\sigma_{\rm cl}}{N}. \tag{93}$$

Because of ergodicity, for large N, $\bar{C}$ does not depend on the statistical operator ρ used in the definition of the correlation function, provided we do not take some non generic state like a single eigenstate $|E_k\rangle$ for instance. If U_0 has symmetries, so that its Hilbert space is split into s components of sizes N_j, the average $\bar{C}$ will be different on different subspaces, $\bar{C}_j = 4\sigma_{\rm cl}/N_j$. Averaging over all invariant subspaces then gives

$$\bar{C} = \frac{4s\sigma_{\rm cl}}{N}, \tag{94}$$

so that $\bar{C}$ is increased by a factor s compared to the situation with only a single desymmetrized subspace. The fidelity decay will start to be dominated by the average plateau (93) at time $t_{\rm H}$ when the quadratic growth takes over, $\bar{C}t_{\rm H}^2 \approx 2\sigma_{\rm cl}t_{\rm H}$,

$$t_{\rm H} = \frac{1}{2}N \propto \hbar^{-d}, \tag{95}$$

which is nothing but the (dimensionless) *Heisenberg time* associated with the inverse (quasi)energy density. Note that for autonomous systems where energy is a conserved quantity, Heisenberg time scales differently $t_{\rm H} \propto \hbar^{1-d}$. Again, if one has s invariant subspaces, the Heisenberg time is reduced $t_{\rm H} = N/(2s)$.

In Fig. 4 we show numerical calculation of the correlation integral (sum) for the chaotic kicked top at $\alpha = 30$. We compare the classical correlation sum (the same data as in Fig. 1) and quantum correlation sum. One can nicely see the crossover from linear growth of quantum correlation sum $2\sigma_{\rm cl}t$ for small times $t < t_{\rm H}$, to the asymptotic quadratic growth due to correlation plateau $\bar{C}$. In addition, numerically fitted asymptotic growth $0.103t/S$ and $0.0077t/S$ nicely agree with formula for $\bar{C}$, using $N = S$ and classical values of transport coefficients $\sigma_{\rm cl} = 0.0515$ and 0.00385 for $\gamma = \pi/6$ and $\gamma = \pi/2$, respectively.

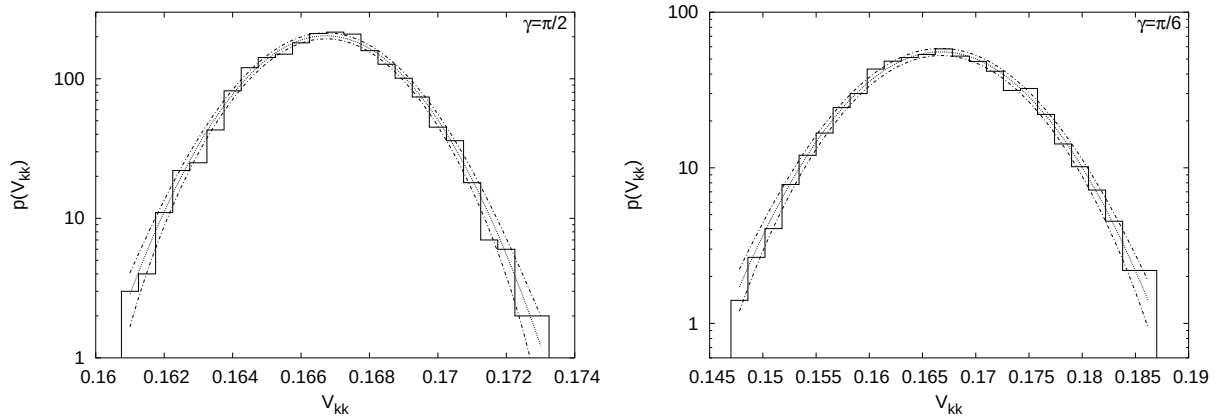

Fig. 5. Histogram of the normalized distribution of the diagonal matrix elements V_{kk} for the chaotic kicked top and $S = 4000$ on OE subspace (B.4). The dotted line is the theoretical Gaussian distribution with the second moment $\bar{C}$ and the two chain lines are expected $\sqrt{N_i}$ statistical deviations if there are N_i elements in the $i-$th bin. Note the different x-ranges in two figures due to different $\sigma_{\rm cl}$ for the two chosen γ.

For times $t > t_{\rm H}$, and provided ε is sufficiently small, the correlation sum will grow quadratically and the linear response fidelity reads

$$F(t) = 1 - \frac{\varepsilon^2}{\hbar^2}\frac{4\sigma_{\rm cl}}{N}t^2. \tag{96}$$

To derive the decay of fidelity beyond the linear response regime one needs higher order moments of diagonal elements of perturbation V. If we use the leading order BCH expression of the echo operator (24), neglecting the term $\Gamma(t)\varepsilon^2$, we have the fidelity amplitude $f(t) = \sum_k \exp\left(-{\rm i}V_{kk}\varepsilon t/\hbar\right)/N$, where we choose an ergodic average $\rho = \mathbb{1}/N$. In the limit $N \to \infty$ we can replace the sum with an integral over the probability distribution of diagonal matrix elements $p(V_{kk}) = p(V)$,

$$f(t) = \int {\rm d}V\, p(V) \exp\left(-{\rm i}V\varepsilon t/\hbar\right). \tag{97}$$

For long times the fidelity amplitude is therefore a Fourier transformation of the distribution of diagonal matrix elements. For classically mixing systems the distribution is conjectured to be Gaussian with the second moment equal to $\bar{C}$ (93). This is confirmed by numerical data in Fig. 5. The mean value of diagonal matrix elements is perturbation specific and is for our choice of the perturbation (B.3) equal to $\sum_k V_{kk}/(2S+1) = (2S+1)(S+1)/12S^2$. From the figure we can see that the distribution is indeed Gaussian with the variance agreeing with the theoretically predicted $\bar{C} = 4\sigma_{\rm cl}/S$. The Fourier transformation of a Gaussian is readily calculated and we get a Gaussian fidelity decay

$$F(t) = \exp\left(-(t/\tau_{\rm p})^2\right), \qquad \tau_{\rm p} = \sqrt{\frac{N}{4\sigma_{\rm cl}}}\frac{\hbar}{\varepsilon}. \tag{98}$$

In order to see a Gaussian fidelity decay for mixing systems the perturbation strength ε must be sufficiently small. Otherwise, the fidelity will decay exponentially (90) to its fluctuating plateau $\bar{F}$ before time $t_{\rm H}$ when the Gaussian decay starts. Requiring that the time-scale of exponential decay $\tau_{\rm m}$ is smaller than $t_{\rm H} = N/2$ gives the critical perturbation strength $\varepsilon_{\rm p}$,

$$\varepsilon_{\rm p} = \frac{\hbar}{\sqrt{\sigma_{\rm cl} N}}. \tag{99}$$

For $\varepsilon < \varepsilon_{\rm p}$ we will have a Gaussian decay (98), otherwise the decay starts as an exponential (90) and goes over to a Gaussian at the Heisenberg time $t_{\rm H}$ (see Section 4 for a uniform theory within a random matrix model). If the decay reaches the plateau $\overline{F}$ before or around $t_{\rm H}$, the decay remains purely exponential (for details see Section 7). Again we illustrate the predicted Gaussian decay for the chaotic kicked top with $\alpha = 30$ and $S = 1500$ and a full trace average over the Hilbert space. The results of numerical simulation, together with the theory are shown in Fig. 6.

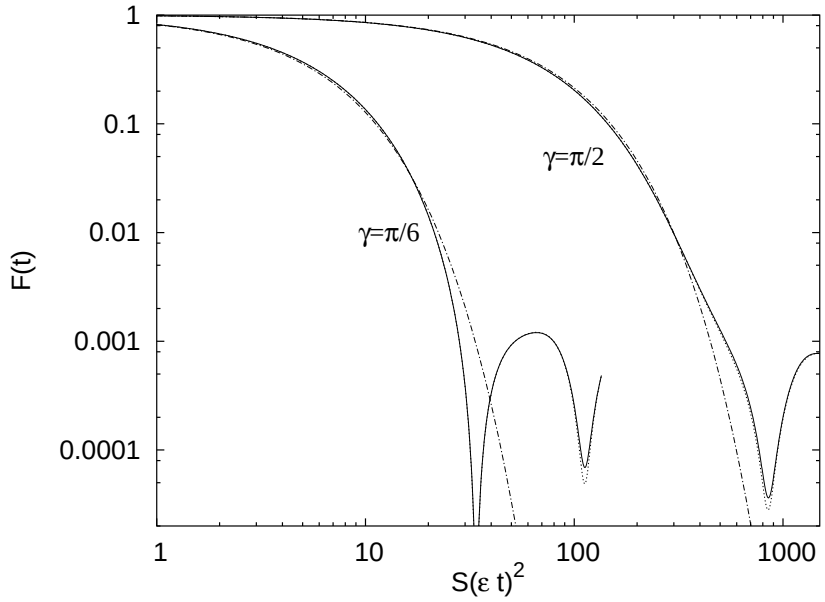

Fig. 6. Quantum fidelity decay for $\varepsilon < \varepsilon_{\rm p}$ in the chaotic regime. For $\gamma = \pi/2$ data for $\varepsilon = 1 \cdot 10^{-6}$ (solid curve) and $5 \cdot 10^{-6}$ (dotted curve) are shown. For $\gamma = \pi/6$, $\varepsilon = 3 \cdot 10^{-7}$ (solid) and $1 \cdot 10^{-6}$ (dotted) are shown. Note that for both γ the curves for both ε practically overlap. The chain curves are theoretical predictions (98) with classically computed $\sigma_{\rm cl}$.

The regime of Gaussian decay is sometimes referred to as the perturbative regime [45,44] because it can be derived using perturbation theory in lowest order. Writing the eigenenergies in first order $E_k^\varepsilon = E_k + V_{kk}\,\varepsilon$ and the overlap matrix in zeroth order $O_{kl} = \delta_{kl} + O(\varepsilon)$ (40), one arrives at the Fourier transform formula (97).

3.2. *Vanishing time averaged perturbation and fidelity freeze*

Here we shall assume that the perturbation is of particular form, namely it can be written as a time derivative of some observable W (29). We will show that a simple semi-classical theory can be developed which describes anomalously slow fidelity decay (fidelity freeze) in such a case. Other types of perturbations with vanishing time-average will be considered within the random matrix framework in Section 4.3.

The presentation here follows Ref. [17]. Based on the general discussion of Section 2.2, we write a semi-classical expression for the fidelity below the time scale $t_2 = O(\varepsilon^{-1})$, which shall be specified later, and above the Ehrenfest time-scale $t_{\rm E}$, $t_{\rm E} < t < t_2$, as

$$F(t) \approx F_{\rm plat} = \left| \langle \exp\left(-\frac{{\rm i}\varepsilon}{\hbar} w\right) \rangle_{\rm cl} \langle \exp\left(\frac{{\rm i}\varepsilon}{\hbar} W\right) \rangle \right|^2 \tag{100}$$

This equation is derived from the general Eq. (35) in three steps: (i) the higher order middle factor in Eq. (35) can be neglected for for $t < t_2$, (ii) we assume that due to *mixing dynamics*, the correlation function of $\exp(-{\rm i}W(t)\varepsilon/\hbar)$ can be factorized for $t > t_{\rm mix}$ as

$$\langle \exp(-{\rm i}W(t)\varepsilon/\hbar) \exp({\rm i}W(0)\varepsilon/\hbar) \rangle \approx \langle \exp(-{\rm i}W(t)\varepsilon/\hbar) \rangle \langle \exp({\rm i}W(0)\varepsilon/\hbar) \rangle,$$

and (iii) for $t > t_{\rm E}$ the average $\langle W(t) \rangle = \langle\!\langle W \rangle\!\rangle$ is approximated by the classical average

$$\langle w \rangle_{\rm cl} = \frac{\int_\Omega {\rm d}\mu x w(\boldsymbol{x})}{\int_\Omega {\rm d}\mu x} \tag{101}$$

where $w(\boldsymbol{x})$ is the classical observable corresponding to the operator W and Ω is the classical invariant ergodic component related to the initial state Ψ, e.g. the energy surface for $E = \langle \Psi | H_0 | \Psi \rangle$.

The plateau of fidelity can be written in a compact form for the two simplest extreme cases of initial states: (a) for a *coherent initial state* (CIS), where the initial state average can be approximated by the classical observable evaluated at the center $\boldsymbol{x}^*$ of the wave packet $\langle W\rangle \approx w(\boldsymbol{x}^*)$, hence $|\langle\exp(-\mathrm{i}W\varepsilon/\hbar)\rangle| \approx 1$, and (b) for a *random initial state* (RIS), where the initial state average is equivalent to an ergodic average, $\langle\exp(-\mathrm{i}W\varepsilon/\hbar)\rangle = \langle\!\langle\exp(-\mathrm{i}W\varepsilon/\hbar)\rangle\!\rangle \approx \langle\exp(-\mathrm{i}w\varepsilon/\hbar)\rangle_{\mathrm{cl}}$. Defining a classical generating function as

$$G(z) = \langle\exp(-\mathrm{i}zw)\rangle_{\mathrm{cl}} \tag{102}$$

one can compactly write

$$F_{\mathrm{plat}}^{\mathrm{CIS}} \approx |G(\varepsilon/\hbar)|^2\,, \qquad F_{\mathrm{plat}}^{\mathrm{RIS}} \approx |G(\varepsilon/\hbar)|^4\,. \tag{103}$$

Note that the two plateau levels satisfying *universal* relation $F_{\mathrm{plat}}^{\mathrm{RIS}} \approx (F_{\mathrm{plat}}^{\mathrm{CIS}})^2$. Curiously, the same relation is satisfied for the case of regular dynamics (see Section 5.3). If the argument $z = \varepsilon/\hbar$ is large, the analytic function $G(z)$ can be calculated generally by the method of stationary phase. In the simplest case of a single isolated stationary point $\boldsymbol{x}^*$ in N dimensions

$$|G(z)| \asymp \left|\frac{\pi}{2z}\right|^{N/2} \left|\det \partial_{x_j}\partial_{x_k} W(\boldsymbol{x}^*)\right|^{-1/2}. \tag{104}$$

This expression gives an asymptotic power law decay of the plateau height independent of the perturbation details. Note that for a finite phase space we will have oscillatory *diffraction corrections* to Eq. (104) due to a finite range of integration $\int \mathrm{d}\mu$ which in turn causes an interesting situation for specific values of z, namely that by increasing the perturbation strength ε we can actually increase the value of the plateau.

Next we shall consider the regime of long times $t > t_2$. Then the second term in the exponential of (24) dominates the first one, however even the first term may not be negligible. Up to terms of order $O(t\varepsilon^3)$ we can factorize Eq. (34) as $M_\varepsilon(t) \approx \exp(-\mathrm{i}\frac{\varepsilon}{\hbar}(W(t)-W(0)))\exp(-\mathrm{i}\frac{\varepsilon^2}{2\hbar}\Sigma_R(t))$. When computing the expectation value $f(t) = \langle M_\varepsilon(t)\rangle$ we again use the fact that in the leading semiclassical order the operator ordering is irrelevant and that any time-correlation can be factorized, so also the second term of $\Gamma(t)$ (25) vanishes. Thus we have

$$F(t) \approx F_{\mathrm{plat}} \left|\langle\exp\left(-\mathrm{i}\frac{\varepsilon^2}{2\hbar}\Sigma_R(t)\right)\rangle\right|^2, \quad t > t_2. \tag{105}$$

This result is quite intriguing. It tells us that apart from a prefactor F_{plat}, the decay of fidelity with residual perturbation is formally the same as fidelity decay with a generic (non-residual) perturbation, Eqs. (7) and (10), when one substitutes the operator V with R and the perturbation strength ε with $\varepsilon_R = \varepsilon^2/2$. The fact that time-ordering is absent in Eq. (105) as compared with (10) is semiclassically irrelevant. Thus we can directly apply the general semiclassical theory of fidelity decay described in previous subsection, using a renormalized perturbation R of renormalized strength ε_R. Here we simply rewrite the key results in the 'non-Lyapunov' (perturbation-dependent regime), namely for $\varepsilon_R < \hbar$. Using a classical transport rate $\sigma := \lim_{t\to\infty} \frac{1}{2t}(\langle\sigma_R^2(t)\rangle_{\mathrm{cl}} - \langle\sigma_R(t)\rangle_{\mathrm{cl}}^2)$ where $\sigma_R(t)$ is a classical observable corresponding to $\Sigma_R(t)$. We have either an exponential decay

$$F(t) \approx F_{\mathrm{plat}} \exp\left(-\frac{\varepsilon^4}{2\hbar^2}\sigma t\right), \quad t < t_{\mathrm{H}} \tag{106}$$

or a (perturbative) Gaussian decay

$$F(t) \approx F_{\mathrm{plat}} \exp\left(-\frac{\varepsilon^4}{2\hbar^2}\sigma\frac{t^2}{t_{\mathrm{H}}}\right), \quad t > t_{\mathrm{H}}, \tag{107}$$

and the crossover again happens at the Heisenberg time t_{H}. This is just the time when the integrated correlation function of $R(t)$ becomes dominated by quantum fluctuation. Comparing the two factors in (106,107), *i.e.* the fluctuations of two terms in (24), we obtain a semiclassical estimate of t_2

$$t_2 \approx \min\left\{\sqrt{\frac{t_H}{\sigma}}\frac{\kappa_{\mathrm{cl}}}{\varepsilon}, \frac{\kappa_{\mathrm{cl}}^2}{\sigma\varepsilon^2}\right\}, \tag{108}$$

where κ_{cl} is dispersion of classical observable corresponding to W,

$$\kappa_{\mathrm{cl}}^2 = \langle w^2\rangle_{\mathrm{cl}} - \langle w\rangle_{\mathrm{cl}}^2. \tag{109}$$

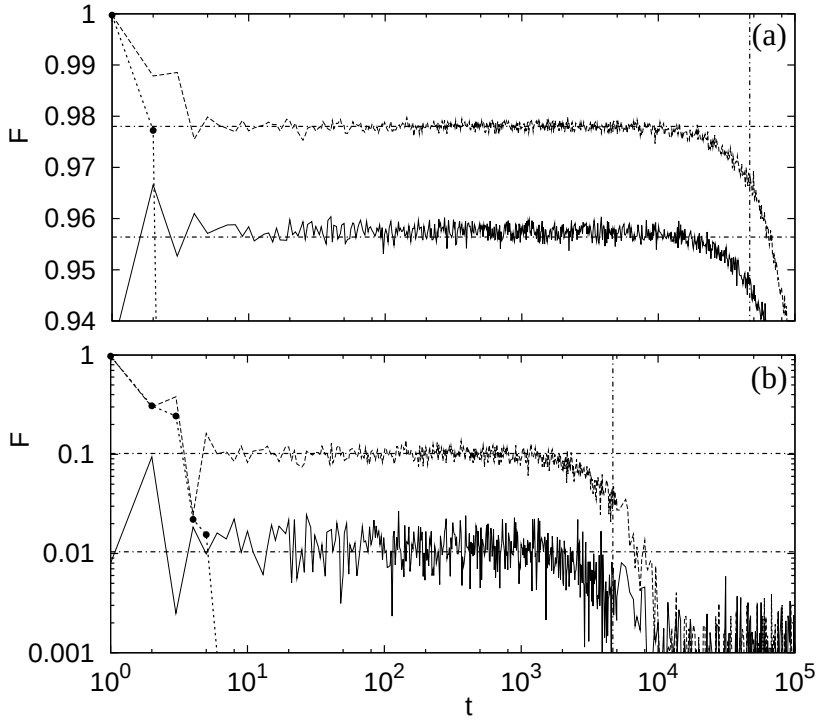

Fig. 7. $F(t)$ for the kicked top, with $\varepsilon = 10^{-3}$ (a), and $\varepsilon = 10^{-2}$ (b), upper curves (dashed) for CIS and the lower curves (full) for RIS. Horizontal lines are theoretical plateau values (103), vertical lines are theoretical values of t_2 (108). Points represent calculation of the corresponding classical fidelity for CIS which follows quantum fidelity up to the Ehrenfest ($\log \hbar$) barrier and exhibits no freezing.

Interestingly, the exponential regime (106) can only take place if $t_2 < t_{\rm H}$. If one wants to keep $F_{\rm plat} \sim 1$, or have exponential decay in the full range until $F \sim 1/\mathcal{N}$, this implies a condition on dimensionality: $d \geq 2$. The quantum fidelity and its plateau values have been expressed entirely (in the leading order in $\hbar$) in terms of classical quantities. While the prefactor $F_{\rm plat}$ depends on the details of the initial state, the exponential factors of (106,107) *do not*. Yet, the freezing of fidelity is a purely quantum phenomenon. The corresponding *classical fidelity* (discussed in Section 6) does not exhibit freezing. Let us illustrate our theoretical findings by numerical examples.

First we consider a quantized kicked top as an example of a one-dimensional system ($d = 1$) with spin quantum number $S = 1000$. The model is described in Appendix B.1, Eqs. (B.6,B.7,B.8). In Fig. 7 we show that the analytical expressions in Eq. (103) for the plateau values agree very well with numerical results, not only for weak perturbation $\varepsilon = 10^{-3}$ shown in Fig. 7(a) where linearized (linear response) expressions for the plateau values could be used, but also for strong perturbation $\varepsilon = 10^{-2}$ as shown in Fig. 7(b). Integration over the sphere yields $G(\varepsilon J) = \sqrt{\frac{\pi}{2\varepsilon J}}\mathrm{erf}(e^{\mathrm{i}\pi/4}\sqrt{\varepsilon J/2})$. Comparing with the asymptotic general formula (104) for $G(z)$ we now also find a diffractive contribution due to the oscillatory behavior of the complex Error function. Small (quantum) fluctuations around the theoretical plateau values in Fig. 7 lie beyond the leading order semiclassical description. In Fig. 7 we also demonstrate that the semiclassical formula (108) for t_2 works very well.

To demonstrate the Gaussian and exponential long-time decay of fidelity (106) with renormalized perturbation strength we look at a system of two ($d = 2$) coupled tops described in Appendix B.1, Eqs. (B.15-B.17). Here we work with the spin quantum number $S = 100$. The results of the numerical simulations are shown in Fig. 8. We show only the long-time decay, since at short times, the behavior is qualitatively the same as for $d = 1$. If the perturbation is sufficiently strong, one obtains an exponential decay as shown in Fig. 8(a), while for a smaller perturbation we obtain a Gaussian decay as shown in Fig. 8(b). Numerical data have been successfully compared with the theory (106,107) using classically calculated $\sigma = 9.2 \cdot 10^{-3}$, and with

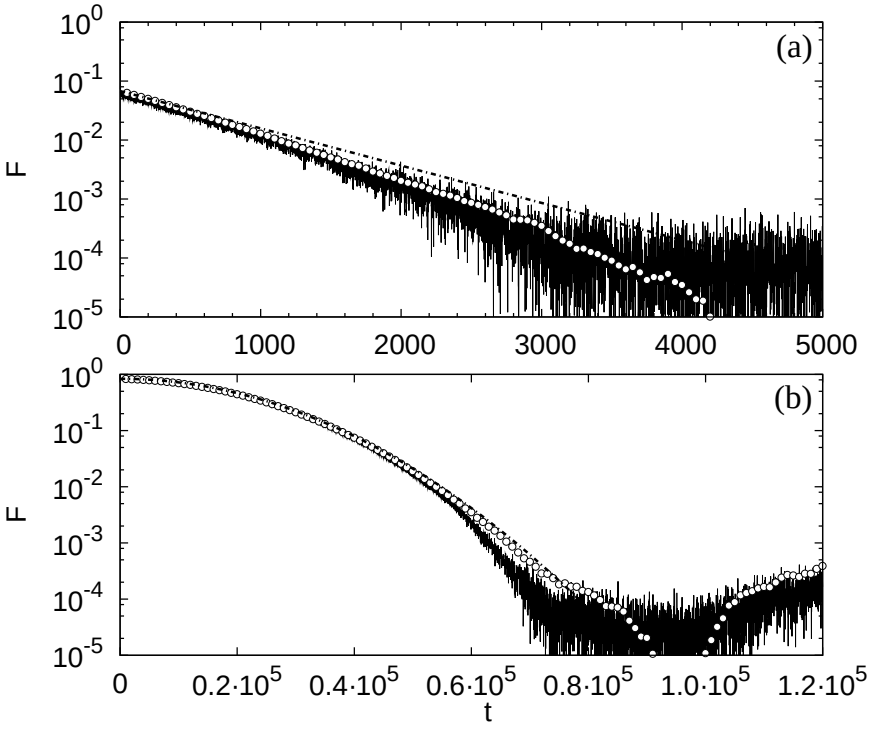

Fig. 8. Long-time fidelity decay in two coupled kicked tops. For strong perturbation $\varepsilon = 7.5 \cdot 10^{-2}$ (a) we obtain an exponential decay, and for smaller $\varepsilon = 2 \cdot 10^{-2}$ (b) we have a Gaussian decay. Chain curves give semiclassical expressions (106,107) using classical inputs, full curves give direct numerical simulations and open circles give "renormalized" numerics in terms of renormalized perturbation operator R and perturbation strength $\varepsilon_R = \varepsilon^2/2$.

the "renormalized" numerics using the operator R.

A similar phenomenon as quantum freeze has been observed in Ref. [102] for small perturbations consisting of a phase space displacement.

3.3. *Composite systems*

As for other measures of echo-dynamics for mixing and ergodic dynamical system we again assume a bipartite decomposition of the Hilbert space $\mathcal{H} = \mathcal{H}_{\rm c} \otimes \mathcal{H}_{\rm e}$. For mixing dynamics the correlations decay and the linear response term will grow linearly with time. For large times one can argue that $\Sigma(t)$ should look like a random matrix and the terms giving the difference between the fidelity and the echo purity and the reduced fidelity can be estimated as

$$\frac{\sum_{j=2}^{\mathcal{N}_{\rm c}} |\langle j;1|\Sigma(t)|1;1\rangle|^2}{\langle 1;1|\Sigma^2(t)|1;1\rangle} \sim \frac{\sum_j |[\Sigma(t)]_{(j;1),(1;1)}|^2}{\sum_{j,\nu} |[\Sigma(t)]_{(1;1),(j,\nu)}|^2} \sim \frac{1}{\mathcal{N}_{\rm e}}, \tag{110}$$

because there are more terms in the sum for fidelity. Therefore we can estimate the difference $F_{\rm P}(t) - F^2(t) \sim 1/\mathcal{N}_{\rm c} + 1/\mathcal{N}_{\rm e}$ and $F_{\rm R}(t) - F(t) \sim 1/\mathcal{N}_{\rm c}$. Provided both dimensions $\mathcal{N}_{\rm c,e}$ are large and for sufficiently long times, so the "memory" of the initial state is lost, we can expect the decay of all three quantities to be the same.

Discussing linear response results (Section 2.6.6) in the case of mixing dynamics we have shown that the linear decay is the same for all three quantities. Similar random matrix arguments as for the linear response can be used also for higher order terms and therefore one expects that in the semiclassical limit of small $1/\mathcal{N}_{\rm c} + 1/\mathcal{N}_{\rm e}$ we will have the same exponential decay (90)

$$F_{\rm P}(t) \approx F_{\rm R}^2(t) \approx F^2(t) = \exp\left(-2t/\tau_{\rm m}\right), \tag{111}$$

with the decay time $\tau_{\rm m} = \hbar^2/2\varepsilon^2\sigma_{\rm cl}$ (90) independent of the initial state. This result is expected to hold when $\Sigma(t)$ can be approximated with a random matrix for large times (110) and V does not contain terms acting on only one subspace. Such terms could cause fidelity to decay while having no influence on purity.

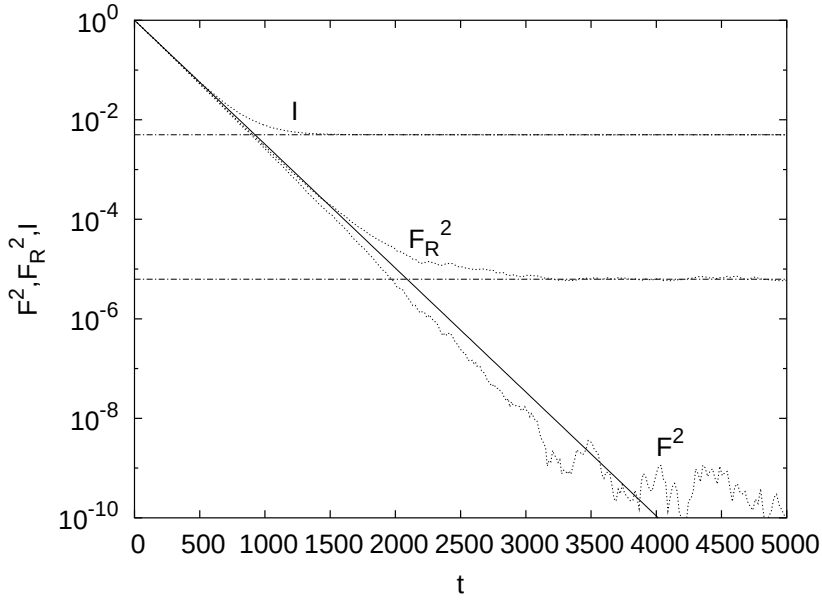

Fig. 9. Decay of $F^2(t), F_{\rm R}^2(t)$ and $I(t)$ (dotted curves) in the mixing regime of the double kicked top. The solid line gives the theoretical exponential decay (111) with $\tau_{\rm m}$ calculated from the classical $\sigma_{\rm cl} = 0.056$. Horizontal chain lines give the saturation values of the purity and the reduced fidelity, $1/200$ and $1/400^2$, respectively.

For a numerical demonstration of this result we chose for the system of coupled kicked tops such parameters that the corresponding classical dynamics is practically completely chaotic and mixing. The exact form of the perturbation and the parameter values are given in Appendix B.1, Eq. (B.20). The unperturbed system consists of two uncoupled kicked tops such that the coupling is due to the perturbation. In this case, echo purity $F_P(t)$ is the same as purity $I(t)$ of the forward evolution of the perturbed system. The perturbation strength and the spin size were chosen as $\varepsilon = 8 \cdot 10^{-4}$ and $S = 200$, respectively, such that $\mathcal{N}_{\rm c,e} = 2S + 1 = 401$. The initial state was chosen as a product of two coherent states placed at the positions $\vartheta^*_{\rm c,e} = \pi/\sqrt{3}$, $\varphi^*_{\rm c,e} = \pi/\sqrt{2}$ on the canonical sphere, for both tops. We show in Fig. 9 the decay of the fidelity $F(t)$, the reduced fidelity $F_{\rm R}(t)$, and the purity $I(t)$. Clean exponential decay is observed in all three cases, on a time scale $\tau_{\rm m}$ (111) given by the classical transport coefficient $\sigma_{\rm cl}$. We numerically calculated the classical correlation function

$$C_{\rm cl}(t) = [\langle z_{\rm c}(t) z_{\rm c}(0)\rangle_{\rm cl}]^2, \tag{112}$$

where we took into account that the unperturbed dynamics is uncoupled and is the same for both subsystems and that $\langle z\rangle_{\rm cl} = 0$. Taking only the first term $C_{\rm cl}(0) = 1/9$ would give $\sigma_{\rm cl} = 1/18$ (88) while the full sum of $C_{\rm cl}(t)$ gives a slightly larger value $\sigma_{\rm cl} = 0.056$. Exponential decay persists up to the saturation value determined by the dimension of the Hilbert space.

We also wish to illustrate what happens if dimension of one of the subspaces, say of the central system $\mathcal{N}_{\rm c}$ is not large, but we only let the dimension of the environment $\mathcal{N}_{\rm e}$ become large. For this purpose we choose a model of a kicked Ising spin chain for parameter values for which the model is non-integrable and operates in the regime of quantum chaos (see Appendix B.2).

We note that in the linear response expression for purity decay, we have a reduced slope of purity echo increase with a factor $1 - (\mathcal{N}_{\rm e} + \mathcal{N}_{\rm c})/(\mathcal{N}_{\rm e}\mathcal{N}_{\rm c})$ with respect to $[F(t)]^2$, whereas for long times, the decay of purity, with the appropriate plateau value subtracted and rescaled, is determined by the asymptotic decay of the echo operator, squared, *i.e.*

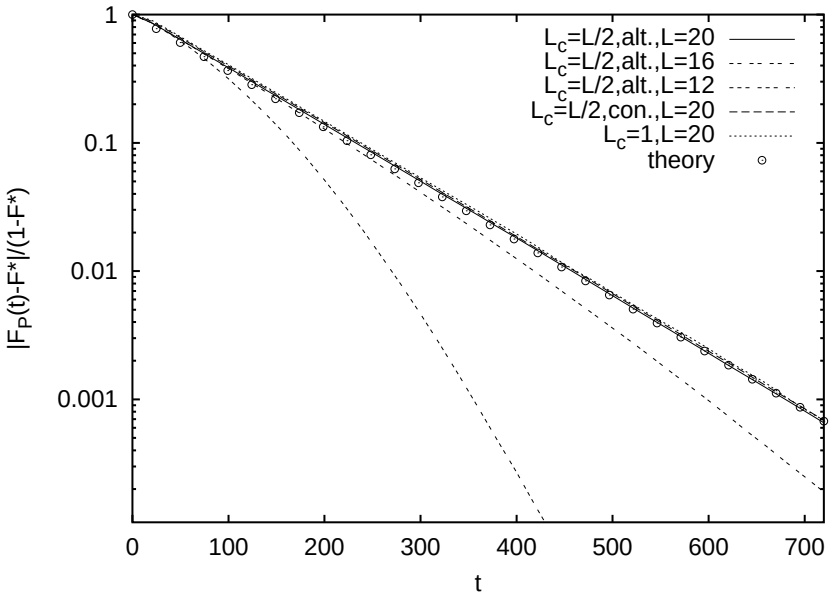

Fig. 10. Decay of echo purity in kicked Ising chain in the mixing regime $h_z = 1.4$ for different types of division [full curve, broken dashed curves = central system is composed of every other spin, dashed curve = central system is a connected half of the chain, dotted curve = central system is a *single* spin] and different sizes L (indicated in the legend) and $\varepsilon' = 0.01$. Theoretical decay (for $L \to \infty$) is given by sampled symbols.

$$\frac{F_{\rm P}(t) - F_{\rm P}^*}{1 - F_{\rm P}^*} \approx [F(t)]^2. \tag{113}$$

This is illustrated in Fig. 10 for different cases of division of the spin chain into the central system and the environment, and discussed in detail in Ref. [51].

For a related work on entanglement growth in chaotic composite systems see [103,104]. Some other aspects of entanglement in chaotic systems have been studied in Refs. [105,106,47,107–114].

3.4. *Semiclassical theories in terms of classical orbits*

In the semiclassical limit (small $\hbar$) quantum fidelity can be calculated using the semiclassical expression for the quantum propagator in terms of classical orbits. Historically this was the method used by Jalabert and Pastawski [7] to derive the perturbation independent Lyapunov decay of quantum fidelity. They used the perturbation consisting of a uniform distribution of scattering potentials with a Gaussian spatial dependence. It is noted that in the absence of the perturbation $F(t) \equiv 1$ is recovered exclusively if only diagonal terms are retained, *i.e.* in the notation we use later this means orbits for which $j_\varepsilon = j_0$, resulting in a single sum over orbits (instead of double). For nonzero perturbation averaging over impurities is argued to "select" only diagonal terms. Later it was shown that the same Lyapunov decay is found also for the classical fidelity [62]. This suggests that quantum Lyapunov decay is a consequence of the quantum-classical correspondence; see Section 6 for more details. The correspondence will hold until the Ehrenfest time when a wave packet is spread over a sufficiently large portion of Hilbert space and quantum interferences become important. We shall discuss in detail parameter ranges and time scales when various regimes of fidelity decay occur in Section 7, and we shall see that a Wigner function representation proposed in Ref. [115] illustrates this nicely. For a detailed discussion of the range of the Lyapunov decay in a Lorentz gas with disorder see Ref. [116]. Fidelity decay for disordered system with diffractive scatterers has been studied using a diagrammatic expansion in Ref. [117]. It is worth mentioning that for sufficiently strong perturbations ($\hbar < \varepsilon < \sqrt{\hbar}$) there are large fluctuations [73,75] and as a consequence the average fidelity decay depends on the way we average. For typical initial packets the evolution is "hypersensitive" to perturbations, resulting in a double

exponential fidelity decay [73], $F \propto \exp(-\text{const} \times \mathrm{e}^{2\lambda t})$. Semiclassics has been used in Refs. [45,44] to derive the so-called Fermi golden rule decay (90), see also [53,54]. The Fermi golden rule decay has been derived independently using correlation function formalism in Refs. [42,46]. Fermi golden rule type expressions involving the correlation function have also appeared as an intermediate step in Ref. [44]. Lyapunov decay in a Lorentz gas was the subject of a numerical study in Ref. [41]. Lyapunov as well as Fermi golden rule regimes in a stadium billiard with disorder have been studied in Ref. [118]. The transition between Fermi golden rule and Lyapunov decay in a Bunimovich stadium has been numerically considered in Ref. [119] while the short time decay of fidelity in the same system has been discussed using local density of states in Ref. [120]. The importance of the delicate interplay between classical perturbation theory and the structural stability of manifolds in chaotic systems has been stressed in selecting the diagonal terms. The argumentation has been further elaborated in Ref. [121], resulting in the so-called dephasing representation [57,58]. Using the dephasing representation it is possible to calculate quantum fidelity decay numerically ranging from the Fermi golden rule to the Lyapunov regime. For strong perturbations one can use dephasing representation to investigate deviations from a simple Lyapunov decay for chaotic systems for which the hyperbolic stretching rate is not uniform across the phase space [122], or perhaps even more interestingly, to investigate new types of perturbation dependent fidelity decay in 'weakly' chaotic systems with classically diffusive behaviour [123].

Semiclassics can also be used to calculate purity. For chaotic systems the exponential decay of purity has been derived in [124], confirming earlier predictions in Refs. [91,125,50]. Chaotic time dependent oscillator is treated in Ref. [126].

Instead of using classical orbits in semiclassical derivations, e.g. in the Van Vleck-Gutzwiller propagator, one can directly use the formalism of Weyl quantization to obtain a semiclassical expression of fidelity. Such an approach has been used in Ref. [127] where the propagation of Gaussian wave packets is studied. Two terms are identified, the position of the center of the packet accounts for its translation while the metaplectic operator takes care of the dispersion. The metaplectic operator represents the symplectic transformation (*i.e.* canonical transformation) of the linearized motion around the central orbit. Independently, a similar approach has been used in Ref. [128].

In the present section we give a brief derivation of the semiclassical expression for fidelity in terms of the Wigner function of the initial state, the so-called dephasing representation derived in Refs. [57,58]. With $\boldsymbol{r}, \boldsymbol{r}'$ denoting points in configuration space, the fidelity amplitude can be written as

$$f(t) = \langle \psi_0(t) | \psi_\varepsilon(t) \rangle = \int \mathrm{d}\boldsymbol{r}' \, \psi_0^*(\boldsymbol{r}'; t) \psi_\varepsilon(\boldsymbol{r}'; t). \tag{114}$$

If $\psi(\boldsymbol{r}, 0)$ is the initial state, the wave function at time t is given by

$$\psi_\varepsilon(\boldsymbol{r}'; t) = \int \mathrm{d}\boldsymbol{r} \, \langle \boldsymbol{r}' | U_\varepsilon(t) | \boldsymbol{r} \rangle \, \psi(\boldsymbol{r}; 0). \tag{115}$$

The step to semiclassics consists in replacing the quantum propagator $\langle \boldsymbol{r}' | U_\varepsilon(t) | \boldsymbol{r} \rangle$ by its semiclassical approximation $K_\varepsilon^{\mathrm{sc}}(\boldsymbol{r}', \boldsymbol{r}, t)$, *i.e.* $\langle \boldsymbol{r}' | U_\varepsilon(t) | \boldsymbol{r} \rangle \to K_\varepsilon^{\mathrm{sc}}(\boldsymbol{r}', \boldsymbol{r}, t)$. The first argument of $K_\varepsilon^{\mathrm{sc}}$ will denote the end point after time t (quantity with prime) and the second argument the initial point (without prime). The semiclassical Van Vleck-Gutzwiller propagator is [129,130],

$$K_\varepsilon^{\mathrm{sc}}(\boldsymbol{r}', \boldsymbol{r}, t) = \sum_{j_\varepsilon} \frac{1}{(2\pi \mathrm{i}\hbar)^{d/2}} \sqrt{C_{j_\varepsilon}} \exp\left(\frac{\mathrm{i}}{\hbar} S_{j_\varepsilon}(\boldsymbol{r}', \boldsymbol{r}, t) - \mathrm{i} \frac{\pi}{2} m_{j_\varepsilon} \right), \tag{116}$$

where the sum extends over all orbits j_ε that connect points $\boldsymbol{r}$ and $\boldsymbol{r}'$ in time t, *i.e.* sum over all initial momenta $\boldsymbol{p}_{j_\varepsilon}$, such that the evolution for time t results in $(\boldsymbol{r}, \boldsymbol{p}_{j_\varepsilon}) \xrightarrow{t} (\boldsymbol{r}', \boldsymbol{p}'_{j_\varepsilon})$. For chaotic systems the number of contributing orbits j_ε will be very large already for small times and will grow exponentially with time, because the sum goes over all momenta, *i.e.* over all energies. The action is given by

$$S_{j_\varepsilon}(\boldsymbol{r}', \boldsymbol{r}, t) = \int_0^t \mathrm{d}t' L_\varepsilon(\tilde{\boldsymbol{r}}(t'), \dot{\tilde{\boldsymbol{r}}}(t'), t'), \tag{117}$$

and $C_{j_\varepsilon} = |\det(\partial^2 S_{j_\varepsilon} / \partial \boldsymbol{r}' \partial \boldsymbol{r})|$ is the absolute value of the Van Vleck determinant. Taking into account that $\partial S_{j_\varepsilon}(\boldsymbol{r}', \boldsymbol{r}, t) / \partial \boldsymbol{r} = -\boldsymbol{p}_{j_\varepsilon}$, where $\boldsymbol{p}_{j_\varepsilon}$ is the initial momentum, we see that C_{j_ε} is the Jacobian of the

transformation between the initial momentum and the final position, $C_{j_\varepsilon} = |\det \frac{\partial \boldsymbol{p}_{j_\varepsilon}}{\partial \boldsymbol{r}'}|$. The integer m_{j_ε} is a Maslov index. Writing the fidelity amplitude (114) in terms of $K_\varepsilon^{\rm sc}$ and $K_0^{\rm sc}$ and taking the expectation value leads to an expression involving a three-fold integral over the positions: $\boldsymbol{r}'$ (the position argument of the propagated wave functions at time t and $\boldsymbol{r}, \tilde{\boldsymbol{r}}$ (the position arguments of the initial states to be propagated). In addition we have a double sum over orbits j_ε of the perturbed dynamics, connecting $(\boldsymbol{r}, \boldsymbol{p}_{j_\varepsilon}) \xrightarrow{t} (\boldsymbol{r}', \boldsymbol{p}'_{j_\varepsilon})$, and orbits j_0 of the unperturbed one, connecting $(\tilde{\boldsymbol{r}}, \tilde{\boldsymbol{p}}_{j_0}) \xrightarrow{t} (\boldsymbol{r}', \tilde{\boldsymbol{p}}'_{j_0})$,

$$f(t) = \frac{1}{(2\pi \mathrm{i}\hbar)^d} \int \mathrm{d}\boldsymbol{r} \mathrm{d}\tilde{\boldsymbol{r}}\, \psi^*(\tilde{\boldsymbol{r}}; 0)\psi(\boldsymbol{r}; 0) \sum_{j_\varepsilon, j_0} \times \int \mathrm{d}\boldsymbol{r}' \sqrt{C_{j_0} C_{j_\varepsilon}} \exp\left(\frac{\mathrm{i}}{\hbar} \{S_{j_\varepsilon}(\boldsymbol{r}', \boldsymbol{r}, t) - S_{j_0}(\boldsymbol{r}', \tilde{\boldsymbol{r}}, t)\} - \mathrm{i}\frac{\pi}{2} \{m_{j_\varepsilon} - m_{j_0}\} \right). \tag{118}$$

In the expression for fidelity $F(t)$ we have twice as many terms! The last expression is still rather involved but for our case of echo dynamics several simplifications are possible. One is to use the shadowing theorem (see references in [57]) to identify those orbits that give the dominating contribution to the phase factor and the other is to transform the integration from the final position to the initial momentum.

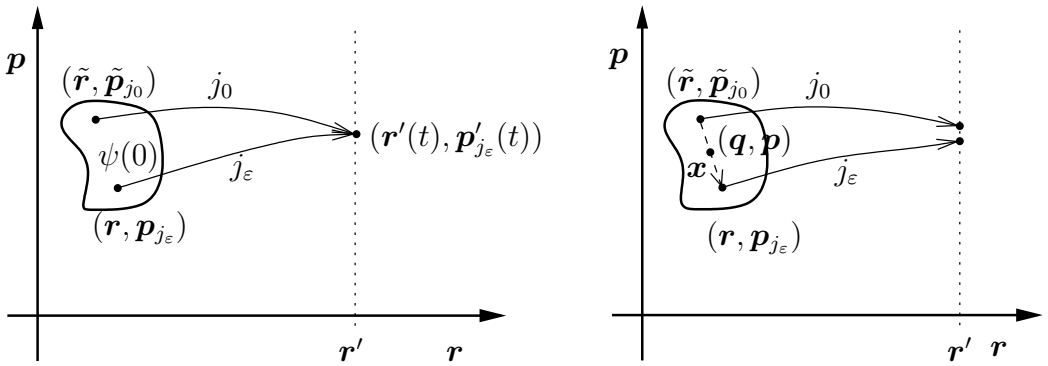

Fig. 11. Orbits involved in the semiclassical calculation of the fidelity amplitude (118) after taking into account matching condition (119). Left figure denotes situation in the classical limit of exact matching and the right one for finite $\hbar$ where shadowing orbit pairs give major contribution.

Note that the semiclassical propagator (116) does not satisfy a semigroup condition, *i.e.* a product of two propagators $K^{\rm sc}(t)$ for time t is only approximately equal to a propagator for twice the time, $K^{\rm sc}(2t)$. To preserve the semigroup property, *i.e.* preserving normalization (unitarity), a product of semiclassical propagators must be supplemented by the "matching" of momenta of two orbits occurring in two propagators. Formally this condition is implemented by making a stationary phase approximation in the integral over $\boldsymbol{r}'$, for details see e.g. [131]. If the semiclassical limit $\hbar \to 0$ is taken prior to integration, the stationary phase condition $\partial S_{j_\varepsilon}/\partial \boldsymbol{r}' - \partial S_{j_0}/\partial \boldsymbol{r}'$ has to be obeyed exactly. Exact matching indeed gives the decay of classical fidelity (see Section 6). The matching condition at time t,

$$\tilde{\boldsymbol{p}}'_{j_0} = \boldsymbol{p}'_{j_\varepsilon}, \tag{119}$$

forces the initial condition for the unperturbed orbit $(\tilde{\boldsymbol{r}}, \tilde{\boldsymbol{p}}_{j_0})$ to be implicitly determined trough the matching condition for a forward perturbed evolution from $(\boldsymbol{r}, \boldsymbol{p}_{j_\varepsilon})$ followed by a backward unperturbed evolution. This suppresses one space integration over $\mathrm{d}\tilde{\boldsymbol{r}}$ in (118). The orbits involved in calculating this classical fidelity are schematically shown in the left panel of Fig. 11. The action difference $\Delta S(\boldsymbol{r}, \boldsymbol{p}, t)$ after forward perturbed evolution followed by backward unperturbed evolution is given by

$$\Delta S(\boldsymbol{r}, \boldsymbol{p}, t) = S_{j_\varepsilon}(\boldsymbol{r}', \boldsymbol{r}, t) - S_{j_0}(\boldsymbol{r}', \tilde{\boldsymbol{r}}, t) = \int_0^t \mathrm{d}t' L_\varepsilon(\boldsymbol{r}(t'), \dot{\boldsymbol{r}}(t')) + \int_t^0 \mathrm{d}t' L_0(\boldsymbol{r}(t'), \dot{\boldsymbol{r}}(t')), \tag{120}$$

where the initial condition for the second integral with L_0 is the final orbit position of the first integral. This difference will, in general, be large for chaotic systems, because perturbed and unperturbed orbits will

explore vastly different regions of phase space. For sufficiently large time the action difference will depend only on the chaotic properties of the system and not on the perturbation strength. This results in the perturbation independent decay of classical fidelity.

For finite $\hbar$, *i.e.* first evaluating the integral and then taking the semiclassical limit, the above matching condition (119) needs to hold only approximately. Approximate continuity of momenta for finite $\hbar$ means that we have to consider also almost continuous orbits for which discontinuity $\tilde{\boldsymbol{p}}'_{j_0} - \boldsymbol{p}'_{j_\varepsilon}$ is sufficiently small. This is shown in the right panel of Fig. 11. Of course, the approximate continuity is automatically taken care of if we perform the stationary phase integration properly. Yet here we would like to identify the dominating contribution by physical arguments, namely using the shadowing theorem. It states for chaotic systems that, while two orbits starting from the same initial condition will generally exponentially diverge, if evolved with two slightly different evolutions, we can find exponentially close initial condition for one evolution such that its orbit will closely follow (shadow) the other one. Because the two initial conditions [5] are exponentially close they should in fact be summed over (for finite $\hbar$) in the formula for the fidelity amplitude $f(t)$ (118). As the orbit and its shadow, a 'shadowing pair', closely follow each other, their action difference ΔS will be small, *i.e.* $\Delta S \sim \mathcal{O}(\varepsilon)$ whereas one has $\Delta S \sim \mathcal{O}(1)$ for non-shadowing pairs. Therefore shadowing pairs cause the largest contribution to $f(t)$. It is thus sufficient to take into account shadowing pairs only. To arrive at the final expression we change the integration variables $\mathrm{d}\boldsymbol{r}$ and $\mathrm{d}\tilde{\boldsymbol{r}}$ in (118) to their difference $\boldsymbol{x} = \boldsymbol{r} - \tilde{\boldsymbol{r}}$ and their mean $\bar{\boldsymbol{q}} = (\boldsymbol{r} + \tilde{\boldsymbol{r}})/2$. As the major contribution to $f(t)$ results from shadowing pairs, due to their small ΔS the difference $\boldsymbol{x}$ will be small and we can expand ΔS around $\bar{\boldsymbol{q}}$ to linear order in $\boldsymbol{x}$,

$$S_{j_\varepsilon}(\boldsymbol{r}', \bar{\boldsymbol{q}} + \boldsymbol{x}/2, t) - S_{j_0}(\boldsymbol{r}', \bar{\boldsymbol{q}} - \boldsymbol{x}/2, t) = S_{j_\varepsilon}(\boldsymbol{r}', \bar{\boldsymbol{q}}, t) - S_{j_0}(\boldsymbol{r}', \bar{\boldsymbol{q}}, t) - \boldsymbol{x}\bar{\boldsymbol{p}} + \cdots . \tag{121}$$

where we denoted the mean initial momentum by $\bar{\boldsymbol{p}} = (\boldsymbol{p}_{j_\varepsilon} + \tilde{\boldsymbol{p}}_{j_0})/2$. This expansion does not depend on the initial state being localized. Next, we transform the integration over the final positions $\boldsymbol{r}'$ to an integration over initial mean momenta $\bar{\boldsymbol{p}}$. Together with the original Jacobian prefactor $\sqrt{C_{j_0} C_{j_\varepsilon}}$ this gives $\sqrt{|\det \frac{\partial \boldsymbol{p}_{j_\varepsilon}}{\partial \bar{\boldsymbol{p}}}||\det \frac{\partial \tilde{\boldsymbol{p}}_{j_0}}{\partial \bar{\boldsymbol{p}}}|}$ which though is close to one for shadowing orbits. For shadowing orbits Maslov indices are equal, $m_{j_\varepsilon} = m_{j_0}$. We thus obtain

$$f(t) = \frac{1}{(2\pi \mathrm{i}\hbar)^d} \int \mathrm{d}\bar{\boldsymbol{q}}\mathrm{d}\bar{\boldsymbol{p}}\mathrm{d}\boldsymbol{x}\, \psi^*(\bar{\boldsymbol{q}} - \frac{\boldsymbol{x}}{2}; 0)\psi(\bar{\boldsymbol{q}} + \frac{\boldsymbol{x}}{2}; 0) \times \\ \times \exp\left(\frac{\mathrm{i}}{\hbar}\{S_{j_\varepsilon}(\boldsymbol{r}', \bar{\boldsymbol{q}}, t) - S_{j_0}(\boldsymbol{r}', \bar{\boldsymbol{q}}, t)\}\right) \exp\left(-\frac{\mathrm{i}}{\hbar}\bar{\boldsymbol{p}}\boldsymbol{x}\right). \tag{122}$$

The action difference $S_{j_\varepsilon}(\boldsymbol{r}', \bar{\boldsymbol{q}}, t) - S_{j_0}(\boldsymbol{r}', \bar{\boldsymbol{q}}, t)$ is calculated by using forward perturbed orbit j_ε followed by an unperturbed backward evolution along shadowing orbit j_0, where the initial condition is such that $(\bar{\boldsymbol{q}}, \bar{\boldsymbol{p}}) = (\boldsymbol{r} + \tilde{\boldsymbol{r}}, \boldsymbol{p}_{j_\varepsilon} + \tilde{\boldsymbol{p}}_{j_0})/2$, the so-called center chord in Weyl formalism [132]. By transforming to initial momenta $\bar{\boldsymbol{p}}$ we have eliminated one summation over momenta in Eq. (118). Therefore, we should sum over all initial conditions with the same center chord $(\bar{\boldsymbol{q}}, \bar{\boldsymbol{p}})$. As shadowing orbits are very close to each other there will be typically only one orbit having a given center chord and furthermore, to lowest order, we can assume that both orbits are actually the same for the purpose of calculating the action difference. For this single orbit we can take the initial condition to be the center chord $(\bar{\boldsymbol{q}}, \bar{\boldsymbol{p}})$. Combining all these simplifications for shadowing orbits and noting that $L_\varepsilon - L_0 = -\varepsilon V$, if V is the perturbing potential, we find $S_{j_\varepsilon}(\boldsymbol{r}', \bar{\boldsymbol{q}}, t) - S_{j_0}(\boldsymbol{r}', \bar{\boldsymbol{q}}, t) \approx \int_0^t \mathrm{d}t' V(\bar{\boldsymbol{q}}(t'), \bar{\boldsymbol{p}}(t'), t')$. We recognize the Wigner function for the state $\psi(\boldsymbol{r}; 0)$ in Eq. (122),

$$W_\rho(\bar{\boldsymbol{q}}, \bar{\boldsymbol{p}}) = \frac{1}{(2\pi\hbar)^d} \int \mathrm{d}\boldsymbol{x}\, \psi^*(\bar{\boldsymbol{q}} - \frac{\boldsymbol{x}}{2}; 0)\psi(\bar{\boldsymbol{q}} + \frac{\boldsymbol{x}}{2}; 0) \exp\left(-\frac{\mathrm{i}}{\hbar}\bar{\boldsymbol{p}}\,\boldsymbol{x}\right), \tag{123}$$

and we finally get

$$f(t) = \int \mathrm{d}\bar{\boldsymbol{q}}\mathrm{d}\bar{\boldsymbol{p}}\, W_\rho(\bar{\boldsymbol{q}}, \bar{\boldsymbol{p}}) \exp\left(-\frac{\mathrm{i}}{\hbar}\varepsilon \int_0^t \mathrm{d}t' V(\bar{\boldsymbol{q}}(t'), \bar{\boldsymbol{p}}(t'), t')\right). \tag{124}$$

[5] In our case there are actually two exponentially close "final" conditions at time t.

The final result (124) is the so-called dephasing representation [57,58]. It has a very appealing form: fidelity is given as the Wigner function average of the phases due to action differences. The importance of this expression is that it is valid from the Lyapunov to the Fermi golden rule regime. It can also in general describe fidelity decay in regular systems, e.g., Gaussian decay or even decay after plateau in quantum freeze [133]. In particular it is very handy for numerical evaluation of quantum fidelity decay in various non-generic situations or for complicated initial states. It should be also useful for systems with many degrees of freedom due to favorable scaling of its running time as compared to exact quantum calculations.

The statistics of action differences has been discussed in Ref. [134]. While in practice the numerical evaluation of the dephasing representation (124) turns out to reproduce the exact quantum fidelity decay in chaotic, regular as well as in mixed systems very well [57,58], there are nevertheless some limitations. For instance, it is unable to describe the perturbative Gaussian decay for small perturbations which occurs due to finite size effects [121].

The exponential term in the expression for $f(t)$ (124) is very reminiscent of our approximate quantum echo operator $M_\varepsilon(t) \approx \exp(-\mathrm{i}\varepsilon\Sigma(t)/\hbar)$ (24) where $\Sigma(t)$ is the integral of the perturbation (15). Indeed, the semiclassical fidelity amplitude could be obtained directly, using the Weyl-Wigner quantization [132], *i.e.* replacing $M_\varepsilon(t)$ by its Weyl symbol and the density matrix ρ by its Wigner function W_ρ we recover the dephasing representation.

4. Random matrix theory of echo dynamics

From the previous section we have a surprising dichotomy. We have two slightly different approaches which yield for weak and very weak perturbation respectively the Fermi Golden rule and the perturbative regime. Both results are based on perturbation expansions, and there should be a unified theory to describe these regimes.

As random matrix models have been extremely successful in describing a wide field of phenomena in physics ranging from elasticity to particle physics [135,86] associated in some sense with chaos, it seems natural to attempt a formulation of echo dynamics in this framework. A number of papers have appeared on this subject [53,54,136]. We shall basically follow the lines of [52], which uses the linear response approximation expressed in terms of correlation integrals, very similar to our reasoning in Section 2.1. This method provides a uniform approximation encompassing both regimes. It proved successful in explaining two independent experiments (see Section 9). Some exact results for the random matrix theory (RMT) model used are also available [56,55,18,137]. We give the outlay of the model and derive a linear response formula for fidelity decay extending its validity to long times in a form valid strictly in the weak perturbation limit. We compare this result to new more detailed calculations or the kicked top and to the exact RMT solution. We then present a considerable body of new material extending this model to purity decay, and with modified perturbations we discuss various situations where quantum freeze can occur [18,137,111].

The RMT model we present, allows to describe fidelity decay in a chaotic system, under a static global perturbation; that model could be extended to treat also noisy perturbations, but at least in the case of uncorrelated noise, a direct statistical treatment is more adequate (see Section 2.1.2). Chaoticity is meant to justify choosing the unperturbed system from one of the Gaussian invariant ensembles [138–140]. With the word "global" we mean that in the eigenbasis of the unperturbed Hamiltonian, the perturbation matrix is not sparse. Banded matrices may occur, as long as their bandwidth is so large, that a full matrix would yield similar results. We shall mainly concentrate on this case, because it is most amenable to analytic treatment. Where other Hamiltonians are used we shall point this out and explain why it is necessary.

We consider a perturbed Hamiltonian in a form, typical for RMT (see e.g. [141,142]):

$$H_{\varepsilon'} = \cos(\varepsilon')\, H_0 + \sin(\varepsilon')\, H_1 \,, \tag{125}$$

where H_0 and H_1 are chosen from one of Cartan's classical ensembles [143,86]. This scheme has the advantage that the perturbation does not change the level density of the Hamiltonian, and thus avoids the need to normalize time in the echo dynamics, as discussed at the end of Section 2.1.3. We will generally be interested in situations where ε' scales as $1/\sqrt{N}$, where N denotes the dimension of the Hamiltonian matrices. In this case, the matrix elements of the perturbation couple a finite number of neighboring eigenstates of the

unperturbed system, largely independent on N. This assumption allows to describe all regimes, from $\varepsilon' = 0$ up to the Fermi golden rule regime, and beyond. For large N, we may therefore linearize the trigonometric functions in Eq. (125). It is then convenient, to fix the average level spacing of H_0 to be one in the center of the spectrum, and to require that the off-diagonal matrix elements of $V = H_1/\sqrt{N}$ have unit variance such that

$$H_\varepsilon = H_0 + \varepsilon\, V\ , \tag{126}$$

where $\varepsilon = \sqrt{N}\varepsilon'$. It is easy to check that corrections to the Heisenberg time are of order $\mathcal{O}(1/N)$. The matrix H_0 can have special properties (for example in Section 4.4 on echo purity), but typically it will be derived from a random matrix taken from the classical ensembles. We may use different ensembles for H_0 and V. In many cases, the ensemble of perturbations is invariant under the transformations that diagonalize H_0. We can then choose H_0 to be diagonal with a spectrum $\{E_j^0\}$ with given spectral statistics. In this situation we can unfold the spectrum that defines H_0, to have average level density one along the entire spectrum, or we can restrict our considerations to the center of the spectrum. This restricts us to situations, where the spectral density may be assumed constant over the energy spread of the initial state. Other cases could be important, but have, to our knowledge, so far not been considered in RMT.

The one parameter family H_ε defines echo dynamics as discussed in Section 2. In what follows, the eigenbasis of H_0 will be the only preferred basis except in Section 4.4, where we deal with entangled subsystems. Unless stated otherwise, we consider initial states to be random, but of finite span in the spectrum of H_0. Eigenstates of H_0 are one limiting case and random states with maximal spectral span the other.

The spectral span of the initial state and the spreading width of the H_0-eigenstates in the eigenbasis of H_ε, determine the only relevant time scales. They should be compared to the Heisenberg time, which has been fixed to $t_H = 1$, by unfolding the spectrum of H_0. In the limit $N \to \infty$, the Zeno time (of order t_H/N; see Section 2.1.1) plays no role.

Here, we are interested in the decay of fidelity or some other measure of echo dynamics. The main results cover essentially the range from the perturbative up to the Fermi golden rule regime [44,45]. The analysis of the quantum freeze and an exact analytical result for the random matrix model will provide additional and/or different regimes. The Lyapunov regime [7,44] as well as the particular behavior of coherent states are certainly not within the scope of RMT.

We shall find that in many situations the fidelity amplitude is self averaging; see Eq. (131). Therefore we mainly concentrate on the fidelity amplitude, and do not bother with the more complicated averages for fidelity itself.

This section is organized as follows: The linear response approximation and the exact analytic treatment of the fidelity amplitude are discussed in Sections 4.1, and 4.2, respectively. The quantum freeze case is studied in Section 4.3. Composite systems (two coupled subsystems) are considered in Sections 4.4 and 4.5.

4.1. *Linear response theory*

Recall that the echo operator $M_\varepsilon(t)$ can be written to second order in ε as [46,52]

$$M_\varepsilon(t) = \mathbf{1} - \mathrm{i}\, 2\pi\varepsilon \int_0^t \mathrm{d}t'\ \tilde{V}(t') - (2\pi\varepsilon)^2 \int_0^t \mathrm{d}t' \int_0^{t'} \mathrm{d}t''\ \tilde{V}(t')\,\tilde{V}(t'') + \mathcal{O}(\varepsilon_0^3)\ . \tag{127}$$

To obtain the fidelity amplitude we have to compute the average of $M_\varepsilon(t)$ with respect to both, the ensemble defining the random perturbation V, and the one defining the spectrum $\{E_\alpha^0\}$ of H_0. Provided that H_0 and V are statistically independent, the linear term in ε averages to zero. The quadratic term is determined by the two-point time correlation function

$$\langle [\tilde{V}(\tau)\,\tilde{V}(\tau')]_{\nu,\nu'} \rangle = \sum_\mu \langle V_{\nu,\mu}\, V_{\mu,\nu'} \rangle\ \langle e^{2\pi \mathrm{i}[(E_\nu - E_\mu)\tau + (E_\mu - E'_\nu)\tau']} \rangle = \delta_{\nu,\nu'}\ \left\{ \frac{2}{\beta_V} + \delta(\tau - \tau') - b_2(\tau - \tau') \right\}\ . \tag{128}$$

The middle expression contains two separate averages, the first is taken over the ensemble of V and the second over the spectral ensemble of the unperturbed Hamiltonian. The average over the matrix elements

of V yields delta functions that allow to rewrite the spectral average in terms of the two-point correlation function of the spectrum; as the spectral ensemble is invariant under rearrangements of the eigenenergies, the result is independent of the index ν. The spectral two-point correlation function is then translational invariant and the spectral form factor b_2 [144] is conveniently introduced. The constant β_V depends on the classical ensemble from which the perturbation was taken. It can take the values 1,2, and 4 for the orthogonal, unitary, and symplectic ensembles, respectively.

Inserting this result into Eq. (7) for the fidelity amplitude we get [52]

$$\langle f_\varepsilon(t)\rangle = 1 - (2\pi\varepsilon)^2 \left[t^2/\beta_V + t/2 - \int_0^t \mathrm{d}\tau' \int_0^{\tau'} \mathrm{d}\tau \; b_2(\tau) \right] + \mathcal{O}(\varepsilon^4) \; . \tag{129}$$

Any stationary ensemble from which H_0 may be chosen, yields a particular two-point function b_2. The correlation integrals over b_2 for the GOE and the GUE are discussed in [52]. To demonstrate the effect of spectral correlations by contrast, we occasionally use a random level sequence. In this case $b_2(t) = 0$ and the last term in (129) vanishes. Typically (at least in the case of the classical ensembles), spectral correlations lead to a positive b_2, such that the fidelity decay will be slowed down.

The result (129) shows two remarkable features: The first is that the linear and the quadratic term in t scale both with ε^2 The second is about the two possibly different ensembles used for the perturbation and for H_0. The characteristics of V affect only the prefactor of the t^2-term, while the characteristics of H_0 affect only the two-point form factor b_2.

In experiments or numerical simulations averaging over H_0 may be unnecessary, due to the self-averaging properties of fidelity. For this to be effective, we need an initial state which covers a sufficiently large number of eigenstates of H_0. The two-point form factor b_2 can then be obtained by averaging over energy or frequency intervals (spectral average).

As an expansion in time, Eq. (129) contains the leading terms for the perturbative as well as the Fermi golden rule results [30,44,45]. Both are exponentials of the corresponding terms. It is then tempting to simply exponentiate the entire ε^2-term to obtain

$$\langle f_\varepsilon(t)\rangle = \exp\left[-(2\pi\varepsilon)^2 \left(t^2/\beta_V + t/2 - \int_0^t \mathrm{d}\tau' \int_0^{\tau'} \mathrm{d}\tau \; b_2(\tau) \right) \right] \tag{130}$$

This expression will prove to be extremely accurate for perturbation strengths up to the Fermi golden rule regime. Some justification for the exponentiation is given in [72]. While exponentiation in the perturbative regime is trivially justified, our result shows that for times $t \ll t_H$, we always need the linear term in t to obtain the correct answer. In experiments the interplay of both terms has been proven to be important [69,70,83]; see also Section 9.2. On the other hand, for stronger perturbations fidelity has decayed before Heisenberg time to fluctuation levels or to levels where our approximation fails. Comparison with the exact result [56,55] (Section 4.2) will show that the exponentiation allows to extend the linear response result from a validity of $\langle f(t)\rangle \approx 1$ to a validity range of $\langle f(t)\rangle \gtrsim 0.1$

Note that the pure linear response result (129) is probably all we need for quantum information purposes, as processes with fidelity less than $1-\eta$, where $\eta \sim 10^{-4}$, are not amenable to quantum error correction schemes [13]. For considerations about stability in echo dynamics, on the other hand, the exponentiated formula (130) gives a clear and simple expression. The exact treatment will show where to expect additional effects, but experiments at this time are still limited to $\langle f(t)\rangle \gtrsim 0.1$ [69,70,83].

Fidelity can be calculated in the linear response approximation along the same lines as above. One obtains [52]:

$$\langle F_\varepsilon(t)\rangle = \langle |f_\varepsilon(t)|^2\rangle = \langle f_\varepsilon(t)\rangle^2 + (2\pi\varepsilon)^2 \; (2/\beta_V) \; ipr \; t^2 \; + \mathcal{O}(\varepsilon^4) \; . \tag{131}$$

Here $ipr = \sum_\nu |\langle E_\nu|\Psi\rangle|^4$ indicates the *inverse participation ratio* of the initial state expanded in the eigenbasis of H_0. This equation displays two extreme effects: On the one hand it shows the self-averaging properties of this system. For states with a large spectral span in H_0 the correction term that marks the difference between $\langle F_\varepsilon(t)\rangle$ and $|\langle f_\varepsilon(t)\rangle|^2$ goes to zero as the inverse participation ratio becomes small ($\sim 1/N$), see also Eq. (46) for the difference between the average fidelity amplitude and the average fidelity. On the other hand, for an eigenstate of H_0, $ipr = 1$, and hence the quadratic term in Eq. (131) disappears. Moreover, the

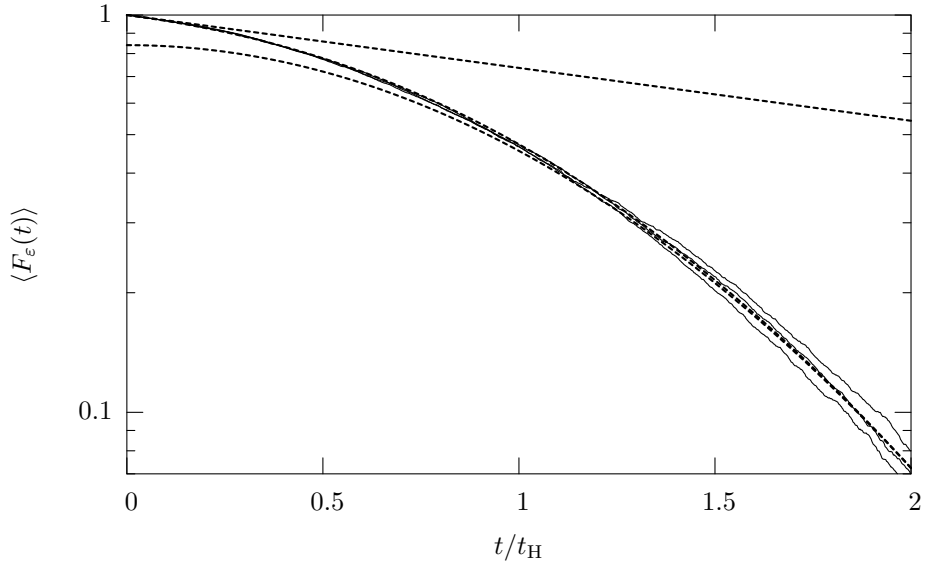

Fig. 12. Simulation of fidelity decay for a dynamical model (the desymmetrized kicked rotor) in the cross-over regime. The three thin solid lines show the result of the simulation (for three different initial conditions), the dashed line the corresponding exponentiated linear response approximation. An additional dashed line shows the exponential part, another one the Gaussian part of that approximation (for details see text). The Heisenberg time is $t_{\rm H} = 1000$.

correlations cancel the linear term after the Heisenberg time. Thus, we find that after Heisenberg time the decay stops for an H_0 taken from a GUE and continues only logarithmically for a GOE [52]. That situation is very similar to the quantum freeze considered in Section 4.3.

Situations involving states with a small spectral span have been analyzed in Ref. [145]. There fidelity decay has been computed for two perturbed Hamiltonians H_ε and $H_{-\varepsilon}$, with perturbations of opposite sign. Under these circumstances, it has been found that the evolving states have maximal overlap for different evolution times. Note that by construction, the Heisenberg times are the same for both evolutions, in distinction to the cases we discuss in the Sections 2.1.3 and 9.2.

We illustrate the above results with the help of dynamical models, the kicked rotor and the kicked top (see Appendix B.1). We show cases, where the time-reversal symmetry is conserved (by both the unperturbed Hamiltonian H_0 and the perturbation V), and other cases, where the time-reversal symmetry is broken (again by both, H_0 and V). The former corresponds to a GOE spectrum, perturbed by a GOE matrix, the latter to a GUE spectrum, perturbed by a GUE matrix.

In Fig. 12 we show fidelity decay in the cross-over regime. The numerical calculations have been carried out by D. F. Martinez [146]. The quantum propagator for the kicked rotor is constructed in position space, such that the Floquet matrix is symmetric [147]. However, we changed the kick potential from $\cos\varphi$ to $\cos\varphi - \sin 2\varphi$ in order to break the reflection symmetry. That assures that the time reversal symmetry is the only remaining symmetry in the system. The perturbation is implemented by a small increment of the kicking strength K, which has been chosen in the regime of complete chaos $K \approx 10$. The perturbation strength $2\pi\varepsilon \approx 0.554$ has been computed from the integrated classical correlation function, $\sigma_{\rm cl}$ as explained in Section 3.1. Thus, in the comparison of theory and numerical experiment, there is no free parameter. We plot three curves, for different initial states. Those were coherent (Gaussian) wave packets located at arbitrarily chosen positions on the $p = 1/2$ axis in phase space. In this way, the initial states have real coefficients in the position basis. The additional dashed lines are just to guide the eye, as to the validity of the Fermi golden rule and the perturbative expressions, respectively.

To check explicitly the scaling in the perturbation strength we finally perform simulations with the kicked top (Appendix B.1). Numerical results for time-reversal invariant kicked top with $S = 400$ (propagator (B.1)) and perturbations ranging over a whole set of kicked top perturbation strengths $\varepsilon_{\rm KT} = 10^{-6}$ to $\varepsilon_{\rm KT} = 10^{-2}$ are shown in Fig. 13. The RMT perturbation parameter ε is given in terms of "physical" kicked top

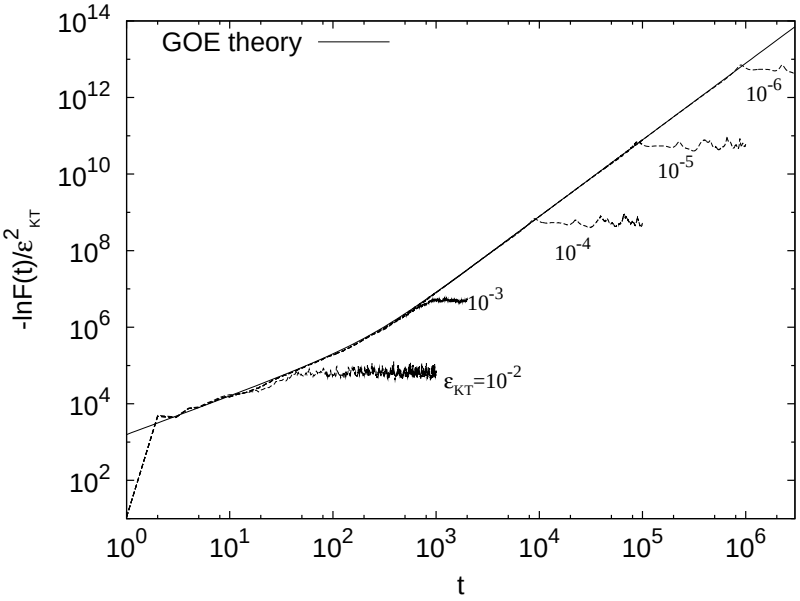

Fig. 13. The scaled logarithm of the fidelity as a function of time for a time-reversal invariant kicked top. The quantity is chosen such that different perturbation strengths ε give the same theoretical curve (solid line), based on the Eq. (130). The crossover between the exponential (Fermi golden rule regime) and Gaussian decay (perturbative regime) occurs around the Heisenberg time $t_{\mathrm{H}} = 400$. The numerical data for different perturbation strengths are shown by dashed curves.

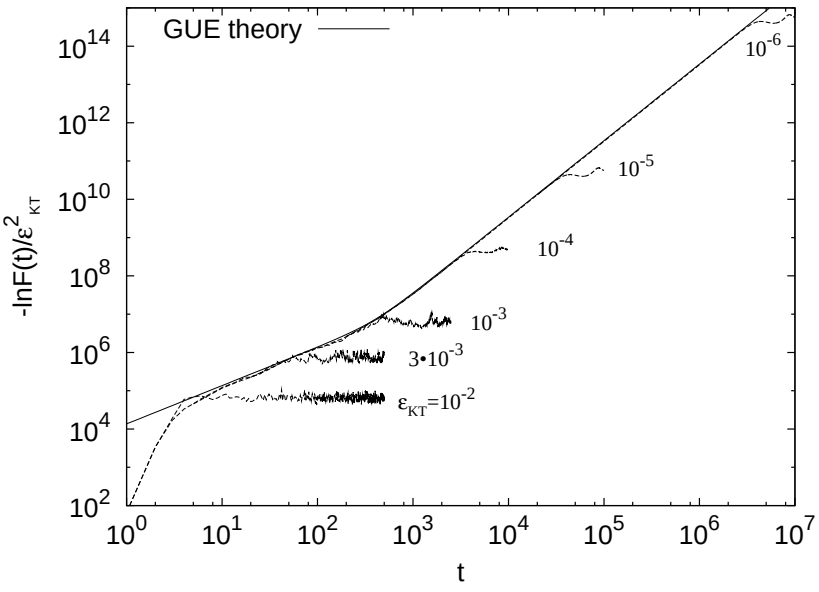

Fig. 14. The scaled logarithm of the fidelity as a function of time for a kicked top, with broken time-reversal invariance (similar graph, as in Fig. 13). The theoretical curve (solid line) is based on the Eq. (130), with $\beta_V = 2$ and $b_2(t)$ describing GUE level fluctuations. The Heisenberg time is $t_H = 400$. The numerical data for different perturbation strengths are shown by dashed curves.

perturbation $\varepsilon_{\mathrm{KT}}$ (written simply as ε in propagators in Appendix B.1) as $2\pi\varepsilon = S\varepsilon_{\mathrm{KT}}\sqrt{2\sigma_{\mathrm{cl}}\mathcal{N}}$, resulting in $2\pi\varepsilon$ ranging from 7.9 to $7.9 \cdot 10^{-4}$ for the shown $\varepsilon_{\mathrm{KT}}$, see also Section 4.3.4 for further details on obtaining ε from $\varepsilon_{\mathrm{KT}}$. Plotting $-{\varepsilon_{\mathrm{KT}}}^{-2} \ln F_\varepsilon(t)$ versus t on a double-log scale has the consequence that all curves should follow a single line given by Eq. (130). However, the numerical results deviate at the very end

and the very beginning. Differences for long times are due to the scaling, since the saturation value of fidelity does actually not depend on ε. At short times the individual properties of the dynamical system show up, and short periodic orbits give the expected non-universal contributions. Figure 13 shows that for most perturbations considered, the exponentiated linear response expression fits very well and explains the transition from linear to quadratic behavior. The strongest perturbation is the exception. Here saturation sets in before non-generic effects have died out, without leaving any space for generic RMT behavior.

To complete the picture, we show in Fig. 14 a similar calculation for a kicked top which breaks the time-reversal symmetry (Appendix B.1, Eq. (B.14)) and spin size $S = 200$. It corresponds to the random matrix model (126), where both parts, H_0 and V are chosen from a GUE. Again we see essentially the same features as in Fig. 13. The comparison with the exponentiated linear response formula shows similar agreement as for the GOE case.

4.2. *Supersymmetry calculation for the fidelity amplitude*

The exponentiated linear response formula (130) agrees very well with dynamical models as we have seen above, and as it has been reported in the literature [52,148]. It also agrees with experiments [69,70,83] on which we shall report in Section 9.2. Nevertheless it is quite clear, that this approach is not justified for perturbations stronger than one, even if we omit the fact, that the exponentiation is only heuristically justified. In the last twenty years many problems in RMT have been solved exactly, and indeed recently Stöckmann and Schäfer [56,55] have solved the model given in Eq. (126) exactly, for GOE or GUE matrices, in the limit of infinite dimensions.

More specifically, they choose H_0 and V independently but both either from the GOE or the GUE, and compute the fidelity amplitude $\langle f_\varepsilon(t)\rangle$ with the help of supersymmetry techniques. A detailed discussion would not be adequate in this review, and we refer to [149] for an introduction to the techniques used and to the original paper [56] for details. They obtain

$$\langle f_\varepsilon(t)\rangle = \frac{1}{t}\int_0^{\min(t,1)} \mathrm{d}u\ (1+t-2u)\ \mathrm{e}^{-(2\pi\varepsilon)^2\,(1+t-2u)\,t/2} \tag{132}$$

for the GUE case and

$$\langle f_\varepsilon(t)\rangle = 2\int_{\max(0,t-1)}^{t} \mathrm{d}u \int_0^u \mathrm{d}v\ \frac{(t-u)(1-t+u)\,v\,((2u+1)\,t-t^2+v^2)}{(t^2-v^2)^2\,\sqrt{(u^2-v^2)((u+1)^2-v^2)}} \times \mathrm{e}^{-(2\pi\varepsilon)^2\,[(2u+1)\,t-t^2+v^2]/2}\ . \tag{133}$$

for the GOE case. These solutions are valid for arbitrary but fixed perturbation strength, in the limit $N \to \infty$.

In Fig. 15, we reproduce two graphs from [56]. The left one, compares the exact and the exponentiated linear response result for $\langle f_\varepsilon(t)\rangle$ for the GOE case. For large perturbations we see there a qualitative difference in the shape of fidelity decay as a shoulder is forming in the exact results. For even stronger perturbations depicted on the right hand side, this becomes notorious as a revival appears at Heisenberg time. Yet, the revival is noticeable only for very small fidelities of the order of 10^{-4} for the GUE and 10^{-6} for the GOE. In all cases agreement with the exponentiated linear response formula is limited to $\langle f(t)\rangle \gtrsim 0.1$. It is thus adequate for most applications, and indeed it was difficult to come up with a dynamical model which can show the revival.

Naturally the random matrix model does not capture the Lyapunov regime, which depends on semi-classical properties. Yet it is not obvious that such a regime always exists. For example for a kicked spin chain we have never discovered this regime, and it may well be that there is no semi-classical regime for this system. This dynamical model has been used [150], to illustrate the partial revival, as shown in Fig. 15. The authors used a multiply kicked Ising spin chain in a Hilbert space spanned by 20 spins, and averaged only over a few initial conditions. The aim was to obtain the partial revival with as little averaging as possible, relying on the self-averaging properties of the fidelity amplitude. It has been checked that the model shows random matrix behavior as far as its spectral statistics is concerned. The result for the decay of the fidelity

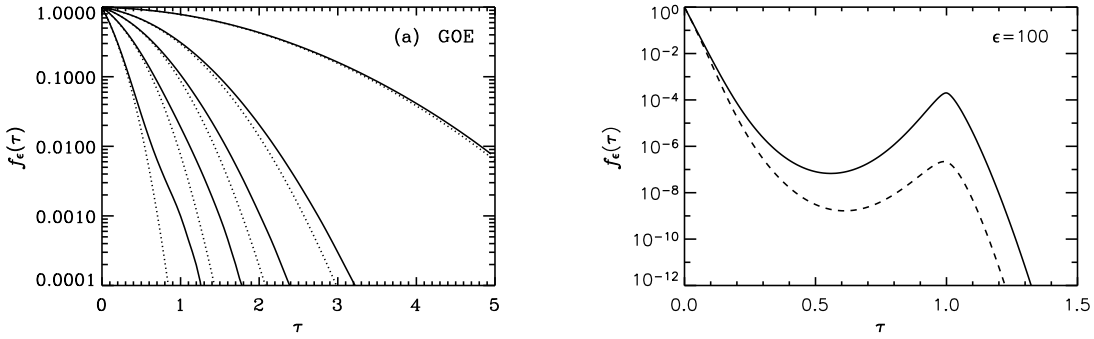

Fig. 15. Fidelity amplitude decay for the random matrix model, defined in Eq. (126) (taken from [56]). Part (a) shows $\langle f_\varepsilon(t)\rangle$ for the GOE case, as obtained from the exact expression, Eq. (133), (solid lines), together with the same quantity, as obtained from the exponentiated linear response result, Eq (130) (dashed lines). The perturbation strength has been set to the following values: $(2\pi\,\varepsilon)^2 = 0.2,\ 1\,,2\,,4$ and 10. Part (b) shows $\langle f_\varepsilon(t)\rangle$ with $(2\pi\,\varepsilon)^2 = 100$ for the GUE case (solid line) and the GOE case (dashed line), as obtained from the exact expressions, Eqs. (132) and (133), respectively.

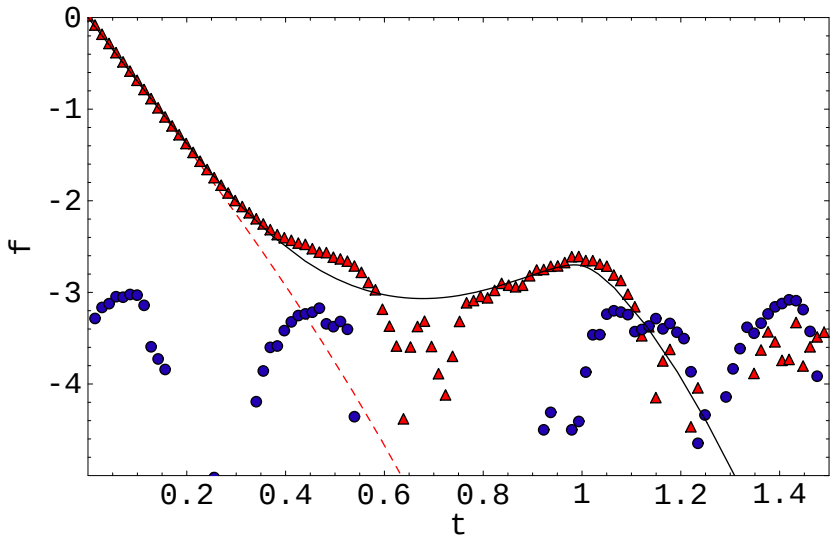

Fig. 16. The decay of the fidelity amplitude in a dynamical system, in the case of broken time-reversal symmetry, in a regime where the partial revival is observable (taken from Ref. [150]). More precisely, $\log_{10}\langle f(t)\rangle$ is plotted. The triangles show the real part of the fidelity amplitude as obtained from the numerical simulation; the circles show the imaginary part, which goes to zero as $1/\sqrt{N}$ due to state averaging. The perturbation strength is $(2\pi\varepsilon)^2 = 31.78$. The solid line shows the exact theoretical result, Eq. (132), the dashed line shows the exponentiated linear response result, Eq. (130).

amplitude is reproduced in Fig. 16. Yet it will probably be difficult to see this effect in an experiment, and we do not know how it may appear in a dynamical system which does display Lyapunov decay at times short compared to the Heisenberg time.

The partial revival of the fidelity amplitude occurs not only in the case of a full GOE (GUE) perturbation as discussed here, but also in the case of a perturbation with vanishing diagonal elements (see Section 4.3, below). In [55] the partial revival has been explained with an analogy to the Debye-Waller factor. A direct, semiclassical and hence dynamical explanation could be obtained by periodic orbit expansions similar to [151,152] (for general chaotic systems) or [153] (for a quantum graph model).

4.3. *Quantum freeze*

In Section 4.1, we found that after the Heisenberg time, fidelity decay is essentially Gaussian [*cf.* discussion below Eq. (130)]. It is determined by the diagonal elements, *i.e.* the time average of the perturbation (in the interaction picture). If this term is zero or very small, we should see a considerable slowing down of fidelity decay. That such a possibility exists in principle was first noted in [16] for integrable systems (see Section 5.3) and in [17] for chaotic systems, as described in Section 3.2. However, in both cases the perturbation was chosen to depend in a very particular way on the unperturbed Hamiltonian, with the effect that fidelity became largely independent of the dynamics in the unperturbed system. We shall discuss that particular choice in the context of RMT at the end of this subsection.

Here we shall mainly consider situations where the perturbation is some RMT matrix with zero diagonal. In the notation of Section 2.2, it means that the off diagonal elements will form the residual interaction $V_{\rm res} = V$. The different options to implement such a scenario have been discussed in Section 2.2. We concentrate here on the case, where H_0 is chosen from a GOE and V is an antisymmetric hermitian random Gaussian matrix. This case is of interest, because it is the only random matrix model, so far, for which an exact analytical result has been obtained [18,137]. We shall show these below, yet we shall mainly concentrate on an extension of the previous linear response treatment, as well as an approach based on second order (time independent) perturbation theory. These approaches give more insight into the mechanism, and they are more easily generalized to other interesting cases. Indeed we shall again find a plateau in fidelity decay, which will be flat if H_0 is chosen from a GUE and almost flat (up to logarithmic corrections) if it is chosen from the GOE. This plateau begins at Heisenberg time, and we are able to describe the decay to the plateau and the plateau itself in terms of the linear response results. The finally ensuing decay is obtained from second order perturbation theory. A brief description of some of these results can be found in [18].

4.3.1. *Linear response approximation*

In linear response, we have seen that the expectation value $\langle V_{ij}\, V_{kl}\rangle$ is the essential ingredient for the calculation of fidelity. We can compute this average with equal ease for the following three ensembles of perturbations: (a) If V is taken from a GOE with deleted diagonal, *i.e.* $\langle V_{ij}\, V_{kl}\rangle = (\delta_{ik}\delta_{jl} + \delta_{il}\delta_{jk})(1-\delta_{ij})$, then we find

$$\langle V_{ik}\, V_{kj}\rangle = (\delta_{ik}\delta_{kj} + \delta_{ij})(1-\delta_{ik}) = \delta_{ij}\,(1-\delta_{ik})\;. \tag{134}$$

(b) If V is taken from a GUE with deleted diagonal, *i.e.* $\langle V_{ij}\, V_{kl}\rangle = \delta_{il}\delta_{jk}\,(1-\delta_{ij})$ then we just obtain the same result for $\langle V_{ik}V_{kj}\rangle$. Thus, in both cases, we obtain:

$$\langle \tilde V(\tau)\,\tilde V(\tau')\rangle_{ij} = \sum_k {\rm e}^{2\pi{\rm i}\,(E_i-E_k)\,\tau}\;\; {\rm e}^{2\pi{\rm i}\,(E_k-E_j)\,\tau'}\;\; \delta_{ij}\,(1-\delta_{ik}) = \delta_{ij}\sum_{k\neq i} {\rm e}^{2\pi{\rm i}\,(E_i-E_k)\,(\tau-\tau')}\;\;. \tag{135}$$

(c) If V is taken from an ensemble of imaginary antisymmetric matrices we may write

$$V = {\rm i}\,A \qquad \langle A_{ij}\, A_{kl}\rangle = \delta_{ik}\delta_{jl} - \delta_{il}\delta_{kj}\;. \tag{136}$$

This yields

$$\langle \tilde V(\tau)\,\tilde V(\tau')\rangle_{ij} = -\sum_k {\rm e}^{2\pi{\rm i}\,(E_i-E_k)\,\tau}\;\; {\rm e}^{2\pi{\rm i}\,(E_k-E_j)\,\tau'}\;\; (\delta_{ik}\delta_{kj} - \delta_{ij}) = \delta_{ij}\sum_{k\neq i} {\rm e}^{2\pi{\rm i}\,(E_i-E_k)\,(\tau-\tau')}\;\;. \tag{137}$$

In all three cases, we obtain the same result, which is in fact quite similar to the cases without deleted diagonal considered in Section 4.1. If we write the sum of exponentials in terms of the spectral two-point correlation function (as it has been done in Eq. (129), we obtain

$$\langle f_\varepsilon(t)\rangle = 1 - (2\pi\varepsilon)^2\left[t/2 - \int_0^t d\tau' \int_0^{\tau'} d\tau\; b_2(\tau)\right] + \mathcal{O}(\varepsilon^4)\;. \tag{138}$$

Comparing this expression to Eq. (129), we note that the t^2-term is missing. This has the peculiar consequence that the characteristics of V [*i.e.* whether we consider case (a), (b), or (c)] have no effect on the linear response result. It solely depends on the spectral statistics of H_0, encoded in the two-point form factor

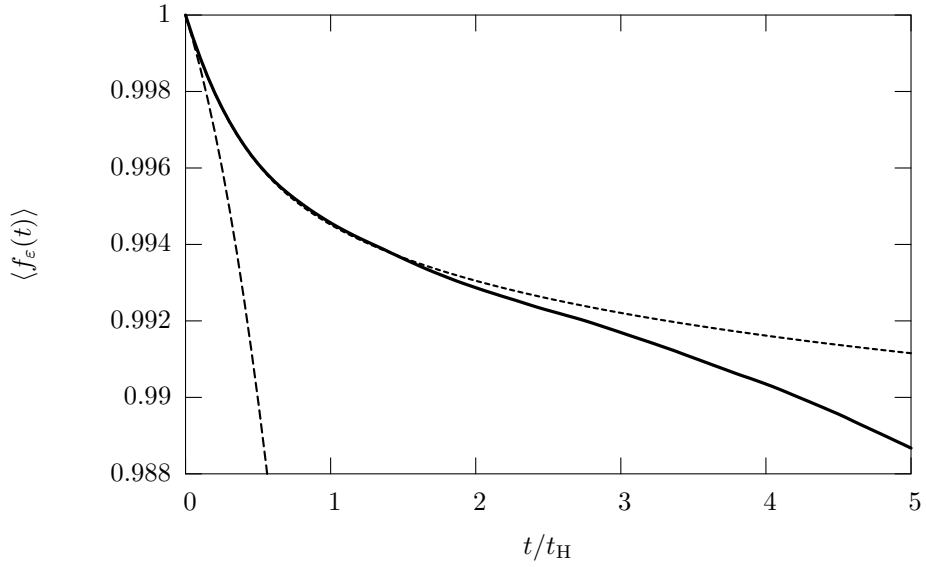

Fig. 17. Numerical simulation of fidelity amplitude decay for a GOE spectrum perturbed with a GOE matrix with deleted diagonal. The perturbation strength was $\varepsilon = 0.025$ (for further details, see text). The thick solid line shows the result of the simulation, the short dashed line shows the linear response result, Eq. (138). The long dashed line shows the linear response result for an ordinary GOE perturbation.

b_2. If we deal with an H_0 taken from a GUE then the decay will stop at Heisenberg time, while for one selected from a GOE we will have a very slow decay, determined by the logarithmic behavior of b_2. We can get explicit formulae for the freeze after Heisenberg time. Evaluating the integral in Eq. (138) for GOE and GUE cases, we get for times $t > t_{\rm H}$,

$$\begin{aligned} \langle f_\varepsilon(t)\rangle &= 1 - (2\pi\varepsilon)^2 \frac{\log(2t)+2}{12} + \mathcal{O}(\varepsilon^4) \quad : \quad \text{GOE} \\ \langle f_\varepsilon(t)\rangle &= 1 - (2\pi\varepsilon)^2 \frac{1}{6} + \mathcal{O}(\varepsilon^4) \quad : \quad \text{GUE}\,. \end{aligned} \tag{139}$$

We can see the time independence for systems without time-reversal symmetry, while for time-reversal invariant systems freezing is not perfect as the plateau value decreases logarithmically, *i.e.* very slowly with time. These predictions are illustrated and compared to simulations for a dynamical model in Figs. 22 and 23 in Section 4.3.4.

In Appendix E we show that the Born series can be computed to fourth order and estimates of higher orders can be given in the limit of large N. This is done both for case (a) and case (c), and again the results agree. By consequence, any difference between the two kinds of perturbations must be of strictly non-perturbative type. That is also confirmed by numerics and thus in Fig. 17, we only show case (a), *i. e.* we give, for a GOE Hamiltonian perturbed by a GOE with deleted diagonal, a comparison of the above formula with a Monte Carlo simulation of the random matrix model. Here we used just a linear rescaling of the unperturbed spectrum to obtain unit average level spacing in the center. Therefore we used rather large matrices of dimension $N = 400$, and random initial states with small spectral span (over the 20 central eigenstates of H_0). With an ensemble of $n_{\rm run} = 2000$, we obtained for the fidelity amplitude the thick solid curve. The linear response approximation, Eq. (138) is plotted by a thin short-dashed line. The agreement is rather good up to $2\,t_{\rm H}$. From then on, we find increasing deviations. This point of departure from the linear response approximation can be moved towards larger times, by decreasing the perturbation strength further. A strict plateau cannot be observed due to the remaining logarithmic decay of the linear response result. The great gain in fidelity can be appreciated by comparing to the decay of the fidelity amplitude for an ordinary GOE perturbation (long-dashed line).

Note that this derivation does not depend in any way on the time averaged perturbation being identically

zero. Rather we use the fact that diagonal and off diagonal elements enter independently, the former influencing the t^2-term in Eq. (129) only. We can therefore equally well deal with diagonal elements which are simply suppressed by a constant factor. That factor would lead to a corresponding suppression of the above mentioned quadratic term. This opens a new range of applications which will have to be considered in the future.

4.3.2. *Beyond fidelity freeze*

Higher order terms in ε will cause an end of the freeze, and we shall use time-independent perturbation theory to describe this phenomenon. Recall that in the case of a standard perturbation such considerations lead to quadratic decay setting in around Heisenberg time [44,45]. It is precisely the absence of this term in the present situation that is responsible for the freeze. Here, we consider the case, where the second order term is needed, e.g. due to the unusually small or vanishing diagonal elements in the perturbation matrix.

In a formally exact manner, the fidelity amplitude can be written in terms of the eigenvalues of the perturbed and the unperturbed system, and the orthogonal transformation between their respective eigenbases (40):

$$f(t) = \sum_{\alpha\beta} \Psi_\alpha^* \Psi_\beta \, \mathrm{e}^{2\pi \mathrm{i}\, E_\alpha \, t} \; O_{\alpha\beta} \; \mathrm{e}^{-2\pi \mathrm{i}\, \tilde{E}_\beta \, t} \; O_{\alpha\beta} \quad . \tag{140}$$

We assume random initial states Ψ with well defined local density of states (in the eigenbasis of H_0). The spectrum of H_0 is denoted by $\{E_\alpha\}$, while the spectrum of H_ε is denoted by $\{\tilde{E}_\alpha\}$. For times which are long compared to the Heisenberg time, we may neglect phases from energies of different states due to phase randomization. This amounts to approximate the above sum by its diagonal contribution $\alpha = \beta$ as

$$f(t) = \sum_{\alpha} |\Psi_\alpha|^2 \; O_{\alpha\alpha}^2 \; \mathrm{e}^{-2\pi \mathrm{i}\, \Delta_\alpha \, t} \qquad \Delta_\alpha = E_\alpha - \tilde{E}_\alpha \; . \tag{141}$$

Finally, we may assume a sufficiently small perturbation, such that $O_{\alpha\alpha}^2$ may be set equal to one. [6] This leads to

$$f(t) \approx \sum_{\alpha} |\Psi_\alpha|^2 \; \left\langle \mathrm{e}^{-2\pi \mathrm{i}\, \Delta_\alpha \, t} \right\rangle \; . \tag{142}$$

In second order perturbation theory, the level shifts Δ_α are given by

$$\Delta_\alpha = \varepsilon V_{\alpha\alpha} + \varepsilon^2 \sum_{\gamma \neq \alpha} \frac{|V_{\alpha\gamma}|^2}{E_\alpha - E_\gamma} + \mathcal{O}(\varepsilon^3) \; . \tag{143}$$

The first order term, containing the diagonal elements of V, is statistically independent from the second order term. As a consequence, the ensemble average inside the sum factorizes into a purely Gaussian decay and a factor which corresponds to the quantum freeze situation

$$f(t) \approx \sum_{\alpha} |\Psi_\alpha|^2 \; \left\langle \mathrm{e}^{-2\pi \mathrm{i}\, \varepsilon V_{\alpha\alpha} \, t} \right\rangle \; \langle S_\tau(E_\alpha) \rangle \qquad S_\tau(E_\alpha) = \left. \mathrm{e}^{-\mathrm{i}\tau \sum_{\gamma > 1} |V_{1\gamma}|^2/(E_1 - E_\gamma)} \right|_{E_1 = E_\alpha} \; , \tag{144}$$

where $\tau = 2\pi\, \varepsilon^2 \, t$. The above construction allows to treat the energy argument in $\langle S_\tau(E) \rangle$ as a free variable. For the following, we discard the exponential which contains the diagonal matrix elements of V (it usually factors out, anyway). In addition we assume that in the eigenbasis of H_0, the initial state has non-zero coefficients only in a narrow region in the center of the spectrum. That allows to remove the sum, and consider $\langle S_\tau(E) \rangle$ at the energy $E = 0$. More general cases can be considered, but require to replace the sum over α by a convolution-type integral. For $E \neq 0$, $\langle S_\tau(E) \rangle$ can be reduced to $\langle S_\tau(0) \rangle$, by employing a principal value integral to express the smooth part of the sum in the exponent.

We thus consider initial states, such that $\langle f_\varepsilon(t) \rangle \approx \langle S_\tau(0) \rangle$. Then, the decay of the fidelity amplitude only depends on the spectral correlations of the ensembles considered. It involves the level curvature $\kappa =$

[6] A more phenomenological assumption of statistically independent eigenvectors and eigenvalues, which would allow to pull the average $\langle O_{\alpha\alpha}^2 \rangle$ out of the sum, does not prove very useful, if compared to the exact analytical result [18].

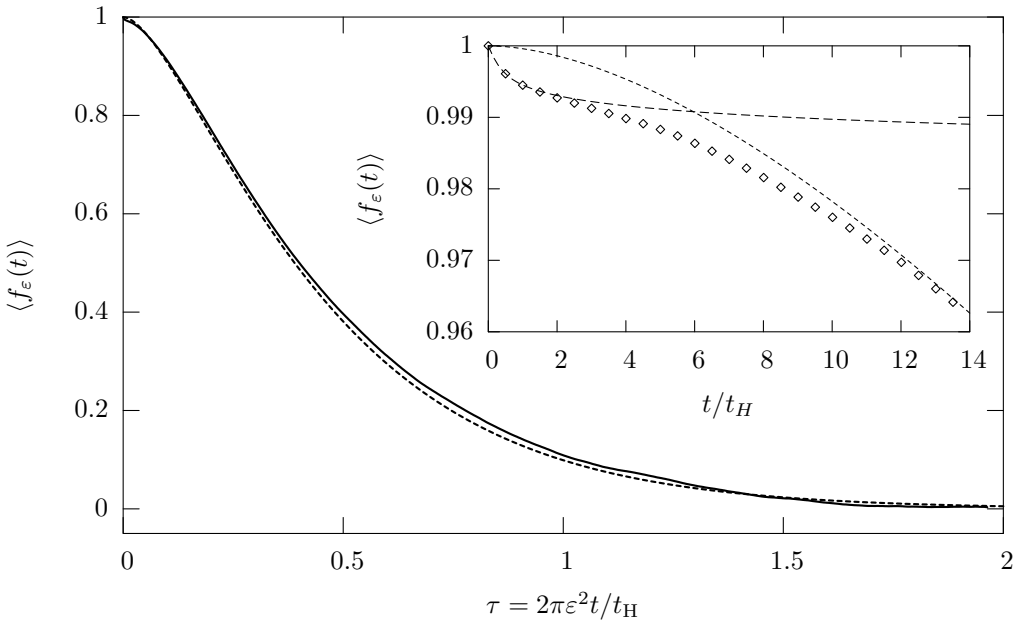

Fig. 18. Numerical simulation of the fidelity amplitude decay for a GOE spectrum perturbed with a GOE matrix with deleted diagonal. The perturbation strength and all other parameters were chosen as in Fig. 17. The thick solid line shows the result of the simulation, the short dashed line shows the result from perturbation theory, Eq. (146) with $\beta = 1$. In the inset, we show the transition from linear response (long dashed line) to time independent perturbation theory (short dashed line). The numerical data are plotted with diamonds.

$\sum_{\gamma>1}^{N} |V_{1\gamma}|^2/E_\gamma - E_1$, which has been studied in some detail in the literature (see Ref. [154–156] and references therein). Using a closed form of the distribution of κ it is a simple exercise to compute $\langle f_\varepsilon(t)\rangle$:

$$\mathcal{P}(\kappa) = \frac{C_\beta}{(\kappa^2+\pi^2)^{1+\beta/2}} \quad : \quad \langle S_\tau(0)\rangle = C_\beta \int \mathrm{d}\kappa \, \frac{\cos\,\tau\kappa}{(\kappa^2+\pi^2)^{1+\beta/2}} \qquad \tau = 2\pi\varepsilon^2\, t\;, \tag{145}$$

where C_β assures proper normalization of $\mathcal{P}(\kappa)$. The cosine integral in Eq. (145) gives

$$\langle f_\varepsilon(t)\rangle \approx \langle S_\tau(0)\rangle = \begin{cases} \mathrm{e}^{-\pi\tau}\;(1+\pi\tau) & : \beta = 2 \\ \pi\tau\; K_1(\pi\tau) & : \beta = 1 \\ \mathrm{e}^{-\pi\tau} & : \beta = 0 \end{cases}, \tag{146}$$

where $K_1(z)$ is the modified Bessel function [157]. The resulting $f_\varepsilon(t)$ gives the decay of fidelity (within the second order perturbative approximation) after the freeze plateau. Note that the decay time scales as $1/\varepsilon^2$ as opposed to $1/\varepsilon$ in the absence of the freeze. In all cases, we assume H_0 to be diagonal. The case $\beta = 2$ describes a GUE spectrum perturbed by a GUE matrix V, with deleted diagonal. It means that the moduli squared $|V_{1\gamma}|^2$ in Eq. (144) have an exponential distribution. The case $\beta = 1$ describes a GOE spectrum perturbed by a GOE matrix, with deleted diagonal. In that case, the moduli squared $|V_{1\gamma}|^2$ have a Porter-Thomas distribution [158]. This perturbation is equivalent to an antisymmetric imaginary random Gaussian matrix. This perturbation has been treated exactly using supersymmetry techniques [18,137]. The last case $\beta = 0$ describes a spectrum with uncorrelated eigenvalues, while V is chosen as in the $\beta = 1$ case. That case has not been considered in [156]. It fits rather accidentally to the formula (145) for $\mathcal{P}(\kappa)$, when setting $\beta = 0$. We include that case, in order to get a more complete overview on the effects of level repulsion on the decay of the fidelity amplitude in the quantum freeze situation. The fact that a spectrum without correlations gives indeed an exponential decay, can be easily checked by direct evaluation of the separable average [159]. Furthermore, one finds that this result only depends on the average of the matrix element $|V_{1\gamma}|^2$, and not on its distribution.

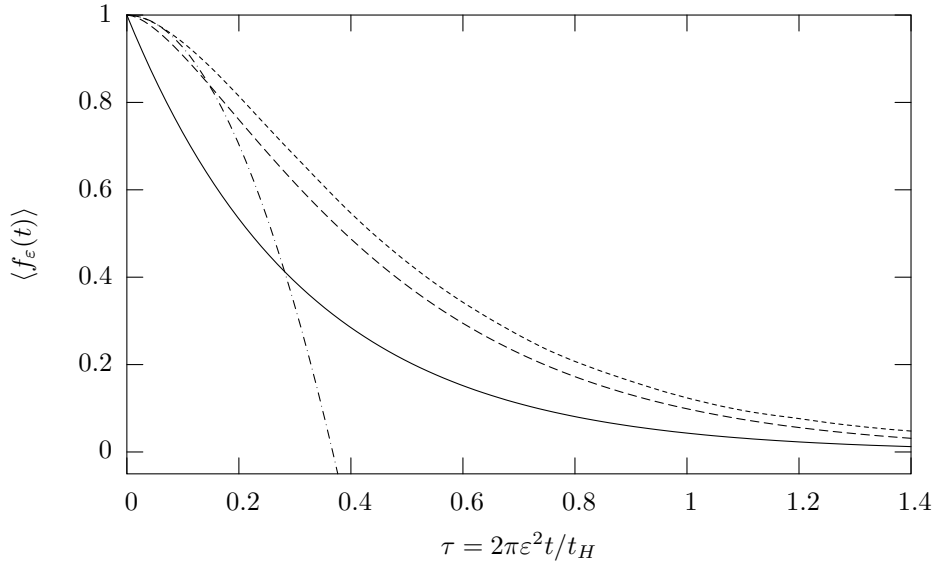

Fig. 19. Numerical simulation of fidelity amplitude decay for different random spectra, perturbed with a GOE matrix with deleted diagonal. For the GOE (long-dashed line) and the Poisson spectrum (solid line) we show the analytical results of Eq. (146). For the GUE spectrum we show a numerical simulation (short-dashed line) and the leading order quadratic behavior (dash-dotted line). For additional details, see text.

In Fig. 18 we show the decay of the fidelity amplitude for a GOE spectrum, perturbed by a GOE matrix with deleted diagonal. The perturbation strength $\varepsilon = 0.025$ and the other parameters are exactly the same as in Fig. 17; but here we show the long time behavior (main graph). The figure shows that our perturbation theory provides a very accurate description of the data. In the inset we focus on smaller times, where the transition from the linear response regime to the perturbative regime can be observed. For the GUE case ($\beta = 2$) and the Poisson case ($\beta = 0$) we obtain similar agreement.

The effect of spectral correlations (level repulsion) In view of Eq. (143), it is clear that level repulsion plays a crucial role for the behavior of the fidelity amplitude. The degree of level repulsion determines whether the level curvature $\kappa = \sum_{\gamma>1}^{N} |V_{1\gamma}|^2/E_\gamma$, has a finite second moment, or not. If it has, we may expand $S_\tau(0)$ in angular brackets in Eq. (144) up to the quadratic term, and average term by term. That would give

$$f_0(E,t) \sim 1 - \frac{\tau^2}{2}\,\langle\kappa^2\rangle\,. \tag{147}$$

It is not difficult to see that $\langle\kappa^2\rangle$ is finite for the GUE spectrum, only. For a GOE spectrum, or a Poisson spectrum (without correlations) that average diverges. Equation (147) will be used below to consider the case of a GUE spectrum perturbed by a GOE matrix with deleted diagonal.

The small time behavior of the fidelity amplitude can be obtained from the exact results, Eq. (146). Here, small time really means small τ; the time t should still be much larger than the Heisenberg time. The corresponding asymptotic expansions yield to lowest order

$$\langle f_\varepsilon(t)\rangle \sim \begin{cases} 1-\pi^2\tau^2/2 & : \text{GUE} \\ 1-\dfrac{1}{2}\left(-\ln(\pi\tau)+\dfrac{1}{2}+\ln 2-\gamma\right)\,\pi^2\tau^2 & : \text{GOE} \\ 1-\pi\tau & : \text{Poisson} \end{cases}, \tag{148}$$

where γ is Euler's gamma constant [157]. These expansions demonstrate that in the GOE and the Poisson case, the second moment of the level curvature κ do not exist.

In Fig. 19, we illustrate the effect of level correlations on the decay of the fidelity amplitude, in the presence of a GOE perturbation (with deleted diagonal). For the GOE and the uncorrelated spectrum, the

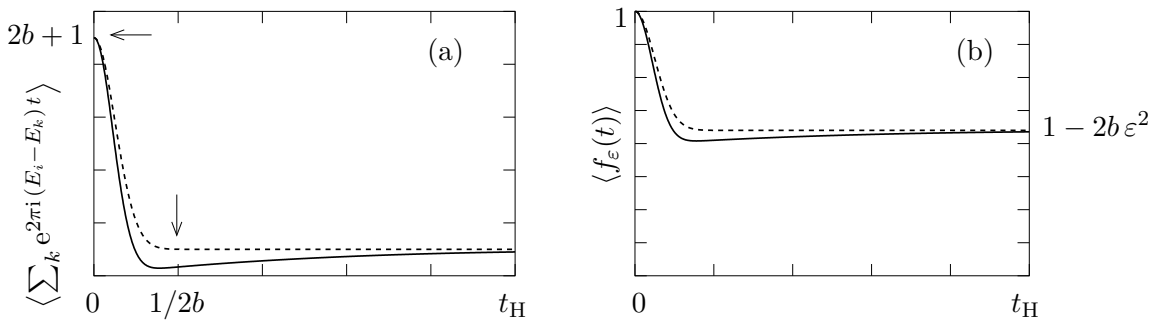

Fig. 20. Schematic behavior of the fidelity amplitude [panel (b)] and the two-point correlations [panel (a)], which are the determining quantities for that behavior (see text for details). For the purpose of illustration, we assume a small band width. The solid lines show the results for a GOE spectrum, the dashed lines that for an uncorrelated (Poisson) spectrum.

curves shown are just the analytical results given in Eq. (146). For the GUE spectrum, there is no complete analytical result available (note that it is a rather artificial situation), and we therefore show an actually quite accurate [7] numerical simulation. The Poisson spectrum has no correlations at all, and by consequence the decay of the fidelity amplitude is the fastest. From $\tau = 0$ it starts of linearly. Next comes the GOE spectrum, with linear level repulsion, and therefore much slower decay $\langle f(t) \rangle$. The GUE spectrum gives leads to the slowest decay of the fidelity amplitude. It is the only case, where the $\langle f(t) \rangle$ behaves quadratically for small τ. The corresponding coefficient will be calculated below; the resulting quadratic decay is plotted with a dash-dotted line.

As mentioned above, a GUE spectrum perturbed by a GOE matrix (with deleted diagonal), is a rather artificial construction. Even though, there is no complete analytical result available (in terms of the perturbation theory, developed above), we may still obtain the leading order behavior at small times. This is due to the fact that for the GUE spectrum, the level curvature has a finite second moment

$$\langle \kappa^2 \rangle = \langle |V_{1\gamma}|^4 \rangle \left\langle \sum_{\gamma=2}^{N} (E_1 - E_\gamma)^{-2} \right\rangle \Bigg|_{E_1 = 0} , \tag{149}$$

where $\langle |V_{1\gamma}|^4 \rangle = 2\,(3)$ for a GUE (GOE) perturbation. By comparison of Eq. (147) with the $\beta = 2$ case in Eq. (148) we find that $\langle f_\varepsilon(t) \rangle \sim 1 - 3\,\pi^2\,\tau^2/4$ (dash-dotted line in Fig. 19).

4.3.3. *Commutator perturbation*

Let us take a perturbation which is proportional to the commutator of a random GOE matrix W with H_0 (in order to remain Hermitean, the perturbation must be imaginary).

$$H = H_0 + \varepsilon\, V \qquad V_{kl} = \mathrm{i} W_{kl}\, (E_k - E_l)\, . \tag{150}$$

In the interaction picture, the perturbation V is equivalent to the time-derivative of W, as detailed in Section 2.2. Here, we use a banded perturbation matrix W_{kl}, and consequently also banded V_{kl}, because otherwise the limit of infinite matrix dimension $N \to \infty$ will be ill defined. It is then convenient to assume that the basis states are arranged in such a way that $E_i < E_j$ for $i < j$ (for technical convenience we also assume a non-degenerate spectrum).

Linear response The crucial quantity is the average

$$\sum_k \langle \tilde{V}_{ik}(\tau)\, \tilde{V}_{kj}(\tau') \rangle = \sum_k \mathrm{e}^{2\pi \mathrm{i}\,(E_i - E_k)\,\tau}\ \mathrm{e}^{2\pi \mathrm{i}\,(E_k - E_j)\,\tau'}\ \langle V_{ik}\, V_{kj} \rangle\, . \tag{151}$$

[7] We expect this simulation to reproduce the result of the perturbation theory exactly, within the finite linewidth in the figure. In particular, we checked that further decrease of ε or increase of N (the dimension of the Hamiltonian matrix) gives no noticeable change on the scales of the figure.

Since W is hermitian, we obtain under the above assumptions:

$$\langle \tilde{V}(\tau)\, \tilde{V}(\tau')\rangle_{ij} = \delta_{ij} \sum_k (E_i - E_k)^2\, \mathrm{e}^{2\pi \mathrm{i}\,(E_i-E_k)\,(\tau-\tau')}\, \langle |W_{ij}|^2\rangle \qquad \langle |W_{ij}|^2\rangle = \theta\big(\, b - |i-j|\,\big)\,, \tag{152}$$

where $\theta(j) = 1$ for $j \geq 0$ and $\theta(j) = 0$ otherwise. That is the simplest case of a banded matrix, but more realistic band profiles can be treated along the same lines. Inserting this into the Eq. (127) for the echo operator in the linear response approximation, we get

$$\begin{aligned}\langle M_\varepsilon(t)\rangle_{ij} &= \delta_{ij}\left[1 + \varepsilon^2 \sum_{k=\max(1,i-b)}^{\min(N,i+b)} \big(\, \mathrm{e}^{2\pi \mathrm{i}\,(E_i-E_k)\,t} - 2\pi \mathrm{i}\,(E_i - E_k)\,t - 1\,\big)\right] \\ &= \delta_{ij}\big[\,1 - \varepsilon^2\, \mathcal{C}(t)\,\big]\,. \end{aligned} \tag{153}$$

For an initial state which stays away from the border of the spectrum, the linear term averages to zero (as a spectral average). In the limit of large band-width, the remaining sum of exponential phases tend to an expression involving the two-point form factor, similar to the case of Eq. (128):

$$\sum_{k=\max(1,i-b)}^{\min(N,i+b)} \mathrm{e}^{2\pi \mathrm{i}\,(E_i-E_k)\,t} \to \delta(t) - b_2(t) + 1\,. \tag{154}$$

With that information in mind, we plot in Fig. 20 the schematic behavior of that sum for finite band width b; panel (a). The solid line shows the result for a GOE spectrum, the dashed line for the case $b_2(t) = 0$ (uncorrelated levels). The time $t = t_H/(2b)$ may be considered as the Ehrenfest time of the system. So we may say that the correlation integral $\mathcal{C}(t)$ increases from zero to some value between $2b$ and $2b+1$, within a time which is of the oder of the Ehrenfest time. Panel (b) of Fig. 20 shows the schematic behavior of the fidelity amplitude; its very fast decay to the practically constant value of $f_{\mathrm{plateau}} = 1 - 2b\,\varepsilon^2$. This shows that a commutator perturbation yields a behavior of the fidelity amplitude which is to a large extent insensitive to the particular dynamics of the unperturbed system. This is in line with the "surprising" similarities of quantum freeze between integrable and chaotic systems [16,17]. For perturbations which have a vanishing diagonal due to other reasons, the situation is different, as we have seen above.

Time independent perturbation theory As the diagonal of the perturbation V is zero, we must evaluate the eigenenergies of H in second order perturbation theory, just as in Eq. (143). For a perturbation of the form (150), the level shifts are given by

$$\Delta_\alpha = \tilde{E}_\alpha - E_\alpha = \varepsilon^2 \sum_{\gamma\neq\alpha} |W_{\alpha\beta}|^2\, (E_\alpha - E_\gamma)\,. \tag{155}$$

For this expression to be valid, the shifts in the eigenenergies must be small compared to the average level distance (which is set equal to one). For definiteness, let us consider the banded random matrix model, Eq. (153), as used in the linear response calculation. Then we obtain, from Eq. (144):

$$\langle f_\varepsilon(t)\rangle \approx \sum_\alpha |\Psi_\alpha|^2\, \left\langle e^{\mathrm{i}\tau\,\Delta_\alpha}\right\rangle \qquad \Delta_\alpha = \sum_{1\leq|\gamma-\alpha|\leq b} |W_{\alpha\beta}|^2\, (E_\alpha - E_\gamma)\,, \tag{156}$$

where $\tau = 2\pi\,\varepsilon^2\, t$. In this equation, we have assumed that the initial state stays away from the matrix borders. Then, as long as the level density remains constant, the phase average $\langle e^{\mathrm{i}\tau\,\Delta_\alpha}\rangle$ is translational invariant, and we obtain

$$\langle f_\varepsilon(t)\rangle \approx \left\langle e^{\mathrm{i}\tau\,\Delta_\alpha}\right\rangle = 1 - \frac{\tau^2}{2}\, \langle \Delta_\alpha^2\rangle + \mathcal{O}(\tau^4)\,. \tag{157}$$

In distinction to the perturbations with deleted diagonal, here the second moment of the level shifts usually exist. We find:

$$\langle \Delta_\alpha^2\rangle \approx 2\, \langle |W_{\alpha\beta}|^4\rangle \left(\int_0^b \mathrm{d}x\; x^2 + b^2/2.\right) = 2\, \langle |W_{\alpha\beta}|^4\rangle \left(\frac{b^3}{3} + \frac{b^2}{2} + \mathcal{O}(b)\right)\,. \tag{158}$$

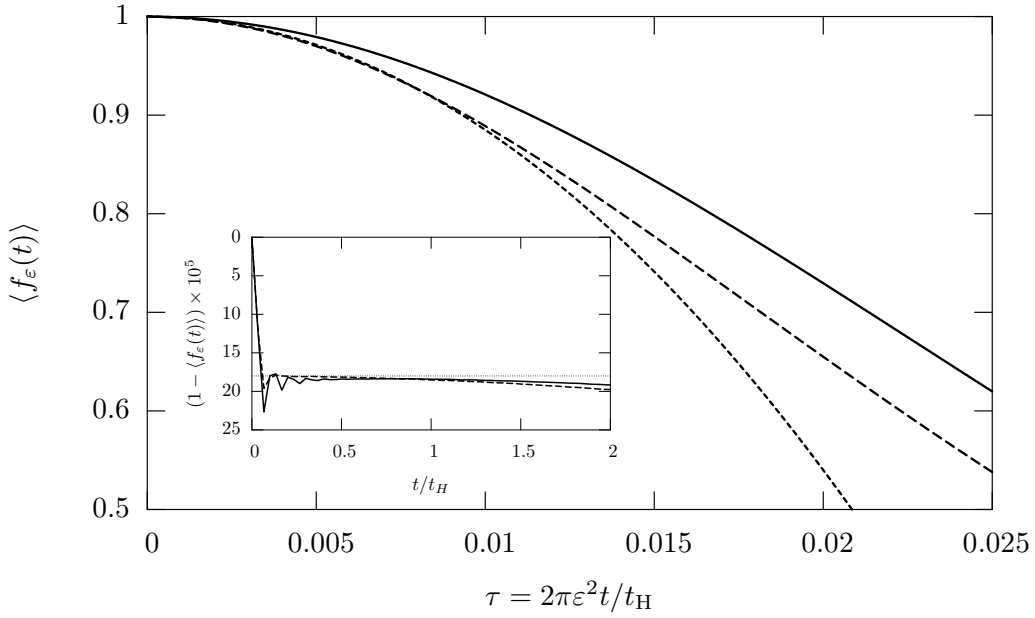

Fig. 21. The fidelity amplitude in the case of a banded commutator perturbation. The case of a GOE spectrum (solid lines) and a Poisson spectrum (long dashed lines). The theoretical expectations based on linear response ($f_{\rm plateau}$; dotted line) and second order perturbation theory (short dashed lines). The main figure shows the long time behavior, where we scaled time to coincide with τ, as used in Eq. (157). The insert shows the short time behavior for times of the order of the Heisenberg time. For details on the parameters used in the simulation, see text.

The sum over γ is here approximated with an integral. Here, we added the next leading term of the Euler-Maclaurin expansion (it amounts to the inversion of the familiar trapezoidal integration rule) [157]. Note that the b^2-term also depends on the spectral correlations. Thus, the expansion above is correct only in the case of an uncorrelated (Poisson) spectrum. For a GOE spectrum, the b^2-term must be modified.

In Fig. 21 we show the behavior of the fidelity amplitude for a banded commutator perturbation. We performed two simulations, one with a GOE spectrum and another one with a Poisson (uncorrelated) spectrum. We use a small band-width $b = 10$ to observe finite size effects in the band-width. The perturbation strength was $\varepsilon = 0.003$, and the dimension of the matrices $N = 100$. We performed an ensemble average over $n_{\rm run} = 40\,000$ realizations, and an average over $n_{\rm tr} = 50$ initial states, which were eigenstates of the unperturbed system, located in the center of the spectrum.

The main figure shows the long time behavior for both simulations, (GOE spectrum: solid line, Poisson spectrum: long dashed line) together with the theoretical expectation, Eq. (157). We find good agreement in the Poisson case, while the correlations in the GOE spectrum lead to a slower decay. As explained above, we expect the difference between correlated and uncorrelated spectra to disappear in the limit of large band-width. The insert shows the short time behavior for times of the order of the Heisenberg time. We compare the simulations with the plateau value $f_{\rm plateau}$ found from the linear response approximation. We find good agreement, and we recognize a weak influence of the two-point form factor, as explained in Fig. 20.

4.3.4. *RMT freeze in dynamical systems*

We will demonstrate the theory for fidelity freeze in RMT by a dynamical model. We again choose the kicked top. As the numerical results for a commutator type perturbations have already been presented (Figs. 7 and 8), we will focus on perturbations whith vanishing diagonal elements, either due to symmetries or due to setting them to zero by hand, see also general discussion in Section 2.2.

First we are going to discuss unperturbed system with time reversal symmetry, therefore corresponding to GOE theory (COE for a kicked system). For this we take a symmetrized chaotic kicked top $U_\varepsilon^{\rm sym}$ given in Appendix B, Eq. (B.12). Because the perturbation for $U_\varepsilon^{\rm sym}$ is complex antisymmetric (in the eigenbasis

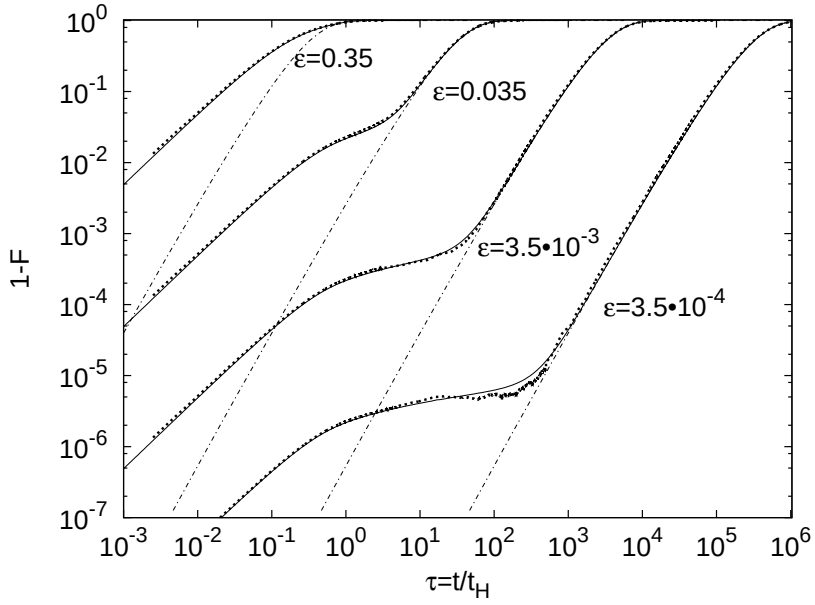

Fig. 22. Log-freeze in a kicked top, GOE case, the same data as in [18]. The solid line shows the exact result obtained by supersymmetry [18], the chain line shows the long-time approximation Eq. (161), the thick dotted lines show numerical simulations with the kicked top. At small times, $1-F$ increases linearly as given by the standard Fermi golden rule decay (159). Around the Heisenberg time $t_{\rm H}=400$ this regime ends and the freeze begins. The logarithmic behavior ends where the asymptotic decay of the freeze begins. This is well described by the long-time approximation.

of unperturbed $U_0^{\rm sym}$) we expect to find quantum freeze. The symmetrization, *i.e.*, splitting operator P in $U_\varepsilon^{\rm sym}$ into two parts, is essential. Without symmetrization there is no freeze and fidelity decays on much shorter time scale. For instance, for parameters used in Fig. 22 fidelity for an unsymmetrized dynamics decays on a time scale which is approximately 1000 times shorter! In order to compare RMT with the numerics we have to re-introduce physical units. The Heisenberg time is $\mathcal{N}=2S$, if S is the spin size, and the second moment of matrix elements of the perturbation is $\langle|V_{jk\to j}|^2\rangle = 2\sigma_{\rm cl}/\mathcal{N}$, where $\sigma_{\rm cl}$ is an integral of the classical correlation function (see Section 3.1). For times smaller than the Heisenberg time fidelity will decrease linearly, according to (87),

$$1-F \approx (\varepsilon_{\rm KT} S)^2 2\sigma_{\rm cl} t, \tag{159}$$

where we temporarily use $\varepsilon_{\rm KT}$ for kicked top perturbation strength (denoted simply by ε in Appendix B.1) to distinguish it from RMT perturbation strength ε, which is given as $2\pi\varepsilon = \varepsilon_{\rm KT}\sqrt{4\sigma_{\rm cl}S^3}$. For intermediate times, when we have a log-freeze (139), we have instead

$$1-F \approx \varepsilon_{\rm KT}^2 S^3 4\sigma_{\rm cl} \frac{\ln(t/2S)+2+\ln 2}{6}\,. \tag{160}$$

For large times we can use the approximate theoretical prediction (146) noting that in physical units we have $\tau = \varepsilon_{\rm KT}^2 S^2 \sigma_{\rm cl} t/\pi$ and thus

$$F = \varepsilon_{\rm KT}^4 S^4 \sigma_{\rm cl}^2 t^2 [K_1(\varepsilon_{\rm KT}^2 S^2 \sigma_{\rm cl} t)]^2\,. \tag{161}$$

In Fig. 22 we compare numerical results with the theoretical prediction (161) as well as with the exact result from [18], all for $S=200$ and different $\varepsilon_{\rm KT}=10^{-6},\ldots,10^{-3}$. We have averaged over 400 independent kicked top realizations, taking one random initial state for each. Independent kicked top realizations are obtained by drawing the parameter α in Eq. (B.12) at random from a Gaussian probability distribution with the center at $\alpha=30$ and unit variance. To ensure statistical independence the standard deviation divided by the number of realizations must be large as compared to the so-called level collision time which scales as $\sim 1/\sqrt{\mathcal{N}}$ and is determined by the level velocity and the mean level spacing. The averaging over independent spectra is here absolutely essential to reproduce the log-freeze. The agreement with the log-freeze (160) holds only up

to the time determined by the smallest level spacing and therefore scales as $\sim \sqrt{m}$, if m is the number of ensembles used in the averaging. The asymptotic result (161) is similarly sensitive to averaging.

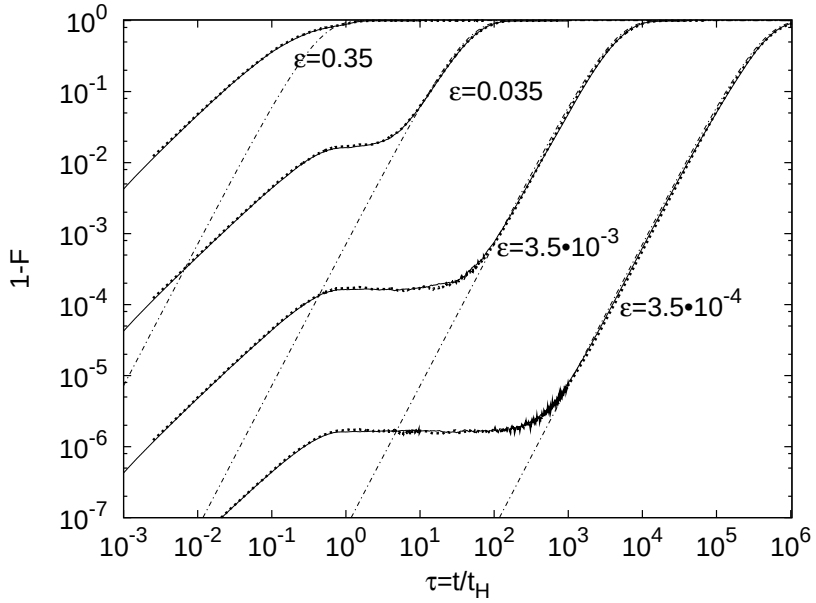

Fig. 23. Freeze in a kicked top, for the GUE case. The diagonal elements are put to zero by hand. The thick dashed lines show the numerical simulations, the solid lines correspond to the exact RMT result from [18], and the chain lines show the asymptotic result (163). The plateau during freeze is constant in the GUE case, as described by Eq. (162).

Next we will give an example for a system without time-reversal symmetry, belonging to the CUE. The one step propagator is given by Eq. (B.14). For the numerical simulations, we use exactly the same paramters as in the GOE case; this refers to the spin magnitude $S = 200$, the random distribution for α, the initial states, and the perturbation strengths. In order to obtain freeze we set diagonal elements of the perturbation to zero by hand. The short time decay does not depend on the symmetry class and it is the same as for the GOE case (159). The plateau during quantum freeze is for the GUE case independent of time,

$$1 - F = \varepsilon_{\rm KT}^2 S^3 4\sigma_{\rm cl} \frac{1}{3} \,. \tag{162}$$

On the other hand, Eq. (146) yields for the long time decay

$$F = (1 + \varepsilon_{\rm KT}^2 S^2 \sigma_{\rm cl} t)^2 \exp\left(-2\varepsilon_{\rm KT}^2 S^2 \sigma_{\rm cl} t\right). \tag{163}$$

In Fig. 23 we again find nice agreement between numerical simulations and theory.

4.4. *Echo purity*

The random matrix model developed in [52] and described above can be generalized to cover the evolution of entanglement following the lines of Refs. [160,161]. The new essential ingredient is to write the Hilbert space $\mathcal{H}$ as a tensor product of two Hilbert spaces $\mathcal{H} = \mathcal{H}_{\rm c} \otimes \mathcal{H}_{\rm e}$, which we will for convenience call "central system" and "environment". For the dimension N of $\mathcal{H}$, we get: $N = n_{\rm c}\, n_{\rm e}$, where $n_{\rm c}$ and $n_{\rm e}$ are the dimensions of $\mathcal{H}_{\rm c}$ and $\mathcal{H}_{\rm e}$, respectively.

We first consider an unperturbed Hamiltonian $H_0 \in$ GOE, which couples the two subspaces randomly and strongly, while the perturbation V will be drawn independently from the same ensemble. The entire argument that follows will go through analogously for $H_0 \in$ GUE. Echo purity, *i.e.* the purity of an initial state evolved with the echo operator, is defined in Section 2.6, Eq. (74). To calculate that quantity we need

a representation of the echo operator $\tilde{M}_\varepsilon(t)$ in a product basis with respect to the two factor spaces. Some orthogonal transformation will yield this as

$$\tilde{M}_\varepsilon(t) = O\ M_\varepsilon(t)\ O^T\ . \tag{164}$$

As H_0 and V are chosen from orthogonally invariant ensembles, the orthogonal transformation O will be random and independent of the product spaces $\mathcal{H}_\mathrm{c}$ and $\mathcal{H}_\mathrm{e}$. We will average over it using the invariant measure of the orthogonal group as in [160,161]. Since purity is of second order in the density matrix the expressions become involved and we have to digress to some formal considerations before actually working out the linear response approximation.

Purity form Since purity is defined as a trace of the square of a density operator, its treatment in RMT usually leads to a rather messy jungle of indices [160,161]. To avoid that, we define a linear form $p[\,.\,]$ on the space of operators in $\mathcal{H}^{\otimes 2}$. To this end we require that for any tensor product of operators ϱ_1, ϱ_2 acting on $\mathcal{H}$ the purity functional evaluates to

$$p[\varrho_1 \otimes \varrho_2] = \mathrm{tr}_\mathrm{c}\big(\,\mathrm{tr}_\mathrm{e}\,\rho_1\ \mathrm{tr}_\mathrm{e}\,\rho_2\,\big)\ . \tag{165}$$

Due to linearity this suffices for a complete definition of the purity form. The purity itself, reads: $I(t) = p[\varrho\otimes\varrho]$. For that expression to be physically meaningful, ϱ should be a density matrix. However, the following algebraic manipulations will eventually involve operators, which are not density operators.

For $H = H_0 + \varepsilon\ V$ and $\rho^M(t)$ denoting the initial state $\rho(0)$ propagated with the echo operator $M(t) = U_0^\dagger(t)\ U(t)$, the echo purity may be written as

$$F_P(t) = p[\rho^M(t) \otimes \rho^M(t)]\ . \tag{166}$$

In order to compute the echo purity in linear response approximation, we use the corresponding expression for the echo operator, Eq. (127) in the eigenbasis of H_0. Due to the bilinearity of the tensor product, we obtain for the linear response expression of the echo operator in the product basis

$$\tilde{M}(t) \approx \mathbf{1} - 2\pi\mathrm{i}\,\varepsilon\ \tilde{I} - (2\pi\varepsilon)^2\ \tilde{J} \tag{167}$$

$$\tilde{I} = O\ I\ O^T \qquad I_{\alpha\beta} = \int_0^t \mathrm{d}\tau\ \mathrm{e}^{2\pi\mathrm{i}\,E_\alpha\,\tau}\ V_{\alpha\beta}\ \mathrm{e}^{-2\pi\mathrm{i}\,E_\beta\,\tau} \tag{168}$$

$$\tilde{J} = O\ J\ O^T \qquad J_{\alpha\beta} = \sum_\xi \int_0^t \mathrm{d}\tau \int_0^\tau \mathrm{d}\tau'\ \mathrm{e}^{2\pi\mathrm{i}\,E_\alpha\,\tau}\ V_{\alpha\xi}\ \mathrm{e}^{-2\pi\mathrm{i}\,E_\xi\,(\tau-\tau')}\ V_{\xi\beta}\ \mathrm{e}^{-2\pi\mathrm{i}\,E_\beta\,\tau'}\ , \tag{169}$$

where $O^T\,H_0\,O = \mathrm{diag}(E_\mu)$. As mentioned above, V will be drawn from a GOE, while the orthogonal matrix O is taken from the orthogonal group provided with the invariant Haar measure. We will see that in linear response approximation, echo purity depends on the spectrum of H_0 only via its two-point correlations, which are conveniently expressed in terms of the two-point form factor b_2. All three components are assumed to be statistically independent. [8]

The starting point is thus more general than what we have considered in Section 2.6, inasmuch as we allow for non-separable (with respect to $\mathcal{H}_\mathrm{c}$ and $\mathcal{H}_\mathrm{e}$) and even non-pure (in $\mathcal{H}$) initial states. While we treat the technical details in Appendix D, we state here, that the echo purity is of the general form

$$F_P(t) \approx p[\rho(0)\otimes\rho(0)] - 2\ (2\pi\varepsilon)^2\ \mathcal{C}_P(t)\ , \tag{170}$$

where the correlation integral $\mathcal{C}_P(t)$ is independent of ε.

In the case of a pure and separable initial state $\rho(0) = |\psi_c(0)\rangle\,\langle\psi_c(0)| \otimes |\psi_e(0)\rangle\,\langle\psi_e(0)|$ we may use the orthogonal invariance of H_0 and V under arbitrary orthogonal transformations, and the invariance of purity under orthogonal transformations in the factor spaces, to obtain the following compact expression:

$$\mathcal{C}_P(t) = 2\,\left(1 - \frac{n_\mathrm{c}+n_\mathrm{e}-2}{N+2}\right)\,\left(t^2 + t/2 - \int_0^t \mathrm{d}\tau' \int_0^{\tau'} \mathrm{d}\tau\ \langle b_2(E,\,\tau)\rangle\right)\ . \tag{171}$$

[8] This assumption is crucial and should be carefully checked, in practice.

Note that the average over the random orthogonal transformation, implies that the decay is influenced by the spectral correlations from everywhere in the spectrum. For that reason we use the notation $\langle b_2(E,\,\tau)\rangle$ which means a global spectral average of the two-point form factor over the whole spectrum. The decay of the echo purity is of the same form as the fidelity amplitude decay, but faster by a factor of $4\,[1-(n_{\rm c}+n_{\rm e}-2)/(N+2)]$. This fact is consistent with the inequality (75) which states that the square of fidelity must be smaller or equal to purity; for our RMT model in linear response approximation the equality holds exactly in the limit $n_{\rm c}, n_{\rm e} \to \infty$.

These results, in particular Eqs. (170) and (171), apply to the quantum simulation of a dynamical model (the kicked Ising spin chain, Appendix B.2) considered in Section 3.3. While those considerations were restricted to the Fermi golden rule regime (exponential decay), the present results cover the whole range from the Fermi golden rule to the perturbative regime. Being obtained from linear response theory, their validity is naturally restricted to time regions where the echo operator is sufficiently close to the identity. However, we expect that this defect can be cured by phenomenological exponentiation of the linear response result, similar to the fidelity amplitude case. If in addition the possibly quite large limit values of the echo purity are taken into account (as described in Section 3.3), we expect to obtain an accurate general theoretical description of echo purity decay. Numerical simulations to check these ideas are considered, but have not been performed, so far. See however, Fig. 10, which presents some cases for relatively small Hilbert space dimensions, where the echo-purity deviates very clearly from an exponential decay. These deviations indicate the presence of an additional term, quadratic in time, which would be in line with Eq. (171). Unfortunately, the presence of a number of discrete symmetries in the dynamical system used, makes a quantitative comparison exceedingly difficult.

Some special cases could be considered. In many dynamical models, such as for the Jaynes-Cummings model with counter-rotating terms [162] the perturbation may only act in one of the two subsystems. As on the other hand the eigenstates of H_0 (when transformed to a product basis) imply a complicated orthogonal transformation, we still expect the above result to provide a reasonable description of the decay of echo purity.

One special case of fundamental importance will be treated in the following Section 4.5. There we shall assume H_0 to be separable, the perturbation providing the only coupling.

4.5. *Purity decay*

The results we developed in the previous subsection (and in particular in Appendix D) can readily be modified to obtain an excellent model for the decay of purity in a pure forward time evolution. To that end, consider a Hamiltonian H_0 which does not establish any interaction between the two subsystems, such that it can be written as $H_0 = h_{\rm c} \otimes \mathbf{1} + \mathbf{1} \otimes h_{\rm env}$, where $h_{\rm c}$ and $h_{\rm env}$ act on $\mathcal{H}_{\rm c}$ and $\mathcal{H}_{\rm e}$, respectively. Clearly the purity of any density matrix for the central system will not be affected by a time evolution with this Hamiltonian. Thus entanglement and purity decay will be entirely due to the forward time evolution. A simulation with a corresponding dynamical model is discussed in Section 3.3, Fig. 9. While the focus there is on the semiclassical behavior which involves quantum mechanically strong perturbations to reach the Fermi golden rule regime, we consider decay times of the order of the Heisenberg time. As before, the results here will therefore cover the whole range from the Fermi golden rule to the perturbative regime.

Assuming that the perturbation V as well as the Hamiltonians $h_{\rm c}$ and $h_{\rm env}$ are taken from appropriate random matrix ensembles, we can still apply our results obtained for echo purity. However, at the level of echo dynamics, we make an additional approximation. Since the additivity of the eigenenergies of $h_{\rm c}$ and $h_{\rm env}$ in the unperturbed system tend to destroy spectral correlations, anyway, we replace the spectrum of H_0 by a sequence of uncorrelated random levels. We approximate the purity decay $I(t)$ of a separable H_0 with the decay of the echo purity $F_P(t)$ of a simpler H_0, which is no longer separable. In this way, we get for the growth of entanglement as measured by the purity of an evolving state with initial density matrix ϱ_0

$$\langle I(t)\rangle \approx \langle F_P(t)\rangle = I(0) - 2\,(2\pi\varepsilon)^2\,\mathcal{C}_P(t) + \mathcal{O}(\varepsilon^4)\;, \tag{172}$$

with a simplified correlation integral due to the absence of correlations in the spectrum of H_0 (see Appendix D.1). For the case of pure initial states we thus get the following linear response result:

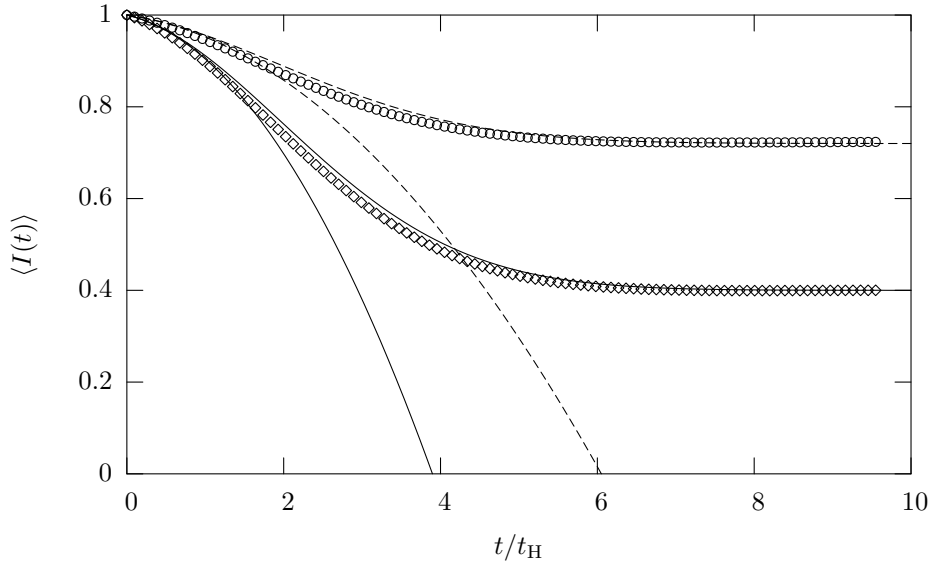

Fig. 24. Purity decay in a random matrix simulation. The initial state is a tensor product of two random states in the respective factor spaces. The simulations are shown by diamonds ($n_{\rm c} = n_{\rm e} = 10$) and by circles ($n_{\rm c} = 2, n_{\rm e} = 50$). The corresponding theoretical curves show that bare linear response result, Eq. (173) together with its exponentiated version for the case $n_{\rm c} = n_{\rm e} = 10$ (solid lines) and the case $n_{\rm c} = 2, n_{\rm e} = 50$ (dashed line). The exponentiated version contains a phenomenological treatment of the asymptotic value (for details, see text).

$$\langle I(t)\rangle \approx 1 - 4\,(2\pi\varepsilon)^2 \left\{ t^2\,\left[\,1 - {\rm Ipr}_2\,\varrho_0\,\right] + \frac{t}{2}\,\left[\,1 - \frac{n_{\rm c}+n_{\rm e}-1-{\rm Ipr}_2\,\varrho_0}{N}\,\right]\right\} + \mathcal{O}(\varepsilon^4)\;, \tag{173}$$

where ${\rm Ipr}_2 = {\rm Ipr}(\,{\rm tr}_{\rm e}\,\varrho_0\,) + {\rm Ipr}(\,{\rm tr}_{\rm c}\,\varrho_0\,) - {\rm Ipr}\,\varrho_0$. Here, we have generalized the inverse participation ratio to density matrices by defining: ${\rm Ipr}\,\varrho = {\rm tr}\,(\,{\rm diag}\,\varrho\,)^2$, where ${\rm diag}\,\varrho$ is the diagonal part of the density matrix ϱ. In the case of pure states, $\varrho = |\psi\rangle\langle\psi|$, this definition reduces to the familiar definition of the inverse participation ratio. Note that even if ϱ_0 is assumed pure in this equation, the partial traces of ϱ_0 are generally not.

Equation (173) can be tested by random matrix simulations. To this end we assume the initial state to be pure and separable, $I(0) = 1$. We choose rather small dimensions of the Hilbert spaces involved, and compare in Figs. 24 and 25 the cases $n_{\rm c} = n_{\rm e} = 10$ (diamonds) and $n_{\rm c} = 2, n_{\rm e} = 50$ (circles). In those figures we show the average purity $\langle I(t)\rangle$ (it equals the average echo purity $\langle F_P(t)\rangle$ in the present model), as a function of time, restricting ourselves to rather small perturbations $\varepsilon = 0.025$. In Fig. 24 we use initial states which are products of random states in the respective subsystems. In that case, ${\rm Ipr}_2\,\varrho_0 = 3/(n_{\rm c}+2) + 3/(n_{\rm e}+2) - 9/((n_{\rm c}+2)(n_{\rm e}+2))$. Here, the perturbation strength is actually strong enough to observe the cross-over from linear to quadratic decay. For each case, $n_{\rm c} = n_{\rm e} = 10$ (solid lines) and $n_{\rm c} = 2, n_{\rm e} = 50$ (dashed lines), we plot two theoretical curves, the behavior according to Eq. (173) and its exponentiated version. For the latter we also took into account the finite limit values of the purity at large times, in the way as described in Section 3.3, Eq. (113)

$$\langle I(t)\rangle \approx F_P^* + (1-F_P^*)\,\exp\left[\,2\,\mathcal{C}_P(t)\,(1-F_P^*)^{-1}\,\right]\,. \tag{174}$$

In the absence of a theoretical prediction for the limit value F_P^*, we fitted it to the numerical simulation. There are noticeable differences between the numerical simulations and the analytical predictions. We believe these differences to be due to the particular form of the level density for H_0 and the fact that we use random initial states with maximal spectral span. Since H_0 is the sum of two random spectra with constant level density, the level density of H_0 has a triangular shape, whereas in the analytical work the level density is assumed to be constant.

Figure 25 shows the purity decay for initial states which are eigenstates of H_0. In that case, the quadratic term in Eq. (173) cancels, and one obtains

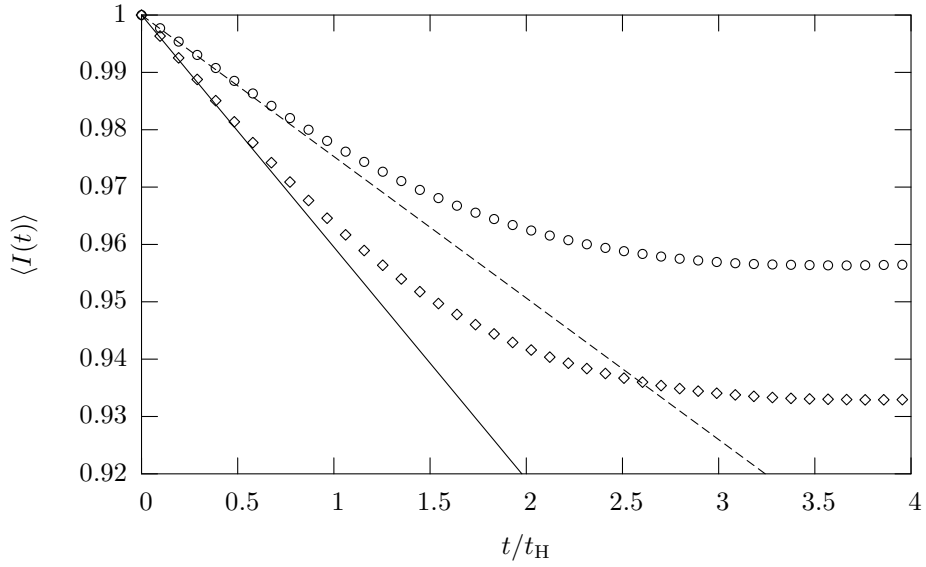

Fig. 25. Purity decay in a random matrix simulation. The initial state is a product state from the product basis of eigenststes of the uncoupled Hamiltonian with an energy located at the center of the spectrum. The simulations are shown by diamonds ($n_{\rm c} = n_{\rm e} = 10$) and by circles ($n_{\rm c} = 2, n_{\rm e} = 50$). The corresponding theoretical curves show the plain linear response result, Eq. (175), by a solid line ($n_{\rm c} = n_{\rm e} = 10$) and a dashed line ($n_{\rm c} = 2, n_{\rm e} = 50$), respectively.

$$\langle I(t)\rangle = 1 - 2\,(2\pi\varepsilon)^2\,t\,\left(1 - \frac{n_{\rm c} + n_{\rm e} - 2}{N}\right) + \mathcal{O}(\varepsilon^4)\,. \tag{175}$$

We find that the linear response result is indeed valid, also for that case. At small times the theoretical curves converge to the numerical results. However, even when the saturation value of purity is taken into account (as done in Fig. 24), the exponentiated linear response formula (not plotted) does not correctly describe the numerical simulations. Note that due to the absence of the t^2-term the saturation values are much higher.

In [111] a similar result is obtained for an even more involved situation relevant for quantum information.

5. Quantum echo-dynamics: Integrable case

We shall now turn our attention to integrable dynamics. The system can actually also have a mixed phase space, provided the initial state is located in the integrable part of phase space so that we can locally define action-angle variables used in the following theoretical derivations. We shall call such systems *regular*. Throughout this section we shall assume for simplicity that the perturbation is time independent [9] in the Schrödinger picture, *i.e.* $V(t) = V$.

The action-angle variables used in the theoretical derivations are introduced in Section 5.1. Afterwards, we discuss fidelity decay for perturbations with non-zero time average (Section 5.2) and then for perturbations with zero time average, resulting in the so-called fidelity freeze (Section 5.3). In Section 5.4 measures for composite systems are discussed, in particular purity. Section 5.5 discusses fidelity decay in systems with mixed phase space, for cases where the purely regular theory exposed in the previous subsections is not sufficient.

If the dynamics is integrable it is useful to define a *time-averaged perturbation* $\bar{V}$ (27),

$$\bar{V} = \lim_{t\to\infty} \frac{1}{t} \int_0^t dt' \tilde{V}(t') = \lim_{t\to\infty} \frac{\Sigma(t)}{t}. \tag{176}$$

[9] This of course does not mean that the perturbation $\tilde{V}(t)$ in the interaction picture is time independent.

For sufficiently small $\hbar$ the above integral converges for some classical averaging time $t_{\rm ave}$. Observe that $\bar{V}$ is by construction a constant of motion, $[\bar{V}, U_0] = 0$. For chaotic dynamics $\bar{V}$ goes to zero in the semiclassical limit. For regular dynamics on the other hand there can be two different situations depending on the operator $\bar{V}$: (i) the typical case where $\bar{V} \neq 0$ and (ii) the special case where $\bar{V} = 0$, which gives rise to an entirely different behavior known as quantum freeze [16], for a general discussion of freeze see Section 2.2. If $\bar{V}$ is nonzero the double integral of the correlation function $C(t', t'')$ (14) will also grow quadratically with time and so one can also define an *time-averaged correlation function* $\bar{C}$,

$$\bar{C} = \lim_{t\to\infty} \frac{1}{t^2} \int_0^t \int_0^t dt'' dt' C(t'', t'). \tag{177}$$

$\bar{C}$ is the plateau value of the correlation function for $t \to \infty$ (or the value around which the correlation function oscillates). Correlation functions in regular systems will typically have a plateau due to the existence of conserved quantities. Equivalently $\bar{C}$ can be written in terms of the average perturbation operator $\bar{V}$,

$$\bar{C} = \langle \bar{V}^2 \rangle - \langle \bar{V} \rangle^2 \,, \tag{178}$$

i.e., $\bar{C}$ is the variance of the time averaged perturbation. For sufficiently small $\hbar$, the quantum correlation function can be replaced by its classical counterpart, *i.e.*, the quantum operator V can be replaced by the classical oservable v, such that $\bar{C}$ is given by classical dynamics. The time scale on which $\bar{C}$ converges is again $t_{\rm ave}$. Physically, this is the time in which the classical correlation functions decay to their asymptotics. The linear response expression for fidelity (13) can now be written as

$$F(t) = 1 - \frac{\varepsilon^2}{\hbar^2} \bar{C} t^2 + \cdots \,, \tag{179}$$

valid for $t > t_{\rm ave}$. The time scale for fidelity decay scales as $\sim 1/\varepsilon$. Here, the quadratic decay is not a consequence of trivial conservation laws, as discussed in Section 2.1.3, but of the regular dynamics with non-decaying correlations. Also it must not be confused with the so-called Zeno decay, Section 2.1.1, which is also quadratic but happens on a very short time-scale on which the correlation function does not yet decay, regardless of the dynamics [66,67]. For a numerical comparison of Zeno time-scale and our quadratic decay; see Fig. 39.

Of course one should keep in mind that the behavior of the correlation function (14) depends on the dynamics as well as on the perturbation V itself. For instance, even for integrable dynamics the correlation function can decay to zero for a sufficiently "random" perturbation. In such a case the fidelity decay in the linear response regime will be linear even for regular dynamics. Indeed, exponential decay of fidelity has been found in Ref. [163] also in a regular regime if a random transformation of the basis is made before applying the perturbation (making the perturbation effectively random). Note that such a random perturbation has no classical limit, nevertheless it could be important for quantum computing where typical errors acting on individual qubits may not have a classical limit [164] either. The application of perturbations which have no classical limit can result in a situation where the presence of symmetries can cause the fidelity decay to be exponential and slower than in the absence of symmetries [165]. A more detailed account of fidelity studies in the context of quantum computing is given in Section 8.

Passing to action-angle operators will turn out to make derivations easier and will furthermore enable us to use classical action-angle variables in the leading semiclassical order, thereby expressing quantum fidelity in terms of classical quantities, even though in some cases quantum and classical fidelity may behave quite differently. Therefore, before proceeding with the evaluation of $F(t)$ beyond the linear response let us have a look at the quantum action-angle operator formalism.

5.1. *Action-angle operators*

Since we assume the classical system to be integrable (in the case of near-integrable systems at least locally, by KAM theorem) we can employ action-angle variables, $\{j_k, \theta_k, k = 1 \dots d\}$, in a system with d degrees of freedom. In the present section, dealing with the regular regime we shall use lowercase letters to

denote *classical variables* and capital letters to denote the corresponding *quantum operators*. For instance, the quantum Hamiltonian will be given as $H(\boldsymbol{J}, \boldsymbol{\Theta})$ whereas its classical limit will be written as $h(\boldsymbol{j}, \boldsymbol{\theta})$.

As our unperturbed Hamiltonian is integrable, it is a function of actions only, *i.e.* $h_0 = h_0(\boldsymbol{j})$. The solution of the classical equations of motion is simply

$$\boldsymbol{j}(t) = \boldsymbol{j}, \qquad \boldsymbol{\theta}(t) = \boldsymbol{\theta} + \boldsymbol{\omega}(\boldsymbol{j})t \pmod{2\pi}, \tag{180}$$

with a dimensionless frequency vector $\boldsymbol{\omega}(\boldsymbol{j}) = \partial h_0(\boldsymbol{j})/\partial \boldsymbol{j}$. In Section 5.3 it will come handy to expand the classical limit $v(\boldsymbol{j}, \theta)$ of a perturbation operator V into a Fourier series,

$$v(\boldsymbol{j}, \boldsymbol{\theta}) = \sum_{\boldsymbol{m} \in \mathbb{Z}^d} v_{\boldsymbol{m}}(\boldsymbol{j}) e^{\mathrm{i}\boldsymbol{m}\cdot\boldsymbol{\theta}}, \tag{181}$$

where the multi-index $\boldsymbol{m}$ has d components. The classical limit of the time-averaged perturbation $\bar{V}$ is $\bar{v} = v_{\boldsymbol{0}}(\boldsymbol{j})$, *i.e.* only the zeroth Fourier mode of the perturbation survives time averaging.

In quantum mechanics, one quantizes the action-angle variables using the EBK procedure (see *e.g.* Ref. [166]) where one defines the action (momentum) operators $\boldsymbol{J}$ and angle operators $\exp(\mathrm{i}\boldsymbol{m}\cdot\boldsymbol{\Theta})$ satisfying the canonical commutation relations, $[J_k, \exp(\mathrm{i}\boldsymbol{m}\cdot\boldsymbol{\Theta})] = \hbar m_k \exp(\mathrm{i}\boldsymbol{m}\cdot\boldsymbol{\Theta}), k = 1, \ldots, d$. As the action operators are mutually commuting they have a common eigenbasis $|\boldsymbol{n}\rangle$ labeled by the d-tuple of quantum numbers $\boldsymbol{n} = (n_1, \ldots, n_d)$,

$$\boldsymbol{J}|\boldsymbol{n}\rangle = \boldsymbol{J}_{\boldsymbol{n}}|\boldsymbol{n}\rangle. \tag{182}$$

Here $\boldsymbol{J}_n = \hbar\{\boldsymbol{n} + \boldsymbol{\alpha}\}$ is an eigenvalue of operator $\boldsymbol{J}$ in an eigenstate $|\boldsymbol{n}\rangle$ and $0 \le \alpha_k \le 1$ are the Maslov indices which are irrelevant for the leading order semiclassical approximation we shall use. It follows that the angle operators act as shifts, $\exp(\mathrm{i}\boldsymbol{m}\cdot\boldsymbol{\Theta})|\boldsymbol{n}\rangle = |\boldsymbol{n} + \boldsymbol{m}\rangle$. The Heisenberg equations of motion can be solved in the leading semiclassical order by using classical equations of motion, *i.e.* replacing quantum $H_0(\hbar\boldsymbol{n}) - H_0(\hbar(\boldsymbol{n} - \boldsymbol{m}))$ with its classical limit $\boldsymbol{m}\cdot\boldsymbol{\omega}(\hbar\boldsymbol{n})$ and disregarding the operator ordering,

$$\begin{aligned} \boldsymbol{J}(t) &= \mathrm{e}^{\mathrm{i}H_0 t/\hbar}\boldsymbol{J}\mathrm{e}^{-\mathrm{i}H_0 t/\hbar} = \boldsymbol{J}, \\ \mathrm{e}^{\mathrm{i}\boldsymbol{m}\cdot\boldsymbol{\Theta}(t)} &= \mathrm{e}^{\mathrm{i}H_0 t/\hbar}\mathrm{e}^{\mathrm{i}\boldsymbol{m}\cdot\boldsymbol{\Theta}}\mathrm{e}^{-\mathrm{i}H_0 t/\hbar} \cong \mathrm{e}^{\mathrm{i}\boldsymbol{m}\cdot\boldsymbol{\omega}(\boldsymbol{J})t}\mathrm{e}^{\mathrm{i}\boldsymbol{m}\cdot\boldsymbol{\Theta}}, \end{aligned} \tag{183}$$

in terms of the frequency operator $\boldsymbol{\omega}(\boldsymbol{J})$. Throughout this paper we use the symbol $\cong$ for 'semiclassically equal', *i.e.* asymptotically equal to leading order in $\hbar$. Similarly, time evolution of any other observable is obtained to leading order by substitution of classical with quantal action-angle variables. For instance the perturbation $\tilde{V}(t)$ (181) is

$$\tilde{V}(t) = \mathrm{e}^{\mathrm{i}H_0 t/\hbar} V \mathrm{e}^{-\mathrm{i}H_0 t/\hbar} \cong \sum_{\boldsymbol{m}} v_{\boldsymbol{m}}(\boldsymbol{J}) \mathrm{e}^{\mathrm{i}\boldsymbol{m}\cdot\boldsymbol{\omega}(\boldsymbol{J})t} \mathrm{e}^{\mathrm{i}\boldsymbol{m}\cdot\boldsymbol{\Theta}}. \tag{184}$$

5.2. *Perturbations with non-zero time average*

In this section we assume $\bar{V} \neq 0$. We have seen (24) that the echo operator for sufficiently small ε can be written as

$$M_\varepsilon(t) \approx \exp\left\{-\frac{\mathrm{i}}{\hbar}\left(\Sigma(t)\varepsilon + \frac{1}{2}\Gamma(t)\varepsilon^2\right)\right\}, \tag{185}$$

where $\Gamma(t)$ (25) grows at most linearly with t. If $\bar{V} \neq 0$, the first term in the exponential will grow as $\Sigma(t) = \bar{V}t$ for times longer than the classical averaging time t_{ave} (176). Therefore, provided $\varepsilon < 1$, the term involving $\Gamma(t)$ will be $1/\varepsilon$ times smaller than the first one and can be neglected. Replacing $\Sigma(t)$ with $\bar{V}t$ we write the fidelity amplitude as

$$f(t) = \langle \mathrm{e}^{-\mathrm{i}\varepsilon t\bar{V}/\hbar}\rangle, \qquad t \gg t_{\mathrm{ave}}. \tag{186}$$

As the average perturbation operator $\bar{V}$ is diagonal in the eigenbasis of actions, $\bar{V}\ |\boldsymbol{n}\rangle = \bar{V}_{\boldsymbol{n}}|\boldsymbol{n}\rangle$, the above expectation value is especially simple in the action eigenbasis $|\boldsymbol{n}\rangle$,

$$f(t) = \sum_{\boldsymbol{n}} \exp\left(-\mathrm{i}\varepsilon t\bar{V}_{\boldsymbol{n}}/\hbar\right) D_\rho(\hbar\boldsymbol{n}), \qquad D_\rho(\hbar\boldsymbol{n}) = \langle\boldsymbol{n}|\rho|\boldsymbol{n}\rangle. \tag{187}$$

Now we make a leading order semiclassical approximation by replacing quantum operator $\bar{V}$ by its classical limit $\bar{v}(\boldsymbol{j})$ and replacing the sum over quantum numbers $\boldsymbol{n}$ with the integral over classical actions $\boldsymbol{j}$ (note small-cap letter). By denoting with $d_\rho(\boldsymbol{j})$ the classical limit of $D_\rho(\hbar\boldsymbol{n})$, we arrive at the fidelity amplitude,

$$f(t) \cong \hbar^{-d} \int \mathrm{d}^d\boldsymbol{j} \exp\left(-\mathrm{i}\frac{\varepsilon}{\hbar} t\bar{v}(\boldsymbol{j})\right) d_\rho(\boldsymbol{j}). \tag{188}$$

This equation will serve us as a starting point for all calculations of fidelity decay in regular systems for non-residual perturbations. The replacement of the sum with the action space integral (ASI) is valid up to such classically long times t_a, that the variation of the argument in the exponential across one Planck cell is small,

$$t_\mathrm{a} = \frac{1}{|\partial_{\boldsymbol{j}}\bar{v}|\varepsilon} \sim \hbar^0/\varepsilon. \tag{189}$$

Subsequently we shall see that the fidelity decays in times shorter than this, and thus the ASI approximation is justified. The ASI representation (188) will be now used to evaluate the fidelity for different initial states $d_\rho(\boldsymbol{j})$.

5.2.1. *Coherent initial states*

First we take the initial state to be a coherent state $|\boldsymbol{j}^*, \boldsymbol{\theta}^*\rangle$ centered at action and angle position $(\boldsymbol{j}^*, \boldsymbol{\theta}^*)$. Expansion coefficients of a general coherent state (a localized wave packet) can be written as

$$\langle \boldsymbol{n}|\boldsymbol{j}^*, \boldsymbol{\theta}^*\rangle = \left(\frac{\hbar}{\pi}\right)^{d/4} |\det\Lambda|^{1/4} \exp\left\{-\frac{1}{2\hbar}(\boldsymbol{J}_{\boldsymbol{n}} - \boldsymbol{j}^*)\cdot\Lambda(\boldsymbol{J}_{\boldsymbol{n}} - \boldsymbol{j}^*) - \mathrm{i}\boldsymbol{n}\cdot\boldsymbol{\theta}^*\right\}, \tag{190}$$

where Λ is a positive symmetric $d \times d$ matrix of squeezing parameters. The classical limit of D_ρ (187) is therefore

$$d_\rho(\boldsymbol{j}) = (\hbar/\pi)^{d/2} |\det\Lambda|^{1/2} \exp(-(\boldsymbol{j} - \boldsymbol{j}^*)\cdot\Lambda(\boldsymbol{j} - \boldsymbol{j}^*)/\hbar). \tag{191}$$

The ASI (188) for the fidelity amplitude can now be evaluated by the stationary phase method with the result [46],

$$F(t) = \exp\left\{-(t/\tau_\mathrm{r})^2\right\}, \qquad \tau_\mathrm{r} = \frac{1}{\varepsilon}\sqrt{\frac{2\hbar}{\bar{\boldsymbol{v}}'\cdot\Lambda^{-1}\bar{\boldsymbol{v}}'}}, \tag{192}$$

where the derivative of the average perturbation is

$$\bar{\boldsymbol{v}}' = \frac{\partial\bar{v}(\boldsymbol{j}^*)}{\partial\boldsymbol{j}}, \tag{193}$$

and is evaluated at the position of the initial packet $\boldsymbol{j}^*$. Comparing the fidelity (192) with the linear response formula (179) we see that the average correlation function for a coherent initial state, $\bar{C} = \frac{1}{2}\hbar(\bar{\boldsymbol{v}}'\cdot\Lambda^{-1}\bar{\boldsymbol{v}}')$, is proportional to $\hbar$ because the size of the packet scales with $\hbar$.

We thus find a Gaussian decay of fidelity for coherent initial states in regular systems. This has very simple physical interpretation. As the fidelity is an overlap of the initial state with the state obtained after an echo, *i.e.* after propagation with $M_\varepsilon(t) = \exp(-\mathrm{i}\bar{V}(\boldsymbol{J})\varepsilon t/\hbar)$, we can see that the effective Hamiltonian for this evolution is $\bar{V}(\boldsymbol{J})$. It depends only on action variables and therefore its classical limit $\bar{v}(\boldsymbol{j})$ generates a very simple classical evolution. Only the frequencies of tori are changed by the amount $\Delta\boldsymbol{\omega} = \varepsilon\bar{\boldsymbol{v}}'$, while the shapes of tori do not change. This change in frequency causes the "echo" packet $M_\varepsilon(t)|\psi(0)\rangle$ to move *ballistically* away from its initial position and as a consequence fidelity decays. The functional form of this decay is directly connected with the shape of the initial packet. For coherent initial states it is Gaussian while for other forms of localized initial packets it will be correspondingly different but with the same dependence of the regular decay time τ_r on the ballistic separation "speed" $\bar{\boldsymbol{v}}'$ and perturbation strength ε. Note that the decay of classical fidelity is more complicated, see Section 6.

In one dimensional systems ($d = 1$) another phenomenon will be observable. After long times the echo packet will make a whole revolution around the torus causing the fidelity to be large again. This will happen after the so-called beating time t_b determined by the condition [10] $\varepsilon\bar{v}'(j^*)t_\mathrm{b} = 2\pi$,

[10] In the presence of symmetries the beating time can be shorter than the one given by Eq. (194).

$$t_{\rm b} = \frac{2\pi}{\bar{v}'\varepsilon}. \tag{194}$$

This beating phenomena is particular to one dimensional systems as in general the incommensurability of frequencies will suppress the revivals of fidelity in more than one degree of freedom systems (*i.e.* $t_{\rm b}$ for derivative of $\bar{v}$ in each action direction would have to be the same), for a numerical example of a two degree of freedom system see Ref. [46]. Strong revivals of fidelity have been discussed also in Ref. [167]. In case of commensurate frequencies one can have revivals also in many-dimensional systems, for an example of $d = 2$ dimensional Jaynes-Cummings model see Refs. [168,51]. In Ref. [169] quantum fidelity has been exactly calculated for a system with the Hamiltonian $H_\varepsilon = p^2/2 + g(t)q^2/2 + \varepsilon/q^2$, with an arbitrary periodic function $g(t)$, and it has been shown that there are perfect periodic recurrences of fidelity.

To illustrate the above theory for fidelity decay we compare it in Fig. 26 with the results of numerical simulation. The model we choose is a kicked top with a unit-step propagator given in Eq. (B.1), using $\gamma = \pi/2$ and small $\alpha = 0.1$ giving regular dynamics. Evaluation of the theoretical formula (192) in the limit of vanishing α gives for this particular perturbation the theoretical fidelity decay

$$F(t) = \exp\left(-\varepsilon^2 S t^2 y^2 (1-y^2)/8\right), \tag{195}$$

if y is the position of the initial coherent state on a sphere. Nice agreement of numerics ($S = 100$ and $\varepsilon = 0.0025$) with the theory can be seen as well as fidelity recurrence at the predicted time $t_{\rm b}$.

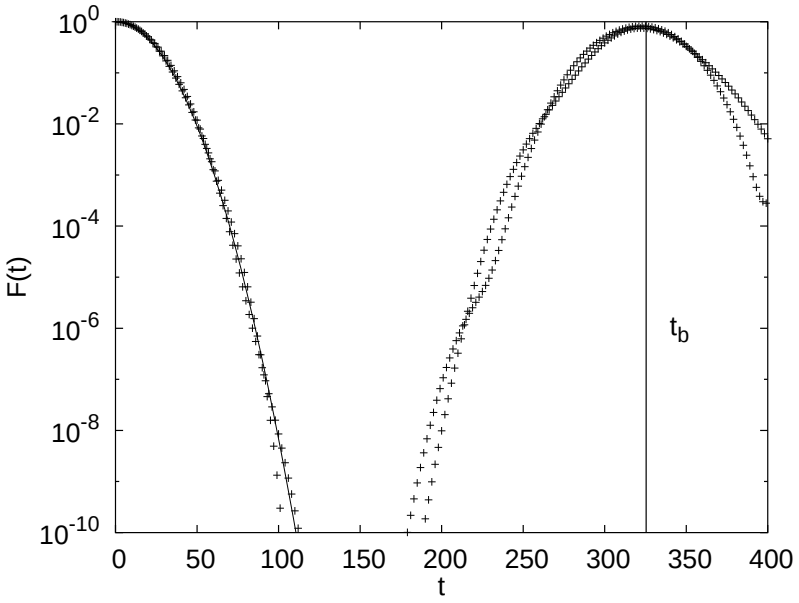

Fig. 26. Quantum fidelity for a coherent initial state of the regular kicked top (B.1) [from [46]]. The solid line shows the predicted Gaussian decay (195), the point symbols "+" show the numerical results. The vertical line indicates the theoretical beating time (194) which is particular to one degree of freedom systems.

5.2.2. *Random initial states*

In this section we shall consider random initial states, that is pure states whose expansion coefficients are independent Gaussian random numbers. In the semiclassical limit, *i.e.* for large Hilbert space dimension $\mathcal{N}$, the expectation value of an echo operator is self averaging, meaning that the fidelity for one particular random state is equal to the fidelity averaged over the whole Hilbert space. Therefore, we calculate $f(t)$ via Eq. (7) choosing the initial state as the density matrix $\rho = \mathbb{1}/\mathcal{N}$. The expansion coefficients take the form $D_\rho(\boldsymbol{J}) = 1/\mathcal{N}$ (187) and the corresponding classical quantity is

$$d_\rho(\boldsymbol{j}) = \frac{(2\pi\hbar)^d}{\mathcal{V}}, \tag{196}$$

where we calculated the dimension of the Hilbert space $\mathcal{N}$ using the Thomas-Fermi rule. For short times the decay of fidelity is again quadratic (179), albeit with a different $\bar{C}$ than for coherent states. For longer times the ASI (188) giving $f(t)$ can be calculated using a stationary phase method if the phase $\varepsilon\bar{v}t/\hbar$ of the echo operator changes fast enough. This is valid for $t > \hbar/\varepsilon$. Note on the other hand, that there is also an upper limit for ASI determined by $t_{\rm a} \sim 1/\varepsilon$ (189). In contrast to the coherent initial state, we can now have more than one stationary point. If we have p points, $\boldsymbol{j}_\eta, \eta = 1, \ldots, p$, where the phase is stationary, $\partial\bar{v}(\boldsymbol{j}_\eta)/\partial\boldsymbol{j} = \boldsymbol{0}$, the ASI gives [46]

$$f(t) = \frac{(2\pi)^{3d/2}}{\mathcal{V}} \left|\frac{\hbar}{t\varepsilon}\right|^{d/2} \sum_{\eta=1}^{p} \frac{\exp\{-\mathrm{i}t\bar{v}(\boldsymbol{j}_\eta)\varepsilon/\hbar - \mathrm{i}\nu_\eta\}}{|\det \bar{\boldsymbol{V}}_\eta|^{1/2}}, \tag{197}$$

where $\{\bar{\boldsymbol{V}}_\eta\}_{kl} = \partial^2\bar{v}(\boldsymbol{j}_\eta)/\partial j_k \partial j_l$ is a matrix of second derivatives at the stationary point $\boldsymbol{j}_\eta$, and $\nu_\eta = \pi(m_+ - m_-)/4$ where $m_\pm$ are the numbers of positive/negative eigenvalues of the matrix $\bar{\boldsymbol{V}}_\eta$. In above derivation we also assumed that phase space is infinite. In a finite phase space we shall have diffractive oscillatory corrections in the stationary phase formula, see numerical results below or Ref. [16]. It is interesting to note the power-law dependence on time and perturbation strength. In the simple case of one stationary point, fidelity will asymptotically decay as

$$F(t) \asymp [\hbar/(t\varepsilon)]^d, \tag{198}$$

where the sign $\asymp$ will denote "in the asymptotic limit" throughout this section. An interesting, though still largely unexplored, question is what happens in the thermodynamic limit $d \to \infty$? From the above formula we see that with increasing dimensionality d of a system the decay gets faster. This allows for a possible crossover to a Gaussian decay when approaching the thermodynamic limit. Such behavior has been observed in a class of kicked spin chains [42]. Agreement with Gaussian or expeonetial decay beyond linear response is frequently observed also for finite d, *e.g.* in a spin model of quantum computation [43].

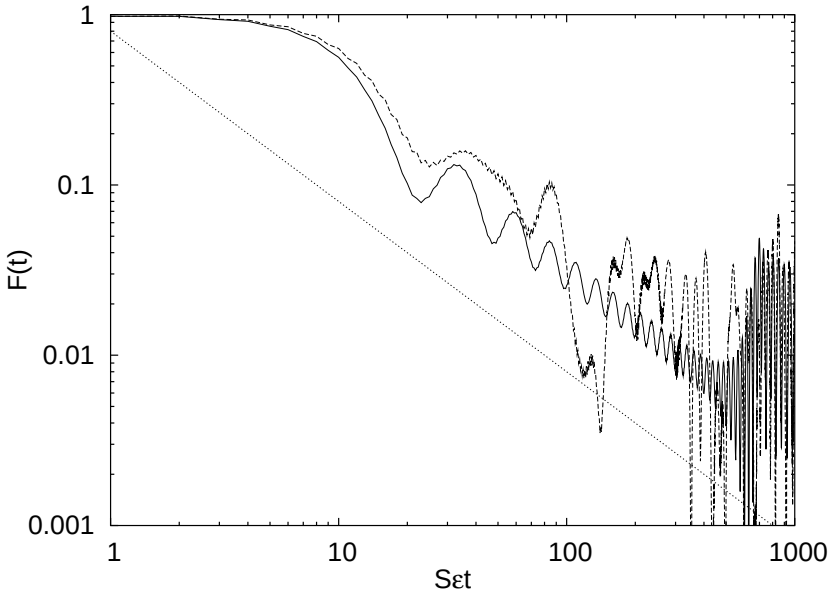

Fig. 27. Power law decay of fidelity for the regular kicked top (B.1) [from [46]] and random initial state. The solid curve gives the results of a numerical simulation for $\rho = \mathbb{1}/\mathcal{N}$, the dotted line gives a predicted asymptotic decay $\propto t^{-1}$, and the wiggling dashed curve represents the numerics for a single random state, $\mathcal{N} = 100$.

In Fig. 27 we show results of numerical simulation for the same regular kicked top used for coherent initial states (B.1). Note the oscillating decay due to finite phase space.

5.2.3. *Average Fidelity for Coherent States*

One might be also interested in fidelity averaged over the position of the initial coherent state,

$$\langle F(t)\rangle_{\boldsymbol{j}} = \frac{(2\pi)^d}{\mathcal{V}} \int \mathrm{d}^d \boldsymbol{j} F(t, \boldsymbol{j}). \tag{199}$$

The asymptotic decay of average fidelity will be dominated by regions in the action space where the decay $F(t, \boldsymbol{j})$ is the slowest. Denoting all $\boldsymbol{j}$ dependent terms by a non-negative scalar function $g(\boldsymbol{j})$, the fidelity decay for a single coherent state can be written as $F(t, \boldsymbol{j}) = \exp\left(-\varepsilon^2 t^2 g(\boldsymbol{j})/\hbar\right)$ (192). For large $\varepsilon^2 t^2/\hbar$ the main contribution to the average will come from regions around zeros of $g(\boldsymbol{j})$, where the fidelity decay is slow. In general there can be many zeros due to divergences in τ_{r} (192), but for simplicity let us assume there is a single zero at $\boldsymbol{j}_*$ of order η. The asymptotic decay can then be calculated and scales as [170]

$$\langle F(t)\rangle_{\boldsymbol{j}} \asymp \left(\frac{\hbar}{\varepsilon^2 t^2}\right)^{d/\eta}. \tag{200}$$

The asymptotic decay is therefore algebraic with the power depending on the number of degrees of freedom d and the order η of the zero. For infinite phase space η can only be an even number, whereas for a finite space η can also be odd. Note that for regular systems the fidelity averaged over the position of coherent states $\langle F(t)\rangle_{\boldsymbol{j}}$ is not necessarily equal to the fidelity for a random initial state (198) [11]. Whereas for fidelity decay of a random initial state zeros of $\bar{v}(\boldsymbol{j})$ matter, for $\langle F(t)\rangle_{\boldsymbol{j}}$ singularities of τ_{r} (192) determine asymptotic decay (*e.g.* zeros of $\bar{\boldsymbol{v}}'$).

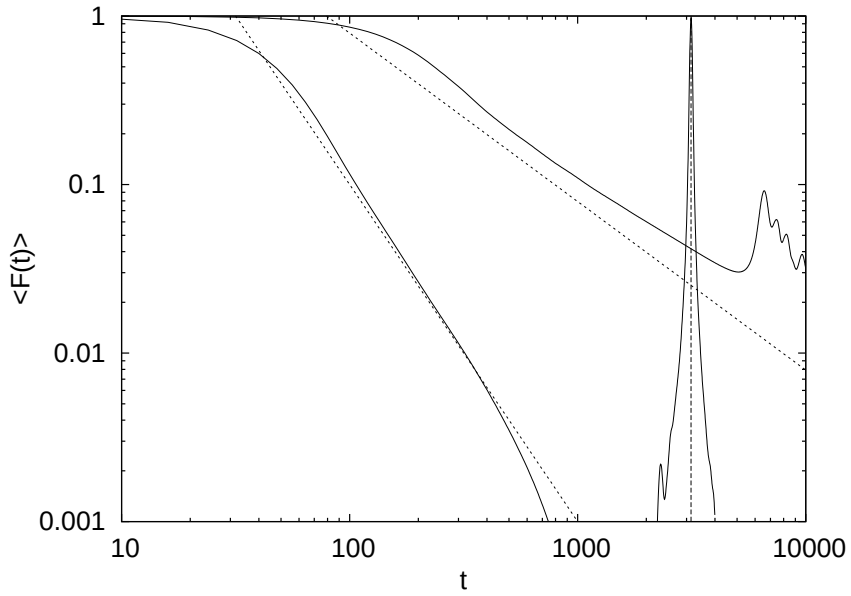

Fig. 28. Average fidelity decay $\langle F(t)\rangle_{\boldsymbol{j}}$ for a regular kicked top [from [170]]. For two different perturbations, Eq. (B.1) and Eq. (B.5), different asymptotic power law is obtained. Top set of curves is for a perturbation in α (B.1) and bottom is for a perturbation in the rotation angle (B.5). Full curves in both cases represent numerics while dotted lines are theoretical predictions (201) and (202) without free fitting parameters.

To illustrate the above points we calculated the average fidelity decay for a kicked top and two different perturbations. In the first case we take the system already used for coherent states (B.1), for which $g(j) = j^2(1-j^2)/8$ (195). We have three zeros, with the asymptotic decay given by the one of highest order, $\eta = 2$, causing asymptotic decay,

$$\langle F(t)\rangle_{\boldsymbol{j}} \asymp \frac{\sqrt{2\pi}}{\varepsilon t\sqrt{S}}. \tag{201}$$

[11] For chaotic systems the two averages of course agree.

As a second example we take the same regular kicked top system and parameters, only the perturbation is now in rotation angle (B.5), whereas before it was in the twist parameter α. The function g is in this case $g(j) = (1 - j^2)/2$. As opposed to the previous case, we now have only two zeros of order $\eta = 1$ at $j_* = \pm 1$. The asymptotic decay is therefore

$$\langle F(t)\rangle_{\boldsymbol{j}} \asymp \frac{1}{\varepsilon^2 t^2 S}. \tag{202}$$

In Fig. 28 the results of a numerical simulation are compared with theory. Good agreement is observed with the asymptotic predictions (201) and (202). Strong revival of fidelity for the case of perturbation in the rotation angle (B.5) seen in the figure is particular to this perturbation because the beating time $t_{\rm b}$ (194) does not depend on j. Generally such revivals are absent from $\langle F(t)\rangle_{\boldsymbol{j}}$. We can therefore see that the asymptotic decay of average fidelity $\langle F(t)\rangle_{\boldsymbol{j}}$ is algebraic with the power being *system dependent*.

5.3. *Perturbations with zero time average*

Above we considered general perturbations, for which the double correlation integral (13) in regular systems was growing quadratically with time, *i.e.* time averaged perturbation $\bar{V}$ is nonzero. In the present section we discuss the situation when this correlation integral does not grow with time (asymptotically for large times), that is the time averaged perturbation is zero, $\bar{V} \equiv 0$. This are the so called *residual* perturbations because $V = V_{\rm res}$. Most of the results have been published in Ref. [16]. We will heavily rely on general derivations presented in Section 2.2. As the short time fidelity is given by the operator $\Sigma(t)$ (31) and its norm does not grow with time, the fidelity will *freeze* at a constant value called the plateau (35). After a sufficiently long time it will again start to decay due to the operator $\Gamma(t)$ (32). The main tool for theoretical derivations will be similar as for non-residual perturbations, that is using action-angle variables and evaluating resulting semiclassical ASI using stationary phase method.

5.3.1. *Coherent initial states*

Similarly as we expanded the perturbation V (181) into a Fourier series we can also expand the operator $W(t)$ which is needed to calculate the freeze plateau (35). We write it in terms of action-angle operators, $W = W(\boldsymbol{J}, \boldsymbol{\Theta})$ and then write the corresponding classical quantity $w(\boldsymbol{j}, \boldsymbol{\theta})$ as,

$$w(\boldsymbol{j}, \boldsymbol{\theta}) = \sum_{\boldsymbol{m}\neq\boldsymbol{0}} w_{\boldsymbol{m}}(\boldsymbol{j}) \mathrm{e}^{\mathrm{i}\boldsymbol{m}\cdot\boldsymbol{\theta}}. \tag{203}$$

The expansion coefficients $w_{\boldsymbol{m}}$ are easily expressed in terms of $v_{\boldsymbol{m}}$,

$$w_{\boldsymbol{m}} = -\mathrm{i}\frac{v_{\boldsymbol{m}}}{\boldsymbol{m}\cdot\boldsymbol{\omega}}. \tag{204}$$

The time dependent value of the plateau (35) is now in the leading semiclassical order

$$f_{\rm plat}(t) \cong \langle \exp\left(-\mathrm{i}\varepsilon w(\boldsymbol{J}, \boldsymbol{\Theta} + \boldsymbol{\omega}t)/\hbar\right) \exp\left(\mathrm{i}\varepsilon w(\boldsymbol{J}, \boldsymbol{\Theta})/\hbar\right)\rangle. \tag{205}$$

For sufficiently large time, say $t > t_1$, the phase $\boldsymbol{\omega}(\boldsymbol{J})t$ in the argument of the first exponential function will change over the initial state by more than 2π. In this case the averaging over initial states will yield the same result as averaging over time. Therefore, for $t > t_1$ we can replace the time dependent $f_{\rm plat}(t)$ with its time average,

$$f_{\rm plat} \cong \lim_{t\to\infty} \frac{1}{t} \int_0^t dt' f(t'). \tag{206}$$

But averaging over time is equal to averaging over angle, so we can write the expression for fidelity plateau as

$$f_{\rm plat} \cong \langle \exp\left(\mathrm{i}\frac{\varepsilon}{\hbar} w(\boldsymbol{J}, \boldsymbol{\Theta})\right) \int \frac{\mathrm{d}^d \boldsymbol{x}}{(2\pi)^d} \exp\left(-\mathrm{i}\frac{\varepsilon}{\hbar} w(\boldsymbol{J}, \boldsymbol{x})\right)\rangle. \tag{207}$$

This is a general expression for $f_{\rm plat}$ valid for any initial state. Now we shall assume the initial state to be a coherent state.

Let us first estimate the time t_1 after which the above averaging is justified. We demand $\boldsymbol{m}\Delta\boldsymbol{\omega}t_1 > 2\pi$, where $\Delta\boldsymbol{\omega}$ is a frequency change over the packet and $\boldsymbol{m}$ is the mode number of certain Fourier mode (203) $w_{\boldsymbol{m}}$. The frequency change over the initial packet is $\Delta\boldsymbol{\omega} \approx \Omega\Delta\boldsymbol{j}$, where $\Omega_{jk} = \partial\omega_j(\boldsymbol{j}^*)/\partial j_k$ and $\Delta\boldsymbol{j}$ is the size of the initial packet. For coherent states (191) it is $\Delta\boldsymbol{j} \approx \sqrt{\hbar/\Lambda}$ so that we get an estimate of t_1 for coherent initial states, $t_1 \approx \sqrt{\Lambda}/(\boldsymbol{m}\Omega\sqrt{\hbar})$. A more rigorous derivation [16] shows that the Fourier mode $w_{\boldsymbol{m}}$ decays with a Gaussian envelope on the time scale t_1,

$$t_1 = \frac{1}{\sqrt{\frac{\hbar}{4}\left(\boldsymbol{m}\cdot\Omega\Lambda^{-1}\Omega^{\mathrm{T}}\boldsymbol{m}\right)}} \propto \hbar^{-1/2}. \tag{208}$$

Therefore, all time dependent terms in $f_{\mathrm{plat}}(t)$ decay with a Gaussian envelope on the above time scale t_1. After t_1, but before t_2 when $\Gamma(t)$ becomes important, the fidelity is constant and we have a fidelity freeze. We proceed to evaluate the plateau value of this freeze f_{plat} (207) for coherent initial states. We shall use the fact that the expectation value of an arbitrary quantity is to leading order equal to this quantity evaluated at the position of the packet, $\langle\exp(-(\mathrm{i}\varepsilon/\hbar)g(\boldsymbol{J},\boldsymbol{\Theta}))\rangle \cong \exp(-(\mathrm{i}\varepsilon/\hbar)g(\boldsymbol{j}^*,\boldsymbol{\theta}^*))$, for sufficiently smooth function g, provided that the size of the wave-packet $\sim\sqrt{\hbar}$ is smaller than the oscillation scale of the exponential $\sim\hbar/\varepsilon$, *i.e.* provided $\varepsilon \ll \hbar^{1/2}$. Then the squared modulus of f_{plat} (207) reads as

$$F_{\mathrm{plat}}^{\mathrm{CIS}} \cong \frac{1}{(2\pi)^{2d}}\left|\int \mathrm{d}^d\boldsymbol{\theta}\exp\left(-\frac{\mathrm{i}\varepsilon}{\hbar}w(\boldsymbol{j}^*,\boldsymbol{\theta})\right)\right|^2, \tag{209}$$

where superscript CIS is abbreviation for coherent initial state, *i.e.* localized wave packet. This equation is the expression for the plateau for arbitrary residual perturbation. The integral over angles can not be done in general but if $\varepsilon < \hbar$ then only the linear response expression for the plateau is needed. Expanding $F_{\mathrm{plat}}^{\mathrm{CIS}}$ we obtain

$$1 - F_{\mathrm{plat}}^{\mathrm{CIS}} = \frac{\varepsilon^2}{\hbar^2}\nu_{\mathrm{CIS}}, \qquad \nu_{\mathrm{CIS}} = \sum_{\boldsymbol{m}\neq\boldsymbol{0}}|w_{\boldsymbol{m}}(\boldsymbol{j}^*)|^2. \tag{210}$$

The integral in Eq. (209) can be done analytically if the perturbation $w(\boldsymbol{j},\boldsymbol{\theta})$ (203) has a *single* nonzero Fourier mode, say $w_{\pm\boldsymbol{m}_0}$. In that case the integral gives

$$F_{\mathrm{plat}}^{\mathrm{CIS}} = J_0^2\left(2\frac{\varepsilon}{\hbar}|w_{\boldsymbol{m}_0}(\boldsymbol{j}^*)|\right), \tag{211}$$

were J_0 is the zero order Bessel function. The plateau for a single mode residual perturbation is therefore given by a Bessel function.

As a simple illustration of the above theory we again take the kicked top with a one-step propagator given in Eq. (B.9). Using classical $w(j,\theta)$ (B.11) and a single-mode formula (211) we get

$$F_{\mathrm{plat}}^{\mathrm{CIS}} = J_0^2\left(\varepsilon S\frac{\sqrt{1-j^{*2}}}{2\sin(\alpha j^*/2)}\right). \tag{212}$$

Comparison of theory with numerics is shown in Fig. 29. We can see that up to time t_1 (208) quantum fidelity follows the classical one (circles in Fig. 29). After t_1 the correspondence breaks as the classical fidelity decays as a power law, while quantum fidelity freezes. For details about classical fidelity see Section 6. The value of the plateau agrees with the linear response formula (210) for weak perturbations and with the full expression (212) for strong perturbation. Vertical chain lines show theoretical values of t_2 (calculated later), which is the time when the plateau ends. Also, at certain times quantum fidelity exhibits resonances or strong revivals. These "spikes" occurring at regular intervals can be seen also in a long time decay of fidelity in Fig. 30. These are called the echo resonances and are particular to one-dimensional systems and localized initial packets, so that the variation of the frequency derivative $\omega' = \mathrm{d}\omega(j)/\mathrm{d}j$ over the wave packet is small. Due to the discreteness of quantum energies, at certain times a constructive interference occurs, resulting in a revival of fidelity. These echo resonances must not be confused with the revivals of fidelity due to the beating phenomenon (194) which is classical, whereas echo resonances are a quantum phenomenon. The time of occurrence of a resonance t_{res} is given by

$$t_{\mathrm{res}} = \frac{2\pi}{\hbar\omega'}, \tag{213}$$

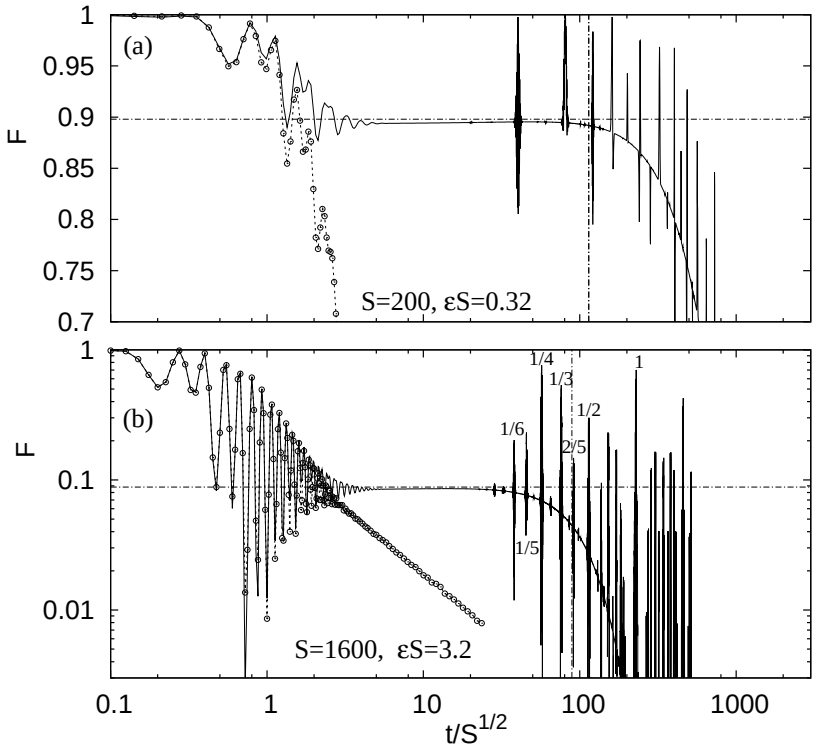

Fig. 29. Fidelity freeze for coherent initial states in a regular kicked top (B.9) [from [16]]. Symbols connected with dashed lines denote the corresponding classical fidelity while the solid line represents a quantum simulation. After the initial decay, when the quantum fidelity agrees with the classical one (until t_1), quantum fidelity freezes at the plateau (horizontal chain line, Eq. (211)). This plateau lasts long (note the log scale) until at t_2 (217), denoted by vertical chain line, decay starts again. In (b) we also indicate fractional k/p resonances with k/p marked on the figure.

or at fractional multiples of basic $t_{\rm res}$. Echo resonances have been described and explained in detail in Ref. [16] and they can also be observed in the numerical results shown in Refs. [167] and [171]. For a more mathematically oriented derivation of the condition under which they occur see also Ref. [128]. The same resonant times are also found for revivals of the wave-packet after just forward evolution studied in Refs. [172] and [173], see also the review [174]. For the quantum kicked rotor in a regime of quantum resonance similar phenomenon as freezing in regular systems can be observed due to the formal similarity of propagator [175]. It is important to realize that freeze is pure quantum phenomenon; classical fidelity does not exhibit freeze (see figure 29) even though the perturbation is exactly the same as in the quantum case!

The operator $\Sigma(t)$ determines the plateau. Long time decay on the other hand will be dictated by the operator $\Sigma_{\rm R}(t)$ (33). For long times, when this decay will take place, we can define a time averaged operator R (32),

$$\bar{R} = \lim_{t\to\infty} \frac{\Sigma_{\rm R}(t)}{t} = \lim_{t\to\infty} \frac{1}{t} \int_0^t dt' R(t'), \tag{214}$$

and approximate $\Gamma(t) \approx \bar{R}t$. This approximation is justified, because the fidelity decay will happen on a long time scale $\sim 1/\varepsilon^2$, whereas the average of R converges in a much shorter classical averaging time $t_{\rm ave}$. For R the semiclassical limit r can be calculated using the Poisson brackets instead of commutators, $r = -\{w, dw/dt\}$. When we average r over time, only the zeroth Fourier mode survives resulting in

$$\Gamma(\boldsymbol{J})/t \cong \bar{r}(\boldsymbol{J}), \qquad \bar{r}(\boldsymbol{j}) = -\sum_{\boldsymbol{m}\neq\boldsymbol{0}} \boldsymbol{m}\cdot\partial_{\boldsymbol{j}} \left\{ |w_{\boldsymbol{m}}(\boldsymbol{j})|^2\, \boldsymbol{m}\cdot\boldsymbol{\omega}(\boldsymbol{j}) \right\}. \tag{215}$$

Provided $\varepsilon/\hbar$ is sufficiently small (*i.e.* the plateau is high) the echo operator can be for long times approximated by $M_\varepsilon \cong \exp\left(-{\rm i}\varepsilon^2 \bar{R}t/2\hbar\right)$. Long time decay of fidelity can then be calculated by evaluating the ASI

in analogy to the procedure developed for non-residual perturbations (188), replacing the perturbation ε with $\varepsilon^2/2$ and $\bar{v}$ with $\bar{r}$. Using formula $F(t) = \exp\left(-(t/\tau_{\rm r})^2\right)$ (192), we obtain long-time fidelity decay for coherent states and residual perturbations,

$$F(t) \cong \exp\left\{-(t/\tau_{\rm rr})^2\right\}, \qquad \tau_{\rm rr} = \frac{1}{\varepsilon^2}\sqrt{\frac{8\hbar}{\bar{\boldsymbol{r}}' \cdot \Lambda^{-1}\bar{\boldsymbol{r}}'}}. \tag{216}$$

The semiclassical value of $\bar{r}$ is given in Eq. (215) and its derivative is $\bar{\boldsymbol{r}}' = \partial_{\boldsymbol{J}}\bar{r}$. The decay time scales as $\tau_{\rm rr} \sim \hbar^{1/2}\varepsilon^{-2}$ and is thus smaller than the upper limit $t_{\rm a} \sim \hbar^0\varepsilon^{-2}$ of the validity of the ASI approximation. Remember that the above formula is valid only if the plateau is close to $F = 1$, such that the term $\Sigma(t)$ can be neglected. For such small ε the crossover time t_2 from the plateau to the long time decay can be estimated by comparing the linear response plateau (210) with the long time decay (216), resulting in $t_2 \approx \tau_{\rm rr}\varepsilon\sqrt{\nu_{\rm CIS}}/\hbar \sim \hbar^{-1/2}\varepsilon^{-1}$. For stronger perturbations, namely up to $\varepsilon \sim \sqrt{\hbar}$ time t_2 can be estimated as $\tau_{\rm rr}$. We therefore have

$$t_2 = \min\{1, \frac{\varepsilon}{\hbar}\nu_{\rm CIS}^{1/2}\}\tau_{\rm rr} = \min\{\text{const } \hbar^{1/2}\varepsilon^{-2}, \text{const } \hbar^{-1/2}\varepsilon^{-1}\}. \tag{217}$$

The theoretical prediction for the departure point t_2 (217) of fidelity from the plateau is plotted as a vertical chain line in Fig. 29. In Fig. 30 we show results of long time numerical simulation for the kicked top (B.9). The agreement with theoretical Gaussian decay (216) is good.

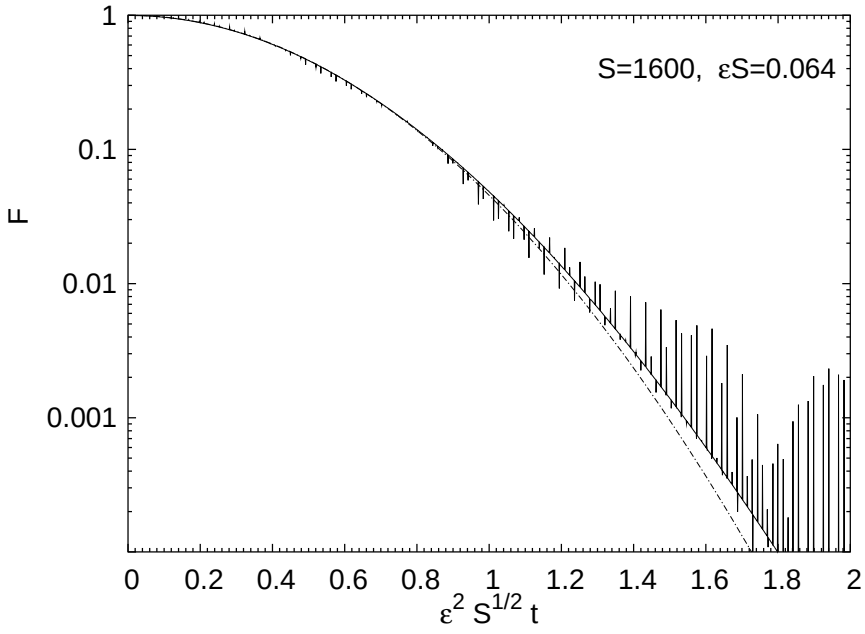

Fig. 30. Long time ballistic decay after the freeze plateau for the regular kicked top (B.9) with coherent initial state and residual perturbation [from [16]]. Chain curves indicate theoretical Gaussian decay (216) with analytically computed coefficients. The decay is the same as for non-residual perturbations but with a "renormalized" perturbation strength $\varepsilon^2/2$ and perturbation $\bar{r}$ instead of $\bar{v}$.

5.3.2. *Freeze in a harmonic oscillator*

The time t_1 (208) when the plateau starts can diverge for systems with vanishing frequency derivatives Ω. Such is the case for instance in harmonic oscillator where $\Omega = 0$. One can show that in this case the plateau is not constant but oscillates and is in the linear response regime by factor $1/\hbar$ *higher* than in systems with $\Omega \neq 0$. The full expression for the plateau for the harmonic oscillator and coherent initial state is [170]

$$F_{\rm plat}^{\rm CIS} = \exp\left(-\frac{\varepsilon^2}{\hbar}\nu_{\rm har}\right), \tag{218}$$

where $\nu_{\rm har}$ is some time-dependent coefficient. This expression must be compared with the Bessel function (211) for systems with nonzero Ω. Because Bessel functions decay asymptotically in an algebraic way, the plateau for large perturbations is *smaller* in harmonic oscillators than in general systems (note that for small perturbations it is *larger*). As opposed to general situation, for harmonic oscillator classical fidelity agrees with the quantum one despite the freeze. Because of inequality (78) there is also freeze in reduced fidelity and purity. The plateau in reduced fidelity scales the same as for fidelity (218) whereas is does not depend on $\hbar$ for purity. The long time decay of fidelity or of reduced fidelity and purity after the plateau ends does not show any peculiarities for the harmonic oscillator. For further details as well as for a numerical example in Jaynes-Cummings system see Ref. [170].

5.3.3. *Rotational orbits*

So far we have always talked about the operator $\bar{V}$ being either zero or not, resulting in a qualitatively different decay of quantum fidelity. Similar behavior as for $\bar{V}=0$ might occur for particular localized initial states provided the expectation value of $\bar{V}$ and its powers are zero, $\langle \bar{V}^n\rangle \equiv 0$, even if on the operator level we have $\bar{V}\neq 0$. Such situation might occur in regular systems having rotational orbits in classical phase space. For these we may have perturbations which have $\langle \bar{v}\rangle_{\rm class}=0$ and correspondingly quantum freeze occurs. Note that for classical fidelity only the functional dependence will change from a Gaussian to a power-law as one puts the initial coherent state in the rotational part of phase space, in both cases depending on εt [63]. Quantum fidelity on the other hand decays as a Gaussian on a time scale $\tau_{\rm r}\sim 1/\varepsilon$ in the case of $\langle V\rangle\neq 0$, while it displays a freeze and later decays on a much longer time scale $\tau_{\rm rr}\sim 1/\varepsilon^2$ for $\langle V\rangle = 0$. Freeze of quantum fidelity and correspondingly short correspondence between quantum and classical fidelity for an initial state put in the rotational part of phase space has been observed in Ref. [167].

Interesting behavior might emerge at borders between regions with $\langle \bar{V}^n\rangle = 0$ and $\langle \bar{V}^n\rangle \neq 0$, for instance close to separatrices that separate rotational parts of a phase space from the rest. The decay of quantum fidelity at such a border has been studied in Ref. [171]. While far away in the rotational part of phase space the freeze has been observed, even though on the operator level one has $\bar{V}\neq 0$, interesting and non-trivial behavior has been seen in the transition region. There fidelity decays as a power law, depending on the product εt, *i.e.* on a time scale $\tau\sim 1/\varepsilon$. Such power-law decay is actually not a complete surprise, as the average fidelity (Section 5.2.3) also decays as a power-law due to regions of phase space with diverging time-scale $\tau_{\rm r}$ of Gaussian decay (192). Still, exact theoretical understanding of the fidelity decay close to separatrices is lacking.

5.3.4. *Random initial states*

Similarly as for non-residual perturbations (Section 5.2.2) we again assume a finite Hilbert space of sufficient size, such that the difference between fidelity for one specific random state and an average over all states can be neglected. We shall replace quantum averages with classical averages, $\langle g(\boldsymbol{J},\boldsymbol{\Theta})\rangle \cong \frac{1}{\mathcal{V}}\int {\rm d}^d\boldsymbol{j}{\rm d}^d\boldsymbol{\theta}\, g(\boldsymbol{j},\boldsymbol{\theta})$. First we calculate the plateau. Calculating the plateau for coherent initial states, we argued that after time t_1 (208) the fidelity is time-independent and we have a plateau. For random initial states the same happens, only the time t_1 is different. One can use the same argumentation as for coherent states, taking into account that the effective size $\Delta\boldsymbol{j}$ of random states is $\Delta\boldsymbol{j}\sim\mathcal{O}(1)$, resulting in

$$t_1 \sim \frac{1}{|\boldsymbol{m}\Omega|}\sim \varepsilon^0\hbar^0. \tag{219}$$

Compared to coherent states, t_1 is now independent of $\hbar$ and is therefore smaller. After averaging time t_1 we can use the general time averaged expression for the value of the plateau (207), arriving at

$$f_{\rm plat}^{\rm RIS}\cong \frac{(2\pi)^d}{\mathcal{V}}\int {\rm d}^d\boldsymbol{j}\left|\int \frac{{\rm d}^d\boldsymbol{\theta}}{(2\pi)^d}\exp\left(-\frac{{\rm i}\varepsilon}{\hbar}w(\boldsymbol{j},\boldsymbol{\theta})\right)\right|^2, \tag{220}$$

where RIS stands for random initial state. Interestingly, the plateau for a random initial state is the *average* plateau for a coherent state squared, where averaging is done over the position of the initial coherent state. If we denote the plateau for a coherent initial state centered at $\boldsymbol{j}^*$ by $F_{\rm plat}^{\rm CIS}(\boldsymbol{j}^*)$ (209), then the plateau for a random initial state $F_{\rm plat}^{\rm RIS}$ is

$$F_{\rm plat}^{\rm RIS} \cong \left| \frac{(2\pi)^d}{\mathcal{V}} \int \mathrm{d}^d \boldsymbol{j} F_{\rm plat}^{\rm CIS}(\boldsymbol{j}) \right|^2 . \tag{221}$$

One word of caution is necessary though concerning the above formula. The $w(\boldsymbol{j}, \boldsymbol{\theta})$ (204) needed in the calculation of $F_{\rm plat}^{\rm CIS}(\boldsymbol{j}^*)$ (209) diverges at points in phase space where $\boldsymbol{m} \cdot \boldsymbol{\omega}(\boldsymbol{j}) = 0$. For a coherent initial state this was no real problem as divergence would occur only if we placed the initial packet at such a point. For random initial state though, there is an average over the entire action space in the plateau formula (221) and if there is a single diverging point somewhere in the phase space it will cause divergence. The solution to this is fairly simple. If we compare the semiclassical formula for $w_{\boldsymbol{m}}$ (204) with its quantum version for matrix elements W_{jk} (30), we see that there are no divergences in W_{jk} as the matrix element V_{jk} is for residual perturbations zero precisely for those j, k which would give divergence due to vanishing $E_j - E_k$. Remembering that the integral in the formula for $F_{\rm plat}^{\rm RIS}$ over $\boldsymbol{j}$ is actually an approximation for a sum over $\hbar\boldsymbol{n}$ the remedy is to retain the original sum over the eigenvalues of the action operator excluding all diverging terms. The formula for the plateau in the case of such divergences is therefore

$$F_{\rm plat}^{\rm RIS} \cong \left| \frac{1}{\mathcal{N}} \sum_{\boldsymbol{n}}^{\boldsymbol{m}\cdot\boldsymbol{\omega}(\hbar\boldsymbol{n})\neq 0} F_{\rm plat}^{\rm CIS}(\hbar\boldsymbol{n}) \right|^2 . \tag{222}$$

In the summation over $\boldsymbol{n}$ we exclude all terms in which, for any constituent Fourier mode $\boldsymbol{m}$, we would have $\boldsymbol{m} \cdot \boldsymbol{\omega}(\hbar\boldsymbol{n}) = 0$. To summarize, if there are no points with $\boldsymbol{m} \cdot \boldsymbol{\omega} = 0$ in phase space on can use the integral formula (221), otherwise a summation formula (222) must be used.

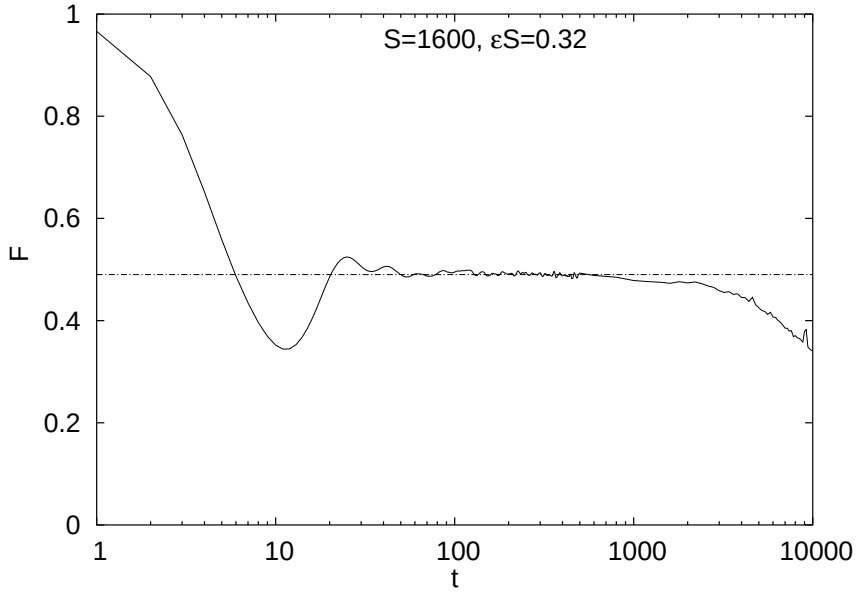

Fig. 31. Fidelity plateau for a random initial state for the regular kicked top (B.9) [from [16]]. The chain line shows the theoretical value of the plateau as computed from Eq. (222). Due to near resonant terms with small $\boldsymbol{m} \cdot \boldsymbol{\omega}(\boldsymbol{j})$ the plateau is lower than in Fig. 29, even though the perturbation is of the same strength.

To illustrate the summation formula for the plateau, we use the same kicked top as for coherent states (B.9). As one can see in Fig. 31 the agreement with numerics is very good. Compared to Fig. 29(a) for coherent state (where the same perturbation strength is used) the plateau is here much lower due to near-diverging terms. For a numerical example of a system with no singularities, where the integral formula (221) can be used, see Ref. [16].

For long times, after the plateau ends at $t_2 \sim 1/\varepsilon$, the fidelity again starts to decrease due to increasing $\Gamma(t)$. The calculation using ASI is analogous to the case of non-residual perturbations, Eq. (197), one just has to replace $\bar{v}$ with $\bar{r}$ and ε with $\varepsilon^2/2$. We shall only give the result,

$$F(t) \asymp \left(\frac{t_{\rm ran}}{t}\right)^d, \qquad t_{\rm ran} = \text{const} \times \frac{\hbar}{\varepsilon^2}. \tag{223}$$

For comparison with numerical simulation see Ref. [16].

Finally, we make a short comment on the behavior of average fidelity (averaged over positions of coherent states) for residual perturbations. For non-residual perturbations we have seen in Section 5.2.3 that the asymptotic decay is determined by the divergences of the decay time $\tau_{\rm r}$. For residual perturbation the situation is very similar. During the plateau, until time t_2, averaging of the plateaus for coherent states gives the plateau for random states. Thus in the average fidelity one still has a plateau of order $1 - F \sim (\varepsilon/\hbar)^2$ (in the linear response). After the plateau, we have to average Gaussian decay (216), where in general divergences of $\tau_{\rm rr}$ will cause a power-law asymptotic decay. The power will depend on the nature of the divergence and therefore on the perturbation The only difference to general perturbations is that the decay depends on the parameter $\varepsilon^2 t$ and not on εt as for non-residual perturbations. Note though that some researchers [176] have predicted a universal $t^{-3d/2}$ decay of average fidelity for residual perturbations, that is with the power depending only on the dimension d and not on perturbation specifics. The reason for the discrepancy between these results is presently unclear.

5.4. *Composite systems and entanglement*

In case of composite systems one might not be interested in the influence of perturbations on the whole system but just on some "central" subsystem of interest. Stability of a subsystem is quantified by reduced fidelity $F_{\rm R}(t)$ (72) and by echo purity $F_{\rm P}(t)$ (74). We shall mostly discuss coherent initial states, *i.e.* a direct product of localized packets for central subsystem and environment, for which semiclassical treatment is the most simple. At the end we shall also comment on other possible choices of initial states.

The calculation of the reduced fidelity is quite analogous to the one for fidelity (192). We again employ a classical time averaged perturbation $\bar v(\mathbf{j})$, where the action vector $\mathbf{j}$ has $d_{\rm c}$ components $\mathbf{j}^{\rm c}$ for the central system and $d_{\rm e}$ components $\mathbf{j}^{\rm e}$ for the environment, $\mathbf{j} = (\mathbf{j}^{\rm c}, \mathbf{j}^{\rm e})$, if $d_{\rm c}$ and $d_{\rm e}$ are the number of degrees of freedom (DOF) of the central subsystem and environment, respectively. The shape of the initial packet is given by squeezing matrices $\Lambda_{\rm c}$ and $\Lambda_{\rm e}$ for the central subsystem and the environment, respectively. The derivatives of the classical $\bar v$ with respect to actions can be written as

$$\bar{\boldsymbol{v}}' = (\bar{\boldsymbol{v}}'_{\rm c}, \bar{\boldsymbol{v}}'_{\rm e}), \qquad \bar{\boldsymbol{v}}'_{\rm c} = \frac{\partial \bar{\boldsymbol{v}}(\boldsymbol{j}^*)}{\partial \boldsymbol{j}^{\rm c}}, \qquad \bar{\boldsymbol{v}}'_{\rm e} = \frac{\partial \bar{\boldsymbol{v}}(\boldsymbol{j}^*)}{\partial \boldsymbol{j}^{\rm e}}. \tag{224}$$

Performing Gaussian integrals in action space gives reduced fidelity [50]

$$F_{\rm R}(t) = \exp\left(-\frac{\varepsilon^2}{\hbar^2}\bar C_{\rm R} t^2\right), \qquad \bar C_{\rm R} = \frac{1}{2}\hbar\left(\bar{\boldsymbol{v}}'_{\rm c}\Lambda_{\rm c}^{-1}\bar{\boldsymbol{v}}'_{\rm c}\right). \tag{225}$$

A single parameter $\bar C_{\rm R}$ determines the reduced fidelity decay. This must be compared with $\bar C = \frac{1}{2}\hbar\left(\bar{\boldsymbol{v}}'_{\rm c}\Lambda_{\rm c}^{-1}\bar{\boldsymbol{v}}'_{\rm c} + \bar{\boldsymbol{v}}'_{\rm e}\Lambda_{\rm e}^{-1}\bar{\boldsymbol{v}}'_{\rm e}\right)$ (192) which governs fidelity decay. Compared to fidelity, reduced fidelity depends understandably only on perturbation derivatives with respect to actions of the central system. But note that the average coupling $\bar v$ depends also on the dynamics of the environment and so $\bar C_{\rm R}$ itself does depend on the environment.

The derivation of echo purity (or in special case of uncoupled unperturbed dynamics of purity) is a little more involved. We have to calculate averages of the form

$$\begin{aligned} F_{\rm P}(t) &\cong \hbar^{-2d}\int d\boldsymbol{j}\, d\tilde{\boldsymbol{j}}\, \exp\left(-{\rm i}\frac{\varepsilon t}{\hbar}\Phi\right) d_\rho(\boldsymbol{j}) d_\rho(\tilde{\boldsymbol{j}}), \\ \Phi &= \bar v(\boldsymbol{j}^{\rm c}, \boldsymbol{j}^{\rm e}) - \bar v(\tilde{\boldsymbol{j}}^{\rm c}, \boldsymbol{j}^{\rm e}) + \bar v(\tilde{\boldsymbol{j}}^{\rm c}, \tilde{\boldsymbol{j}}^{\rm e}) - \bar v(\boldsymbol{j}^{\rm c}, \tilde{\boldsymbol{j}}^{\rm e}), \end{aligned} \tag{226}$$

with $d_\rho(\boldsymbol{j})$ being the initial density (191) of the wave packet. When expanding $\bar v(\mathbf{j})$ around the position $\mathbf{j}_*$ of the initial packet, the constant term, the linear terms as well as the diagonal quadratic terms cancel exactly, regardless of the position of the initial packet. The lowest non-vanishing contribution comes from non-diagonal quadratic term

$$-{\rm i}\frac{\varepsilon t}{\hbar}\left[(\boldsymbol{j}^{\rm c} - \tilde{\boldsymbol{j}}^{\rm c})\cdot \bar v''_{\rm ce}(\boldsymbol{j}_*)(\boldsymbol{j}^{\rm e} - \tilde{\boldsymbol{j}}^{\rm e})\right], \tag{227}$$

where $\bar{v}''_{\rm ce}$ is a $d_{\rm c} \times d_{\rm e}$ matrix of mixed second derivatives of $\bar{v}$ evaluated at the position of the initial packet,

$$(\bar{v}''_{\rm ce})_{kl} = \frac{\partial^2 \bar{v}}{\partial (\boldsymbol{j}^{\rm c})_k \partial (\boldsymbol{j}^{\rm e})_l}. \tag{228}$$

After performing integrations we get the final result (see Ref. [177] for details)

$$F_{\rm P}(t) = \frac{1}{\sqrt{\det\left(\mathbb{1} + (\varepsilon t)^2 u\right)}}, \quad u = \Lambda_{\rm c}^{-1} \bar{v}''_{\rm ce} \Lambda_{\rm e}^{-1} \bar{v}''_{\rm ec}, \tag{229}$$

where u is a $d_{\rm c} \times d_{\rm c}$ matrix involving $\bar{v}''_{\rm ce}$ and its transpose $\bar{v}''_{\rm ec}$. Note that the matrix u is a classical quantity (independent of $\hbar$) that depends only on the observable $\bar{v}$ and on the position of the initial packet. For small εt we can expand the determinant and we get initial quadratic decay in the linear response regime (special case of Eq. (84)),

$$F_{\rm P}(t) = 1 - \frac{1}{2}(\varepsilon t)^2 \,{\rm tr}\, u + \cdots . \tag{230}$$

The most prominent feature of the expression (229) for the echo purity (or purity) decay for initial product wave packets is its $\hbar$ independence. In the linear response calculation this $\hbar$-independence has been theoretically predicted in Ref. [162] as well as numerically confirmed [50]. We see that the scaling of the decay time $\tau_{\rm P}$ of $F_{\rm P}(t)$ is $\tau_{\rm P} \sim 1/\varepsilon$. This means that echo purity will decay on a very long time scale and so localized wave packets are universal pointer states [178], *i.e.* states robust against decoherence [91]. For large times we use the fact that $\det(\mathbb{1} + zu)$ is a polynomial in z of order $r = {\rm rank}\,(u)$ and find asymptotic power law decay $F_{\rm P}(t) \asymp {\rm const}\,(\varepsilon t)^{-r}$. Note that the rank of u is bounded by the smallest of the subspace dimensions, *i.e.* $1 \leq r \leq \min\{d_{\rm c}, d_{\rm e}\}$, since the definition (74) is symmetric with respect to interchanging the roles of the subspaces "c" and "e". Let us give two simple examples: (i) For $d_{\rm c} = 1$ and for *any* $d_{\rm e}$ we shall always have asymptotic power law decay with $r = 1$. If a *single* DOF of the subsystem "c" is coupled with *all* DOF of the subsystem "e", *e.g.* $\bar{v} = j^{\rm c} \otimes (j^{\rm e1} + j^{\rm e2} + \cdots)$, then $|\bar{v}''|^2 \propto d_{\rm e}$ and we have $F_{\rm P}(t) \asymp 1/(\varepsilon t \sqrt{d_{\rm e}})$; (ii) Let us consider a multidimensional system where the matrix u is of rank one so it can be written as a direct product of two vectors, $u = \boldsymbol{x} \otimes \boldsymbol{y}$. The determinant occurring in $F_{\rm P}(t)$ is $\det\left(\mathbb{1} + (\varepsilon t)^2 u\right) = 1 + (\varepsilon t)^2 \boldsymbol{x} \cdot \boldsymbol{y}$. Such is the case for instance if we have a coupling of the same strength between all pairs of DOF. The dot product is then $\boldsymbol{x} \cdot \boldsymbol{y} \propto d_{\rm c} d_{\rm e}$ and we find $F_{\rm P}(t) \asymp 1/(\varepsilon t \sqrt{d_{\rm c} d_{\rm e}})$. The power of the algebraic decay is independent of both $d_{\rm c}$ and $d_{\rm e}$. The bottom line is, that the power law of the asymptotic decay depends on the perturbation. In Refs. [124,179] the author predicted $\sim t^{-d}$ decay of purity for intermediate times and universal $\sim t^{-2d}$ decay for large times. While the intermediate decay is in accord with our theory, its long time decay is not. For numerical examples where asymptotic decay of purity exhibits different powers see Ref. [177].

To demonstrate the theory of reduced fidelity and echo purity decay we again take two coupled kicked tops, using a regular propagator in Eq. (B.18). We take $S = 100$, coupling $\varepsilon = 0.01$ and coherent initial state. As the unperturbed dynamics is uncoupled $F_{\rm P}(t)$ is actually equal to purity $I(t)$. The results of the numerical simulation are plotted in Fig. 32 together with the theoretical predictions (225) for reduced fidelity and for purity (229). No fitting is involved.

In the above paragraph we have discussed coherent initial states. What about other choices? We shall consider two possibilities: (i) superposition of two coherent states - so called cat states and (ii) random initial states. In both cases we assume that the unperturbed evolution is uncoupled, so echo purity equals purity. Let us first describe the decay of purity $I(t)$ for cat states,

$$|\psi(0)\rangle = \frac{1}{\sqrt{2}} \left(|\psi_{\rm c1}(0)\rangle + |\psi_{\rm c2}(0)\rangle\right) \otimes |\psi_{\rm e}(0)\rangle, \tag{231}$$

where the initial positions of the wave packets $\psi_{\rm c1}(0)$, $\psi_{\rm c2}(0)$ and $\psi_{\rm e}(0)$ are $\boldsymbol{j}^{*{\rm c1}}$, $\boldsymbol{j}^{*{\rm c2}}$ and $\boldsymbol{j}^{*{\rm e}}$, respectively. Assuming that the initial packets of the central subsystem are orthogonal the initial reduced density matrix is

$$\rho_{\rm c}(0) = \frac{1}{2} \left(|\psi_{\rm c1}(0)\rangle\langle\psi_{\rm c1}(0)| + |\psi_{\rm c2}(0)\rangle\langle\psi_{\rm c2}(0)| + |\psi_{\rm c2}(0)\rangle\langle\psi_{\rm c1}(0)| + |\psi_{\rm c1}(0)\rangle\langle\psi_{\rm c2}(0)|\right), \tag{232}$$

and represents coherent superposition of two macroscopically separated packets – superposition of "dead and alive cat" [180] – see also a popular account in Ref. [91]. What we would like to illustrate is decoherence.

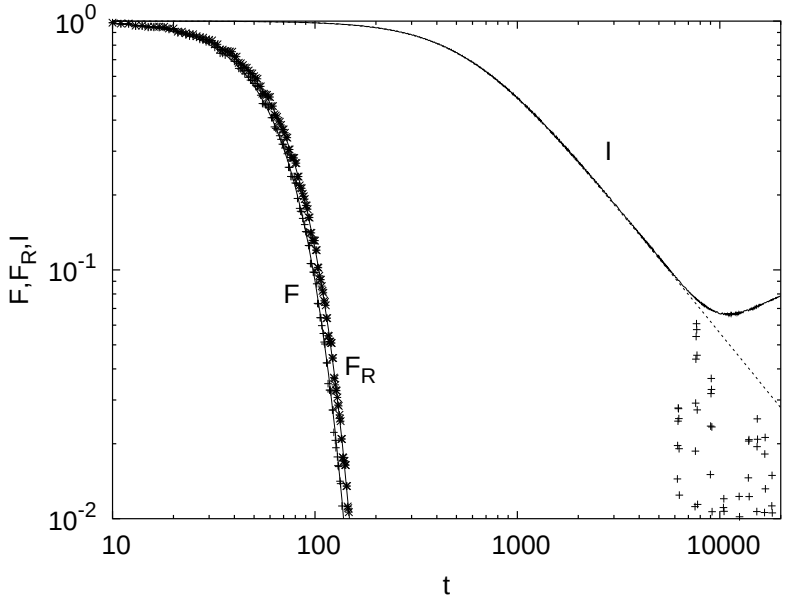

Fig. 32. Decay of fidelity $F(t)$, reduced fidelity $F_{\rm R}(t)$ and purity $I(t)$ for integrable dynamics and localized initial packets [from [170]]. The theoretical Gaussian decay for the fidelity (192) and the reduced fidelity (225) overlaps with the numerics (symbols). Purity decays asymptotically as a power law (229) and also nicely agrees with the numerics (full curve), until a finite size saturation level is reached. Note that purity decays on a much longer time scale than fidelity and reduced fidelity due to independence of its decay time on the small parameter $\hbar$.

Decoherence is a process where off diagonal matrix elements of the initial reduced density matrix dissappear due to the coupling with the environment, so that the resulting reduced density matrix $\rho_{\rm c}^{\rm mix}(\tau_{\rm dec})$ is a statistical mixture of two diagonal contributions only,

$$\rho_{\rm c}^{\rm mix}(\tau_{\rm dec}) = \frac{1}{2}\left(|\psi_{\rm c1}(\tau_{\rm dec})\rangle\langle\psi_{\rm c1}(\tau_{\rm dec})| + |\psi_{\rm c2}(\tau_{\rm dec})\rangle\langle\psi_{\rm c2}(\tau_{\rm dec})|\right), \tag{233}$$

with $\tau_{\rm dec}$ being decoherence time. Here we already used the fact that purity for individual localized packets decays on a long $\hbar$ independent time scale (229) and because we expect $\tau_{\rm dec}$ to be much shorter, we can use propagated packets as pointer states. During the process of decoherence purity will decay from $I(0) = 1$ for the initial reduced density matrix $\rho_{\rm c}(0)$ to $I(\tau_{\rm dec}) = 1/2$ for decohered matrix $\rho_{\rm c}^{\rm mix}(\tau_{\rm dec})$. Using similar techniques as for the calculation of echo purity for individual coherent states (229), one can also calculate purity for cat states, the result being [181]

$$I(t) = \frac{1}{4}(I_1(t) + I_2(t) + 2F_{\rm e}(t)), \tag{234}$$

where $I_{1,2}(t)$ are purities (229) for individual constituent coherent states, that is for $\psi_{\rm c1,c2}(0) \otimes \psi_{\rm e}(0)$, while $F_{\rm e}(t)$ is a cross-correlation quantity similar to reduced fidelity. Explicitly, it is given by

$$F_{\rm e}(t) = \exp\left(-t^2/\tau_{\rm dec}^2\right), \qquad \tau_{\rm dec} = \sqrt{\hbar/C_{\rm e}}/\varepsilon$$
$$C_{\rm e} = \frac{1}{2}\left(\bar{v}'_{\rm e}(\boldsymbol{j}^{*\rm c1}) - \bar{v}'_{\rm e}(\boldsymbol{j}^{*\rm c2})\right)\Lambda_{\rm e}^{-1}\left(\bar{v}'_{\rm e}(\boldsymbol{j}^{*\rm c1}) - \bar{v}'_{\rm e}(\boldsymbol{j}^{*\rm c2})\right). \tag{235}$$

Decoherence for regular systems can now be understood from the very different time scales on which $I_{1,2}$ and $F_{\rm e}$ decay. $F_{\rm e}(t)$ decays fast as a Gaussian on an $\hbar$-dependent time scale while $I_{1,2}(t)$ decay slowly on an $\hbar$-independent time scale. At the point when $F_{\rm e}(t)$ becomes negligibly small, purity will be simply $I(t) \approx (I_1(t) + I_2(t))/4$ and therefore approximately equal to $1/2$. The decay of $F_{\rm e}(t)$ therefore signifies decoherence with the decoherence time scale $\tau_{\rm dec}$ being simply equal to the decay time of $F_{\rm e}(t)$ (235). On the other hand, the decay of $I_{1,2}(t)$ is a signal of relaxation of individual packets to equilibrium. In the simple case when $\bar{v}$ has coupling terms between all pairs of degrees of freedom one can see [181] that $C_{\rm e}$ scales as

$C_\mathrm{e} \sim d_\mathrm{c} d_\mathrm{e} (\boldsymbol{\jmath}^{*\mathrm{c}1} - \boldsymbol{\jmath}^{*\mathrm{c}2})^2$ and therefore the decoherence time scales as $\tau_\mathrm{dec} \sim \sqrt{\hbar/(d_\mathrm{c} d_\mathrm{e})}/(\varepsilon |\boldsymbol{\jmath}^{*\mathrm{c}1} - \boldsymbol{\jmath}^{*\mathrm{c}2}|)$. It therefore goes to zero in any of the following four limits: the semiclassical limit $\hbar \to 0$, the thermodynamic limit of large environment and/or large central subsystem, $d_\mathrm{c,e} \to \infty$, the limit of macroscopic superpositions, *i.e.* of large packet separation, $|\boldsymbol{\jmath}^{*\mathrm{c}1} - \boldsymbol{\jmath}^{*\mathrm{c}2}| \to \infty$ and finally the limit of strong coupling. Note that these are exactly the limits one needs to explain the lack of cat states in classical macroscopic world of large objects! One should note that irreversible decoherence is possible only in the thermodynamic limit. For a finite integrable system there will be partial revivals of purity at large times. This revivals get less prominent and happen at larger times with increasing dimensionality d or decreasing $\hbar$. Also, due to high sensitivity of systems to perturbation, reversing the process of decoherence will be in practice close to impossible. Therefore, for all practical purposes one can observe decoherence also in a sufficiently large but finite regular system. For the theory presented here (234) we needed that the average perturbation $\bar{V}$ converged, *i.e.* time is larger than the classical averaging time t_ave. But for sufficiently separated packets decoherence time τ_dec will eventually get very small [182–184], even smaller than t_ave. We can circumvent this difficulty by noting that for very short times one can instead of the time averaged $\bar{V}$ use just an instantaneous time independent $V(0)$. Then our theory can again be used [181]. The theory developed here therefore applies to truly macroscopic superpositions of localized wave packets (for which τ_dec is very small) regardless whether the dynamics are regular or chaotic.

Let us now demonstrate the decay of purity for cat states (234) by a numerical experiment. We take a system of two coupled anharmonic oscillators with $\hbar = 1/500$ and coupling $\varepsilon = 0.01$, for details see Ref. [181]. The results are shown in Fig. 33, where one can nicely see two different regimes of purity decay. In the first one fast Gaussian decoherence happens until purity reaches $I = 1/2$ at $\tau_\mathrm{dec} \sim 30$, and in the second one a slow algebraic relaxation takes place.

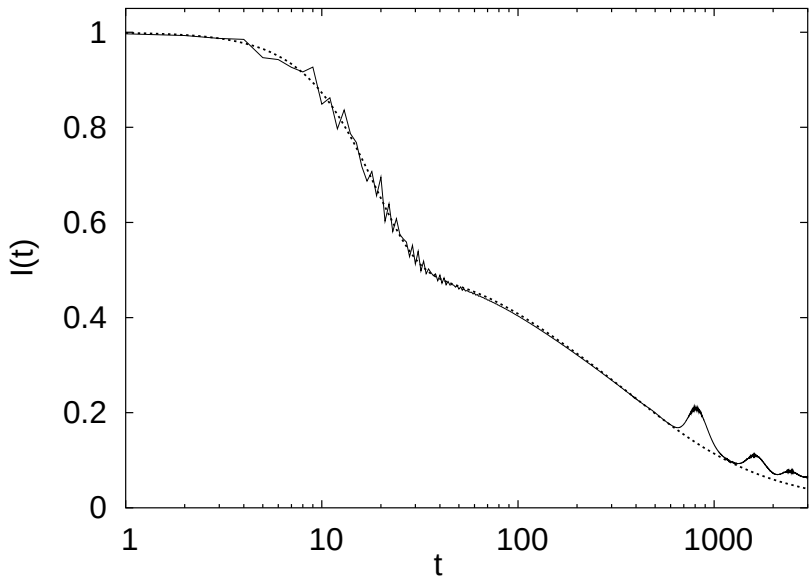

Fig. 33. Decay of purity $I(t)$ (234) in a regular system for an initial cat state (231) [from [181]]. The dotted curve shows the theoretical prediction (234) with no fit parameters, and the full curve shows numerics. The initial decay of purity until $\tau_\mathrm{dec} \sim 30$ is given by a fast Gaussian decay of $F_\mathrm{e}(t)$ (235). At the end of decoherence purity is $I(\tau_\mathrm{dec}) = 1/2$, then the relaxation of individual packets begins, visible as a slow power-law decay of purities $I_{1,2}(t)$ (229).

In the context of quantum information perhaps more interesting than coherent states are random initial states. For regular dynamics echo purity will initially decay quadratically, but on $\hbar$ dependent scale that is typically much shorter than for coherent initial states. Echo purity for random states in a spin chain (a system having no classical limit) has been studied in Ref. [49]. In the linear response regime a quadratic decay has been observed and interestingly the full functional form of the decay approached a Gaussian in

the thermodynamical limit. Quadratic decay of concurrence, a quantity describing entanglement for mixed states, has been observed for an integrable spin chain [110]. In Ref. [185] the initial entanglement production rate (time derivative of purity) as well as its asymptotic saturation value have been studied for random state averaging and for coherent state averaging. In the integrable regime the initial entanglement production rate is much larger for random state averages than for coherent state averages due to a different $\hbar$ dependence of the corresponding correlation functions. Decoherence in a system of two $\frac{1}{2}$ spins coupled to a bath composed of a number of spin $\frac{1}{2}$ particles has been studied in Ref. [186]. It has been numerically found that decoherence is faster when the internal bath dynamics is chaotic than when it is regular. Interestingly, in a certain regime of parameters decoherence decreases by increasing coupling strength to the bath.

An interesting question is to what extent the decay of e.g. purity can be described classically. The classical analog of decoherence has been considered in Refs. [187–190]. Using a perturbative approach the influence of the type of the perturbation and of the dynamics on the quantum-classical correspondence were explored, see also Ref. [191] for a study of quantum-classical correspondence of entanglement in coupled harmonic oscillators.

We shall not discuss the decay of reduced fidelity or of echo purity in the case of freeze. Based on the general inequality between the three quantities (78), we can immediately state that reduced fidelity and echo purity will also exhibit freeze. For an example of purity freeze in a harmonic oscillator see Ref. [170] and also Section 5.3.2.

5.5. *Mixed phase space*

For classically mixed situation, with coexisting regular and chaotic regions in phase space, much less is known than for purely regular (Section 5) or chaotic (Section 3) dynamics. If a localized packet is started completely within a region of phase space having regular/chaotic structure one can use the appropriate theory for quantum fidelity. One should be cautious though as there can be different time-scales involved that are not present in purely regular or chaotic situations. The behavior of fidelity in the border region between regular and chaotic components might be particularly tricky. Two effects can be important at such a border: (i) classical dynamics in border region is "sticky", *i.e.* diffusive, causing a slow power-law decay of various classical quantities [192–194]. Here the value of $\hbar$ might be very important for the impact this classical phenomenon has on quantum fidelity decay. On the other hand, there are also pure quantum effects that will influence fidelity decay, (ii) the transition between $\langle \bar{V} \rangle \neq 0$ for regular region (in typical situation) and $\langle \bar{V} \rangle \to 0$ in chaotic region occurs at the border. We have seen that for regular dynamics the fidelity typically decays as a power-law at points with vanishing average perturbation (actually vanishing $\bar{v}'$), for instance around separatrices. Similarly, average fidelity (200) also has a power-law decay. Therefore, both effects suggest a power-law decay of quantum fidelity at the border between chaotic and regular regions of phase space. The fidelity decay in such region has been numerically studied in Ref. [195]. They were able to fit a two-parameter power-law formula to the numerically obtained fidelity decay, although the results were less than convincing as the power-law covered less than one order of magnitude. To numerically evaluate quantum fidelity for systems with mixed classical phase space on can use the dephasing representation. In Refs. [57,58] it has been shown that the dephasing representation works well in such situations. Other numerical results are reported in Ref. [148].

Another point worth mentioning is the actual transition from regular to chaotic behavior as some parameter of the system is varied. Due to finite $\hbar$ the transition will generally not happen at the same parameter value as for classical dynamics. In particular, in Ref. [105] the parameter region of weak chaoticity in a saw-tooth map has been studied and deviations from the Fermi golden rule and Lyapunov regime of quantum fidelity decay have been observed. The authors studied fidelity decay around the transition point between the Fermi golden rule and Lyapunov regime, occurring at $\varepsilon \sim \varepsilon_{\mathrm{r}} \propto \hbar$. By increasing $\varepsilon/\hbar$ the deviation from the Fermi golden rule starts first, after which the decay rate of quantum fidelity approaches the classical Lyapunov exponent in an oscillatory way. The reason for this transitional behavior are strong fluctuations in the fidelity amplitude, causing deviations between $|\langle f \rangle|^2$ and $\langle F \rangle$.

6. Classical echo-dynamics

In this section we shall define the corresponding classical quantity, characterizing classical Loschmidt echoes, namely the *classical fidelity*. One can use a strategy which is completely analogous to the quantum case to derive a theoretical description of the decay of the classical fidelity. The results found here may be of interest for themselves, or can serve as a reference for the quantum results. For example, within the time scale of the order of Ehrenfest time ($\sim \log \hbar$ for chaotic systems), classical fidelity and quantum fidelity should strictly agree.

Classical fidelity has been considered in several papers. In [46] a definition and a linear response treatment has been given. Benenti and Casati [59] considered it in the context of quantum classical correspondence in a diffusive system with dynamical localization. Eckhardt [60] treated its generalization to stochastic flows, whereas Benenti et al. [63,61] considered the asymptotic decay of the classical fidelity, both in the case of regular and chaotic dynamics. In Refs. [62,196] a theory has been developed for the short-time regime of classical fidelity decay and its relation to the Lyapunov spectrum.

The classical fidelity $F_{\rm cl}(t)$ can be defined as

$$F_{\rm cl}(t) = \int_\Omega {\rm d}\boldsymbol{x} \rho_\varepsilon(\boldsymbol{x},t)\rho_0(\boldsymbol{x},t), \tag{236}$$

where the integral is extended over the phase space, and

$$\rho_0(\boldsymbol{x},t) = \hat{U}_0^t \rho(\boldsymbol{x},0), \quad \rho_\varepsilon(\boldsymbol{x},t) = \hat{U}_\varepsilon^t \rho(\boldsymbol{x},0) \tag{237}$$

give the classical Liouvillean evolution for time t of the initial phase space density $\rho(\boldsymbol{x},0)$. In order to have $F_{\rm cl}(t) = 1$, we have to require that the phase space density is square normalized $\int {\rm d}\boldsymbol{x}\rho^2(\boldsymbol{x},0) = 1$. We note that classical dynamics of L^2 phase space densities is unitary due to phase volume conservation, *i.e.* the Liouville theorem. Therefore, we can also build a classical echo picture and form a unitary *classical echo propagator* that composes perturbed forward evolution with the unperturbed backward evolution which is also unitary and is given by

$$\hat{U}_{\rm E}(t) = \hat{U}_0^\dagger(t)\,\hat{U}_\varepsilon(t). \tag{238}$$

Writing the phase space density after an echo as

$$\rho_{\rm E}(\boldsymbol{x},t) = U_{\rm E}(t)\rho_0(\boldsymbol{x},0) \tag{239}$$

we rewrite the classical Loschmidt echo as

$$F_{\rm cl}(t) = \int_\Omega {\rm d}\boldsymbol{x} \rho_{\rm E}(\boldsymbol{x},t)\rho_0(\boldsymbol{x},0). \tag{240}$$

The above definitions (236,240) can be shown to correspond to the classical limit of quantum fidelity, if written in terms of Wigner functions [46,47]. In the ideal case of a perfect echo ($\varepsilon = 0$), fidelity does not decay, $F_{\rm cl}(t) = 1$. However, due to chaotic dynamics, when $\varepsilon \neq 0$ the classical echo decay sets in after a time scale

$$t_\varepsilon \sim \frac{1}{\lambda} \ln\left(\frac{\nu}{\varepsilon}\right), \tag{241}$$

required to amplify the perturbation up to the size ν of the initial distribution. Thus, for $t \gg t_\varepsilon$ the recovery of the initial distribution via the imperfect time-reversal procedure fails, and the fidelity decay is determined by the decay of correlations for a system which evolves forward in time according to the Hamiltonians H_0 (up to time t) and H_ε (from time t to time $2t$). This is conceptually similar to the "practical" irreversibility of chaotic dynamics: Due to the exponential instability, any amount of numerical error in computer simulations rapidly erases the memory about the initial distribution. In the present case, the coarse-graining which leads to irreversibility is not due to round-off errors but to a perturbation in the Hamiltonian.

Another somehow related concept named quantum-classical fidelity has recently been introduced and studied [197], which measures L^2 distance between the Wigner function and the corresponding classical phase space density as a function of time. It is a very suitable tool for precise definitons of various Ehrenfest time-scales and a detailed study of quantum-classical correspondence. Quantum-classical fidelity can also be interpreted as a "classical" fidelity if the Plack constant $\hbar$ is treated as a perturbation.

6.1. *Short time decay of classical fidelity*

The analysis presented below follows Refs. [46,62]. The propagation of classical densities in phase space is governed by the unitary Liouville evolution $\hat{U}_\varepsilon(t)$

$$\frac{\mathrm{d}}{\mathrm{d}t}\hat{U}_\varepsilon(t) = \hat{L}_{H_\varepsilon(\boldsymbol{x},t)}\hat{U}_\varepsilon(t) \tag{242}$$

where $\hat{L}_{A(\boldsymbol{x},t)} = (\boldsymbol{\nabla}A(\boldsymbol{x},t))\cdot \mathrm{J}\boldsymbol{\nabla}$, A is any observable, and

$$H_\varepsilon(\boldsymbol{x},t) = H_0(\boldsymbol{x},t) + \varepsilon V(\boldsymbol{x},t), \tag{243}$$

is a generally time-dependent family of classical Hamiltonians with perturbation parameter λ. The matrix J is the usual symplectic unit. Similarly, $\mathrm{d}\hat{U}^\dagger_\varepsilon(t)/\mathrm{d}t = -\hat{U}^\dagger_\varepsilon(t)\hat{L}_{H_\varepsilon(\boldsymbol{x},t)}$. Using Eqs. (242,243,238) and writing $\hat{U}_\varepsilon(t) = \hat{U}_0(t)\hat{U}_\mathrm{E}(t)$ we get

$$\frac{\mathrm{d}}{\mathrm{d}t}\hat{U}_\mathrm{E}(t) = \left\{\hat{U}^\dagger_0(t)\hat{L}_{\varepsilon V(\boldsymbol{x},t)}\hat{U}_0(t)\right\}\hat{U}_\mathrm{E}(t). \tag{244}$$

Classical dynamics have the nice property that the evolution is governed by characteristics that are simply the classical phase space trajectories, so the action of the evolution operator on any phase space density is given as $\hat{U}_0(t)\ \rho = \rho\circ\boldsymbol{\phi}_t^{-1}$, where $\boldsymbol{\phi}_t^{-1}$ denotes the backward (unperturbed) phase space flow from time t to time 0. Similarly, the backward evolution is given by $\hat{U}^\dagger_0(t)\ \rho = \rho\circ\boldsymbol{\phi}_t$, where ϕ_t represents the forward phase space flow from time 0 to time t. Here and in the following we assume the dynamics to start at time 0.

We note that echo-dynamics (238) can be treated as Liouvillean dynamics in the *interaction picture*, since

$$\begin{aligned}
&\left\{\hat{U}^\dagger_0(t)\hat{L}_{A(\boldsymbol{x},t)}\hat{U}_0(t)\rho\right\}(\boldsymbol{x}) = \\
&= \hat{U}^\dagger_0(t)\left(\boldsymbol{\nabla}_{\boldsymbol{x}}A(\boldsymbol{x},t)\right)\cdot \mathrm{J}\boldsymbol{\nabla}_{\boldsymbol{x}}\rho\left(\boldsymbol{\phi}_t^{-1}(\boldsymbol{x})\right) = \\
&= \left(\boldsymbol{\nabla}_{\boldsymbol{\phi}_t(\boldsymbol{x})}A(\boldsymbol{\phi}_t(\boldsymbol{x}),t)\right)\cdot \mathrm{J}\boldsymbol{\nabla}_{\boldsymbol{\phi}_t(\boldsymbol{x})}\rho\left(\boldsymbol{\phi}_t^{-1}\left(\boldsymbol{\phi}_t(\boldsymbol{x})\right)\right) = \\
&= \left(\boldsymbol{\nabla}_{\boldsymbol{x}}A(\boldsymbol{\phi}_t(\boldsymbol{x}),t)\right)\cdot \mathrm{J}\boldsymbol{\nabla}_{\boldsymbol{x}}\rho(\boldsymbol{x}) = \left\{\hat{L}_{A(\boldsymbol{\phi}_t(\boldsymbol{x}),t)}\ \rho\right\}(\boldsymbol{x}).
\end{aligned} \tag{245}$$

In the last line we used the invariance of the Poisson bracket under the flow. This extends Eq. (244) to the form (242)

$$\frac{\mathrm{d}}{\mathrm{d}t}\hat{U}_\mathrm{E}(t) = \hat{L}_{H_\mathrm{E}(\boldsymbol{x},t)}\ \hat{U}_\mathrm{E}(t) \tag{246}$$

where the *echo Hamiltonian* is given by

$$H_\mathrm{E}(\boldsymbol{x},t) = \varepsilon V\left(\boldsymbol{\phi}_t(\boldsymbol{x}),t\right). \tag{247}$$

The function H_E is nothing but the perturbation part εV of the original Hamiltonian, which, however, is evaluated at the point that is obtained by forward propagation with the unperturbed original Hamiltonian. It is important to stress that this is not a perturbative result but an exact expression. Also, even if the original Hamiltonian system was time independent, the echo dynamics obtains an explicitly time dependent form. Trajectories of the echo-flow are given by Hamilton equations

$$\dot{\boldsymbol{x}} = \mathrm{J}\ \boldsymbol{\nabla}H_\mathrm{E}(\boldsymbol{x},t). \tag{248}$$

At this point we limit our discussion to time independent Hamiltonians and perturbations. The slightly more general case of periodically driven systems reducible to symplectic maps shall be discussed later.

Inserting (247) into Eq. (248) yields

$$\dot{\boldsymbol{x}} = \varepsilon\mathrm{J}\boldsymbol{\nabla}_{\boldsymbol{x}}V(\boldsymbol{\phi}_t(\boldsymbol{x})) = \varepsilon\mathrm{J}\mathrm{M}_t^T(\boldsymbol{x})(\boldsymbol{\nabla}V)(\boldsymbol{\phi}_t(\boldsymbol{x})). \tag{249}$$

Here we have introduced the *stability matrix* $\mathrm{M}_t(\boldsymbol{x})$, $[\mathrm{M}_t(\boldsymbol{x})]_{i,j} = \partial_j[\boldsymbol{\phi}_t(\boldsymbol{x})]_i$.

6.1.1. *Linear response regime for Lipschitz continuous initial density*

Let us first discuss the classical echo dynamics in the *linear response regime*, *i.e.* in the case where the total *echo displacement*

$$\Delta\boldsymbol{x}(t) = \int_0^t \dot{\boldsymbol{x}}\mathrm{d}t' = \varepsilon \int_0^t \mathrm{d}t' \mathrm{J}\mathrm{M}_{t'}^T(\boldsymbol{x})(\boldsymbol{\nabla}V)(\boldsymbol{\phi}_{t'}(\boldsymbol{x})) \tag{250}$$

is small compared to all other classical phase space scales. Writing classical fidelity in the symmetric representation we immediately arrive at the simple linear response result

$$\begin{aligned} F_{\mathrm{cl}}(t) &= \int_\Omega \mathrm{d}\boldsymbol{x}\rho(\boldsymbol{x}+\Delta\boldsymbol{x}(t)/2)\rho(\boldsymbol{x}-\Delta\boldsymbol{x}(t)/2) \\ &= 1 - \frac{1}{4}\varepsilon^2\mathrm{d}t' \int_\Omega \mathrm{d}\boldsymbol{x}\left(\nabla\rho(\boldsymbol{x})\cdot\int_0^t \mathrm{d}t'\mathrm{J}\mathrm{M}_{t'}^T(\boldsymbol{x})(\boldsymbol{\nabla}V)(\boldsymbol{\phi}_{t'}(\boldsymbol{x}))\right)^2 \end{aligned} \tag{251}$$

Now it's easy to specialize the above formula to the cases of chaotic and regular dynamics. In the case of chaotic dynamics, the stability matrix $\mathrm{M}_t(\boldsymbol{x})$ will after a short time t expand any initial vector with exponential $\exp(\lambda_{\max}t)$ where $\lambda_{\max}$ is the maximal Lyapunov exponent of the flow. Since the time integral of an exponential is still an exponential, the expression in the big bracket on the RHS of Eq. (251) can be written as $2C[\rho]\exp(\lambda_{\max}t)$ where $C[\rho]$ is a constant depending only on the initial density. Hence

$$F_{\mathrm{cl}}^{\mathrm{ch}}(t) = 1 - \varepsilon^2 C[\rho]^2\exp(2\lambda_{\max}|t|) + O(\varepsilon^4). \tag{252}$$

For sufficiently strong perturbations, $\varepsilon > \hbar$, and typical initial packets quantum fidelity decays in a similar way [73]. On the other hand, for regular dynamics, the stability matrix is of parabolic type (all eigenvalues 1 but having defective Jordan canonical form) so it always stretches an arbitrary initial vector linearly in time and

$$F_{\mathrm{cl}}^{\mathrm{reg}}(t) = 1 - \varepsilon^2 C'[\rho]^2 t^2 + O(\varepsilon^4) \tag{253}$$

where $C'[\rho]$ is another constant depending on the initial density ρ only.

However, please note that in deriving the expression (251) we have assumed that the initial density $\rho(\boldsymbol{x})$ was *smooth* and *differentiable*. In fact, the above result still holds for general Lipschitz continuous densities [196].

6.1.2. *Linear response regime for discontinuous initial density*

It is interesting though, that the result is quite different for discontinuous initial densities, like for example characteristic functions on sets in phase space which may be of considerable interest in classical statistical mechanics. In such a general case it is useful to rewrite the classical fidelity as

$$F_{\mathrm{cl}}(t) = 1 - \frac{1}{2}\int_\Omega [\rho(\boldsymbol{x}) - \rho(\boldsymbol{x}+\Delta\boldsymbol{x}(t))]^2 \tag{254}$$

This representation is a trivial consequence of the square normalizability of phase-space density and Liouville theorem for the echodynamics $\boldsymbol{x}+\Delta\boldsymbol{x}(t)$. Now it is easy to see that for Lipschitz continuous densities the previous results (252,253) follow, while for *discontinuous* densities the main contribution to the integral, for small ε, *i.e.* for small $|\Delta\boldsymbol{x}|$, comes from the set of phase space points $\boldsymbol{x}$ where $\rho(\boldsymbol{x})$ is discontinuous, where the contribution is proportional to discontinuity gap times $|\Delta\boldsymbol{x}|$, namely

$$F_{\mathrm{cl}}(t) = 1 - \int_\Omega \mathrm{d}\boldsymbol{x} D_\rho(\boldsymbol{x})|\Delta\boldsymbol{x}(t)| \tag{255}$$

where $D_\rho(\boldsymbol{x})$ is a certain *distribution* taking account for the discontinuity gaps of the density $\rho(\boldsymbol{x})$. So, the main distinction from the continuous case is that the fidelity drop is proportional to the length of the echo displacement $|\Delta\boldsymbol{x}|$ instead of its square. Since the latter asymptotically expands as $e^{\lambda_{\max}|t|}$ or $|t|$ for chaotic and regular dynamics, respectively, we obtain a universal linear response formulae for fidelity decay of discontinuous densities

$$F_{\rm cl}^{\rm ch,dis}(t) = 1 - |\varepsilon| C''[\rho] \exp(\lambda_{\max} t) + O(\varepsilon^2),$$
$$F_{\rm cl}^{\rm reg,dis}(t) = 1 - |\varepsilon| C'''[\rho] |t| + O(\varepsilon^2),$$

where $C''[\rho]$ and $C'''[\rho]$ are constants depending only on the details of the initial density ρ.

6.1.3. *General (multi-)Lyapunov decay for chaotic few body systems*

From now on we assume that the flow $\boldsymbol{\phi}_t$ has very strong ergodic properties, *e.g.* it is uniformly hyperbolic and Anosov, and consider to what extend can classical echo dynamics be explored in order to understand classical fidelity decay beyond the linear response approximation. To understand the dynamics (249) we need to explore the properties of M_t. We start by writing the matrix

$$\mathrm{M}_t^T(\boldsymbol{x})\mathrm{M}_t(\boldsymbol{x}) = \sum_j e^{2\lambda_j t} d_j^2(\boldsymbol{x},t) \boldsymbol{v}_j(\boldsymbol{x},t) \otimes \boldsymbol{v}_j(\boldsymbol{x},t) \tag{256}$$

expressed in terms of orthonormal eigenvectors $\boldsymbol{v}_j(\boldsymbol{x},t)$ and eigenvalues $d_j^2(\boldsymbol{x},t)\exp(2\lambda_j t)$. After the ergodic time $t_{\rm e}$ necessary for the echo trajectory to explore the available region of phase space, Oseledec theorem [198] guarantees that the eigenvectors of this matrix converge to Lyapunov eigenvectors being independent of time, while $d_j(\boldsymbol{x},t)$ grow slower than exponentially, so the leading exponential growth defines the Lyapunov exponents λ_j. Similarly, the matrix

$$\mathrm{M}_t(\boldsymbol{x})\mathrm{M}_t^T(\boldsymbol{x}) = \sum_j e^{2\lambda_j t} c_j^2(\boldsymbol{x}_t,t) \boldsymbol{u}_j(\boldsymbol{x}_t,t) \otimes \boldsymbol{u}_j(\boldsymbol{x}_t,t), \tag{257}$$

where $\boldsymbol{x}_t = \boldsymbol{\phi}_t(\boldsymbol{x})$, has the same eigenvalues $[c_j^2(\boldsymbol{x}_t,t) \equiv d_j^2(\boldsymbol{x},t)]$, and its eigenvectors depend on the final point $\boldsymbol{x}_t$ only, as the matrix in question can be related to the backward evolution. The vectors $\{\boldsymbol{u}_j(\boldsymbol{x}_t)\}$, $\{\boldsymbol{v}_j(\boldsymbol{x})\}$, constitute left, right, part, respectively, of the *singular value decomposition* of $\mathrm{M}_t(\boldsymbol{x})$, so we write for $t \gg t_{\rm e}$

$$\mathrm{M}_t(\boldsymbol{x}) = \sum_{j=1}^{N} \exp(\lambda_j t)\ \boldsymbol{e}_j(\boldsymbol{\phi}_t(\boldsymbol{x})) \otimes \boldsymbol{f}_j(\boldsymbol{x}) \tag{258}$$

assuming that the limits $\boldsymbol{e}_j(\boldsymbol{x}) = \lim_{t\to\infty} c_j(\boldsymbol{x},t)\boldsymbol{u}_j(\boldsymbol{x},t)$, $\boldsymbol{f}_j(\boldsymbol{x}) = \lim_{t\to\infty} d_j(\boldsymbol{x},t)\boldsymbol{v}_j(\boldsymbol{x},t)$ exist. Rewriting Eq. (249) by means of Eq. (258) we obtain

$$\dot{\boldsymbol{x}} = \varepsilon \sum_{j=1}^{N} \exp(\lambda_j t)\ W_j(\boldsymbol{\phi}_t(\boldsymbol{x}))\ \boldsymbol{h}_j(\boldsymbol{x}) \tag{259}$$

where $\boldsymbol{h}_j(\boldsymbol{x}) = \mathrm{J}\boldsymbol{f}_j(\boldsymbol{x})$, and introducing new observables

$$W_j(\boldsymbol{x}) = \boldsymbol{e}_j(\boldsymbol{x}) \cdot \boldsymbol{\nabla} V(\boldsymbol{x}). \tag{260}$$

Note that for general hyperbolic systems the signs of the vector fields $\boldsymbol{e}_j(\boldsymbol{x})$, $\boldsymbol{f}_j(\boldsymbol{x})$ may actually not be unique, so they rigorously exist only as *director* fields, *i.e.* rank one tensor fields. But since from a physics point of view this represents only a technical difficulty [196], we shall ignore the problem in the following discussions.

For small perturbations the echo trajectories remain close to the initial point $\boldsymbol{x}(0)$ for times large in comparison to the internal dynamics of the system ($t_{\rm e}$, Lyapunov times, decay of correlations, etc), and in this regime the echo evolution can be linearly decomposed along different independent directions $\boldsymbol{h}_j(\boldsymbol{x}(0))$

$$\boldsymbol{x}(t) = \boldsymbol{x}(0) + \sum_{j=1}^{N} y_j(t)\ \boldsymbol{h}_j(\boldsymbol{x}(0)). \tag{261}$$

For longer times, the point $\boldsymbol{x}(t)$ moves away from the initial point, but the dynamics is still governed by the local unstable vectors at the evolved point. Therefore the decay of fidelity is governed by the spreading of the densities along the conjugated unstable manifolds defined by the conjugate vector fields $\boldsymbol{h}_j(\boldsymbol{x}) = J\boldsymbol{f}_j(\boldsymbol{x})$.

Inserting (261) into (259) we obtain for each direction $\boldsymbol{h}_j$

$$\dot{y}_j = \varepsilon \ \exp(\lambda_j t) W_j(\boldsymbol{\phi}_t(\boldsymbol{x})). \tag{262}$$

For *stable* directions with $\lambda_j < 0$, after a certain time, the variable y_j becomes a constant of the order ε.

For *unstable* directions with $\lambda_j > 0$, we introduce a new variable z_j as $y_j = \varepsilon \exp(\lambda_j t) z_j$ and rewrite the above equation as

$$\dot{z}_j + \lambda_j z_j = W_j(\boldsymbol{\phi}_t(\boldsymbol{x})). \tag{263}$$

The right hand side of this equation is simply the evolution of the observable W_j starting from a point in phase space $\boldsymbol{x} = \boldsymbol{x}(0)$. Due to assumed ergodicity of the flow $\boldsymbol{\phi}_t$, $W_j(\boldsymbol{\phi}_t(\boldsymbol{x}))$ has well defined and *stationary* statistical properties such as averages and correlation functions. The linear damped Eq. (263) is formally equivalent to a Langevin equation (with deterministic noise) and hence its solution $z_j(t)$ has a well defined time- and ε-independent probability distribution $P_j(z_j)$. Its moments can be expressed in terms of moments and correlation functions of the deterministic noise W_j, in particular $\overline{W_j} = 0$. The analysis generalizes to the case of explicitly time-dependent W_j.

Going back to the original coordinate y_j we obtain its distribution as $K_j(y_j) = P_j(z_j)\mathrm{d}z_j/\mathrm{d}y_j$, or $K_j(y_j) = P_j\left(\exp(-\lambda_j t) y_j/\varepsilon\right) \exp(-\lambda_j t)/\varepsilon$. This probability distribution tells us how, on average, points within some initial (small) phase space set of characteristic diameter ν spread along a locally well defined unstable Lyapunov direction j and therefore represents an averaged kernel of the evolution of such densities along this direction. Starting from the initial localized density ρ_0, of small width ν such that the decomposition (261) does not change appreciably along ρ_0, echo dynamics yields for the densities $\rho_t(\boldsymbol{y}) = \int \mathrm{d}^N \boldsymbol{y}' \rho_0(\boldsymbol{y}') \prod_j K_j(y_j - y_j')$. For the stable directions j we set $K_j(y_j) = \delta(y_j)$, as the shift of y_j (of order ε) can be neglected as compared to unstable directions. This also implies that the assumption $\varepsilon \ll \nu$ is necessary in order to get any echo at all after not too short times. Classical fidelity (240) can now be written as $F_{\mathrm{cl}}(t) = \int \mathrm{d}^N \boldsymbol{y}\ \rho_0(\boldsymbol{y})\ \rho_t(\boldsymbol{y})$. As long as the width ν_j of ρ_0 along the unstable direction j is much larger than the width of the kernel K_j, there is no appreciable contribution to fidelity decay in that direction. At time

$$t_j = (1/\lambda_j) \log(\nu_j/(\varepsilon \gamma_j)), \tag{264}$$

where γ_j is a typical width of the distribution P_j, the width of the kernel is of the order of the width of the distribution along the chosen direction. After that time, the overlap between the two distributions along the chosen direction starts to decay with the same rate as the value of the kernel in the neighborhood of $y_j = 0$, which is $\propto \exp(-\lambda_j t)$. The total overlap decays as

$$F_{\mathrm{cl}}(t) \approx \prod_{j;\ t_j < t} \exp\left[-\lambda_j (t - t_j)\right], \tag{265}$$

where only those unstable directions contribute to the decay for which $t_j > t$. As the time t_j is shorter the higher the corresponding Lyapunov exponent λ_j, fidelity will initially decay with the largest Lyapunov exponent λ_1. In chaotic systems with more than two degrees of freedom we, however, expect to observe an increase of decay rate after the time t_2, etc. Eq. (265) provides good description for classical fidelity as long as $F_{\mathrm{cl}}(t)$ does not approach the saturation value $F_\infty \sim \nu^N$ where the asymptotic decay of classical fidelity is then given by the leading eigenvalue of Perron-Frobenius operator [61].

The result (265) does not only explain a simple Lyapunov decay of Loschmidt echoes as observed in many numerical experiments on two dimensional systems, but also predicts a cascade of decays with increasing rates given by the sums of first few Lyapunov exponent for few body chaotic systems. For example, in the first non-trivial case of a four dimensional dynamics with two positive Lyapunov exponents one can have two distinct behaviors. In the simple *doubly hyperbolic* case of well separated individual Lyapunov exponents $\lambda_1 > \lambda_2$ the decay is expected to go through a cascade of increasing rates, first λ_1 and then $\lambda_1 + \lambda_2$, whereas in the *loxodromic* case $\lambda_1 = \lambda_2$ the rate is $2\lambda_1$. We illustrate this numerically for fourdimensional cat maps, *i.e.* 4-volume preserving automorphisms on a 4-torus, $\boldsymbol{x}' = \mathrm{C}\boldsymbol{x} \pmod 1$, $\boldsymbol{x} \in [0,1)^4$. The choices

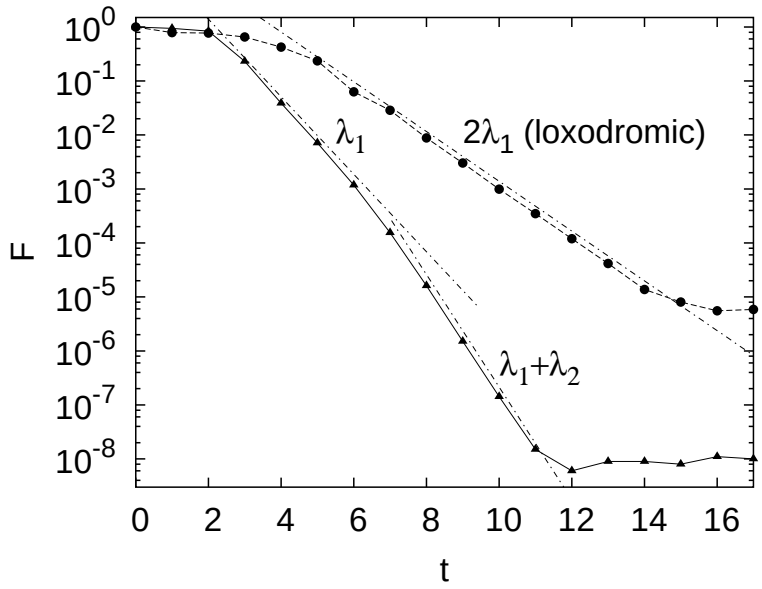

Fig. 34. Decay of classical fidelity for two examples of 4D cat maps perturbed as explained in text [taken from [62]]. Triangles refer to doubly-hyperbolic case where initial set was a 4-cube $[0.1, 0.11]^4$, and $\varepsilon = 2 \cdot 10^{-4}$, whereas circles refer to loxodromic case where initial set was $[0.1, 0.15]^4$, and $\varepsilon = 3 \cdot 10^{-3}$. In both cases initial density was sampled by 10^9 points. Chain lines give exponential decays with theoretical rates, $\lambda_1 = 1.65, \lambda_1 + \lambda_2 = 2.40$ (doubly-hyperbolic), and $2\lambda_1 = 1.06$ (loxodromic).

$$\mathrm{C_{d-h}} = \begin{bmatrix} 2 & -2 & -1 & 0 \\ -2 & 3 & 1 & 0 \\ -1 & 2 & 2 & 1 \\ 2 & -2 & 0 & 1 \end{bmatrix}, \ \mathrm{C_{lox}} = \begin{bmatrix} 0 & 1 & 0 & 0 \\ 0 & 1 & 1 & 0 \\ 1 & -1 & 1 & 1 \\ -1 & -1 & -2 & 0 \end{bmatrix}$$

are two examples representing the doubly-hyperbolic and loxodromic case. The matrix $\mathrm{C_{d-h}}$ has the unstable eigenvalues $\approx 5.22, 2.11$, while the largest eigenvalues of $\mathrm{C_{lox}}$ are $\approx 1.70 \exp(\pm i 1.12)$. The perturbation for both cases was done by applying an additional map at each time step $\bar{x}_1 = x'_1 + \varepsilon \sin(2\pi x_3) \pmod 1$, $\bar{x}_{2,3,4} = x'_{2,3,4}$. In Fig. 34 we show the two types of decay which agree with theoretical predictions.

6.2. *Asymptotic long time decay for chaotic dynamics*

However, our theory above is valid only up to a time-scale in which the echo-dynamics spreads all over the available phase space. After that time, one should use a different approach to understand asymptotic (long time) decay of classical fidelity. In this regime, there does not yet exist any rigorous approach to fidelity decay, hence we describe a heuristic approach of the paper [61], also demonstrating different regimes of classical fidelity decay in chaotic classical maps. We illustrate the general phenomena in a standard model of classical chaos, namely the *sawtooth map* which is defined by

$$\overline{p} = p + F_0(\theta), \quad \overline{\theta} = \theta + \overline{p} \pmod{2\pi}, \tag{266}$$

where (p, θ) are conjugated action-angle variables, $F_0 = K_0(\theta - \pi)$, and the over-bars denote the variables after one map iteration. We consider this map on the torus $0 \le \theta < 2\pi$, $-\pi L \le p < \pi L$, where L is an integer. For $K_0 > 0$ the motion is completely chaotic and diffusive, with Lyapunov exponent given by $\lambda = \ln\{(2 + K_0 + [(2 + K_0)^2 - 4]^{1/2})/2\}$. For $K_0 > 1$ one can estimate the diffusion coefficient D by means of the random phase approximation, obtaining $D \approx (\pi^2/3)K_0^2$. In order to compute the classical fidelity, we choose to perturb the kicking strength $K = K_0 + \varepsilon$, with $\varepsilon \ll K_0$. In practice, we follow the evolution of a

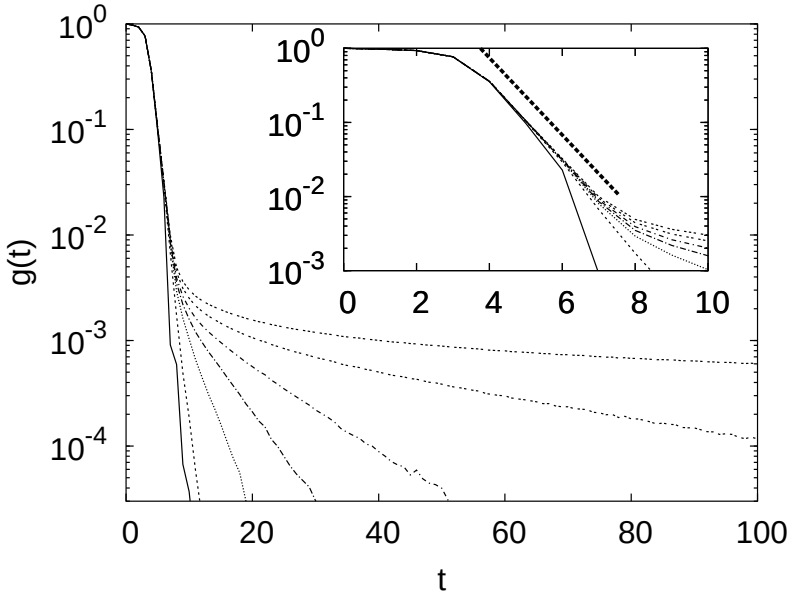

Fig. 35. Decay of the fidelity $g(t)$ for the sawtooth map with the parameters $K_0 = (\sqrt{5}+1)/2$ and $\varepsilon = 10^{-3}$ for different values of $L = 1, 3, 5, 7, 10, 20, \infty$ from the fastest to the slowest decaying curve, respectively [taken from [61]]. The initial phase space density is chosen as the characteristic function on the support given by the $(q, p) \in [0, 2\pi) \times [-\pi/100, \pi/100]$. Note that between the Lyapunov decay and the exponential asymptotic decay there is a $\propto 1/\sqrt{t}$ decay, as expected from diffusive behavior. Inset: magnification of the same plot for short times, with the corresponding Lyapunov decay indicated as a thick dashed line.

large number of trajectories, which are uniformly distributed inside a given phase space region of area A_0 at time $t = 0$. The fidelity $f(t)$ is given by the percentage of trajectories that return back to that region after t iterations of the map (266) forward, followed by the backward evolution, now with the perturbed strength K, in the same time interval t. In order to study the approach to equilibrium for fidelity, we consider the quantity

$$g(t) = (f(t) - f(\infty))/(f(0) - f(\infty)) \; . \tag{267}$$

Thus, $g(t)$ drops from 1 to 0 as t goes from 0 to ∞. We note that $f(0) = 1$ while, for a chaotic system, $f(\infty)$ is given by the ratio A_0/A_c, with A_c the area of the chaotic component to which the initial distribution belongs.

The behavior of $g(t)$ is shown in Fig. 35, for $K_0 = (\sqrt{5}+1)/2$ and different L values. One can see that only the short time decay is determined by the Lyapunov exponent λ, $f(t) = \exp(-\lambda t)$. In this figure we demonstrate that the Lyapunov decay is followed by a power law decay $\propto 1/\sqrt{Dt}$, a manifestation of deterministic diffusion taking place on the cylindrical phase space (for large L) [59], up to the diffusion time $t_D \sim L^2/D$, and then the asymptotic relaxation to equilibrium takes place exponentially, with a decay rate γ (shown in Fig. 36) ruled not by the Lyapunov exponent but by the largest Ruelle-Pollicott resonance.

These resonances have been determined for the sawtooth map by diagonalizing a discretized (coarse-grained) classical propagator [61] and determining the spectral gap between the modulus of the largest eigenvalue and the unit circle. In Fig. 36 we illustrate the good agreement between the asymptotic decay rate of fidelity (extracted from the data of Fig. 35) and the decay rate γ as predicted by the gap in the discretized Perron-Frobenius spectrum.

More generally, one can conclude that the long time asymptotics of the (shifted) classical fidelity $g(t)$ behaves in the same way as a typical temporal correlation function of the (forward) dynamics at time $2t$. This is true even for systems where the decay of correlations is given by power laws and the spectral gap of the Perron-Frobenius operator vanishes, *e.g.* for the stadium billiard [61].

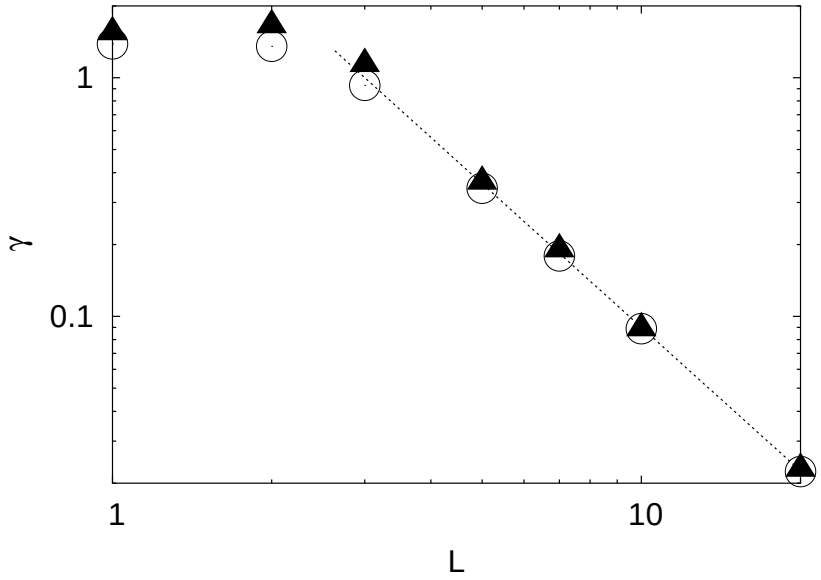

Fig. 36. Asymptotic exponential decay rates of fidelity for the sawtooth map ($K_0 = (\sqrt{5}+1)/2$, $\varepsilon = 10^{-3}$) as a function of L [taken from [61]]. The rates are extracted by fitting the tails of the fidelity decay in the Fig. 35 (triangles) and from the discretized Perron-Frobenius operator (circles). The line denotes the $\propto 1/L^2$ behavior of the decay rates, as predicted by the Fokker-Planck equation.

6.3. *Asymptotic decay for regular dynamics*

As for the decay of classical fidelity in the regime of regular classical, the theory has been developed in Ref. [63]. We shall not outline the details here but just repeat the main result.

The evolution of initial phase space density $\rho(\boldsymbol{x}, 0)$ under regular dynamics is quite trivial, as it evolves quasi-periodically on the set of neighboring tori as can be expressed explicitly in the action-angle coordinates [63]. We note that a perturbation of an integrable system, being of KAM (Kolmogorov-Arnold-Moser) type i.e. sufficiently smooth in the phase space variables, can cause two main effects on the KAM tori of an unperturbed system: (i) either the shape of the tori changed, or (ii) the frequencies of the motion changed. Depending on whether one of the two effects is dominant, we have two different types of decay: (i) algebraic decay $f(t) \propto t^{-d}$, where d is the number of degrees of freedom if mainly the shape of the tori is changed, (ii) ballistic decay, which is basically determined by the shape of the initial density $\rho(\boldsymbol{x}, 0)$, i.e. Gaussian if the latter is a Gaussian, if mainly the frequencies of the tori are changed.

In Fig. 37 we show an example of classical fidelity decay in an integrable rectangular billiard, with the action-angle Hamiltonian ($d = 2$)

$$H_0 = \frac{\alpha_1}{2} I_1^2 + \frac{\alpha_2}{2} I_2^2 \tag{268}$$

which is perturbed by a generic perturbation of the form

$$V = \cos(\beta)\cos(\Theta_1)\cos(\Theta_2) + \sin(\beta) I_1 I_2.$$

Depending on the value of the parameter β, the perturbation mainly affects either the shape of the tori or their frequencies.

6.4. *Classical fidelity in many-body systems*

In systems with increasing, macroscopic number of degrees of freedom the above theoretical considerations can still be applied though somehow qualitatively different behavior is obtained. The details can be found

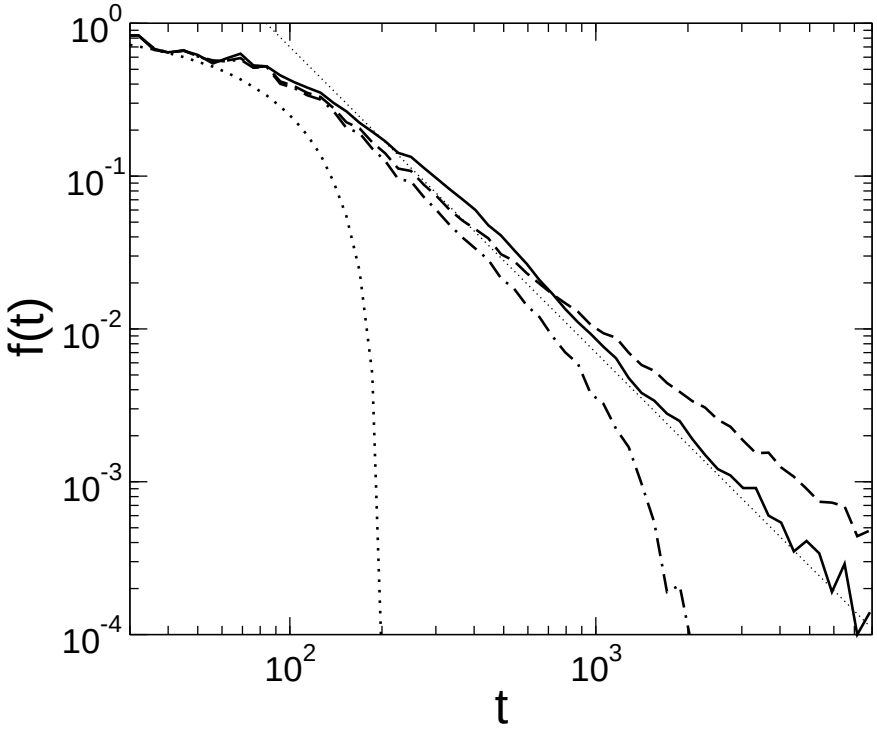

Fig. 37. Fidelity decay for the rectangular billiard for various values of the parameter $\beta = 0$ (full line), 0.232 (dashed), 0.3 (dot-dashed) and $\pi/2$ (dotted) [taken from [63]]. The parameters of the system have been chosen as follows: $\alpha_1 = (\sqrt{5}+1)/2$, $\alpha_2 = 1$. In all cases the initial phase space density is a hyper-rectangle centered around $I_1 = 1$, $I_2 = 1$, $\Theta_1 = 1$ and $\Theta_2 = 1$ with all sides of length $\nu_{I_1} = \nu_{I_1} = \nu_{\Theta_1} = \nu_{\Theta_2} = 0.02$. The perturbation parameter is $\varepsilon = 3 \times 10^{-4}$ and the number of trajectories $N = 10^5$. The $\propto 1/t^2$ decay is shown as a thin dotted line.

in Ref. [196].

The central result of that analysis is that the fidelity of a many-body system (in the larger d limit), which is perturbed by a *global* perturbation (i.e. the one which perturbs all degrees of freedom in an approximately uniform way), and for which Lyapunov exponents around the maximal one $\lambda_{\max}$ are smoothly distributed with a well defined density in the thermodynamic limit $d \to \infty$, decays with a doubly exponential law

$$F_{\rm cl}(t) = \exp(-Ad\varepsilon^{\beta} \exp(\beta \lambda_{\max} t)) \; . \tag{269}$$

A is some system specific constant which does not depend on d, ε, t. As we have discussed already within the classical linear response approximation, it turns out that it is of crucial importance whether the initial phase space density is (Lipschitz) continuous or not, namely we have index $\beta = 1$ for discontinuous distribution, and $\beta = 2$ for Lipschitz continuous one.

6.5. *Universal decay in dynamically mixing systems which lack exponential sensitivity to initial conditions*

Recently, another possibility of relaxation and mixing behavior in classical dynamical systems has been investigated [199,200], which does not require exponential sensitivity on initial conditions. Even though it may appear quite exotic at the first sight, such a situation can arise quite often, for example in polygon billiards of two and higher dimensions, hard point gases in one dimension, etc. The decay of classical fidelity for such situations has been addressed in Ref. [201]. It has been found that under quite general dynamical conditions of mixing and marginally stable (parabolic) dynamics (being a consequence of the lack of exponential sensitivity to initial conditions), the fidelity decay exhibits a universal form (for small perturbations ε) namely

$$F_{\rm cl}(t) = \phi(B|\varepsilon|^{2/5} t) \tag{270}$$

where B is some constant depending on details of temporal correlation decay of the perturbation and $\phi(x)$ is a *universal* function with the following asymptotic properties: $1-\phi(x) \propto |x|^{5/2}$, for $|x| \to 0$, and $\phi(x) = \exp(-|x|)$, for $|x| \to \infty$.

7. Time scales and the transition from regular to chaotic behavior

It is instructive to summarize all different time scales involved in the decay of fidelity for regular and chaotic dynamics. As for general, or generic perturbations one does not have freeze, we will limit our discussion to the situation with a nonzero time averaged perturbation.

7.1. *Chaotic dynamics*

The exposition here closely follows the one in Ref. [46]. For chaotic dynamics there are six relevant time scales (even seven for coherent initial states): the (short) Zeno time, the classical mixing time $t_{\rm mix}$ on which correlation function decays; the quantum decay time of the fidelity $\tau_{\rm m}$ (90); the Heisenberg time $t_{\rm H}$ (95) after which the system starts to "feel" finiteness of Hilbert space and effectively begins to behave as an integrable system; the decay time $\tau_{\rm p}$ (98) of perturbative Gaussian decay present after $t_{\rm H}$; the time t_∞ when the fidelity reaches the finite size plateau; for coherent initial states we have in addition the Ehrenfest time $t_{\rm E}$ up to which we have quantum-classical correspondence. Depending on the interrelation of these time scales, *i.e.* depending on the perturbation strength ε, Planck's constant $\hbar$ and the dimensionality d, we will also have different decays of fidelity. All different regimes can be reached by *e.g.* fixing $\hbar$ and increasing ε. Let us follow different decay regimes as we increase ε (shown in Fig. 38):

(a) For $\varepsilon < \varepsilon_{\rm p}$ we will have $t_{\rm H} < \tau_{\rm m}$. This means that at the Heisenberg time, the fidelity due to exponential decay (90) will still be close to 1, $F(t_{\rm H}) \approx 1$, and we will see mainly a Gaussian decay due to finite Hilbert space (98). The critical $\varepsilon_{\rm p}$ below which we will see this regime has already been calculated and is (99)

$$\varepsilon_{\rm p} = \frac{\hbar}{\sqrt{\sigma_{\rm cl}\mathcal{N}}} = \hbar^{d/2+1}\frac{(2\pi)^{d/2}}{\sqrt{\sigma_{\rm cl}\mathcal{V}}}. \tag{271}$$

For $\varepsilon < \varepsilon_{\rm p}$ the fidelity will have Gaussian decay with the decay time $\tau_{\rm p}$ (98)

$$\tau_{\rm p} = \frac{\hbar^{1-d/2}}{\varepsilon}\sqrt{\frac{\mathcal{V}}{4\sigma_{\rm cl}(2\pi)^d}}. \tag{272}$$

(b) For $\varepsilon_{\rm p} < \varepsilon < \varepsilon_{\rm s}$ we will have a crossover from the initial exponential decay (90) to the asymptotic Gaussian decay (98) at time $t_{\rm H}$ illustrated in Figs. 13 and 14. This regime occurs if $\tau_{\rm m} < t_{\rm H} < t_\infty$. With increasing perturbation, t_∞ will decrease and the upper border $\varepsilon_{\rm s}$ is determined by the condition $t_\infty = t_{\rm H}$. Denoting a finite size plateau by $F(t) \sim 1/\mathcal{N}^\mu$, with μ lying between 1 and 2, depending on the initial state (see Appendix A), we have the condition $\exp\left(-(t_{\rm H}/\tau_{\rm p})^2\right) = 1/\mathcal{N}^\mu$ which gives

$$\varepsilon_{\rm s} = \frac{\hbar}{\sqrt{\sigma_{\rm cl}\mathcal{N}}}\sqrt{\mu\ln\mathcal{N}} = \varepsilon_{\rm p}\sqrt{\mu\ln\mathcal{N}}. \tag{273}$$

Further increasing the perturbation, we reach perhaps the most interesting regime, in which quantum fidelity can decay faster the more chaotic the systems is. In this regime the exponential decay persists until the plateau is reached.

(c) For $\varepsilon_{\rm s} < \varepsilon < \varepsilon_{\rm mix}\,(\varepsilon_{\rm E})$ we will have an exponential decay until t_∞. The upper border $\varepsilon_{\rm mix}$ is determined by the condition $\tau_{\rm m} = t_{\rm mix}$ which is a point where the argument leading to the factorization of $n-$point correlation function breaks down. For random initial states we get

$$\varepsilon_{\rm mix} = \frac{\hbar}{\sqrt{2\sigma_{\rm cl}t_{\rm mix}}} = \varepsilon_{\rm p}\sqrt{\frac{\mathcal{N}}{2t_{\rm mix}}}. \tag{274}$$

Note that the relative size of this window $\varepsilon_{\rm mix}/\varepsilon_{\rm s} = \sqrt{\mathcal{N}/2\mu t_{\rm mix}\ln\mathcal{N}}$ increases both in the semiclassical $\hbar \to 0$ and in the thermodynamic $d \to \infty$ limit.

For coherent initial states the quantum correlation function relaxes on a slightly longer time scale than $t_{\rm mix}$, namely on the Ehrenfest time $t_{\rm E} \sim -\ln\hbar/\lambda$. Until $t_{\rm E}$ quantum packet follows the classical trajectory and afterwards interferences start to build leading to the breakdown of quantum-classical correspondence. Equating $\tau_{\rm m} = t_{\rm E}$ gives the upper border for coherent states

$$\varepsilon_{\rm E} = \frac{\hbar}{\sqrt{-\ln\hbar}}\sqrt{\frac{\lambda}{2\sigma_{\rm cl}}} = \varepsilon_{\rm mix}\sqrt{\frac{\lambda t_{\rm mix}}{-\ln\hbar}}. \tag{275}$$

(d) For $\varepsilon > \varepsilon_{\rm mix}$ the perturbation is so strong that the quantum fidelity decays before $t_{\rm mix}$, *i.e.* perturbed and unperturbed dynamics are essentially unrelated and fidelity decays almost instantly.

For coherent initial states the upper border of regime (c) is at $\varepsilon_{\rm E}$ which is smaller than the lower border $\varepsilon_{\rm mix}$ of regime (d), which opens up the possibility of another regime between (c) and (d), namely for $\varepsilon_{\rm E} < \varepsilon < \varepsilon_{\rm mix}$ the fidelity will decay within the Ehrenfest time which grows logarithmically with the number of contributing states $\mathcal{N}$ (i.e. with $\log(1/\hbar)$). In this regime the decay of quantum fidelity is the same as the decay of classical fidelity and can be explained in terms of classical Lyapunov exponents [62]. The relative width of this regime $\varepsilon_{\rm mix}/\varepsilon_{\rm E} = \sqrt{\ln(1/\hbar)/\lambda t_{\rm mix}}$ again grows logarithmically with $1/\hbar$. In regime (d), that is for $\hbar < \varepsilon < \sqrt{\hbar}$, quantum dynamics acctually becomes "hypersensitive" to perturbations [73]. For typical initial packets the decay is double exponential, $F \propto \exp(-\text{const} \times \mathrm{e}^{2\lambda t})$. Due to large fluctuations between different initial conditions for times smaller than the Ehrenfest time the average fidelity depends on the way we average. For instance, averaging fidelity one obtains exponential Lyapunov-like decay, $\langle F(t)\rangle \propto \mathrm{e}^{-\lambda_1 t}$, whereas by averaging the logarithm of the fidelity one gets a double exponential decay, $\langle \log F(t)\rangle \propto \mathrm{e}^{2\lambda_{-2} t}$, see Ref. [73] for details.

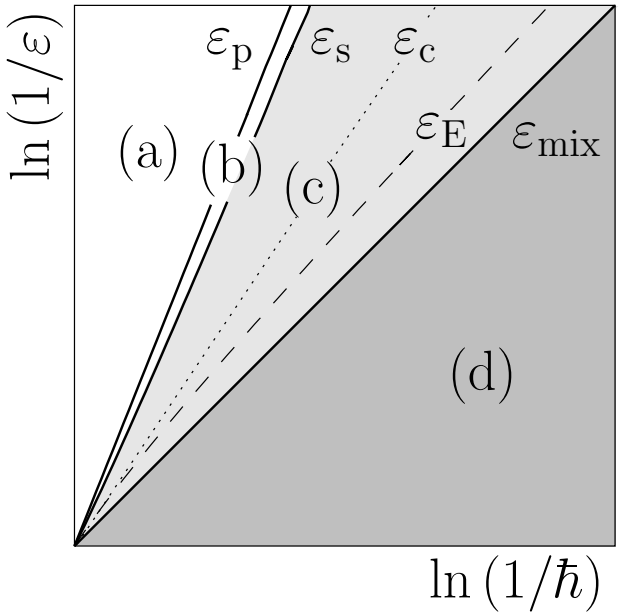

Fig. 38. Schematic view of different fidelity decay regimes for mixing dynamics [from [46]]. For instance, by increasing the perturbation fidelity goes through a Gaussian perturbative regime (a), then exponential Fermi golden rule (c) and finally for $\varepsilon > \varepsilon_{\rm mix}$ it decays almost instantly. The limits $\hbar \to 0$ and $\varepsilon \to 0$ do not commute! For details see text.

Similar information as from Fig. 38 can be gained from Fig. 6 in Ref. [116].

For composite systems we have seen in Section 3.3 that reduced fidelity and echo purity decay semiclassically on the same time scale as fidelity, the difference between time scales being $\sim 1/\mathcal{N}_{\rm c} + 1/\mathcal{N}_{\rm e}$ if $\mathcal{N}_{\rm c,e}$ are dimensions of two subspaces. Therefore, time scales involved in the decay of either reduced fidelity or echo purity (purity) are exactly the same as for fidelity.

Similar regimes as for the fidelity decay were also obtained in Refs. [202,26,203] when studying energy spreading in parametrically driven systems, see also Ref. [204] for a connections between fidelity and local density of states.

7.2. *Regular dynamics*

For regular dynamics the situation is much simpler. We have only three relevant time scales: (i) the classical averaging time $t_{\rm ave}$ in which the average perturbation operator converges to $\bar{V}$ (176), (ii) the quantum fidelity decay time $\tau_{\rm r}$ and, (iii) the time t_∞ when the fidelity reaches a fluctuating plateau due to the finite dimension of Hilbert space. For times smaller than $t_{\rm ave}$ decay is system and state specific and can not be discussed in general. After $t_{\rm ave}$ the fidelity decay is first quadratic in time as dictated by the linear response formula (179). The decay time $\tau_{\rm r}$ scales as $\sim \sqrt{\hbar}/\varepsilon$ (192) for coherent initial states and as $\sim \hbar/\varepsilon$ (197) for random initial states. Beyond linear response the functional dependence of the decay is typically a Gaussian for coherent initial states and power law for random initial states with the before mentioned decay time $\tau_{\rm r}$ (by the decay time in the case of power law dependence we mean the time when the fidelity reaches a fixed value, e.g., $\frac{1}{2}$). For weak perturbation this decay persists until $t_{\rm infty}$ when the finite size effects take in and fidelity approaches a time-averaged saturation value (42). However, for stronger perturbations and very small $\hbar$, such that the time-scale $t_{\rm a}$ (189) of applicability of action space integral approximation may be shorter than t_∞, one may observe another regime of asymptotic fidelity decay after $t_{\rm a}$ [171], which is typically again a power law (however, of different origin than for random initial states). Detailed semiclassical theory of this regime can be found in Ref. [205].

The time t_∞ again depends on the initial state as well as on the Hilbert space dimension $\mathcal{N}$. For random initial states the power law decay gets faster with increasing dimensionality d of the system, and is conjectured to approach a Gaussian decay in the thermodynamic limit [42].

In contrast to chaotic systems, for regular systems the decay time scale of reduced fidelity and of echo purity for composite systems differs from that of fidelity. For coherent initial states the reduced fidelity decays as a Gaussian on a time scale $\tau \sim \sqrt{\hbar}/\varepsilon$ (225), i.e. with the same scaling as fidelity (192) but with a different prefactor. Echo purity (or purity) for coherent initial states on the other hand initially decays quadratically but then asymptotically goes into a power law decay, $F_{\rm P} \sim 1/(\varepsilon t)^r$ (229), where the power r depends on the perturbation and is bounded by $1 \leq r \leq \min(d_{\rm c}, d_{\rm e})$ if $d_{\rm c,e}$ are the numbers of degrees of freedom of two subsystems. The important point though is that the whole decay does not depend on $\hbar$. For small $\hbar$ the decay of echo purity is therefore much slower than that of fidelity. If the initial state of the central subsystem is a superposition of two packets, the so-called cat state, the decay time of purity is much smaller and scales the same as for reduced fidelity or fidelity for a single coherent state, *i.e.* as $\tau_{\rm dec} \sim \sqrt{\hbar}/\varepsilon$ (234). For random initial states echo purity and reduced fidelity decay on a time scale $\tau \sim \hbar/\varepsilon$.

7.3. *Comparison, chaotic vs. regular*

Let us compare decay time scales of chaotic and regular systems. One might expect that quantum fidelity will decay faster for chaotic systems than for regular, at least such is the case for classical fidelity (Section 6). As we will see, this is not necessarily the case. Quantum fidelity decay can be faster for regular systems!

The fidelity decay time scales as $\sim 1/\varepsilon$ for regular systems, while it is $\sim 1/\varepsilon^2$ for mixing dynamics. This opens up an interesting possibility: it is possible that the fidelity decays *faster* for regular system than for chaotic one. Demanding $\tau_{\rm r} < \tau_{\rm m}$ we find that for sufficiently small ε one will indeed have faster fidelity decay in regular systems. This will happen for

$$\varepsilon < \begin{cases} \varepsilon_{\rm r} = \hbar\, \bar{C}^{1/2}/2\sigma_{\rm cl} \propto \hbar & \text{random init. state} \\ \varepsilon_{\rm c} = \hbar^{3/2}\sqrt{\bar{\boldsymbol{v}}' \cdot \Lambda^{-1}\bar{\boldsymbol{v}}'/8\sigma_{\rm cl}^2} \propto \hbar^{3/2} & \text{coherent init. state} \end{cases} . \tag{276}$$

We explicitly wrote the result for random initial states $\varepsilon_{\rm r}$ and coherent initial states $\varepsilon_{\rm c}$ as the two have different scaling with $\hbar$. We can see that for random initial states $\varepsilon_{\rm r}$ scales in the same way as $\varepsilon_{\rm mix}$ and

so one has faster decay of fidelity in regular systems provided $\varepsilon < \varepsilon_{\rm r} \sim \varepsilon_{\rm mix}$. For a coherent initial state this can be satisfied above the perturbative border $\varepsilon > \varepsilon_{\rm p}$ only in more than one dimension $d > 1$. In one dimensional systems $\varepsilon_{\rm p}$ and $\varepsilon_{\rm c}$ have the same scaling with $\hbar$ and whether we can observe faster decay of fidelity in regular systems than in chaotic ones depends on the values of $\sigma_{\rm cl}$ and $\bar{\boldsymbol{v}}'$. We stress that our result does not contradict any of the existing findings on quantum-classical correspondence. For example, a growth of quantum dynamical entropies [206,207] persists only up to logarithmically short Ehrenfest time $t_{\rm E}$, which is also the upper bound for the Lyapunov decay of quantum fidelity [7] and within which one would always find $F^{\rm reg}(t) > F^{\rm mix}(t)$ (for coherent states) above the perturbative border $\varepsilon > \varepsilon_{\rm p}$, whereas the theory discussed here reveals new nontrivial quantum phenomena with a semiclassical prediction (but not correspondence!) much beyond that time. If we let $\hbar \to 0$ first, and then $\varepsilon \to 0$, *i.e.* we keep $\varepsilon \gg \varepsilon_{\rm r,c}(\hbar)$, then we recover the result supported by classical intuition, namely that the regular (non-ergodic) dynamics is more stable than the chaotic (ergodic and mixing) dynamics. On the other hand, if we let $\varepsilon \to 0$ first, and only after that $\hbar \to 0$, *i.e.* satisfying Eq. (276), we find somewhat counterintuitive result saying that chaotic (mixing) dynamics is more stable than the regular one. How can we understand this? Finite $\hbar$ causes that there is a lower limit on the size of structures, see for instance figures of Wigner functions in Section 7.5. Therefore, for sufficiently small perturbations quantum fidelity can not exhibit Lyapunov decay because the latter implies occurrence of smaller and smaller structures as time progresses. So what comes into play for quantum fidelity are correlations between perturbations applied at different times. If correlations are small, like in a chaotic system, perturbations will "add up" in a slow random way, causing a slow decay of quantum fidelity.

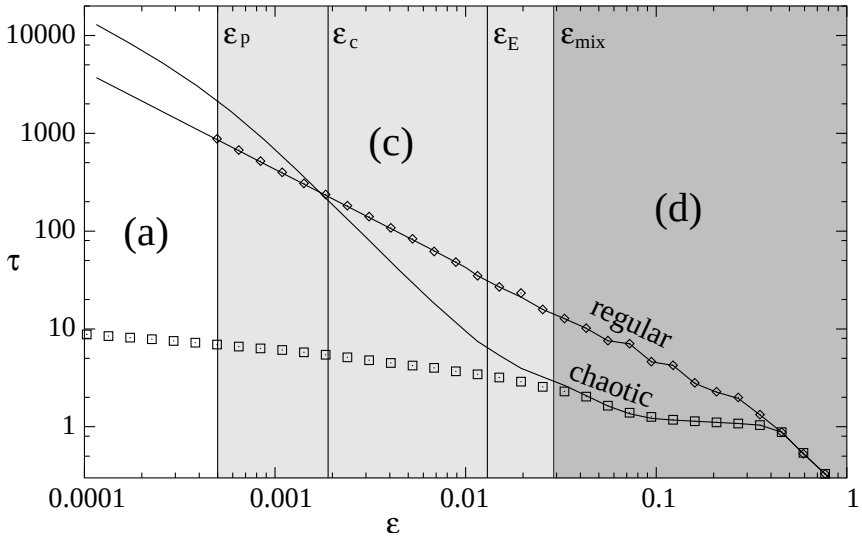

Fig. 39. Numerically calculated decay time of the quantum and classical fidelity for the double kicked top (B.20) in regular and chaotic regimes. The two solid lines show numerically calculated decay times of quantum fidelity for chaotic and regular regimes. Symbols are decay times of classical fidelity, diamonds for the regular and squares for the chaotic regime. Vertical lines show the position of perturbation borders (277). The shading and the letters (a),(c) and (d) correspond to the regimes described in Fig. 38. The Zeno regime corresponds to very short times $\tau < 1$ (i.e. strong perturbations $\varepsilon > 0.4$).

Let us now demonstrate the above regimes by a numerical example (Fig. 39). As already noted, for a one dimensional system ($d = 1$), the 'surprising' behavior of the regular decay time being smaller than the mixing one, $\tau_{\rm r} < \tau_{\rm m}$, is for coherent initial states possible only around the border $\varepsilon_{\rm p}$ (unless $\sigma_{\rm cl}$ is very small) where the exponential decay in the mixing regime goes over to a Gaussian decay due to finite $\mathcal{N}$. However, for more than one degree of freedom, such behavior is generally possible well above the finite size perturbative border $\varepsilon_{\rm p}$. To have general situation we will therefore use double kicked top ($d = 2$). The propagator is given in Appendix B.1, Eq. (B.20). Depending on the parameters the corresponding classical system is chaotic or regular. As initial state we take a product of spin coherent states (B.22) $|\vartheta, \varphi\rangle \otimes |\vartheta, \varphi\rangle$ with $(\vartheta, \varphi) = (\pi/\sqrt{3}, \pi/\sqrt{2})$ and $S = 100$. We numerically calculated the dependence of the decay time τ

(when fidelity reached $1/e \approx 0.37$) on the perturbation strength ε for chaotic and regular cases. We then compared these numerical data with theoretical predictions. Using classically calculated $\sigma = 0.058$ one gets chaotic decay time $\tau_{\rm m}$ (90) $\tau_{\rm m} = \frac{8.6}{\varepsilon^2 S^2}$. To determine the decay time of quantum fidelity for regular situation, Eq. (192), one needs the coefficient $\sqrt{\overline{v}'\Lambda^{-1}\overline{v}'}$. We determined it by fitting the dependence of $\tau_{\rm r}$, such that $\tau_{\rm r} = \frac{4.5}{\varepsilon\sqrt{S}}$, which gives $\sqrt{\overline{v}'\Lambda^{-1}\overline{v}'} = 0.31$. Note that the coefficient $\sqrt{\overline{v}'\Lambda^{-1}\overline{v}'}$ has been obtained by numerical fitting only for convenience. In principle it could be obtained from classical dynamics, but we would again have to resort to numerical calculations as the regular system is not completely integrable but is rather in a mixed KAM-like regime. The values of σ and $\sqrt{\overline{v}'\Lambda^{-1}\overline{v}'}$ can then be used to calculate various perturbation borders as discussed before. For our numerical values we get (271,276,275,274)

$$\varepsilon_{\rm p} = 0.0005, \quad \varepsilon_{\rm c} = 0.0019, \quad \varepsilon_{\rm E} = 0.013, \quad \varepsilon_{\rm mix} = 0.029. \tag{277}$$

In addition to the decay time of quantum fidelity we also numerically computed the decay time of classical fidelity. All these data are shown in Fig. 39. We can see that in the regular regime the quantum and the classical fidelity agree in the whole range of ε. In the chaotic regime things are a bit more complicated. By decreasing perturbation from $\varepsilon = 1$ we are at first in regime of very strong perturbation where the fidelity decay happens faster than any dynamical scale and it does not depend on whether we look at chaotic or regular system or quantum or classical fidelity. There the fidelity decays within the Zeno times-scale, see Section 2.1.1. For smaller ε the regular and chaotic decays start to differ. In chaotic situation the quantum and classical fidelity still agree. This correspondence breaks down around $\varepsilon_{\rm mix}$ where the quantum fidelity starts to follow the theoretical $\tau_{\rm m}$, while the classical fidelity decay is $\tau_{\rm clas} = \log(0.25/\varepsilon)/\lambda$, with 0.25 being a fitting parameter (depending on the width of the initial packet) and $\lambda = 0.89$ is the Lyapunov exponent, read from Fig. 40. For an explanation of this classical decay see Section 6. Incidentally, in our chaotic system the classical mixing time is very short, $t_{\rm mix} \sim 1$, and we see that the correspondence breaks down already slightly before $\varepsilon_{\rm E}$. The quantum fidelity decay time $\tau_{\rm m}$ is valid until a perturbative border $\varepsilon_{\rm p}$ is reached, when finite Hilbert space dimension effects become important and the decay times become equal to $\tau_{\rm p}$. Note that for $\varepsilon < \varepsilon_{\rm c}$ we indeed have faster fidelity decay for *chaotic* than for *regular* dynamics.

7.4. *Increasing chaoticity*

In Fig. 39 we saw there is a range of perturbations for which quantum fidelity decay is faster for regular than for chaotic situation. Another interesting aspect of our correlation function formalism can also be seen for chaotic dynamics alone. Because the decay rate of the fidelity in a chaotic situation is proportional to the integral of the correlation function σ, a stronger chaoticity will typically result in a *faster decay* of the correlation function $C(t)$ and therefore in smaller σ, resulting in slower fidelity decay. This means that *increasing* chaoticity (of the classical system) will *increase* quantum fidelity, i.e. stabilize quantum dynamics. Of course, for this to be observable we have to be out of the regime of quantum-classical correspondence. This phenomenon is illustrated in Fig. 40, where we show similar decay times as in Fig. 39, i.e. the same system and initial condition, but this time depending on the parameter κ of the double kicked top (B.20). The parameter κ controls the chaoticity of the classical dynamics, i.e. at $\kappa = 1$ we are in the quasi-regular regime and for larger κ we get into the chaotic regime. This can also be seen from the dependence of the Lyapunov exponent on κ in the right panel of the figure. Data is shown for six different perturbation strengths ε. We can see that in the regular regime ($\kappa < 2$) the classical fidelity agrees with the quantum one regardless of ε. In the chaotic regime though, the agreement is present only for the two largest ε shown, where we have $\varepsilon > \varepsilon_{\rm mix}$ (277). For $\varepsilon < \varepsilon_{\rm c}$ and for chaotic dynamics (three smallest ε) we get into the non-intuitive regime (shaded region in Fig. 40) where the quantum fidelity will increase if we increase chaoticity. Note that this growth of the decay time stops at around $\kappa \sim 4$ because the classical mixing time $t_{\rm mix}$ gets so small that the transport coefficient is given by its time independent first term $\sigma = C(0)/2$ alone and so σ cannot be decreased any further. From the figure one can also see that the decay time in the transition region, where the corresponding classical system has a mixed phase space, does not change monotonically with κ. Such a behavior is system specific; for some additional results for the kicked top, see Ref. [148].

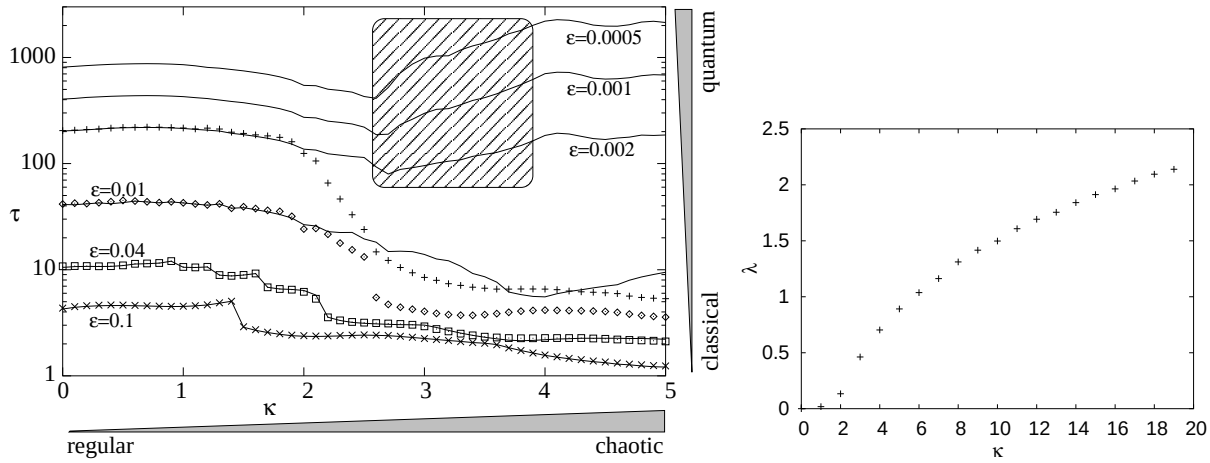

Fig. 40. Numerically calculated dependence of quantum (solid lines) and classical (symbols) fidelity decay times on the parameter κ for the double kicked top (B.20). Different curves are for different perturbation strengths ε. By increasing κ the classical dynamics goes from regular to chaotic, see also the right panel showing the dependence of the largest Lyapunov exponent on κ. By decreasing ε, on the other hand, we go from the regime of quantum-classical correspondence for $\varepsilon > \varepsilon_{\rm E}$, towards a genuinely quantum regime in which for chaotic dynamics we can *increase* the decay time by *increasing* chaoticity – shaded region for the three smallest ε.

At the end let us make a brief comparison of decay times of purity for coherent initial states. In chaotic situation purity decays in the same way as fidelity, $\tau \sim \hbar^2/\varepsilon^2$, so there is nothing new. On the other hand for regular dynamics purity decays on an $\hbar$ independent time scale, $\tau \sim 1/\varepsilon$, which is therefore for small $\hbar$ much larger than for chaotic dynamics. Still, because of different dependence on perturbation strength ε (*i.e.* coupling) one can have situation where purity decay in regular system is faster than in chaotic one. Comparing time scales of decays (229,111) within the range of linear response we see that in order to have such a situation we must have

$$\varepsilon < \varepsilon_{\rm c}^{\rm I} = \hbar^2\sqrt{\mathrm{tr}\, u}/(4\sigma_{\rm cl}) \propto \hbar^2, \tag{278}$$

where u is $\hbar$-inedependent matrix of second derivatives used in (229).

7.5. *Echo measures in terms of Wigner functions*

In Section 3.4 we have derived a semiclassical expression for fidelity in terms of the Wigner function of the initial state (124). That was just an approximation. On the other hand, one can also express fidelity in terms of two Wigner function exactly. Wigner functions, or more generally Weyl symbols for quantum operators, have a nice property that the trace of a product of two operators is equal to the overlap integral of two corresponding Weyl symbols, $\mathrm{tr}\, AB = \int W_{\rm A} W_{\rm B} {\rm d}\Omega$, where $W_{\rm A,B}$ are the corresponding Weyl symbols and the integral is over the whole phase space. Here we will need a special case of this equality for density matrices,

$$\mathrm{tr}\,(\rho_{\rm A}\rho_{\rm B}) = \int W_{\rho_{\rm A}} W_{\rho_{\rm B}} {\rm d}\Omega, \tag{279}$$

where $\rho_{\rm A,B}$ are now two density matrices and $W_{\rho_{\rm A,B}}$ the corresponding Wigner functions. For more information about Wigner functions for systems described by a canonical variables $[q,p] = {\rm i}\hbar$ see, e.g. book [208], whereas for the definition of Wigner function for spin systems (*e.g.* our kicked top models) see Ref. [209]. Remembering that the fidelity can be written as a trace of the product of the initial density matrix $\rho(0)$ and density matrix after an echo, $\rho^{\rm M}(t) = M_\varepsilon(t)\rho(0)M_\varepsilon^\dagger(t)$, or equivalently, as a trace of two forward propagated density matrices $\rho^\varepsilon(t) = U_\varepsilon(t)\rho(0)U_\varepsilon^\dagger(t)$ and $\rho^0(t) = U_0(t)\rho(0)U_0^\dagger(t)$, we have

$$F(t) = \mathrm{tr}\,\rho(0)\rho^{\rm M}(t) = \int W_{\rho(0)} W_{\rho^{\rm M}(t)} {\rm d}\Omega = \int W_{\rho^0(t)} W_{\rho^\varepsilon(t)} {\rm d}\Omega. \tag{280}$$

Similarly, one can write the reduced fidelity (72) and echo purity (74) in terms of Wigner functions of the reduced density matrices $\rho_{\rm c} = \mathrm{tr}_{\rm e}[\rho]$,

$$F_{\rm R}(t) = \int W_{\rho_{\rm c}(0)} W_{\rho_{\rm c}^{\rm M}(t)} {\rm d}\Omega_{\rm c}, \tag{281}$$

and echo purity

$$F_{\rm P}(t) = \int \left[W_{\rho_{\rm c}^{\rm M}(t)}\right]^2 {\rm d}\Omega_{\rm c}. \tag{282}$$

All these expressions are exact. The classical quantity analogous to Wigner function is just the classical density in phase space, therefore these expressions are handy for comparison with classical quantities. But note that the Wigner function is not necessarily positive whereas the classical density is (the positivity of Wigner function is a necessary but not sufficient condition for the classicality of quantum state). In the next subsection we are going to illustrate the decay of fidelity and echo purity in terms of Wigner functions. Specifically, we will compare chaotic and regular dynamics to see how is different decay of fidelity reflected in the corresponding Wigner functions.

7.5.1. *Illustration with Wigner functions*

Again we will take our standard kicked top (B.1) with parameters $\gamma = \pi/2$ and $\alpha = 30$ for the chaotic case and $\alpha = 0.1$ for the regular one. The spin size is $S = 100$ and we choose a coherent initial state at $(\vartheta^*, \varphi^*) = \pi(1/\sqrt{3}, 1/\sqrt{2})$. The perturbation strength is $\varepsilon = 1.5 \cdot 10^{-2}$. In Fig. 41 we show the fidelity decay for both cases (regular case is the same as in Fig. 26) and an illustration of states in terms of Wigner functions. For the chaotic (triangles in the fidelity plot and pictures above) and the regular case (pluses in the fidelity plot and pictures below) we show two series of Wigner functions at times $t = 0, 60, 120$: the Wigner function after the unperturbed forward evolution (row labeled "forward") and the Wigner function after the echo (row labeled "echo"). In the first frame we also show the structure of the classical phase space being either regular with KAM tori or chaotic. In the inset the data for the fidelity decay is shown on a longer time scale and the vertical line shows the theoretical position of the beating time $t_{\rm b}$ (194). In terms of Wigner functions the fidelity can be visualized as the overlap between the echo Wigner function and the initial Wigner function. The initial Wigner function shows two maxima (white regions of high value) because we have projected the initial coherent state to the invariant OE subspace, resulting in a certain symmetry of the resulting Wigner function. For chaotic dynamics the forward Wigner function develops negative values around the Ehrenfest time after which the quantum-classical correspondence is lost. For regular dynamics this correspondence persist much longer, namely until the Ehrenfest time of regular dynamics $\sim \hbar^{-1/2}$ after which the initial wave packet of size $\sim \hbar^{1/2}$ spreads over the phase space. For a detailed study of Wigner functions in chaotic systems see Refs. [210,211] and references therein. The echo Wigner function for regular dynamics moves ballistically from the initial position, causing the Gaussian decay of fidelity. We also see that for regular dynamics the echo Wigner function does not necessarily have negative values even if they occur in the forward Wigner function. In our case quantum fidelity agrees with the classical one for regular dynamics. In a chaotic case on the other hand, the echo image stays at the initial position and "diffusively" decays in amplitude, causing the fidelity to decay slower than in the regular case. Classical fidelity follows quantum fidelity in the chaotic regime only up to Ehrenfest time.

The previous figure demonstrated the possibility of faster fidelity decay in regular than in chaotic systems, provided inequality (276) is fulfilled. Let us now show that the same can happen also for echo purity. From inequality (278) we see, that either $\hbar$ has to be large (*i.e.* strong quantum regime) or the perturbation has to be weak. As a numerical model we use the Jaynes-Cummings model [212,213], describing a system of harmonic oscillator coupled to a spin. As opposed to kicked top systems, the Jaynes-Cummings model has a time independent Hamiltonian, and time is a continuous variable. Regular (integrable) dynamics is obtained if only the co-rotating coupling term is present, while predominantly chaotic dynamics takes place in the presence of both co- and counter-rotating terms, see Ref. [51] for details about numerical parameters. In Fig. 42 we show the decay of echo purity for relatively small perturbation $\varepsilon = 0.005$ in spin energy, *i.e.* perturbation is the so-called detuning, and large $\hbar = 1/4$, so that the condition $\varepsilon < \varepsilon_{\rm c}^{\rm I}$ (278) is satisfied. In addition, we show a set of pictures for times $t = 50, 100, 150$ and 200 representing square of the Wigner

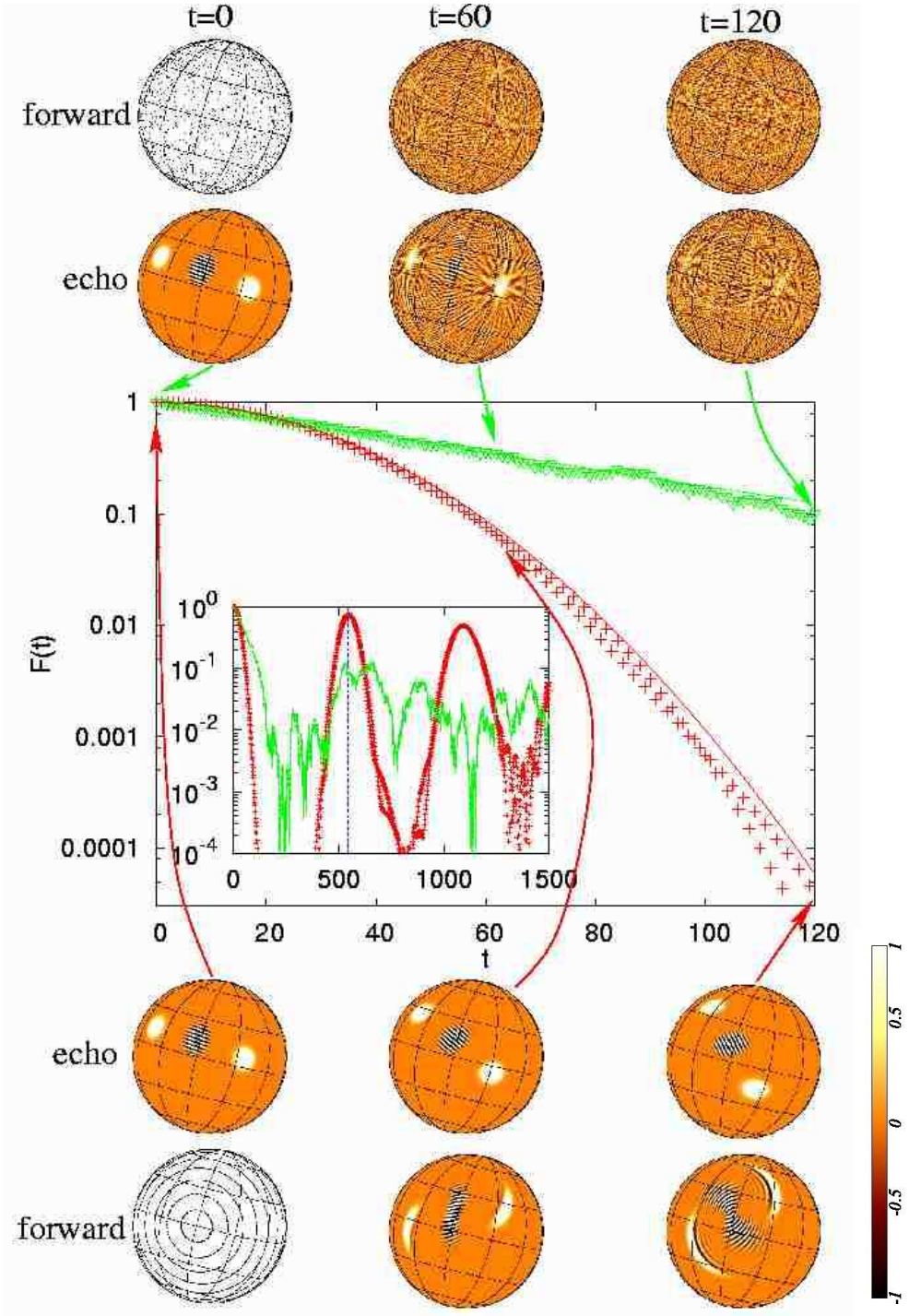

Fig. 41. Fidelity decay for chaotic (top curve and pictures) and regular (bottom curve and pictures) kicked top (B.1). Initial conditions and the perturbation are the same in both cases (see text for details). Wigner functions after forward and echo evolution are shown.

function of the reduced density matrix $\rho_{\rm c}^{\rm M}(t)$ after an echo. The integral of this quantity directly gives echo purity (282). The central subsystem is chosen to be the spin degree of freedom, so the phase space is the surface of a sphere. The top set of pictures is for chaotic and the bottom one for regular dynamics. From the

Wigner function plots one can see that the blob of maximal value of the Wigner function changes its position with time for regular dynamics while it stays at the same place for chaotic dynamics. More importantly, the height of this peak decays faster for regular dynamics than for chaotic one, reflected in a faster decay of echo purity. We should not forget that this regime of faster decay for regular dynamics is reached only for

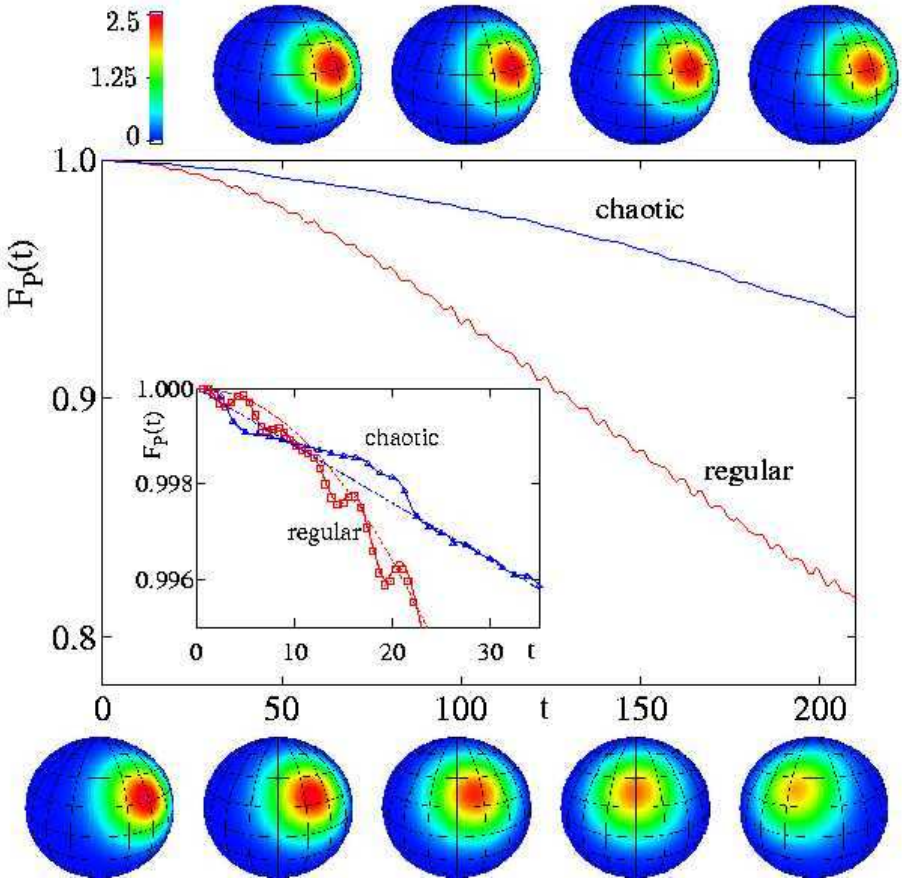

Fig. 42. Echo purity decay in the Jaynes-Cummings model for regular and chaotic dynamics [from [162]]. In the inset the same data is shown for smaller times. Full curves are numerics while dashed ones are theoretical predictions. For small $\varepsilon = 0.005$ and large $\hbar = 1/4$ used here, echo purity decay can be faster in regular than in chaotic system. Top set of pictures shows the square of the Wigner function of the reduced density matrix $\rho_c^M(t)$ for chaotic dynamics and the bottom one for regular dynamics. Its integral gives echo purity.

sufficiently large $\hbar$ (or small ε), see Eq. (278), and that in general, echo purity in regular systems will decay very slowly due to its $\hbar$ independence (229).

7.5.2. *Wigner function approach*

We have seen that the Wigner function often gives an alternate and sometimes very physical view of echo evolution, particularly if we start with a coherent state as an initial state. Note that for a random state the Wigner function is essentially a mess and does not present, to our knowledge, any useful insight. In this context we wish to discuss two papers that reach similar results. In Ref. [115] the authors develop an analogy to the formalism used in the treatment of decoherence, despite of the fact, that they do not consider coupling to some environment. For this purpose the authors consider an ensemble of perturbations. Yet they proceed quite differently than in the case of the RMT treatment offered in Section 4, in that they do not consider unitary evolution and average over the resulting fidelity amplitudes or fidelities. The Wigner function is the density operator in the phase space representation of quantum mechanics. In this picture we obtain a clear

distinction between the evolution of the diminishing coherent part of the Wigner function and the one of the emerging rapidly oscillating part. The fidelity is then given as the trace of the product of the average of the perturbed density matrices $\langle\rho(t)\rangle$ with the $\rho_0(t)$ evolving according to the unperturbed evolution

$$\langle F_z(t)\rangle = \mathrm{tr}\left(\langle\rho(t)\rangle\ \rho_0(t)\right) = \int \mathrm{d}\boldsymbol{p}\,\mathrm{d}\boldsymbol{q}\ \langle W(\boldsymbol{q},\boldsymbol{p},t)\rangle\ W(\boldsymbol{q},\boldsymbol{p},t), \tag{283}$$

which in phase space representation can be written as an integral over the Wigner function $W(\boldsymbol{q},\boldsymbol{p},t)$ and the average Wigner function $\langle W(\boldsymbol{q},\boldsymbol{p},t)\rangle$, averaged over an ensemble of perturbations.

The use of an average density matrix approaches us to concepts usually used in decoherence and induces the authors of this paper to introduce an ensemble of perturbations solely in terms of the time dependence where they assume white noise. This allows them to propose a master equation which can be solved. It is important to note, that the fidelity decay for each element of the ensemble is dominated by the decay of correlations in time through the white noise.

As an initial condition a coherent state is used, and they conclude that with perturbation strength above some threshold, they recover the exponential decay by limiting the integration to the area where the Wigner function varies slowly. The rate of this decay is perturbation independent and is determined by the (maximal) Lyapunov exponent of the underlying classical mechanics. An integration over the remaining area, where we have the well known fast oscillations developing rapidly, will produce a second term, that yields the perturbation dependent Fermi golden rule decay. The Gaussian perturbative regime is never reached in this analysis, because strong perturbations are assumed from the outset.

While the approximations in this paper are uncontrolled and several assumptions are very special, it provides very important qualitative insight: First the somewhat surprising fact that the Lyapunov decay is independent of the perturbation strength becomes intuitively clear, and second a close relation to the dynamics of decoherence is established. A similar picture was used in Ref. [116] to describe the transition between the two regimes in more detail.

Regarding fast oscillations of Wigner functions for sufficiently extended states, it has been argued in Refs. [214,47] that such sub-Planck structure enhances sensitivity of quantum systems to perturbations. When an initial state ψ has been prepared by a "preparation" evolution starting from a localized wave packed ψ_0, $\psi = \exp(-\mathrm{i}H_0 t)\psi_0$, an enhanced sensitivity has been observed when increasing the preparation time t [47]. This has been explained as being due to the small structure in Wigner function of the initial state ψ. The observed dependence though is just due to the dependence of fidelity decay in the initial state and can be explained by classical Lyapunov exponents [215] and therefore can not depend on quantum intereference effects caused by the sub-Planck structures in Wigner function, see also discussion in Ref. [216].

8. Application to Quantum Information

Quantum information theory is a relatively recent endeavor, for a review see Refs. [217–219,13]. Its beginnings go back to the 1980's and in recent years theoretical concepts have been demonstrated in experiments. While quantum cryptography, a method of provably secure communication, is already commercially available, quantum computation is still limited to small laboratory experiments.

Errors and error correction are among the main concerns in quantum information. In the present chapter we are going to discuss, how the techniques and results developed for fidelity decay can be used to design quantum operations that are less prone to errors. We will divide the whole exposition into two parts. In the first part we will show how a straightforward application of fidelity theory can help us understand the dependence of errors on various parameters. In the second part we are going to describe how one can actually decrease errors.

8.1. *Fidelity studies*

We present a partial overview of results obtained by numerically studying fidelity in quantum computation for various kinds of errors. Note that due to the extensiveness of the literature on the subject the list is by

no means exhaustive.

One of the first studies of the sensitivity to errors of quantum algorithms appeared shortly after Shor's discovery of the factoring algorithm. In Ref. [220] the influence of Markovian errors (*e.g.* due to the coupling with the environment) on the workings of Shor's algorithm has been studied. At random instances of time a random qubit was chosen to decay with a certain probability to its zero state. In subsequent work [221] the stability of Shor's algorithm running on an ion trap quantum computer is analyzed in the presence of random phase drift errors due to pulse length inaccuracies. Fidelity is found to depend exponentially on the perturbation strength ε^2 and time t as one expects for uncorrelated errors, see Section 2.1.2 or Eq. (290). In a series of papers [222,223] the influence of unwanted intrinsic qubit-qubit couplings has been studied. The dependence of fidelity on the computation time has been found to be Gaussian. This agrees with a Gaussian fidelity decay for perturbations with non-decaying correlation function. Note that such "regular" (*i.e.* Gaussian) decay of fidelity is not unexpected as the individual one or two-qubit gates, due to their simplicity, can decrease correlation function only in a very limited way, thus causing a slow decay of correlations and consequently a fast Gaussian-like decay of fidelity.

A number of numerical studies has been done by the groups of Shepelyansky and Casati. In Ref. [224,225] the question was addressed, how inter-qubit couplings change the eigenstate structure of a quantum computer, see also Refs. [226–228]. Above some threshold coupling chaos sets in and the authors advocated that quantum computation fails. This result looks like the opposite to our conclusions, where more chaos can mean more stability. One should bear in mind though, that there is no straightforward connection between eigenvector statistics and the actual dynamical fidelity which is a natural quantity measuring the stability. In [225] as well as in [229] survival probability of register states (i.e., fidelity of an unperturbed eigenstate) has been studied. The decay rate has been found to be given by the local density of states. That the eigenstate mixing is not the most relevant quantity is confirmed also by data from nuclear experiments [230]. In Ref. [231] the stability of a quantum algorithm simulating saw-tooth map has been numerically considered for static and random errors, pointing out that static imperfection are more dangerous. Similar study has been performed in Ref. [232] for the quantum kicked rotator. For random errors the fidelity has been found to decay exponentially with ε^2 and the number of gates. Such exponential decay can be shown to be general for uncorrelated (in time) errors [43], independent of the quantum algorithm, see also Eq. (290). For static errors a faster Gaussian decay has been observed, which can again be understood by the linear response formalism. In Ref. [233] the influence of random and static imperfection has been studied, confirming that static imperfections can be more dangerous [43,231]. The influence of errors on the working of quantum computer has been studied also in Ref. [136]. Static imperfections can be decreased by doing rotations between the gates, *i.e.*, introducing "randomizing" gates during the evolution [43]. Similar idea is used in the so-called PAREC (Pauli Random Error Correction) method [234,235].

The group of G. P. Berman studied in detail the stability of the Ising quantum computer, see Refs. [236–239] and references therein. The Ising quantum computer consists of a series of spin $\frac{1}{2}$ particles placed in a magnetic field with a strong gradient. The magnetic gradient allows selective addressing of individual qubits having different resonant frequencies. The nearest neighbor Ising coupling on the other hand enables the execution of two-qubit gates. All gates are performed by applying rectangular pulses of a circularly polarized electro-magnetic field lying in the plane perpendicular to the applied magnetic field. Different gates can be applied by choosing appropriate frequencies, phases and lengths of pulses. Perturbation theory has been used to explain the dependence of fidelity on errors in various physical parameters of the Ising quantum computer.

In Ref. [164] the stability of a quantum algorithm simulating the quantum saw-tooth map is studied with respect to errors in the parameters of the map (classical errors) and with respect to uncorrelated random unitary errors of gates (quantum errors). As expected from the theory [43], the fidelity decay for uncorrelated errors is found to be exponential and independent of the dynamics of the classical map. Similar results have been obtained also for the decay of concurrence in the presence of uncorrelated unitary errors [240]. In Ref. [241] noisy unitary errors were also considered theoretically. A quadratic bound (in the number of applied errors) on the error is obtained, the result being a trivial consequence of the linear response expression for fidelity, Eq. (13). Unitary noise in Grover's algorithm has been studied in Ref. [242].

Summarizing, the plethora of numerical investigations has shown that the dependence of errors on various

parameters like *e.g.* perturbation strength ε, the number of gates etc., can be readily understood within the linear response formalism of fidelity decay. Furthermore, as one is predominantly interested in large values of fidelity, linear response is all that is needed.

8.2. *Decreasing the errors*

Once we have identified the errors and their dependence on various parameters, we can try to decrease or even better to entirely eliminate such errors. We will more closely discuss two possibilities: (i) We can change the algorithm, *i.e.* apply a different set of quantum gates, so that the resulting sequence of gates is more resistant against a given kind of errors; (ii) If one is able to perform certain unitary operations with sufficiently small errors, one can do the actual quantum calculation in a transformed frame, called the *logical* frame, in which the influence of errors is suppressed. Such procedure is known as *dynamical decoupling* [14].

There are other approaches to reduce errors like *quantum error correction*, *decoherence-free subspaces* and procedures using the *quantum Zeno effect*. In the limit of ideal and infinitely short measurements quantum Zeno procedures have certain similarities [243] to the so-called "bang-bang" [244] limit of dynamical decoupling. One should be careful though as dynamical decoupling consists of unitary manipulations of dynamics while quantum Zeno effect involves quantum measurements. Fidelity theory could help to understand errors present in these methods in the non-ideal limit, for some studies see Refs. [15,245]. Another possibility to combat errors is by *quantum error correction* [246–249]. We won't discuss it in detail as we have to first be able to implement individual gates sufficiently well for the error correction to work. Also, quantum error correction can efficiently cure only errors that are correlated over just a few qubits. Its success relies on the fact that errors are local, so that information can be "hidden" in nonlocal states, whose change then serves to diagnose the error and correct them. The efficiency therefore sharply decreases for correlated multi-qubit errors. For study of error correcting codes and decoherence-free subspaces in the presence of errors see Ref. [250,251]. Using decoherence-free subspaces [252–255] one exploits certain symmetries of the coupling (like *e.g.* permutation symmetry) enabling a part of the Hilbert space to be free of decoherence for a given coupling.

In the next section we shall show an illustrative, though not very realistic example of the use of fidelity theory to improve the stability of the Quantum Fourier transformation against a certain kind of perturbations.

8.2.1. *Modifying the algorithm*

We shall first briefly present the language of quantum computation which is slightly different than the so far used framework of continuous-time Hamiltonian dynamics. We will focus on a standard quantum computation where the propagator is decomposed into quantum gates. There are other approaches to quantum computation, for instance, utilizing the ground state to perform computation, like in adiabatic quantum computation [256,257] or using holonomies in degenerate subspaces, as in holonomic quantum computation [258]. For applications of the linear response approach to the stability of holonomic quantum computation see [259–261].

A quantum computer is composed of n elementary two-level quantum systems — called *qubits*. The union of all n qubits is called a quantum register $|\mathrm{r}\rangle$. The size of the Hilbert space $\mathcal{N}$ and therefore the number of different states of a register grows with the number of qubits as $\mathcal{N} = 2^n$. A quantum algorithm is a unitary transformation U acting on register states. In the standard framework of quantum computation a quantum algorithm U which acts on $\mathcal{N}$ dimensional space is decomposed into simpler units called *quantum gates*, U_t, where t is a discrete time counting gates. Typically, quantum gates act on either a single qubit or on two-qubits. Ideal quantum computation with no errors then consists of a series of ideal gates:

$$U(T) = U_T \cdots U_2 U_1. \tag{284}$$

A quantum algorithm is called *efficient* if the number of needed elementary gates T grows at most *polynomially* in $n = \log_2 \mathcal{N}$, and only in this case it can generally be expected to outperform the best classical (digital) algorithm. Decomposition of a given algorithm U into individual gates U_t is of course not unique.

There are many decompositions with different Ts, resulting in the same algorithm $U = U(T)$. At present only few efficient quantum algorithms are known.

The above ideal situation without errors cannot be achieved in practice. Generally, at each time step there will be errors caused by perturbations (*i.e.* unwanted evolution). These can result from the coupling of qubits with external degrees of freedom or from the non-perfect evolution of qubits within the real algorithm in contrast to the ideal one. We shall model both perturbations on a given gate U_t by a unitary perturbation [12] of the form

$$U_t^\varepsilon = \exp(-\mathrm{i}\varepsilon V(t))U_t. \tag{285}$$

We set $\hbar = 1$ and use the superscript ε to denote a perturbed gate. We allow for different perturbations $V(t)$ at different gates. The perturbed algorithm is a product of perturbed gates, $U^\varepsilon(T) = U_T^\varepsilon \cdots U_1^\varepsilon$. Please note that U_j (subscript) is a single gate, that is a transformation acting between time $t = j$ and $t = j + 1$, while we use $U(t)$ for a propagator from the beginning to time t, *i.e.* $U(t) = U_t \cdots U_1$. Fidelity will again serve as a measure of stability so we have

$$F(T) = |\langle M_\varepsilon(T)\rangle|^2, \qquad M_\varepsilon(T) = U^\dagger(T)U^\varepsilon(T). \tag{286}$$

Note that here the discrete total time T is not a free parameter but is fixed by the number of gates, although we could in principle also look at the fidelity as it changes during the course of exectution of the algorithm.

We have seen in Section 7 that we can generally have higher fidelity in chaotic systems than in regular ones. For chaotic evolution fidelity decays linearly in time, while it decays quadratically for regular dynamics. Therefore, one might expect that an algorithm will be the more stable (have higher fidelity) against a given perturbation the more "chaotic" it is. A nontrivial important question then is, for which decomposition of the algorithm U shall we have the highest fidelity? In the present section we give a concrete example of such optimization. The presentation closely follows Ref. [43].

As quantum computer will work adequately only if fidelity is extremely high, the linear response expansion of $F(T)$ is all we need. Writing the echo operator in the interaction picture we have,

$$M_\varepsilon = \mathrm{e}^{-\mathrm{i}\varepsilon\tilde{V}(T)} \cdots \mathrm{e}^{-\mathrm{i}\varepsilon\tilde{V}(2)}\mathrm{e}^{-\mathrm{i}\varepsilon\tilde{V}(1)}, \tag{287}$$

where $\tilde{V}(t) = U^\dagger(t)V(t)U(t)$ is the perturbation of the t-th gate $V(t)$ propagated with the unperturbed gates $U(t) = U_t \cdots U_1$. Be aware that $\tilde{V}(t)$ is time dependent for two reasons; due to the use of the interaction picture (propagation with $U(t)$) and due to the explicit time dependence of the perturbation itself, *i.e.* the fact that different perturbations occur at different gates. To assess the typical performance of a quantum algorithm independent of a particular initial state of the register, we average over Hilbert space of initial states as $\langle\bullet\rangle = \frac{1}{\mathcal{N}}\operatorname{tr}(\bullet)$. Expanding fidelity we obtain to lowest order

$$F(T) = 1 - \varepsilon^2 \sum_{t,t'=1}^{T} C(t,t'), \qquad C(t,t') = \frac{1}{\mathcal{N}}\operatorname{tr}[\tilde{V}(t)\tilde{V}(t')]. \tag{288}$$

Two situation can now be distinguished depending on the time dependence of the perturbation $V(t)$ at different gates.

The extreme case of time-dependent $V(t)$ is *uncorrelated noise*. This can result from coupling to a many body chaotic system, for which the matrix elements of $V(t)$ may be assumed to be *Gaussian random* variables, uncorrelated in time,

$$\langle V_{jk}(t)V_{lm}(t')\rangle_{\text{noise}} = \frac{1}{\mathcal{N}}\delta_{jm}\delta_{kl}\delta_{tt'}. \tag{289}$$

Hence one finds $\langle C(t,t')\rangle_{\text{noise}} = \delta_{tt'}$, where we have averaged over noise. In fact the average of the product in M_ε (287) equals the product of the average and yields the noise-averaged fidelity to all orders

$$\langle F(T)\rangle_{\text{noise}} = \exp(-\varepsilon^2 T), \tag{290}$$

which is *independent* of the quantum algorithm $U(T)$. This result is completely general provided that the correlation time of the perturbation $V(t)$ is *smaller* than the duration of a single gate.

[12] We treat only unitary errors here. Quantum computation is expected to require probability conservation. To treat non-unitary effects we would have to include "environment" into our picture.

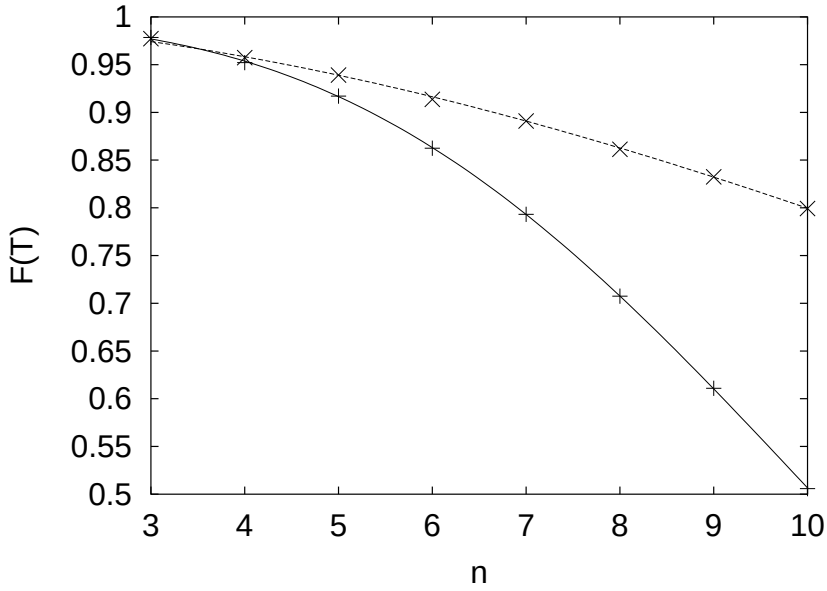

Fig. 43. Dependence of the fidelity $F(T)$ on the number of qubits n for the QFT (pluses) and the IQFT algorithms (crosses), for fixed $\varepsilon = 0.04$ [from [43]]. The full curve is $\exp(-\varepsilon^2\{0.47n^3 - 0.76n^2 + 2.90n\})$ and the dashed one $\exp(-\varepsilon^2\{1.22n^2 + 1.78n\})$. An "improved" IQFT algorithm, being more random, has a higher fidelity, which furthermore decreases slower with n than for the original QFT algorithm. All is for a static random matrix perturbation.

On the other hand, for a *static* perturbation, $V(t) \equiv V$, one may expect *slower* correlation decay, depending on the "regularity" of the evolution operator $U(T)$, and hence faster decay of fidelity. Note that in a physical situation, where the perturbation is expected to be a combination $V(t) = V_{\rm static} + V_{\rm noise}(t)$, the fidelity drop due to a static component is expected to *dominate* long-time quantum computation $T \to \infty$ (i.e. large numbers of qubits n) as compared to the noise component, as soon as the quantum algorithm exhibits long time correlations of the operator $V_{\rm static}$. The fact that static imperfections can be more dangerous than time-dependent ones (*e.g.* noise) has been also observed in numerical experiments done in Ref. [231]. Therefore, in the following we shall concentrate on static perturbations as they are more dangerous. We concentrate on the Quantum Fourier Transformation algorithm (QFT) [262,263] and shall consider its stability against static random perturbations. The perturbation $V(t) \equiv V$ will be a random hermitian matrix from a Gaussian unitary ensemble (GUE) [144]. The GUE matrices have been extensively used to model quantum statistical properties of classically chaotic Hamiltonians without time-reversal invariance [19,86,20]. Note that a GUE matrix acts on the whole Hilbert space and therefore represents a perturbation that affects correlations between all n qubits. Quantum error correction methods for instance do not work for this type of errors. Second moments of a GUE matrix V are normalized as

$$\langle V_{jk} V_{lm} \rangle_{\rm GUE} = \delta_{jm}\delta_{kl}/\mathcal{N}, \tag{291}$$

where the averaging is done over a GUE ensemble. Using this in the general expression for the correlation function (288) we arrive at the correlation function for a static GUE perturbation,

$$\langle C(t,t') \rangle_{\rm GUE} = \left| \frac{1}{\mathcal{N}} \operatorname{tr} U(t,t') \right|^2 , \tag{292}$$

where $U(t,t')$ is the unperturbed propagator from gate $t'+1$ to t, $U(t,t') = U_t \cdots U_{t'+1}$, with the convention $U(t,t) \equiv \mathbb{1}$. The correlation sum must then be evaluated for the QFT algorithm. For the usual decomposition of the QFT algorithm into gates we have $T \sim n^2/2$ gates, namely n one-qubit Hadamard gates and $n^2/2$ diagonal two qubit "B" gates, $\mathrm{B}_{jk} = \mathrm{diag}\{1,1,1,\exp(\mathrm{i}\theta_{jk})\}$, with $\theta_{jk} = \pi/2^{k-j}$. The correlation sum $\nu = \sum_{t,t'=1}^{T} C(t,t')$ scales as $\nu_{\rm QFT} \propto n^3$. Cubic growth can be understood from the special block structure of the QFT. There are n blocks, each containing one Hadamard gate and j "B"-gates, $j = 0, \ldots, n-1$. These "B"-

gates, which are almost identities, are responsible for the correlation function to decay very slowly, resulting in $\nu \propto n^3$, see Ref. [43] for details. The idea how to modify the QFT algorithm is to get rid of *bad* "B"-gates. This can in fact be done [43], obtaining the so-called improved QFT (IQFT) algorithm. The IQFT has twice as many gates as the QFT, but retains the same scaling $T_{\mathrm{IQFT}} \sim n^2$. Although the perturbation is applied twice as often during the evolution of IQFT the correlation sum is smaller, because the correlation function is greatly decreased. More importantly, the correlation sum grows only quadratically with n, $\nu_{\mathrm{IQFT}} \propto n^2$. The dependence of fidelity $F(T)$ on the number of qubits n can be seen in Fig. 43. Both the QFT and the IQFT are represented, and we see the considerable advantage of the modification for large n.

A few comments are in place at this point. The high fidelity of the IQFT algorithm depends on the perturbation being a GUE matrix. The optimization is therefore somewhat perturbation specific. We should point out that the optimization of the QFT algorithm becomes more difficult if the perturbation results from a two-body (two-qubit) GUE ensemble [86,264]. This is connected with the fact that quantum gates are two-body operators and can perform only a very limited set of rotations on full Hilbert space and consequently have a limited capability of reducing the correlation function in a single step. For such errors fidelity will typically decay with the square of the number of errors T, *i.e.* the number of gates, like $\sim \exp(-\varepsilon^2 T^2)$, that is the same as for regular systems. This means that the very fact that the algorithm is efficient, having a polynomial number of gates, makes it very hard to reduce the correlation function and therefore causes fast fidelity decay.

In this section we presented a result for optimizing the QFT if the perturbation acts after each individual gate. In experimental implementations each gate is usually composed of many simple pulses. Provided the perturbation is GUE, the IQFT will be more stable even if the perturbation acts after each pulse (*i.e.* many times during a single gate). This is for instance the case in Ref. [239] where the same gain as here has been numerically verified for a QFT algorithm running on the Ising quantum computer.

8.2.2. *Dynamical decoupling*

Our approach to the analysis of fidelity consisted in exploring how $F(t)$ decays for different perturbations and/or initial states for a given unperturbed dynamics H_0. The question can be turned around though. One can ask, what we can infer about the fidelity $F(t)$ if we have a given perturbation V, but are free to choose the unperturbed evolution H_0. This question is of immediate interest if we want to suppress the unwanted evolution caused by $V(t)$. By appropriately choosing $H_0(t)$ we want to suppress unwanted effects of $V(t)$ as much as possible. Of course, just setting $H_0(t) = -V(t)$ will do the trick. But the rule of the game is, that we are not able to generate an arbitrary H_0, but just some subset. One can, for instance, imagine that $V(t)$ is an unwanted coupling with the environment. In such case $V(t)$ includes also environmental degrees of freedom which we are not able to control. So one can allow H_0 to act only on the the central system and not on the environment.

Such a dynamical suppression of unwanted evolution is known as *a dynamical decoupling* [14,265,15,244,266]. Let us assume that we are able to perform operations $U_0(t)$ from a group $\mathcal{G}$ without errors and infinitely fast [13]. In the case of a discrete group $\mathcal{G}$ time t is a discrete index counting the elements of a group. U_0 can be thought of as generated by some Hamiltonian $H_0(t)$. Usually cyclic conditions are assumed, $U_0(t+T_{\mathrm{c}}) = U_0(t)$, where T_{c} is the period. Due to the presence of the unwanted term $V(t)$, the evolution is actually given by $U_\varepsilon(t)$ applying both $H_0(t)$ and $V(t)$. Because $U_0(t)$ can be executed exactly, we can define a new computational frame called the *logical frame* (interaction frame in fidelity language), in which there is no evolution due to U_0. Mathematically, the propagator in the logical frame is

$$U_{\log}(t) = U_0^\dagger(t) U_\varepsilon(t). \tag{293}$$

We can see, that $U_{\log}(t)$ is nothing but the echo operator $M_\varepsilon(t)$ (6), so we have

$$U_{\log}(t) = \hat{T} \exp\left(-\frac{\mathrm{i}}{\hbar}\varepsilon \int_0^t \mathrm{d}t' \tilde{V}(t') \right), \tag{294}$$

[13] The condition of infinitely fast, so-called "bang-bang" [244] execution, can be relaxed [265].

where $\hat{T}$ denotes a time-ordering and $\tilde{V}(t) = U_0^\dagger V(t) U_0(t)$. The goal of dynamical decoupling is to make evolution in the logical frame $U_{\log}$ as close to identity $\mathbb{1}$ as possible or more generally, to make it a tensor product of evolution of the central system and the environment, $U_{\log}(t) \to U_{\rm sys} \otimes U_{\rm bath}$, *i.e.* to decouple our system from the environment. While in the laboratory frame there are contribution due to H_0 and $V(t)$, in the logical frame there is only a contribution due to logical $\tilde{V}(t)$. By appropriate choice of $U_0(t)$ such that $\tilde{V}(t)$ "averages" out, suppression of evolution due to $V(t)$ can be achieved in the logical frame. Two approaches are possible, depending on how we choose the correcting dynamics $U_0(t)$:

– The first one is called a *deterministic dynamical decoupling* [14], because $U_0(t)$ is chosen to deterministically traverse all the elements of the group $\mathcal{G}$. Applying the BCH formula (Section 2.1.4) on $U_{\log}$ we get

$$U_{\log}(t) = \exp\left\{-\frac{\mathrm{i}}{\hbar}\left(\varepsilon \bar{V} t + \frac{1}{2}\varepsilon^2 \Gamma(t) + \dots\right)\right\}, \tag{295}$$

with the known expressions for $\bar{V}$ (176) and $\Gamma(t)$ (25). If we are able to choose $H_0(t)$ such that $\bar{V} \equiv 0$ dynamical decoupling is achieved and is said to be of the 1st order. Dynamical decoupling therefore exactly corresponds to the freeze of quantum fidelity, either in integrable systems (Section 5.2) or in chaotic (Section 3.2). The fact that going into a different computational frame can dramatically change the influence of errors has been also numerically verified in the Ising quantum computer [239].

– Even if one might not be able to make $\bar{V} = 0$, one might be able to reduce it. A standard measure of success of such a suppression is fidelity, *i.e.* the expectation value of $U_{\log}(t)$. Learning from the results of fidelity decay, we can expect that the suppression will be the larger, the more "chaotic" the evolution $U_0(t)$ is [42,43,46]. In the maximally random case the $U_0(t)$ at different times are totally uncorrelated. Dynamical decoupling for such uncorrelated $U_0(t)$ has been recently proposed [15] and named *random dynamical decoupling*. Lowest order of the error probability has been estimated [15] and is equal to the linear response approximation to fidelity for chaotic dynamics (87), see also Section 2.1.2 on fidelity decay for uncorrelated perturbations.

Summarizing, the idea of dynamical decoupling is to suppress unwanted evolution $V(t)$ by applying unitary corrections $U_0(t)$ and doing quantum operations in the logical frame defined by $U_0(t)$. This can be achieved either by making $\bar{V} = 0$ or by making $U_0(t)$ uncorrelated in time, so the error correlations are decreased. The idea of applying some additional pulses to correct for unwanted evolution is extensively used in NMR. In the quantum computer context it has been for instances used by the group of Berman to suppress near-resonant errors in the Ising quantum computer, see Ref. [267] and references therein.

9. A report on experiments

The first experiments of echo dynamics go back to Hahn [8] in nuclear magnetic resonance (NMR) and in the introduction we have given a historical rundown of NMR techniques. In this section we shall limit our discussion to a few experiments or potential experiments, that relate directly to the theory presented in this paper. In this context recent experiments with microwaves and elastic waves are remarkable, in that they yield very good agreement with random matrix theory, but we shall actually start with some recent NMR experiments by the Cordoba group, which at this point cannot be explained and provide some intriguing riddles. Finally we shall discuss extensively potential experiments in atomic optics expanding on an idea by Gardiner Cirac and Zoller [33,34,48].

9.1. *Echo experiments with nuclear magnetic resonance*

The first real *interacting* many-body echo experiment was done in solids by Rhim et al. [9]. Time reversal, *i.e.* changing the sign of the interaction, is achieved for a dipolar interaction whose angular dependence can change sign for a certain "magic" angle, that causes the method to be called magic echo. Still, the magic echo showed strong irreversibility. Much later a sequence of pulses has been devised enabling a *local* detection of polarization [10,268] (*i.e.* magnetic moment). They used a molecular crystal, ferrocene $Fe(C_5H_5)_2$, in which the naturally abundant isotope ^{13}C is used as an "injection" point and a probe, while a ring of protons

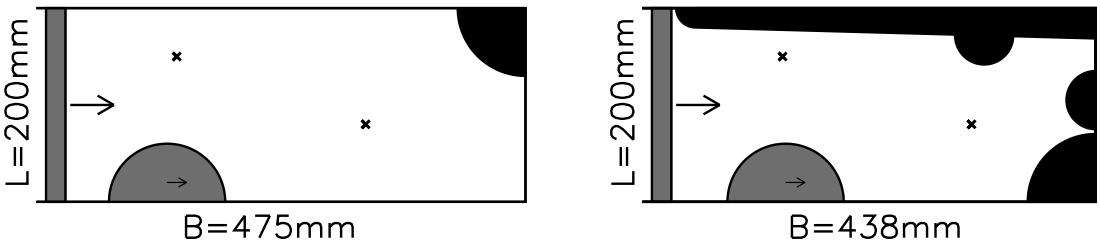

Fig. 44. Geometry of the billiards (figure taken from [69]). In the billiard in the right figure bouncing ball orbits have been avoided by inserting additional elements.

^{1}H constitutes a many-body spin system interacting by dipole forces. The experiment proceeds in several steps: first the ^{13}C is magnetized, then this magnetization is transfered to the neighboring ^{1}H. We thus have a single polarized spin, while others are in "equilibrium". The system of spins then evolves freely, *i.e.* spin diffusion takes place, until at time t the dipolar interaction is reversed and by this also spin diffusion. After time $2t$ the echo is formed and we transfer the magnetization back to our probe ^{13}C enabling the detection of the *polarization echo* (66). Note that in the polarization echo experiments the total polarization is conserved as the dipole interaction has only "flip-flop" terms of the form $S_+^j S_-^{j+1}$, which conserve the total spin. To detect the spin diffusion one therefore needs a local probe. With the increase of the reversal time t the polarization echo – the fidelity – decreases in approximately exponential way. The nature of this decay in spin-diffusion reversal experiment has been furthermore elaborated by Pastawski et al. [38]. The group of Pastawski then performed a series of NMR experiments where they studied in more detail the dependence of the polarization echo on various parameters [11,39,40]. They were able to control the size of the residual part of the Hamiltonian, which was not reversed in the experiment and is assumed to be responsible for the polarization echo decay. In presence of strong perturbations, such as magnetic or quadrupolar impurities, the Echo decays according to a perturbation dependent exponential law as prescribed by the Fermi golden rule. However, in pure systems, where residual interactions are made small, the decay enters a Gaussian regime where the decay rate is perturbation independent. Notice that the experiments are constrained to move from a naturally big perturbation and, while one can reduce it, the full cancellation of perturbation can not be achieved. A similar situation was observed in liquid crystals where a molecule involves a few tens of spins [269]. This is consistent with the original interpretation [38,39] that the many body spectrum is so dense, that almost any small perturbation can place the Echo dynamics in a regime where it is perturbation independent. These surprising results triggered a number of numerical studies and theoretical investigations.

In Ref. [270] quantum Baker map has been experimentally implemented on a 3-qubit system within NMR context. They also studied the influence of perturbations on the dynamics and could by measuring the resulting density matrices calculate the fidelity. For some other NMR measurements of fidelity see also [271].

9.2. *Measuring fidelity of classical waves*

The dynamics of classical electromagnetic waves in a thin resonator is equivalent to a single-particle two dimensional Schrödinger equation, *i.e.* single particle quantum mechanics. This is exploited in the microwave resonator experiments, where properties of two dimensional quantum billiards can be studied. The Marburg group considered a cavity consisting of a rectangle with inserts that assure a chaotic ray behavior, Fig. 44. Both situations with and without parabolic manifolds leading to so-called bouncing ball states were considered. One wall was movable in small steps, this change causing the perturbation occurring in an echo experiment. It is important to note that the shift of the wall changes the mean level density and thus the Heisenberg time. This trivial perturbation, which would cause very rapid correlation decay is eliminated in this case by measuring all times in proper dimensionless units, *i.e.* in terms of the Heisenberg time as proposed in Section 4. Two antennae allow to measure both reflection and transmission channels. The experiment was carried out in the frequency domain. Afterwards the Fourier transform is used to obtain

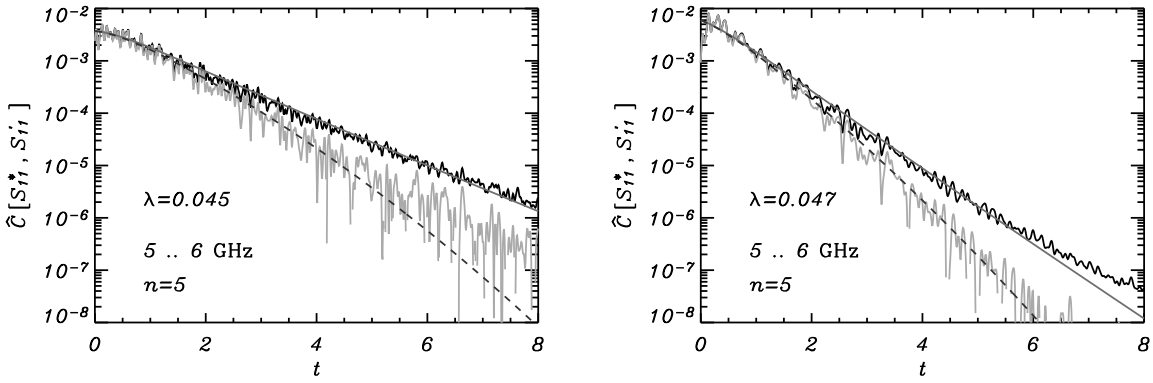

Fig. 45. (Figure taken from [69]) Logarithmic plot of the correlation function $\hat{C}[S^*_{11}, S'_{11}]$ for the billiard with bouncing balls (left), and for the one without bouncing-balls (right). The experimental results for the auto correlation are shown in black, while the correlation of perturbed and unperturbed system are shown in grey. The smooth solid curve corresponds to the theoretical autocorrelation function, and the dashed curve to the product of autocorrelation function and fidelity amplitude.

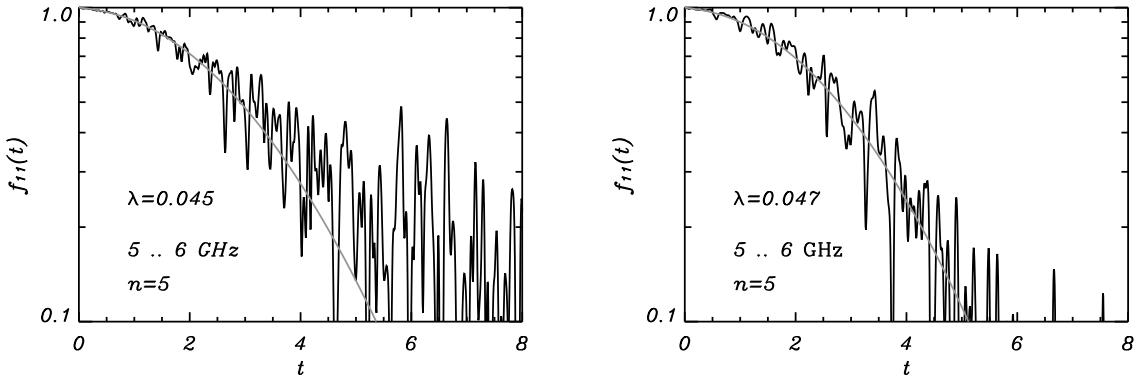

Fig. 46. Logarithmic plot of the corresponding fidelity amplitudes (figure taken from [69]). The smooth curve shows the linear-response result. For the billiard without bouncing balls, the perturbation parameter λ was obtained from the variance of the level velocities; in the other case it was fitted to the experimental curve.

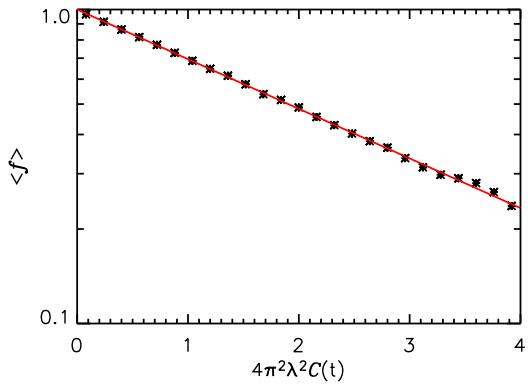

Fig. 47. (Figure taken from [69]) Average of the experimental fidelity amplitude on a rescaled axis $x = 4\pi^2\lambda^2 C(t)$. The solid line corresponds to $g(x) = \exp(-\alpha x)$ with $\alpha = \lambda^2_{\rm exp}/\lambda^2 = 0.36$.

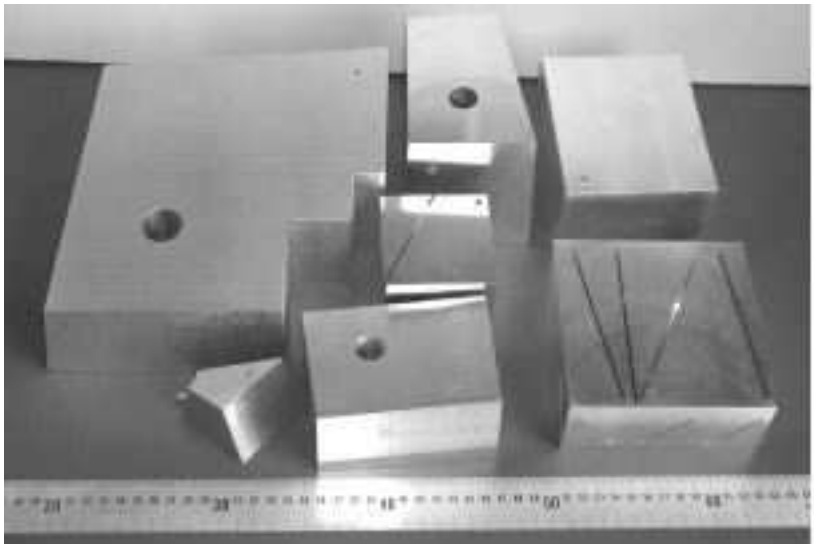

Fig. 48. Different aluminum block specimens (figure taken from [68]).

correlation functions in the time domain. Recall (Section 2.6.1) that these functions are used to define scattering fidelity which, for weak coupling and chaotic dynamics, agrees with standard fidelity. In Fig. 45 the correlation functions are shown for two different systems. Observe that the cross-correlation agrees with the random matrix prediction in time up to six times the Heisenberg time and in magnitude of the cross-correlation function over five orders of magnitude. In the case with bouncing ball states the agreement with RMT is understandably much poorer. In Fig. 46, the scattering fidelity itself is reproduced; as we are in the range of isolated resonances, *i.e.* in a weak coupling situation this should be standard fidelity, and indeed the agreement with fidelity as obtained from RMT is excellent. The perturbation strength in this case was determined independently from the level dynamics and, understandably, for low energies it does not agree with its semi-classical limit. It is more surprising that the shape of fidelity as obtained for RMT in Eq. (130) holds for some stretch beyond the weak coupling limit. This can be seen in Fig. 47, where a wide range of data for chaotic systems has been averaged over, and the validity of scaling with $\lambda^2\ C(t)$ is assumed. This in turn implies scaling with λ^2 as well as with the time dependence and the dependence on Heisenberg time as it appears in the correlation integral $C(t)$. Indeed if we scale the time dependence with the function obtained in the linear response approximation of RMT and average over all results that are available for different systems and frequency ranges we find that exponentiation of linear response is an excellent approximation in the range of the present experiment.

Lobkis and Weaver [68] have performed an interesting experiment on cross-correlations of the long time signal, usually called "coda", of elastic signals at different temperatures for a number of aluminum blocks, Fig. 48. Both the excitation and the readout were transmitted with the same piezo-element, that connected the specimen with the pulse generator and analyzer isolating the latter from the former by a reed relay. The sample was kept in vacuum and with strict control of the uniformity of temperature. The purpose of the measurement was to investigate the normalized cross-correlation of these signals for the same block at different temperatures T_1 and T_2,

$$X(\varepsilon) = \frac{\int \mathrm{d}\tau\ S_{T_1}(\tau)\ S_{T_2}(\tau(1+\varepsilon))}{\sqrt{\int \mathrm{d}\tau\ S_{T_1}^2(\tau)\ \int \mathrm{d}\tau\ S_{T_2}^2(\tau(1+\varepsilon))}}. \tag{296}$$

The correlation integral is calculated around some time t, which the authors call the "age" of the sample. Temperature steps of 4° were chosen. The biggest effect termed dilation is simply due to changes in volume and in the speeds of propagation of the waves. This should show in the correlation functions as a maximum of size 1 at a time difference determined by factors well known for elastic media. In fact we find a maximum at the predicted time, but it is smaller than 1 (see Fig. 49). These maxima as a function of the age t of the

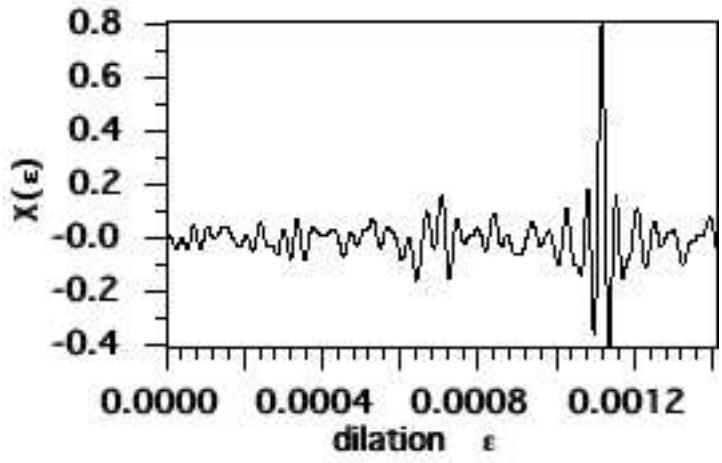

Fig. 49. The typical form a a correlation function computed according to Eq. (296) (figure taken from [68]).

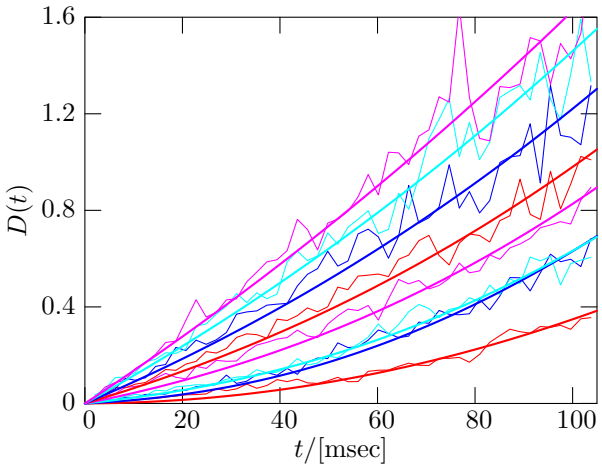

Fig. 50. (Color online) The distortion as a function of time, for the cuboid (figure taken from [83]). The thick solid lines correspond to measurements in the frequency ranges from 100kHz to 800kHz, in steps of 100kHz (from bottom to top). The thin solid lines show the best fits with $-\ln[f(t)]$ where $f(t)$ is given in Eq. (130) with $\beta_V = 1$. The fit values for λ_0 can be found in [83].

sample, are called distortions $D(t)$.

The correlation function (296) suggests that the distortion can be related to the logarithm of scattering fidelity and indeed it is easy to show [83] that $D(t) = -\ln f_s(t)$ holds. The timeshift in the correlation maximum exactly compensates for the trivial dilation effect, and in this sense is equivalent to measuring time in units of Heisenberg time, as was done in the microwave experiment.

As the piezo-element provides weak coupling and the environment of the samples is evacuated, we are in a weak coupling limit, which implies that distortion is also equal to fidelity. In [83] this equivalence is shown in detail. Furthermore for a block for which we expect "chaotic" split ray behavior good agreement with RMT results is demonstrated. In this case perturbation strength as obtained from a fit of RMT is in fair agreement with an estimate resulting from elastomechanics assuming chaotic split ray dynamics.

Actually RMT also fits very well the results for a regular aluminum brick (upper right sample in Fig. 48); see Fig. 50. While this seems at first sight surprising it is in line with findings of GOE spectral statistics [272] confirming that the corresponding wave system displays what one may loosely call wave chaos.

9.3. *Fidelity decay and decay of coherences*

Under special circumstances the time evolution of two coupled systems can show an interesting relation between decay of coherences in one subsystem and fidelity decay in the other one. Basically two types of coupling are described in [48] for which this occurs. On one hand we can have what we might call a dephasing situation, with a Hamiltonian of the form

$$H = H_c + H_e + O_c\, V_e\ , \quad [O_c, H_c] = 0\ . \tag{297}$$

Here as usual operators with indices c and e operate only on either of two subsystems termed somewhat arbitrarily central system and environment, and O_c is some operator commuting with the Hamiltonian with eigenvalues o_j when applied to some eigenfunction ϕ_ν with $H_c\ \phi_\nu\ =\ \epsilon_\nu\, \phi_\nu$. Then it is easy to prove, that for an initial state $(1/\sqrt{2})\,(\phi_j + \phi_k) \otimes \chi_0$ the elements of the density matrix of the central system, *i.e.* the coherences relate to fidelity decay in the environment as

$$\rho^c_{j,k}(t) = \mathrm{e}^{-\mathrm{i}(\epsilon_j - \epsilon_k)}\ \langle\chi_0|\, \mathrm{e}^{-\mathrm{i}t(o_j V_e + H_e)}\, \mathrm{e}^{\mathrm{i}t(o_k V_e + H_e)}\, |\chi_0\rangle = \mathrm{e}^{-\mathrm{i}(\epsilon_j - \epsilon_k)}\ \ f(t). \tag{298}$$

Up to the phase factor the righthand side is clearly the fidelity amplitude resulting for the function χ_0 which can be chosen arbitrarily in the environment with an unperturbed Hamiltonian $o_j V_e + H_e$ and a perturbed Hamiltonian $o_k V_e + H_e$.

If we can measure the coherences, we can measure fidelity, which does not depend on the phases. Moreover, if we know the phases, we actually can measure the fidelity amplitude.

A particularly simple situation occurs if the internal evolution of the central system for some reason is irrelevant. This can occur, if the two states defining the density matrix element we consider, are degenerate, or if the evolution of the internal system is so slow, that coherence decays on a much shorter time scale. It has been argued [182–184] that this can occur if $|o_j - o_k|$ is just large enough. On the other hand Gardiner, Cirac and Zoller [33,34] proposed long ago an experiment to test the sensitivity to changes of dynamics of chaotic systems. Actually the idea they proposed can be generalized and contains much of what was exposed above. Experiments along the lines given above can be carried out in atomic optics. The non-evolution of the central system as assumed in the original papers by the above authors typically holds, though we saw, that it is not essential. We shall describe below a proposition for such an experiment for a kicked rotor in more detail following Ref. [148].

Yet there is another interesting option presented in [48]. As usual quadratic Hamiltonians present additional opportunities. A harmonic oscillator is coupled linearly to a bath of oscillators as

$$H = H^{\mathrm{c}} + H^{\mathrm{e}} + H^{\mathrm{int}} = \hbar\Omega\ a^\dagger a + \sum_\lambda \hbar\omega_\lambda b^\dagger_\lambda b_\lambda + \sum_\lambda \hbar g_\lambda \left(a b^\dagger_\lambda + a^\dagger b_\lambda\right). \tag{299}$$

Here $a, a^\dagger$ are the annihilation and creation operators for the central oscillator and $b_\lambda, b^\dagger_\lambda$ the corresponding operators for the bath oscillators. Ω and ω_λ are the corresponding frequencies and g_λ the coupling constants. Now a coherent state basis will produce an adequate factorized basis, which will remain factorized for very long times, and allow a similar development. The distance between complex "positions" z of the coherent states in the central system will determine the strength of the perturbation. We find that the decay of the coherences in the density matrix determines the fidelity decay of an initially not excited environment of oscillators. As we are dealing with an eigenstate of the unperturbed oscillator we expect Fermi golden rule behavior, *i.e.* exponential decay with the square of the strength of the perturbation, and indeed recover the famous relation $|\varrho^{\mathrm{c}}_{12}(t)|^2 = \exp(-\gamma t|z_1(0) - z_2(0)|^2)\ |\varrho^{\mathrm{c}}_{12}(0)|^2$, [273,91,125]. Historically, it is quite interesting to notice, that the Paris experiment [274] that shows decoherence explicitly can be reinterpreted as a measurement of fidelity decay of the environment at least for large angles. This follows directly from the fact, that the relation between the decoherences and fidelity decay is equally true for well separated Gaussian wave packets.

9.3.1. *The Gardiner-Cirac-Zoller approach and the kicked rotor*

In [33,34] the authors proposed an experiment to study quantum dynamics of the center of mass motion of a trapped atom. Indeed they use the internal degree of freedom of the trapped atom, both to disturb the

dynamics and to measure the effect of this perturbation. While they do not use the word explicitly, they propose a measurement of the fidelity amplitude using the properties of particular couplings of two-level quantum systems. As mentioned above their method is a special case of the general theory outlined in [48] and reported above. It is though important to note that the basic idea is given in this reference. A more detailed proposition along these lines to measure fidelity decay for the kicked rotor *e.g.* is given in [148], which we shall follow in this subsection.

The kicked rotor can be modeled experimentally by an atom in a standing light wave [275–277]. For such an experiment typically an atom of mass M is chosen, which has two electronic levels with spacing ω_0. The states shall be denoted by $|1\rangle$ and $|e\rangle$ for the lower and the excited one. They are driven by two counter–propagating laser fields.

The dipole $\boldsymbol{\mu}$ of this transition is coupled to the electromagnetic field $\boldsymbol{E}(x,t) = \mathcal{E}\boldsymbol{\epsilon}\cos(k_{\rm L}x+\varphi_{\rm L})e^{-i\omega t}+$c.c. of the lasers with wave number $k_{\rm L}$, frequency ω, complex amplitude $\mathcal{E}$, polarization $\boldsymbol{\epsilon}$ and phase $\varphi_{\rm L}$. In the rotating wave approximation the Hamiltonian describing this interaction reads as

$$\hat{H}_{\rm int} = \frac{\hat{p}^2}{2M} + \hbar\omega_0|e\rangle\langle e| + \left[\frac{\hbar\Omega}{2}\cos\left(k_{\rm L}x+\varphi_{\rm L}\right)e^{-i\omega t}|e\rangle\langle 1| + \text{H.c.}\right] , \tag{300}$$

with the Rabi–frequency $\Omega = \boldsymbol{\mu}\boldsymbol{\epsilon}\mathcal{E}/\hbar$. A large detuning $\Delta = \omega_0 - \omega$ allows to adiabatically eliminate the excited state $|e\rangle$ leading to the Hamiltonian

$$\hat{H}_1 = \frac{\hat{p}^2}{2M} + \hbar\kappa_1[\sin(2k_{\rm L}x)+1]\,\delta_T(t) \tag{301}$$

for the state $|1\rangle$ in a frame rotating with the laser frequency. The interaction strength is given by $\kappa_1 = \Omega^2/(8\Delta)$ and we choose the phase $\varphi_{\rm L}$ appropriately. Moreover, the periodic kicks theoretically described by the train of δ–functions in Eq. (301) can be approximately realized by rapidly switching on and off the laser fields with period T. Therefore, the Hamiltonian Eq. (301) corresponds to the Hamiltonian of the kicked rotor.

In order to measure fidelity a similar setup can be applied using atom interferometry [278,277]. For this reason we take again an atom with excited electronic state $|e\rangle$ but two hyperfine ground states $|1\rangle$ and $|2\rangle$ separated by the hyperfine–splitting $\omega_{\rm hf}$, as illustrated in Fig. 51.

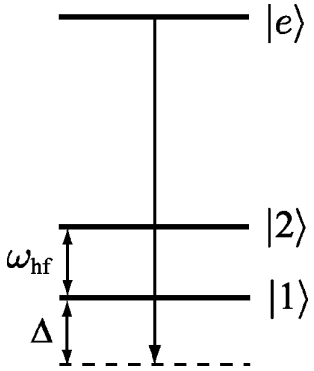

Fig. 51. Level scheme for the measurement of the Loschmidt–echo (taken from [148]). A classical laser drives the transitions $|e\rangle \leftrightarrow |1\rangle$ and $|e\rangle \leftrightarrow |2\rangle$ of a three–level atom with excited electronic state $|e\rangle$ and two hyperfine ground states $|1\rangle$ and $|2\rangle$ which have a level spacing of $\omega_{\rm hf}$. The laser is detuned by Δ from the transition $|e\rangle \leftrightarrow |1\rangle$ and by $\Delta + \omega_{\rm hf}$ from the transition $|e\rangle \leftrightarrow |2\rangle$.

As above for large detuning Δ we can eliminate the excited level and find for the lower hyperfine doublet the Hamiltonian $\hat{H}_{\rm g} = \hat{H}_1|1\rangle\langle 1| + \hat{H}_2|2\rangle\langle 2|$ with

$$\hat{H}_2 = \frac{\hat{p}^2}{2M} + \{\hbar\kappa_2[\sin(2k_{\rm L}x)+1] + \hbar\omega_{\rm hf}\}\;\delta_T(t)\,. \tag{302}$$

Here we analogously defined a second interaction strength

$$\kappa_2 = \frac{\Omega^2}{8(\Delta+\omega_{\rm hf})} = \kappa_1 - d\ , \tag{303}$$

where $d = \kappa_1\omega_{\rm hf}/(\Delta+\omega_{\rm hf})$. We mention that the physical quantity d is then the perturbation strength, which has to be rescaled if results are to be compared *e.g.* with a random matrix model.

The state for the motion of the atom, prepared in a internal superposition of states $|1\rangle$ and $|2\rangle$, propagates in two different potentials described by the Hamiltonians $\hat{H}_1$ and $\hat{H}_2$, Eqs. (301) and (302), respectively. Indeed, this is exactly the situation we need, in order to realize a measurement of the fidelity amplitude.

$$\tilde{f}_N = \langle\psi_0|\,\hat{U}_2^{-N}\,\hat{U}_1^N\,|\psi_0\rangle\ , \tag{304}$$

where $\hat{U}_i$ describes the time evolution with the Hamiltonian $\hat{H}_i$. To achieve this the atomic state must be initially in a superposition of the internal states $|1\rangle$ and $|2\rangle$,

$$|\Psi\rangle = \frac{1}{\sqrt{2}}\big(\,|1\rangle + |2\rangle\,\big)\,|\psi_0\rangle \tag{305}$$

of the composite system of internal and external degrees of freedom. Here $|\psi_0\rangle$ represents the initial state of the center–of–mass motion. The time evolution leads to

$$|\Psi(t=NT)\rangle = \frac{1}{\sqrt{2}}\left[|1\rangle|\psi_N\rangle + |2\rangle|\phi_N\rangle\right]\ . \tag{306}$$

Fidelity can now be extracted by determining the probability $W_N(\theta) \equiv \int dx\,|\langle j(\theta)|\langle x|\,\Psi_N\rangle|^2$ to find the atom in the internal state $|j(\theta)\rangle \equiv \frac{1}{\sqrt{2}}\left[|1\rangle + e^{-i\theta}|2\rangle\right]$. Here we used the position states $|x\rangle$ in order to trace over the external degrees of freedom. We find

$$W_N(\theta) = 1 + {\rm Re}\left[e^{-i\theta}\langle\phi_N|\,\psi_N\,\rangle\right] \tag{307}$$

from which we can finally calculate the real and imaginary part of the fidelity amplitude

$${\rm Re}\tilde{f}_N = W_N(0) - 1 \qquad {\rm Im}\tilde{f}_N = W_N(\pi/2) - 1\ . \tag{308}$$

Due to the constant potential terms in the Hamiltonians $\hat{H}_1$ and $\hat{H}_2$, Eqs. (301) and (302), the measured fidelity amplitude $\tilde{f}_N$ picks up a constant phase factor $\exp[-i(\omega_{\rm hf}-d)N]$. Thus the desired fidelity amplitude as defined in Eq. (4) is related to the measured fidelity amplitude via

$$f_N = e^{i(\omega_{\rm hf}-d)N}\tilde{f}_N\ . \tag{309}$$

For a specific implementation of the above scheme, the authors in [276] propose to use the D2 level of Sodium. More technical details are given in [148]. It is important to note, that we have specifically selected the example of the kicked rotor, because it has recently received attention [276,175] and because of the paradigmatic character it acquired in chaos theory due to many important contributions of Chirikov and others. Yet the original proposal referred to the movement in some trap [33,34] and due to the flexibility that lasers permit, many different Hamiltonians can be studied in this way. Also the perturbation strength can easily be varied.

Similar experiments have been performed [279–281], using certain variants of the idea of Gardiner, Cirac and Zoller, leading to related quantities.

10. Summary

Echo-dynamics and studies about fidelity decay have received considerable additional attention as we were writing this paper, and we apologize, if we missed some recent developments, though we believe that the basic ideas are covered and we are more likely to miss some applications. Echo-dynamics is basically defined by the forward evolution with some unitary dynamics, followed by a backward evolution with a perturbed one. We have focused on Hamiltonian time evolution and based our treatment on the fact that the two-point time correlation function in the interaction picture essentially describes the process, at least for the functions or observables that are usually considered. The most common object of research is fidelity, *i.e.* the autocorrelation function of some initial state under echo dynamics. This quantity is particularly important,

because it is equivalent to the cross correlation function of some initial state evolved with an ideal and a perturbed Hamiltonian, which often serves as a benchmark for the reliability of quantum information processes. The behaviour of other quantities, such as expectation values of operators, purity or S-matrix elements, were also considered. The basis of the entire analysis resides in the observation, that a system is the more stable under perturbations, the shorter the temporal correlations of the perturbation operator in the interaction picture. This leads directly to the relative harmlessness of noisy perturbations, but also to the slightly counterintuitive result that typically a time independent or time periodic perturbation will affect stability more strongly in integrable systems then in chaotic ones. It also leads to a way of stabilizing quantum information processes by introducing chaotic or random elements, or outright engineering rapid decay of the correlations of unavoidable errors by adequate gates.

Most of the standard results are obtained from linear response approximation or in other words from the fist non-vanishing term in a Born expansion. The remarkable fact arises, that in most instances the simple exponentiation of this term gives a result of wide validity, which can be proven in some instances, and in others is confirmed by comparison with numerics. Our treatment considers integrable and chaotic situations, as well as random matrix models for the latter. The concept of integrability and chaos carries over to situations with no classical analogue by considering the behaviour of correlation functions but is supported by spectral statistics.

When surveying experiments, we find that measurements of the fidelity amplitude are possible due to a proposal by Gardiner Cirac and Zoller, which is somewhat dated, but has never been strictly implemented, though related more complicated quantities have been measured. On the other hand, fidelity of S-matrix elements has been tested directly or via Fourier transform of measurements in the energy domain. For chaotic systems scattering fidelity is a good approximation for the standard fidelity, particularly if ensemble averages are taken as was the case in both experiments. Then a good agreement with the results of random matrix theory was observed. The experiments performed show clearly, that effects as observed in the energy domain have no clear signature, thus justifying the general interest in the time domain studies. The experiments are at this point limited to weak and intermediate perturbation strength. The intriguing Lyapunov regime, which shows decay independent of perturbation strength for some time range and sufficiently strong perturbation has not yet been reached, and neither has the revival at Heisenberg time, predicted by exact solutions of the random matrix models. Both experiments will be quite challenging, as they imply measurements of very low fidelities.

While we have concentrated on the correlation function approach, we mention other approaches, that were used to obtain results in different regimes. Vanicek's semi classical approach seems to be the most flexible, as he is also able to obtain essentially all the regimes. Yet we have treated systems such as kicked spin chains that have no known classical analogue and nevertheless can be treated with the correlation function method.

Fidelity decay of mixed systems has been treated on the margin only, as only limited studies exist, and the matter seems in first approximation to result in a separate treatment of integrable and chaotic parts.

For future developments, the evolution of expectation values of relevant operators seems to be a promising field, but also scattering fidelity has at this point only been used where it is equivalent to fidelity in a chaotic system. Perturbations of scattering channels are an interesting alternative. Also the use of quantum freeze of fidelity in information processes presents interesting perspectives.

Acknowledgements

We acknowledge the hospitality of Dr. Brigitte Ibing and of the Centro Internacional de Ciencias, Cuernavaca, which hosted us during a significant part of the effort to write this article. We are grateful to L. Kaplan, H.M. Pastawski, J. H.-J. Stoeckmann and J. Vanicek who sent us many useful comments after reading the manuscript. We also wish to thank G. Benenti, R. Blatt, G. Casati, B. Georgeot, R. Jalabert, H. Haefner, H. Kohler, C. Lewenkopf, F. Leyvraz, C. Pineda, M. Raizen, W. Strunz and G. Veble. Financial support from the Slovenian Research Agency under program P1-0044 and project J1-7437, CONACyT projects # 41000-F and 48937-F as well as UNAM-DAPA project IN-101603F are acknowledged. TG acknowledges

financial support from the EU Human Potential programme No. HPRN-CT-2000-00156 at the initial stage of the work. MŽ acknowledges a fellowship of Alexander von Humboldt Foundation and a hospitality of the Department of Quantum Physics of the University of Ulm.

Appendix A. Time averaged fidelity

In this appendix we discuss and illustrate the time-averaged fidelity for different initial states (eigenstates of H_0, random pure states, or completely mixed states) and in the crossover regime between weak and strong perturbation [46,282].

The point of crossover $\epsilon_{\rm rm}$ from weak (43) to strong (44) perturbation regime is system dependent and can not be discussed in general apart from expecting it to scale with $\hbar$ similarly as a mean level spacing $\epsilon_{\rm rm} \sim \hbar^d$. We will discuss the value of $\bar{F}$ for three different initial states:

(i) First, let us consider the simplest case when the initial state is an *eigenstate* of U_0 say, $\rho = |E_1\rangle\langle E_1|$ with matrix elements $\rho_{lm} = \delta_{l,1}\delta_{m,1}$. For *weak perturbations* this gives (43) $\bar{F}_{\rm weak} = 1$, therefore the fidelity does not decay at all. This result can be generalized to the case when ρ is a superposition or even a mixture of a number of eigenstates, say K of them, all with approximately the same weight, so that one has diagonal density matrix elements of order $\rho_{ll} \sim 1/K$, resulting in $\bar{F}_{\rm weak} \sim 1/K$. On the other hand, for *strong perturbations* $\varepsilon \gg \varepsilon_{\rm rm}$ we get $\bar{F}_{\rm strong} = (4-\beta)/N$ for an initial eigenstate. Here $\beta = 1$ for systems with anti-unitary symmetry where the eigenstates of H_0 can be chosen real and $\beta = 2$ for the case where anti-unitary symmetries are absent. Summarizing, for an initial eigenstate we have time averaged values of fidelity

$$\bar{F}_{\rm weak} = 1, \qquad \bar{F}_{\rm strong} = (4-\beta)/N. \tag{A.1}$$

With this simple result we can easily explain the numerical result of Peres [31] where almost no decay of fidelity was found for a coherent initial state sitting in the center of an elliptic island, thus being a superposition of a very small number of eigenstates (it is almost an eigenstate). The behavior in a generic case may be drastically different as described in the present work.

(ii) Second, consider the case of a *random pure* initial state $|\Psi\rangle = \sum_m c_m |E_m\rangle$, giving $\rho_{ml} = c_m c_l^*$. The coefficients c_m are independent random complex Gaussian variables with variance $1/N$, resulting in averages $\langle|\rho_{lm}|^2\rangle = 1/N^2$ for $m \neq l$ and $\langle\rho_{ll}^2\rangle = 2/N^2$ (average is over Gaussian distribution of c_m). Using this in the expressions for average fidelity (43) and (44) we get

$$\bar{F}_{\rm weak} = 2/N, \qquad \bar{F}_{\rm strong} = 1/N. \tag{A.2}$$

The result for weak perturbations agrees with case (i) where we had $\bar{F}_{\rm weak} \sim 1/K$ if there were K participating eigenvectors.

(iii) Taking a non-pure initial density matrix $\rho = N^{-1}\,\mathbb{1}$, we have

$$\bar{F}_{\rm weak} = 1/N, \qquad \bar{F}_{\rm strong} = (4-\beta)/N^2. \tag{A.3}$$

As expected, the fluctuating plateau is the smallest for maximally mixed states and strong perturbation.

Observe that the average fidelity $\bar{F}$ (42) is of fourth order in matrix elements of O, the same as the inverse participation ratio (IPR) of the perturbed eigenstates. Actually, in the case of initial eigenstate, our case (i), the average fidelity (42) can be rewritten as $\bar{F} = \sum_m |O_{1m}|^4$, which is exactly the IPR. We recall that $O_{mn} = \langle E_m | E_l^\varepsilon \rangle$ is the overlap matrix between perturbed and unperturbed eigenstates. The inverse of the IPR, *i.e.* the participation ratio, is a number between 1 and N which can be thought of as giving the approximate number of unperturbed eigenstates represented in the expansion of a given perturbed eigenstate. For an average over the mixed states, case (iii), we have instead $\bar{F} = \sum_{l,m} |O_{lm}|^4/N^2$, i.e. the average IPR divided by N. The time averaged fidelity is thus directly related to the *localization* properties of eigenstates of U_ε in terms of eigenstates of U_0. Therefore, fidelity will decay only until it reaches the value of finite size fluctuations and will fluctuate around $\bar{F}$ thereafter. The time t_∞ when this happens, $F(t_\infty) = \bar{F}$, depends on the decay of fidelity and is discussed in Section 7.

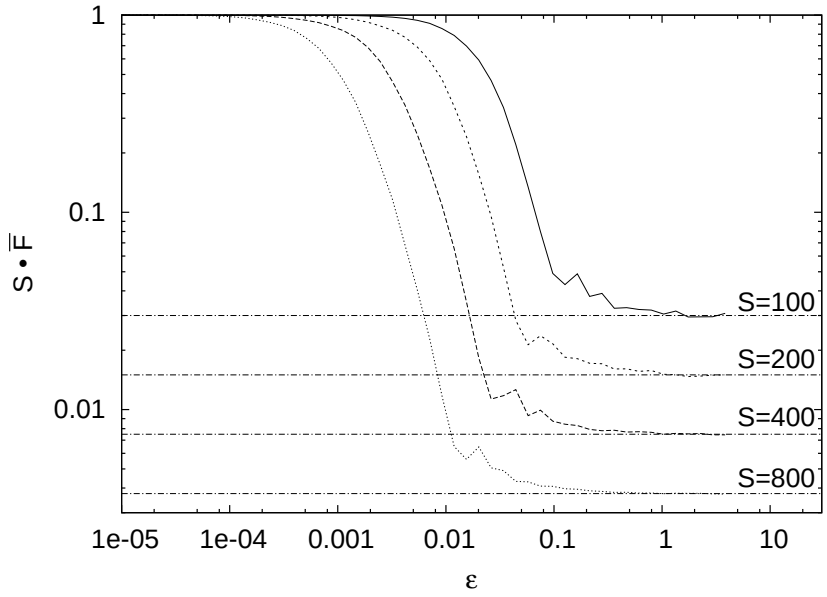

Fig. A.1. Dependence of time averaged fidelity (multiplied by the Hilbert space size $N = S$) $\bar{F}$ on ε is shown for a chaotic kicked top system and Hilbert space average $\rho = \mathbb{1}/N$, i.e. our case (iii). The transition from weak to strong perturbation regime is seen (A.3). Horizontal full lines are the theoretical predictions $\bar{F}_{\rm strong}$ (A.3), while the theoretical result for the weak regime corresponds to 1.

To illustrate the above theory we have calculated the average fidelity (42) for a kicked top with a propagator (B.1). As an initial state we used $\rho = \mathbb{1}/N$, i.e. the case (iii), where the dimension of the Hilbert space is determined by the spin magnitude: $N = S$ (OE subspace). We calculated the dependence of $S\,\bar{F}$ on ε for two cases: a chaotic one for kicked top parameters $\alpha = 30$, $\gamma = \pi/2$ shown in Fig. A.1 and a regular one for $\alpha = 0.1$, $\gamma = \pi/2$ shown in Fig. A.2. In both cases one can see a transition from the weak perturbation regime $\bar{F}_{\rm weak} = 1/N$ to the strong regime $\bar{F}_{\rm strong} = 3/N^2$ for large ε. In the chaotic case the critical $\varepsilon_{\rm rm}$ can be seen to scale as $\varepsilon_{\rm rm} \sim \hbar = 1/S$. In the regular situation, the strong perturbation regime is reached only for a strong perturbation $\varepsilon \sim 4$, where the propagator U_ε itself becomes chaotic. (The transition from the regular to chaotic regime in the kicked top happens at around $\alpha = 3$, see e.g. [31].) Still, if one defines $\varepsilon_{\rm rm}$ as the points where the deviation from the weak regime starts (point of departure from 1 in Fig. A.2) one has scaling $\varepsilon_{\rm rm} \sim 1/S$ also in the regular regime.

Appendix B. Models for numerics

Here we shall give a brief overview of models we used to perform numerical experiments to demonstrate various theoretical results. Except for several occasions, we use kicked systems, for which the Hamiltonian is time periodic, consisting of free time evolution, interrupted periodically by instantaneous "kicks". For such systems, time is a discrete variable, given by the number of kicks. These systems can frequently be simulated much more efficiently, than time-independent systems, if chaoticity is required. Most extensively, we use the kicked top (Section B.1) and the kicked Ising chain (Section B.2). In some occasions, we use the sawtooth map [283] and the famous kicked rotor [284]. In addition to kicked models we also use the Jaynes-Cummings system, well known in quantum optics [285], and a system of coupled anharmonic oscillators. These are the only specific numerical models with a time independent Hamiltonian we are discussing in this review. Jaynes-Cummings model is used only once (Fig. 42), and for further details, we refer the interested reader to Ref. [162], from which Fig. 42 has actually been taken. Anharmonic oscillators are used in Section 5.4 with more details available in the original Ref. [181].

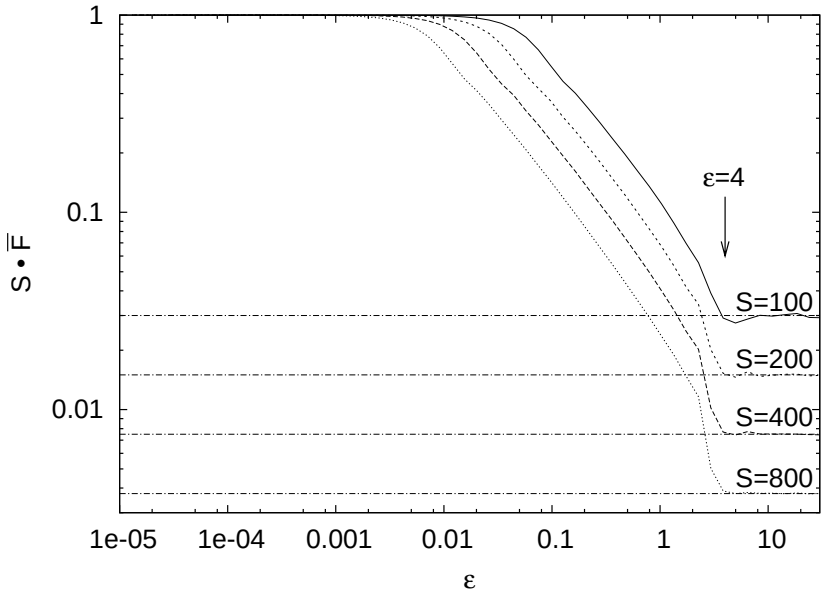

Fig. A.2. The same as Fig. A.1 but for a regular kicked top.

B.1. *The Kicked Top*

The kicked top has been introduced by Haake, Kuś and Scharf [286] and has served as a numerical model in numerous studies ever since [19,287,288,206,207,289]. The kicked top might also be experimentally realizable [290]. We shall use different versions of the kicked top leading to different propagators depending on the phenomenon we want to illustrate. All of them are composed as a product of unitary propagators, each depending on standard spin operators, $S_{\mathrm{x,y,z}}$. The latter fulfill the following commutator relations: $[S_k, S_l] = \mathrm{i}\varepsilon_{klm}\, S_m$ (ε_{klm} is the Levi-Civita symbol). The half-integer (integer) spin S determines the size of the Hilbert space, since $\mathcal{N} = 2S + 1$, and therefore the value of the effective Planck constant $\hbar = 1/S$. The semiclassical limit corresponds to the limit of large spins $S \to \infty$.

Mostly we use the standard kicked top whose one step propagator (Floquet operator) is given by

$$U_\varepsilon = \exp\left(-\mathrm{i}\gamma S_\mathrm{y}\right) \exp\left(-\mathrm{i}(\alpha+\varepsilon)\frac{S_\mathrm{z}^2}{2S}\right). \tag{B.1}$$

Here ε determines the perturbation strength, while the parameters α and γ are two parameters, which allow to change the dynamical properties of the system. The propagator for t steps is simply a power $(U_\varepsilon)^t$. The Hamiltonian which generates U_ε is given by

$$H_\varepsilon = (\alpha+\varepsilon)\frac{1}{2}\left(\frac{S_\mathrm{z}}{S}\right)^2 + \gamma\frac{S_\mathrm{y}}{S}\sum_{k=-\infty}^{\infty}\delta(t-k), \tag{B.2}$$

where the perturbation is

$$V = \frac{1}{2}\left(\frac{S_\mathrm{z}}{S}\right)^2, \tag{B.3}$$

which has the classical limit $V \to v = z^2/2$ (we use lower case letters for corresponding classical observables). In that limit $S \to \infty$, and the area preserving map corresponding to U_ε can be written as a map on the unit sphere. Its explicit form can be obtained from the Heisenberg equations for the spin operators. The angle γ in Eq. (B.1) is usually set to $\pi/2$, whereas we shall either use $\gamma = \pi/2$ or $\gamma = \pi/6$. For these two cases, the decay of the classical correlation function displays two different behaviors, monotonic decay for $\gamma = \pi/6$ and oscillatory decay for $\gamma = \pi/2$, see Fig. 1. In addition, the symmetries are different. For $\gamma = \pi/2$ the propagator U_0 commutes with the operator $\exp\left(-\mathrm{i}\pi S_\mathrm{y}\right)$, which describes a π rotation around the y-axis.

The Hilbert space can be decomposed into three invariant subspaces. Following Peres's book [31] we denote them with $\mathcal{H}_{\rm EE}$, $\mathcal{H}_{\rm OO}$ and $\mathcal{H}_{\rm OE}$, with the basis states

$$\begin{aligned}
&\text{EE}: \ |0\rangle, \{|2m\rangle + |-2m\rangle\}/\sqrt{2} && \mathcal{N}_{\rm EE} = S/2+1 \\
&\text{OO}: \ \{|2m-1\rangle - |-(2m-1)\rangle\}/\sqrt{2} && \mathcal{N}_{\rm OO} = S/2 \\
&\text{OE}: \ \{|2m\rangle - |-2m\rangle\}/\sqrt{2}, \{|2m-1\rangle + |-(2m-1)\rangle\}/\sqrt{2} && \mathcal{N}_{\rm OE} = S,
\end{aligned} \tag{B.4}$$

where we assume S to be even. Here, m runs from 1 to $S/2$ and $|m\rangle$ are standard eigenstates of $S_{\rm z}$. For $\gamma \neq \pi/2$ the subspaces $\mathcal{H}_{\rm EE}$ and $\mathcal{H}_{\rm OO}$ coalesce and we have just two invariant subspaces. Unless stated otherwise, we always work in the subspace $\mathcal{H}_{\rm OE}$. Regardless of the angle γ, the kicked top propagator (B.1) has an anti-unitary symmetry. The parameter α determines the degree of chaoticity of the corresponding classical map. The classical map is mostly regular for small values of α (by regular we mean close to integrable), at $\alpha \sim 3$ (see *e.g.* Ref. [31]) most of the tori disappear while for larger $\alpha > 3$ the system becomes numerically fully chaotic. We use $\gamma = \pi/2$ and $\alpha = 0.1$ to simulate regular dynamics. The small value of α allows to use the integrable dynamics for $\alpha = 0$, to compute $\bar{v}$ in Eq. (176) in an approximate way: $\bar{v} \approx (1-z^2)/4$. To simulate chaotic dynamics, we use $\gamma = \pi/2$ or $\pi/6$ and $\alpha = 30$. For $\gamma = \pi/6$ the integral of the classical correlation function is $\sigma_{\rm cl} = 0.0515$ while it is much smaller, $\sigma_{\rm cl} = 0.00385$, for $\gamma = \pi/2$ due to the oscillating nature of the correlation function.

In Section 5.2.3 we describe fidelity decay averaged over the position of initial coherent states for regular dynamics and a perturbation with non-zero time average. For that purpose we use a different perturbation (as compared to the propagator in Eq. (B.1)):

$$U_\varepsilon = \exp\left(-{\rm i}(\gamma+\varepsilon)S_{\rm y}\right)\exp\left(-{\rm i}\alpha\frac{S_{\rm z}^2}{2S}\right), \tag{B.5}$$

with $\alpha = 0.1$ and $\gamma = \pi/2$ as before.

A third version of the kicked top is used to demonstrate the fidelity freeze. For the chaotic case discussed in Section 3.2 we use the following propagator

$$U_\varepsilon = \exp\left(-{\rm i}\alpha\frac{S_{\rm z}^2}{2S}\right)\exp\left(-{\rm i}\frac{\pi}{2}S_{\rm y}\right)\exp\left(-{\rm i}\varepsilon\frac{S_{\rm x}^2 - S_{\rm z}^2}{2S}\right), \tag{B.6}$$

with $\alpha = 30$. For that perturbation, there is an associated operator W such that V is given as a time-derivative [see Eq. (29)] of

$$W = \frac{1}{2}\left(\frac{S_{\rm z}}{S}\right)^2. \tag{B.7}$$

Note that in contrast to the time-independent case, considered in Section 2, for kicked systems one has [17] $V = W_1 - W_0$, where $W_t = U_0^{-t} W U_0^t$. For the semiclassical calculation of the plateau height the classical limit $w = z^2/2$ is needed. The long time decay beyond t_2, the duration of the freeze, is governed by the operator R (32). In the present case, it is given by

$$R = -\frac{S_{\rm x}S_{\rm y}S_{\rm z} + S_{\rm z}S_{\rm y}S_{\rm x}}{2S^3}. \tag{B.8}$$

The classical correlation integral corresponding to this operator is $\sigma_{\rm R} = 5.1 \cdot 10^{-3}$.

In Section 5.3, fidelity freeze in regular systems is discussed. There, we use the propagator

$$U_\varepsilon = \exp\left(-{\rm i}\alpha\frac{S_{\rm z}^2}{2S}\right)\exp\left(-{\rm i}\varepsilon S_{\rm x}\right), \tag{B.9}$$

with $\alpha = 1.1$. For the calculation of the plateau, one needs to represent the unperturbed system in action angle variables. In a spherical coordinate system,these variables are given by

$$x = \sqrt{1-j^2}\cos\theta, \qquad y = \sqrt{1-j^2}\sin\theta, \qquad z = j. \tag{B.10}$$

The classical limit of the perturbation, expressed in terms of the action j and the angle θ is $v = \sqrt{1-j^2}\cos\theta$, while the classical limit w of the associated operator W reads as

$$w(j,\theta) = \frac{1}{2}\sqrt{1-j^2}\,\frac{\sin(\theta-\omega/2)}{\sin(\omega/2)}, \tag{B.11}$$

where $\omega = \alpha j$ is the frequency of the unperturbed system.

In Section 4.3.4, discussing quantum freeze in RMT, we need a propagator having an anti-unitary or a unitary symmetry, *i.e.*, belonging to COE or CUE class. So far all kicked top models described had an orthogonal symmetry. Specifically, to demonstrate freeze for a perturbation that breaks time-reversal symmetry we used

$$U_\varepsilon^{\mathrm{sym}} = P^{1/2}\exp(-\mathrm{i}\pi S_\mathrm{y}/2.4)P^{1/2}\exp(-\mathrm{i}\varepsilon S_\mathrm{x}), \quad P = \exp\left(-\mathrm{i}\alpha\frac{S_\mathrm{z}^2}{2S} - \mathrm{i}S_\mathrm{z}\right), \tag{B.12}$$

with standard $\alpha = 30$. For $\varepsilon = 0$ the propagator belongs to COE symmetry class while only unitary symmetry remains for nonzero perturbation ε. Symmetrized version of the propagator is chosen (half of twist P before and half after the rotation) in order to have zero time average of the perturbation S_x. In the eigenbasis of unperturbed U_0^{sym} the matrix of S_x is complex antisymmetric. The classical correlation integral of the perturbation is $\sigma_{\mathrm{cl}} = 0.16$. To see the radical difference between the freeze and non-freeze fidelity decay we also show numerics for an unsymmetrized propagator,

$$U_\varepsilon^{\mathrm{nosym}} = P\exp(-\mathrm{i}\pi S_\mathrm{y}/2.4)\exp(-\mathrm{i}\varepsilon S_\mathrm{x}), \tag{B.13}$$

for which the matrix for S_x does not have zeroes on the diagonal in the eigenbasis of U_0^{nosym}. Evolution with $U_\varepsilon^{\mathrm{nosym}}$ will therefore not result in a quantum freeze, whereas for a symmetrized version $U_\varepsilon^{\mathrm{sym}}$ we are going to have freeze.

To show the agreement between RMT for the unitary case and numerics we used the following one step propagator

$$U_\varepsilon = P\exp\left(-\mathrm{i}\frac{\pi}{2.4}S_\mathrm{y}\right)\exp\left(-\mathrm{i}10\frac{S_\mathrm{x}^2}{2S} - \mathrm{i}(1+\varepsilon)S_\mathrm{x}\right), \tag{B.14}$$

with the same P as for the orthogonal case (B.12). In this case the integral of the correlation function is slightly larger, $\sigma_{\mathrm{cl}} = 0.17$. Note that in order to see freeze for this case we have to set the diagonal elements of the perturbation to zero by hand.

B.1.1. *Two coupled kicked tops*

On several occasions we will use a double kicked top. Its propagator is composed of the coupling term and two single kicked top propagators.

To illustrate the dependence of fidelity freeze in chaotic systems (described in Section 3.2) on the number of degrees of freedom we use two coupled kicked tops with the one step propagator

$$U_\varepsilon = \exp(-\mathrm{i}\kappa S_\mathrm{z}^\mathrm{c}S_\mathrm{z}^\mathrm{e})\exp(-\mathrm{i}\pi S_\mathrm{y}^\mathrm{c}/2)\exp(-\mathrm{i}\pi S_\mathrm{y}^\mathrm{e}/2)\exp(-\mathrm{i}\varepsilon VS), \tag{B.15}$$

with a strong coupling $\kappa = 20$ to ensure chaotic dynamics. The perturbation V is chosen similar to that of a single kicked top (B.6) as

$$V = \frac{(S_\mathrm{x}^\mathrm{c})^2 - (S_\mathrm{z}^\mathrm{c})^2 + (S_\mathrm{x}^\mathrm{e})^2 - (S_\mathrm{z}^\mathrm{e})^2}{2S^2}. \tag{B.16}$$

This perturbation can be generated from

$$W = \frac{1}{2}\left(\frac{S_\mathrm{z}^\mathrm{c}}{S}\right)^2 + \frac{1}{2}\left(\frac{S_\mathrm{z}^\mathrm{e}}{S}\right)^2. \tag{B.17}$$

With the superscripts c and e, we denote the Hilbert spaces ("central" system or "environment"), on which the respective operator acts. For numerical simulations we desymmetrized the system. For that purpose, we project the initial state to an invariant subspace of dimension $\mathcal{N} = S(S+1)$ spanned by $\{\mathcal{H}_{\mathrm{OE}} \otimes \mathcal{H}_\mathrm{r}\}_{\mathrm{sym}}$, where $\mathcal{H}_\mathrm{r} = \mathcal{H} \setminus \mathcal{H}_{\mathrm{OE}}$ and $\{\cdot\}_{\mathrm{sym}}$ is a subspace symmetric with respect to the exchange of the two tops. The integral of the classical correlation function corresponding to the operator R is $\sigma_\mathrm{R} = 9.2 \cdot 10^{-3}$.

To study the reduced fidelity and echo purity for regular systems (Section 5.4), we use

$$U_\varepsilon = \exp\left(-\mathrm{i}\gamma_\mathrm{c} S_\mathrm{y}^\mathrm{c}\right)\exp\left(-\mathrm{i}\gamma_\mathrm{e} S_\mathrm{y}^\mathrm{e}\right)\exp\left(-\mathrm{i}\varepsilon (S_\mathrm{z}^\mathrm{c})^2 (S_\mathrm{z}^\mathrm{e})^2/S^3\right), \tag{B.18}$$

where it is important to choose incommensurate parameters, $\gamma_\mathrm{c} = \pi/2.1$ and $\gamma_\mathrm{e} = \pi/\sqrt{7}$ to avoid resonant behavior. Note that here the unperturbed dynamics is uncoupled. Therefore echo purity and purity coincide. For this system, the classical actions are given by the coordinates $y_{\mathrm{c,e}}$, so the classical time averaged perturbation is

$$\bar{v} = \frac{1}{4}(1-j_\mathrm{c}^2)(1-j_\mathrm{e}^2). \tag{B.19}$$

In Sections 7 and 3.3 we use

$$U_\varepsilon = U_\mathrm{c} U_\mathrm{e} \exp\left(-\mathrm{i}(\kappa+\varepsilon) S_\mathrm{z}^\mathrm{c} S_\mathrm{z}^\mathrm{e}/S\right), \tag{B.20}$$

with standard single kicked top propagators

$$U_{\mathrm{c,e}} = \exp\left(-\mathrm{i}\gamma_{\mathrm{c,e}} S_\mathrm{y}^{\mathrm{c,e}}\right)\exp\left(-\mathrm{i}\alpha_{\mathrm{c,e}}\frac{1}{2}\left(\frac{S_\mathrm{z}^{\mathrm{c,e}}}{S}\right)^2\right). \tag{B.21}$$

In Section 7 where we compare timescales of fidelity decay in regular and chaotic system we use $\alpha_{\mathrm{c,e}} = 0$, $\gamma_{\mathrm{c,e}} = \pi/2$ and the coupling $\kappa = 5$ for chaotic and $\kappa = 1$ for regular dynamics. For chaotic dynamics the integral of the correlation function is $\sigma_\mathrm{cl} = 0.058$. On the other hand in Section 3.3 demonstrating purity decay for chaotic dynamics we use $\alpha_{\mathrm{c,e}} = 30$ and $\gamma_{\mathrm{c,e}} = \pi/2.1$ and uncoupled unperturbed system, $\kappa = 0$, giving the integral of the correlation function $\sigma_\mathrm{cl} = 0.056$.

In all single kicked top simulations, the initial state $|\psi(0)\rangle$ used for the computation of fidelity decay, is either a random state with the expansion coefficients $c_m = \langle m|\psi(0)\rangle$ being independent Gaussian complex numbers or a coherent state. For double kicked top the initial coherent states are products of coherent states for each top. A coherent state centered at the position $\mathbf{r}^* = (\sin\vartheta^*\cos\varphi^*, \sin\vartheta^*\sin\varphi^*, \cos\vartheta^*)$ is given by

$$\begin{aligned}|\vartheta^*,\varphi^*\rangle &= \sum_{m=-S}^{S}\binom{2S}{S+m}^{1/2}\cos^{S+m}(\vartheta^*/2)\sin^{S-m}(\vartheta^*/2)\mathrm{e}^{-\mathrm{i}m\varphi^*}|m\rangle \\ &= \frac{\mathrm{e}^{-\mathrm{i}\varphi^* S}}{(1+|\tau|^2)^S}\exp(\tau S_-)|S\rangle, \qquad \tau = \mathrm{e}^{\mathrm{i}\varphi^*}\tan(\vartheta^*/2),\end{aligned} \tag{B.22}$$

with $S_\pm = S_\mathrm{x} \pm \mathrm{i}S_\mathrm{y}$. In the semiclassical limit of large spin S the expansion coefficients of the above state tend to $c_m = \langle m|\vartheta^*,\varphi^*\rangle \asymp \exp\left(-S(m/S - z^*)^2/2(1-z^{*2})\right)\mathrm{e}^{-\mathrm{i}m\varphi^*}$, therefore the squeezing parameter is

$$\Lambda = \frac{1}{\sin^2\vartheta^*}\,. \tag{B.23}$$

Coherent states have a well defined classical limit and this enables us to compare quantum fidelity for coherent initial states with the corresponding classical fidelity. The initial classical phase space density corresponding to a coherent state is [288]

$$\rho_\mathrm{clas}(\vartheta,\varphi) = \sqrt{\frac{2S}{\pi}}\exp\left\{-S[(\vartheta-\vartheta^*)^2 + (\varphi-\varphi^*)^2\sin^2\vartheta]\right\}. \tag{B.24}$$

The above density is square-normalized as $\int \rho_\mathrm{clas}^2 \mathrm{d}\Omega = 1$.

B.2. *The kicked Ising-chain*

As an example of a generic interacting quantum many body model, which may be of some interest also for illustrations relevant for quantum information, we consider the kicked Ising (KI) model [42,49] with the Hamiltonian

$$H_\mathrm{KI}(t) = \sum_{j=0}^{L-1}\left\{J_z\,\sigma_z^j\sigma_z^{j+1} + \delta_p(t)\,(h_x\sigma_x^j + h_z\sigma_z^j)\right\} \tag{B.25}$$

where $\delta_p(t) = \sum_m \delta(t-mp)$ is a periodic train of delta functions with period p. The operators $\sigma_{x,y,z}^j$ are the standard Pauli spin matrices satisfying the canonical commutation relations $[\sigma_\alpha^j, \sigma_\beta^k] = 2\mathrm{i}\,\delta_{jk}\,\epsilon_{\alpha\beta\gamma}\,\sigma_\gamma^j$. The

model represents a chain of L interacting spins 1/2 with periodic boundary conditions $L \equiv 0$, subject to a tilted magnetic field. Integrating over one period p we arrive at the Floquet operator:

$$U = \exp(-\mathrm{i} J_z \sum_j \sigma_z^j \sigma_z^{j+1}) \exp(-\mathrm{i} \sum_j (h_x \sigma_x^j + h_z \sigma_z^j)) \tag{B.26}$$

where we chose units such that $p = \hbar = 1$. The KI model depends on three independent parameters (J_z, h_x, h_z). It is integrable for longitudinal ($h_x = 0$) and transverse ($h_z = 0$) magnetic fields. The KI model is likely to be non-integrable everywhere else. Numerical investigations of the general case of a tilted magnetic field have revealed finite regions of parameter space where the system has an ergodic and mixing behavior, or non-ergodic quasi-integrable behavior, when approaching the thermodynamic limit. For the numerical illustrations of this paper we consider only three typical cases - points on a line in 3d parameter space with fixed parameters $J = 1, h_x = 1.4$ and a varying parameter h_z exhibiting three different types of dynamics [42]: $h_z = 0$ (*integrable*), $h_z = 0.4$ (*intermediate*, *i.e.* non-integrable and non-ergodic), and $h_z = 1.4$ (*ergodic* and *mixing* or simply "chaotic").

The non-trivial integrability of a transverse kicking field, which somehow inherits the solvable dynamics of its well-known autonomous version [291,292], is quite remarkable since it was shown [293] that the Heisenberg dynamics can be calculated explicitly for observables which are bilinear in the Fermi operators $c_j = (\sigma_j^y - i\sigma_j^z) \prod_{j'}^{j'<j} \sigma_{j'}^x$ with time correlations decaying to the non-ergodic stationary values as $\sim t^{-3/2}$ [293].

Appendix C. Scattering fidelity in different approximations

C.1. *Limit of weak coupling, diagonal S-matrix elements*

For non-diagonal S-matrix elements, the weak coupling limit has been treated in Section 2.6.1, with the result, Eq. (63). That was the important case, since it really makes sure that the scattering fidelity $f_{ab}^s(t)$ tends to the standard fidelity of a closed chaotic system.

For $a = b$, however, we find:

$$\begin{aligned}
\langle \hat{S}_{aa}(t)^* \, \hat{S}'_{aa}(t) \rangle &\sim 4\pi^2 \; w_a \, w_b \; \theta(t) \; \mathrm{e}^{-\gamma_W \, t} \left\{ \sum_{j,l} \langle |v_{ja}|^4 \rangle \; O_{jl}^2 \; \mathrm{e}^{2\pi \mathrm{i}(E_j - E'_l)t} + \sum_{j \neq k, l} \langle |v_{ja}|^2 \rangle \; \langle |v_{ka}|^2 \rangle \; O_{kl}^2 \; \mathrm{e}^{2\pi \mathrm{i}(E_j - E'_l)t} \right\} \\
&= 4\pi^2 \; \frac{w_a \, w_b}{N} \; \theta(t) \; \mathrm{e}^{-\gamma_W \, t} \; \frac{1}{N} \sum_j \left\{ \sum_l \mathrm{e}^{2\pi \mathrm{i}(E_j - E'_l)t} \left(3 O_{jl}^2 + \sum_{k \neq j} O_{kl}^2 \right) \right\} \\
&= 4\pi^2 \; \frac{w_a \, w_b}{N} \; \theta(t) \; \mathrm{e}^{-\gamma_W \, t} \; \left\{ 3 \; f(t) + \frac{1}{N} \sum_{jl} \mathrm{e}^{2\pi \mathrm{i}(E_j - E'_l)t} \; \sum_{k \neq j} O_{kl}^2 \right\} \; ,
\end{aligned} \tag{C.1}$$

whereas

$$\langle |\hat{S}_{aa}(t)|^2 \rangle \sim 4\pi^2 \; w_a \, w_b \; \theta(t) \; \mathrm{e}^{-\gamma_W \, t} \left\{ 3 + \frac{1}{N} \sum_j \sum_{l \neq j} \mathrm{e}^{2\pi \mathrm{i}(E_j - E_l)t} \right\} \; . \tag{C.2}$$

While the first term separates again as desired into an auto-correlation part and the fidelity amplitude, the second term, in general, does not. Only in the perturbative regime, where me may assume $O_{kl}^2 = \delta_{kl}$ and treat the perturbed spectrum to first order in λ, we again find the factorization into fidelity amplitude and autocorrelation function.

C.2. *Rescaled Breit-Wigner approximation and the perturbative regime*

For this purpose we refer to the rescaled Breit-Wigner approximation [294], which amounts to a treatment of the anti-Hermitian part in H_{eff} in first order perturbation theory. The main point is that due to the

rescaling this gives useful results even at relatively strong coupling to the continuum. Here, we also treat the perturbation λW in first order perturbation theory. In the eigenbasis of H_0 we have

$$\langle \hat{S}_{ab}(t)^* \, \hat{S}'_{ab}(t) \rangle = 4\pi^2 \theta(t) \sum_{jk} V^*_{ja} \; \mathrm{e}^{2\pi \mathrm{i}(E_j + \mathrm{i}\Gamma_j/2)t} \; V_{jb} \, V^*_{kb} \left(\sum_l O^2_{kl} \; \mathrm{e}^{-2\pi \mathrm{i}(E'_l - \mathrm{i}\Gamma_l/2)t} \right) V_{ka} \; , \tag{C.3}$$

where O is again the orthogonal matrix that transforms the eigenbasis of H'_0 into the eigenbasis of H_0. The numbers Γ_j and Γ'_j denote the diagonal element of the anti-Hermitian part of H_{eff} and H'_{eff} in the respective bases. As we treat λW in first order perturbation theory we have $O^2_{kl} = \delta_{kl}$, $\Gamma'_j = \Gamma_j$, and $E'_l = E_l + \lambda W_{ll}$. Therefore

$$\begin{aligned} \langle \hat{S}_{ab}(t)^* \, \hat{S}'_{ab}(t) \rangle &= 4\pi^2 \theta(t) \sum_{jk} V^*_{ja} \, V_{jb} \, V^*_{kb} \, V_{ka} \; \mathrm{e}^{-\pi(\Gamma_j + \Gamma_k)t} \; \mathrm{e}^{-2\pi \mathrm{i}(E'_k - E_j)t} \\ &= \sum_k \mathrm{e}^{-2\pi \mathrm{i} \lambda \, W_{kk} \, t} \sum_j V^*_{ja} \, V_{jb} \, V^*_{kb} \, V_{ka} \; \mathrm{e}^{-\pi(\Gamma_j + \Gamma_k)t} \; \mathrm{e}^{-2\pi \mathrm{i}(E_k - E_j)t} \; . \end{aligned} \tag{C.4}$$

Under the assumption that W is a random perturbation, uncorrelated with the dynamics of the unperturbed system, we may average over $\exp[2\pi \mathrm{i} \lambda \, W_{kk} \, t]$ independently, which yields the fidelity amplitude $f(t)$. What remains is just the autocorrelation function of the S-matrix element S_{ab} and we find

$$\langle \hat{S}_{ab}(t)^* \, \hat{S}'_{ab}(t) \rangle = f(t) \; \langle |\hat{S}_{aa}(t)|^2 \rangle \; . \tag{C.5}$$

Note that is has not been necessary to actually perform the rescaling (of the Breit-Wigner approximation). It just serves as an argument for the enlarged region of validity of the approximation presented.

C.3. *Rescaled Breit-Wigner approximation and linear response*

Here, we use the rescaled Breit-Wigner approximation to obtain the decaying dynamics for the unperturbed system. We then compute the scattering fidelity in linear response approximation.

$$\begin{aligned} &\hat{S}_{ab}(t)^* \, \hat{S}'_{ab}(t) = 4\pi^2 \; w_a \, w_b \; \theta(t) \; \langle v_b | \, U_0^\dagger \, | v_a \rangle \; \langle v_a | \, U_1 \, | v_b \rangle \\ &U_1 = \mathrm{e}^{-2\pi \mathrm{i} \, H'_{\mathrm{eff}} \, t} \qquad U_0 = \mathrm{e}^{-2\pi \mathrm{i} \, H_{\mathrm{eff}} \, t} = \sum_j |j\rangle \; \mathrm{e}^{-2\pi \mathrm{i}(E_j - \mathrm{i}\Gamma_j/2)t} \; \langle j| \; , \end{aligned} \tag{C.6}$$

Only U_1 depends on the perturbation W (assumed random), so we may write U_1 in linear response approximation and average the result over W:

$$U_1 = U_0 \left\{ \mathbb{1} - 2\pi \mathrm{i} \lambda \int_0^t \mathrm{d}\tau \; \tilde{W}(\tau) - 4\pi^2 \lambda^2 \int_0^t \mathrm{d}\tau \int_0^\tau \mathrm{d}\tau' \; \tilde{W}(\tau) \; \tilde{W}(\tau') \right\} \; , \tag{C.7}$$

where $\tilde{W}(t) = U_0(t)^{-1} \, W \, U_0(t)$. Note that U_0 is not unitary, so that $U_0(t)^{-1} \neq U_0(t)^\dagger$. Averaging over W yields:

$$\overline{U_1} = U_0 \left[\mathbb{1} - 4\pi^2 \lambda^2 \; \mathcal{C}(t) \right] \qquad \mathcal{C}(t) = \int_0^t \mathrm{d}\tau \int_0^\tau \mathrm{d}\tau' \; \mathrm{diag} \left[1 + \textstyle\sum_k \mathrm{e}^{-2\pi \mathrm{i}(E_j - E_k) \, \tau'} \, \mathrm{e}^{\pi(\Gamma_j - \Gamma_k) \, \tau'} \right] \; , \tag{C.8}$$

where we assumed that W is taken from the Gaussian orthogonal ensemble, such that $\langle W_{ij} W_{kl} \rangle = \delta_{ik}\delta_{jl} + \delta_{il}\delta_{kj}$. Apart from the additional factor $\mathrm{e}^{\pi(\Gamma_j - \Gamma_k) \, \tau'}$ we have here precisely the linear response expression of the fidelity amplitude as obtained in [52]. This factor, which depends on the widths of the resonances, tends to smooth out possible level correlations. However, the two dominant features, the quadratic decay for small λ (perturbative regime) and the linear decay for larger λ (Fermi golden rule regime) remain present. In [52], we found that the level correlations have at most a 15% effect on the fidelity decay curve.

Note that both, U_0 and $\overline{U_1}$ are diagonal in the eigenbasis of H_0. Therefore, we obtain for the cross correlation function above:

$$\hat{S}_{ab}(t)^* \, \hat{S}'_{ab}(t) = 4\pi^2 \; w_a \, w_b \; \theta(t) \; \sum_{jk} v^*_{jb} \; \mathrm{e}^{2\pi \mathrm{i}(E_j + \mathrm{i}\Gamma_j/2) \, t} \; v_{ja} \; v^*_{ka} \; \mathrm{e}^{-2\pi \mathrm{i}(E_k - \mathrm{i}\Gamma_k/2) \, t} \; \left[1 - 4\pi^2 \lambda^2 \; \mathcal{C}_k(t) \right] \; v_{kb} \; . \tag{C.9}$$

In the case $a \neq b$ this simplifies to:

$$\hat{S}_{ab}(t)^* \, \hat{S}'_{ab}(t) = 4\pi^2 \, w_a \, w_b \, \theta(t) \, \sum_j |v_{jb}|^2 \, |v_{ja}|^2 \; \mathrm{e}^{-2\pi\Gamma_j \, t} \; \left[1 - 4\pi^2\lambda^2 \, \mathcal{C}_j(t)\right] \tag{C.10}$$

If we neglect the dependence of $\mathcal{C}(t)$ on the resonance widths, we may average independently over the "autocorrelation part" in each term of he sum. In this way, we obtain

$$\langle \hat{S}_{ab}(t)^* \, \hat{S}'_{ab}(t) \rangle = \langle |\hat{S}_{ab}(t)|^2 \rangle \; \Big[1 - 4\pi^2\lambda^2 \; N^{-1} \textstyle\sum_j \mathcal{C}_j(t)\Big] = \langle |\hat{S}_{ab}(t)|^2 \rangle \; f(t) \; , \tag{C.11}$$

i.e. a product of the autocorrelation function and the fidelity amplitude. Note that again it was not necessary to actually perform the rescaling (of the Breit-Wigner approximation).

For the case $a = b$ we obtain an additional term in Eq. (C.10):

$$\begin{aligned} \hat{S}_{aa}(t)^* \, \hat{S}'_{aa}(t) = {} & 4\pi^2 \, w_a^2 \, \theta(t) \, \sum_j |v_{ja}|^4 \; \mathrm{e}^{-2\pi\Gamma_j \, t} \; \left[1 - 4\pi^2\lambda^2 \, \mathcal{C}_j(t)\right] \\ & + 4\pi^2 \, w_a \, w_b \, \theta(t) \, \sum_{j\neq k} |v_{ja}|^2 \, |v_{ka}|^2 \; \mathrm{e}^{-2\pi\mathrm{i}(E_j - E_k)\, t} \; \mathrm{e}^{-\pi(\Gamma_j + \Gamma_k)\, t} \; \left[1 - 4\pi^2\lambda^2 \, \mathcal{C}_k(t)\right] \; . \end{aligned} \tag{C.12}$$

As long as level correlations are not important in the fidelity amplitude $f(t)$, we may average over the autocorrelation part and the fidelity amplitude part independently, and obtain the desired result:

$$\hat{S}_{aa}(t)^* \, \hat{S}'_{aa}(t) = \langle |\hat{S}_{aa}(t)|^2 \rangle \; f(t) \; . \tag{C.13}$$

It will be interesting to investigate situations where the separate averages are still possible, but effects of the width fluctuations on the fidelity amplitude, Eq. (C.8) become noticeable.

Appendix D. Echo purity in RMT: technicalities

In Eq. (167), $\mathbb{1}$, $\tilde{I}$, and $\tilde{J}$ denote operators (matrices) on the Hilbert space $\mathcal{H}$. Note that in general $\tilde{I}$ is hermitian while $\tilde{J}$ is not. Keeping only terms of order up to $(2\pi\varepsilon)^2$, we find

$$\begin{aligned} \varrho^M(t) \otimes \varrho^M(t) = {} & \left[\, (\mathbb{1} - 2\pi\mathrm{i}\varepsilon \; \tilde{I} - (2\pi\varepsilon)^2 \; \tilde{J}) \; \varrho_0 \; (\mathbb{1} + 2\pi\mathrm{i}\varepsilon \; \tilde{I} - (2\pi\varepsilon)^2 \; \tilde{J}^\dagger) \, \right] \; \otimes \; \left[\, \ldots \, \right] + \mathcal{O}(\varepsilon^3) \\ = {} & \varrho_0 \otimes \varrho_0 - 2\pi\mathrm{i}\varepsilon \big[\tilde{I} \, \varrho_0 \otimes \varrho_0 - \varrho_0 \, \tilde{I} \otimes \varrho_0 + \varrho_0 \otimes \tilde{I} \, \varrho_0 - \varrho_0 \otimes \varrho_0 \, \tilde{I} \big] \\ & + (2\pi\varepsilon)^2 \big[\tilde{J} \, \varrho_0 \otimes \varrho_0 + \varrho_0 \, \tilde{J}^\dagger \otimes \varrho_0 + \varrho_0 \otimes \tilde{J} \, \varrho_0 + \varrho_0 \otimes \varrho_0 \, \tilde{J}^\dagger \big] \\ & + (2\pi\varepsilon)^2 \big[\tilde{I} \, \varrho_0 \, \tilde{I} \otimes \varrho_0 - \tilde{I} \, \varrho_0 \otimes \tilde{I} \, \varrho_0 + \tilde{I} \, \varrho_0 \otimes \varrho_0 \, \tilde{I} + \varrho_0 \, \tilde{I} \otimes \tilde{I} \, \varrho_0 - \varrho_0 \, \tilde{I} \otimes \varrho_0 \, \tilde{I} + \varrho_0 \otimes \tilde{I} \, \varrho_0 \, \tilde{I} \big] \\ & + \mathcal{O}(\varepsilon^3) \; , \end{aligned}$$

where ϱ_0 is completely general. If the initial state is separable: $\varrho_0 = \varrho_\mathrm{c} \otimes \varrho_\mathrm{e}$ then it can be shown that the linear terms vanish. If, in addition, the initial state is pure (in the full Hilbert space) than the above expression can be reduced to Eq. (84) in Section 2.6.6. In what follows the linear terms are ignored, because they become zero when averaged over the perturbation V.

The tensor form $p[\,.\,]$ obeys a number of symmetry relations, which may be used to reduce the number of terms in the above expression. By writing this form, given in Eq. (165), explicitely in the product basis of the full Hilbert space $\mathcal{H}$, we find

$$p[A \otimes B] = p[A^\dagger \otimes B^\dagger]^* = p[B \otimes A] = p[B^\dagger \otimes A^\dagger]^* \; . \tag{D.1}$$

Therefore we have

$$\begin{aligned} F_P(t) \approx {} & p[\varrho_0 \otimes \varrho_0] - 2\,(2\pi\varepsilon)^2 \big(\, A_J - A_I \, \big) \\ A_J = {} & 2\,\mathrm{Re}\; p[\tilde{J} \, \varrho_0 \otimes \varrho_0] \\ A_I = {} & p[\tilde{I} \, \varrho_0 \, \tilde{I} \otimes \varrho_0] - \mathrm{Re}\; p[\tilde{I} \, \varrho_0 \otimes \tilde{I} \, \varrho_0] + p[\tilde{I} \, \varrho_0 \otimes \varrho_0 \, \tilde{I}] \; . \end{aligned} \tag{D.2}$$

If the initial state is pure and separable, this expression reduces to the one in Eq. (84) in Section 2.6.6 term by term.

We start by averaging over V. In the case of A_J, this is particularly simple. Let us use Greek letters $\mu, \nu, \ldots$ as indeces which run over the basis states in the full Hilbert space $\mathcal{H}$ (these basis states need not be product states). In view of Eq. (169) and applying the rule $\langle V_{\alpha\beta}\, V_{\gamma\delta}\rangle = \delta_{\alpha\gamma}\delta_{\beta\delta} + \delta_{\alpha\delta}\delta_{\beta\gamma}$ we obtain

$$J_{\mu\nu} = \delta_{\mu\nu}\, C_\mu(t) \qquad C_\mu(t) = \int_0^t \mathrm{d}\tau \int_0^\tau \mathrm{d}\tau' \left(1 + \sum_\xi \mathrm{e}^{-2\pi\mathrm{i}\,(E_\mu - E_\xi)\,(\tau-\tau')} \right) . \tag{D.3}$$

We finally average $\tilde{J}$ over $O \in \mathcal{O}(N)$ the orthogonal group and obtain:

$$\langle \tilde{J} \rangle = \sum_{\mu\nu} |\mu\rangle \sum_\xi O_{\xi\mu}\, C_\xi(t)\, O_{\xi\nu}\, \langle\nu| = \sum_\mu |\mu\rangle \left(\tfrac{1}{N} \textstyle\sum_\xi C_\xi(t) \right) \langle\mu| = \left(\tfrac{1}{N} \textstyle\sum_\xi C_\xi(t) \right)\, \mathbb{1} \,, \tag{D.4}$$

such that

$$A_J = 2\,\mathcal{C}(t)\, p[\varrho_0 \otimes \varrho_0] \qquad \mathcal{C}(t) = \mathrm{Re}\, \frac{1}{N} \sum_\xi C_\xi(t) = \frac{1}{N} \sum_\xi C_\xi(t) \,, \tag{D.5}$$

as this sum is always real. This is precisely the same correlation integral, which appeared in the linear response study of the fidelity amplitude, Section 4.1. As in Eq. (128), we may replace the sum of phases with the spectral form factor. This leads to the expression in squared brackets of Eq. (129) for $\mathcal{C}(t)$. As $I(0) = p[\varrho_0 \otimes \varrho_0]$ factors out from A_J, we find:

$$F_P(t) = I(0)[1 - 4\,(2\pi\varepsilon)^2\, \mathcal{C}(t)\,] + 2\,(2\pi\varepsilon)^2\, A_I \,. \tag{D.6}$$

If we could neglect the term A_I, the echo-purity decay of an initially pure state would be given by the decay of the fourth power of the fidelity amplitude.

For the second part of the echo purity, we have to average the matrix $\tilde{I}\,\varrho_0\,\tilde{I}$, as well as the higher rank tensors: $\tilde{I}\,\varrho_0 \otimes \tilde{I}\,\varrho_0$ and $\tilde{I}\,\varrho_0 \otimes \varrho_0\,\tilde{I}$. The average over V yield

$$I_{\alpha\beta}\, I_{\gamma\delta} = C^+_{\alpha\beta}\, \delta_{\alpha\gamma}\, \delta_{\beta\delta} + C^-_{\alpha\beta}\, \delta_{\alpha\delta}\, \delta_{\beta\gamma} \,) \,, \qquad C^\pm_{\alpha\beta} = \int_0^t \mathrm{d}\tau \int_0^t \mathrm{d}\tau'\ \mathrm{e}^{2\pi\mathrm{i}\,(E_\alpha - E_\beta)\,(\tau \pm \tau')} \,, \tag{D.7}$$

$$\tilde{I}_{\alpha\beta}\, \tilde{I}_{\gamma\delta} = \sum_{\mu\nu\xi\rho} O_{\mu\alpha}\, I_{\mu\nu}\, O_{\nu\beta}\, \ldots\, O_{\xi\gamma}\, I_{\xi\rho}\, O_{\rho\delta} \,. \tag{D.8}$$

Generally, these terms appear within sums which run over all indeces $\alpha, \beta, \gamma, \delta$, and for that case we find

$$\begin{aligned} \sum_{\alpha\beta\gamma\delta} \tilde{I}_{\alpha\beta}\, \tilde{I}_{\gamma\delta}\, X_{\alpha\beta\gamma\delta} &= \sum_{\alpha\beta\gamma\delta} \sum_{\mu\nu} O_{\mu\alpha}\, O_{\nu\beta} \big(C^+_{\mu\nu}\, O_{\mu\gamma}\, O_{\nu\delta} + C^-_{\mu\nu}\, O_{\nu\gamma}\, O_{\mu\delta} \,\big)\, X_{\alpha\beta\gamma\delta} \\ &= A \sum_{\alpha\neq\gamma} X_{\alpha\alpha\gamma\gamma} \;+\; \sum_{\alpha\neq\beta} \big(B\, X_{\alpha\beta\alpha\beta} + C\, X_{\alpha\beta\beta\alpha} \,\big) + D \sum_\alpha X_{\alpha\alpha\alpha\alpha} \\ &= \sum_{\alpha\beta} \big(A\, X_{\alpha\alpha\beta\beta} + B\, X_{\alpha\beta\alpha\beta} + C\, X_{\alpha\beta\beta\alpha} \,\big) + (D - A - B - C) \sum_\alpha X_{\alpha\alpha\alpha\alpha} \,, \end{aligned} \tag{D.9}$$

where X is an arbitrary tensor, and

$$\begin{aligned} A &= \sum_{\mu\nu} \big(C^+_{\mu\nu} + C^-_{\mu\nu} \,\big)\, O_{\mu\alpha}\, O_{\mu\gamma}\, O_{\nu\alpha}\, O_{\nu\gamma} & B &= \sum_{\mu\nu} \big(C^+_{\mu\nu}\, O^2_{\mu\alpha}\, O^2_{\nu\beta} + C^-_{\mu\nu}\, O_{\mu\alpha}\, O_{\mu\beta}\, O_{\nu\alpha}\, O_{\nu\beta} \,\big) \\ D &= \sum_{\mu\nu} \big(C^+_{\mu\nu} + C^-_{\mu\nu} \,\big)\, O^2_{\mu\alpha}\, O^2_{\nu\alpha} & C &= \sum_{\mu\nu} \big(C^+_{\mu\nu}\, O_{\mu\alpha}\, O_{\mu\beta}\, O_{\nu\alpha}\, O_{\nu\beta} + C^-_{\mu\nu}\, O^2_{\mu\alpha}\, O^2_{\nu\beta} \,\big) \,. \end{aligned} \tag{D.10}$$

Distinguishing between the cases $\mu = \nu$ and $\mu \neq \nu$ allows to evaluate the group integrals. In this way, we obtain

$$\begin{aligned} A &= \frac{1}{N+2} \left[2\,t^2 - \frac{1}{N-1} \big(\mathcal{C}_+ + \mathcal{C}_- \,\big) \right] \,, & B &= \frac{1}{N+2} \left[2\,t^2 + \frac{1}{N-1} \big(\,(N+1)\,\mathcal{C}_+ - \mathcal{C}_- \,\big) \right] \,, \\ D &= \frac{1}{N+2} \left[6\,t^2 + \mathcal{C}_+ + \mathcal{C}_- \right] \,, & C &= \frac{1}{N+2} \left[2\,t^2 + \frac{1}{N-1} \big(\,(N+1)\,\mathcal{C}_- - \mathcal{C}_+ \,\big) \right] \,. \end{aligned} \tag{D.11}$$

The new coefficients $\mathcal{C}_\pm$ are related to double integrals over the spectral form factor as follows:

$$\mathcal{C}_\pm = \frac{1}{N}\sum_{\mu\neq\nu} C^\pm_{\mu\nu} \sim -B_\pm(t) + \begin{cases} 0 & : + \text{case} \\ t & : - \text{case} \end{cases}, \qquad B_\pm(t) = \int_0^t \mathrm{d}\tau \int_0^t \mathrm{d}\tau' \, \langle b_2(E,\, \tau \pm \tau')\rangle \, . \tag{D.12}$$

Due to the symmetric sums, the coefficients $\mathcal{C}_\pm$ are strictly real quantities – and so are A, B, C and D. As the two point form factor may depend on the energy range, we include here a global average over the full length of the spectrum.

Due to $D = A + B + C$ we have

$$\sum_{\alpha\beta\gamma\delta} \tilde{I}_{\alpha\beta}\, \tilde{I}_{\gamma\delta}\, X_{\alpha\beta\gamma\delta} = \sum_{\alpha\beta} \big(A\, X_{\alpha\alpha\beta\beta} + B\, X_{\alpha\beta\alpha\beta} + C\, X_{\alpha\beta\beta\alpha} \big) \, . \tag{D.13}$$

Let us start with $\tilde{I}\, \varrho_0\, \tilde{I}$. With the help of Eq. (D.13), we find

$$\begin{aligned} \tilde{I}\, \varrho_0\, \tilde{I} &= \sum_{\alpha\beta\gamma\delta} |\alpha\rangle\, \tilde{I}_{\alpha\beta}\, \varrho^0_{\beta\gamma}\, \tilde{I}_{\gamma\delta}\, \langle\delta| = \sum_{\alpha\beta} \big(A\, |\alpha\rangle\, \varrho^0_{\alpha\beta}\, \langle\beta| + B\, |\alpha\rangle\, \varrho^0_{\beta\alpha}\, \langle\beta| + C\, \langle\alpha|\, \varrho^0_{\beta\beta}\, \langle\alpha| \big) \\ &= A\, \varrho_0 + B\, \varrho_0^T + C\, \mathbb{1} \, . \end{aligned} \tag{D.14}$$

Next we consider

$$\begin{aligned} \tilde{I}\, \varrho_0 \otimes \tilde{I}\, \varrho_0 &= \sum_{\alpha\beta\gamma\delta} \sum_{\varepsilon\xi} |\alpha\rangle\, \tilde{I}_{\alpha\beta}\, \varrho^0_{\beta\varepsilon}\, \langle\varepsilon| \;\otimes\; |\gamma\rangle\, \tilde{I}_{\gamma\delta}\, \varrho^0_{\delta\xi}\, \langle\xi| \\ &= \sum_{\varepsilon\xi} \sum_{\alpha\beta} \big(A\, |\alpha\rangle\, \varrho^0_{\alpha\varepsilon}\, \langle\varepsilon| \;\otimes\; |\beta\rangle\, \varrho^0_{\beta\xi}\, \langle\xi| + B\, |\alpha\rangle\, \varrho^0_{\beta\varepsilon}\, \langle\varepsilon| \;\otimes\; |\alpha\rangle\, \varrho^0_{\beta\xi}\, \langle\xi| \\ &\qquad + C\, |\alpha\rangle\, \varrho^0_{\beta\varepsilon}\, \langle\varepsilon| \;\otimes\; |\beta\rangle\, \varrho^0_{\alpha\xi}\, \langle\xi| \big) \\ &= A\, \varrho_0 \otimes \varrho_0 + \sum_{\alpha\beta} \big(B\, |\alpha\rangle\langle\beta|\, \varrho_0 \;\otimes\; |\alpha\rangle\beta|\, \varrho_0 + C\, |\alpha\rangle\langle\beta|\, \varrho_0 \;\otimes\; |\beta\rangle\langle\alpha|\, \varrho_0 \big) \, . \end{aligned} \tag{D.15}$$

Finally we find

$$\begin{aligned} \tilde{I}\, \varrho_0 \otimes \varrho_0\, \tilde{I} &= \sum_{\alpha\beta\gamma\delta} \sum_{\varepsilon\xi} |\alpha\rangle\, \tilde{I}_{\alpha\beta}\, \varrho^0_{\beta\varepsilon}\, \langle\varepsilon| \;\otimes\; |\xi\rangle\, \varrho^0_{\xi\gamma}\, \tilde{I}_{\gamma\delta}\, \langle\delta| \\ &= \sum_{\varepsilon\xi} \sum_{\alpha\beta} \big(A\, |\alpha\rangle\, \varrho^0_{\alpha\varepsilon}\, \langle\varepsilon| \;\otimes\; |\xi\rangle\, \varrho^0_{\xi\beta}\, \langle\beta| + B\, |\alpha\rangle\, \varrho^0_{\beta\varepsilon}\, \langle\varepsilon| \;\otimes\; |\xi\rangle\, \varrho^0_{\xi\alpha}\, \langle\beta| \\ &\qquad + C\, |\alpha\rangle\, \varrho^0_{\beta\varepsilon}\, \langle\varepsilon| \;\otimes\; |\xi\rangle\, \varrho^0_{\xi\beta}\, \langle\alpha| \big) \\ &= A\, \varrho_0 \otimes \varrho_0 + \sum_{\alpha\beta} \big(B\, |\alpha\rangle\langle\beta|\, \varrho_0 \;\otimes\; \varrho_0\, |\alpha\rangle\langle\beta| + C\, |\alpha\rangle\langle\beta|\, \varrho_0 \;\otimes\; \varrho_0\, |\beta\rangle\langle\alpha| \big) \, . \end{aligned} \tag{D.16}$$

Collecting all terms, we obtain

$$\begin{aligned} A_I &= p[X] \\ X &= A\, \varrho_0 \otimes \varrho_0 + B\, \varrho_0^T \otimes \varrho_0 + C\, \mathbb{1} \otimes \varrho_0 \\ &\qquad - \mathrm{Re}\left[|\alpha\rangle\langle\beta|\, \varrho_0 \otimes \big(B\, |\alpha\rangle\langle\beta|\, \varrho_0 + C\, |\beta\rangle\langle\alpha|\, \varrho_0 \big) \right] \\ &\qquad + |\alpha\rangle\langle\beta|\, \varrho_0 \otimes \big(B\, \varrho_0\, |\alpha\rangle\langle\beta| + C\, \varrho_0\, |\beta\rangle\langle\alpha| \big) \, , \end{aligned} \tag{D.17}$$

where summation over α and β is assumed. There are seven different tensors, appearing in the expression for X. We compute the purity functional for each of them:

$$p[\varrho_0 \otimes \varrho_0] = I(0) \tag{D.18}$$
$$p[\varrho_0^T \otimes \varrho_0] = I'(0) \tag{D.19}$$
$$p[\mathbb{1} \otimes \varrho_0] = n_\mathrm{e} = \dim \mathcal{H}_\mathrm{e} \tag{D.20}$$
$$p\big[\textstyle\sum_{\alpha\beta} |\alpha\rangle\langle\beta| \, \varrho_0 \otimes |\alpha\rangle\langle\beta| \, \varrho_0 \big] = \sum_{\alpha\beta} (\varrho^0_{\alpha\beta})^2 = \mathrm{tr}\big(\varrho_0^T \, \varrho_0 \big) \tag{D.21}$$
$$p\big[\textstyle\sum_{\alpha\beta} |\alpha\rangle\langle\beta| \, \varrho_0 \otimes |\beta\rangle\langle\alpha| \, \varrho_0 \big] = \mathrm{tr}_\mathrm{e}\big[(\mathrm{tr}_\mathrm{c} \, \varrho_0)^2 \big] = p_\mathrm{dual}[\varrho_0 \otimes \varrho_0] = I_\mathrm{dual}(0) \tag{D.22}$$
$$p\big[\textstyle\sum_{\alpha\beta} |\alpha\rangle\langle\beta| \, \varrho_0 \otimes \varrho_0 \, |\alpha\rangle\langle\beta| \big] = \sum_{ij,kl} \langle ij| \, \varrho_0 \, |kl\rangle \, \langle kj| \, \varrho_0 \, |il\rangle = I_2(0) \tag{D.23}$$
$$p\big[\textstyle\sum_{\alpha\beta} |\alpha\rangle\langle\beta| \, \varrho_0 \otimes \varrho_0 \, |\beta\rangle\langle\alpha| \big] = n_\mathrm{c} \, \mathrm{tr} \, \varrho_0^2 \qquad m_\mathrm{c} = \dim \mathcal{H}_\mathrm{c} \; , \tag{D.24}$$

where we have used nothing but the fact that ϱ_0 is a density matrix, *i.e.* $\varrho_0 = \varrho_0^\dagger$ and $\mathrm{tr} \, \varrho_0 = 1$. Latin indices are used to indicate basis states of the factor spaces $\mathcal{H}_\mathrm{c}$ and $\mathcal{H}_\mathrm{e}$. With the help of the symmetry relations of the purity functional, Eq. (D.1), we can show that all quantities except for (D.21) are real. We find that

$$A_I = A \, I(0) + B \, \big[\, I'(0) - \mathrm{Re} \, \mathrm{tr}(\varrho_0^T \, \varrho_0) + I_2(0) \, \big] + C \, \big[\, n_\mathrm{c} + n_\mathrm{e} \, \mathrm{tr} \, \varrho_0^2 + I_\mathrm{dual}(0) \, \big] \; . \tag{D.25}$$

This expression must be invariant under arbitrary unitary transformations in the factor spaces $\mathcal{H}_\mathrm{c}$ and $\mathcal{H}_\mathrm{e}$. Note that $p[\varrho_0 \otimes \varrho_0] = p_\mathrm{dual}[\varrho_0 \otimes \varrho_0]$ only if ϱ_0 is a pure state. Therefore A_I needs not be invariant under exchange of the factor spaces, as long as ϱ_0 is not a pure state.

If ϱ_0 is a pure state, *i.e.* if $\varrho_0 = |\Psi\rangle\langle\Psi|$, some of above quantities simplify, and we obtain

$$A_I = (A - C) \, I(0) + C \, (n_\mathrm{c} + n_\mathrm{e}) + B \, \big[\, I'(0) + I_2(0) - \mathrm{Re} \, \mathrm{tr}(\, \varrho_0^T \, \varrho_0 \,) \, \big] \; . \tag{D.26}$$

Further simplifications rely not so much on the separability of the initial state, but rather on the possibility to choose a product basis, in which the initial state ϱ_0 has real elements. If this is possible, $I'(0) = I_2(0) = I(0)$ and $\mathrm{tr}(\, \varrho_0^T \, \varrho_0 \,) = 1$, such that

$$A_I = (A + 2B - C) \, I(0) + C \, (n_\mathrm{c} + n_\mathrm{e}) - B \; . \tag{D.27}$$

If, finally, the initial state is also separable, we have $I(0) = 1$. Then using $A + B = D - C$, we find:

$$A_I = D + (n_\mathrm{c} + n_\mathrm{e} - 2) \, C \; . \tag{D.28}$$

In the limit of large N, D and some parts of C may be neglected. We then find

$$A_I = \frac{n_\mathrm{c} + n_\mathrm{e} - 2}{N + 2} \, \big(\, 2t^2 + t - B_-(t) \, \big) \; , \qquad B_-(t) = 2 \int_0^t \mathrm{d}\tau \int_0^\tau \mathrm{d}\tau' \, \langle b_2(E, \, \tau) \rangle \; . \tag{D.29}$$

Due to the latter relation, we obtain for the purity echo decay:

$$F_P(t) = 1 - 4\lambda_0^2 \left(1 - \frac{n_\mathrm{c} + n_\mathrm{e} - 2}{N + 2} \right) \left(t^2 + t/2 - \int_0^t \mathrm{d}\tau \int_0^\tau \mathrm{d}\tau' \, \langle b_2(E, \, \tau) \rangle \right) \; . \tag{D.30}$$

This decay is of the same form as the decay of the fourth power of the absolute value of the fidelity amplitude but faster by a factor of $[1 - (n_\mathrm{c} + n_\mathrm{e} - 2)/(N + 2)]$.

D.1. *The decoupled case*

For that case, we work in the eigenbasis of H_0. It might be strictly separable, but another interesting situation would be a weak coupling, treatable by first order perturbation theory and thus breaking the separability of the Hamiltonian without affecting its separable eigenbasis. For echo purity in the linear response approximation, Eq. (D.2) remains valid, but when calculating A_J and A_I we have to replace $\tilde{J}$ and $\tilde{I}$ with their bare counterparts J and I. We find that Eq. (D.6) remains valid (if we may perform an independent spectral average), and that only A_I needs to be modified. Due to the (almost) separable Hamiltonian H_0 it is not realistic to assume that H_0 corresponds to chaotic dynamics. The best we can then

do with RMT, is to assume that H_0 has an uncorrelated Poisson spectrum. In our approach this amounts to setting the spectral two-point form factor to zero. For A_J, this yields:

$$A_J = 2\, I(0)\, (t^2 + t/2)\,. \tag{D.31}$$

In order to compute A_I we use Eq. (D.7), which gives the average of the product of two matrix elements of I and find

$$\sum_{\alpha\beta\gamma\delta} I_{\alpha\beta}\, I_{\gamma\delta}\, X_{\alpha\beta\gamma\delta} = \sum_{\alpha\beta} \big(\, C^+_{\alpha\beta}\, X_{\alpha\beta\alpha\beta} + C^-_{\alpha\beta}\, X_{\alpha\beta\beta\alpha}\,\big)\,. \tag{D.32}$$

This gives

$$\begin{aligned}
I\,\varrho_0\, I &= \sum_{\alpha\beta} \big(\, C^+_{\alpha\beta}\, |\alpha\rangle\, \varrho^0_{\beta\alpha}\, \langle\beta| + C^-_{\alpha\beta}\, |\alpha\rangle\, \varrho^0_{\beta\beta}\, \langle\alpha|\,\big) \\
I\,\varrho_0 \,\otimes\, I\,\varrho_0 &= \sum_{\alpha\beta} \big(\, C^+_{\alpha\beta}\, |\alpha\rangle\langle\beta|\, \varrho_0 \,\otimes\, |\alpha\rangle\langle\beta|\, \varrho_0 + C^-_{\alpha\beta}\, |\alpha\rangle\langle\beta|\, \varrho_0 \,\otimes\, |\beta\rangle\langle\alpha|\, \varrho_0\,\big) \\
I\,\varrho_0 \,\otimes\, \varrho_0\, I &= \sum_{\alpha\beta} \big(\, C^+_{\alpha\beta}\, |\alpha\rangle\langle\beta|\, \varrho_0 \,\otimes\, \varrho_0\, |\alpha\rangle\langle\beta| + C^-_{\alpha\beta}\, |\alpha\rangle\langle\beta|\, \varrho_0 \,\otimes\, \varrho_0\, |\beta\rangle\langle\alpha|\,\big)\,.
\end{aligned} \tag{D.33}$$

Neglecting level correlations in the spectrum of H_0, we may set $C^+_{\alpha\beta} = \delta_{\alpha\beta}\, t^2$ and $C^-_{\alpha\beta} = \delta_{\alpha\beta}\, t^2 + (1-\delta_{\alpha\beta})\, t/N$. Note however, in the case of separable H_0, the matrices $C^+_{\alpha\beta}$ and $C^-_{\alpha\beta}$ are also separable. That might need special treatment. Disregarding this possibility, we find

$$\begin{aligned}
I\,\varrho_0\, I &= \big(\, 2t^2 - \frac{t}{N}\,\big)\, \sum_\alpha |\alpha\rangle\langle\alpha|\, \varrho_0\, |\alpha\rangle\langle\alpha| + \frac{t}{N}\, \mathbb{1} \\
I\,\varrho_0 \,\otimes\, I\,\varrho_0 &= \big(\, 2t^2 - \frac{t}{N}\,\big)\, \sum_\alpha |\alpha\rangle\langle\alpha|\, \varrho_0 \otimes |\alpha\rangle\langle\alpha|\, \varrho_0 + \frac{t}{N}\, \sum_{\alpha\beta} |\alpha\rangle\langle\beta|\, \varrho_0 \otimes |\beta\rangle\langle\alpha|\, \varrho_0 \\
I\,\varrho_0 \,\otimes\, \varrho_0\, I &= \big(\, 2t^2 - \frac{t}{N}\,\big)\, \sum_\alpha |\alpha\rangle\langle\alpha|\, \varrho_0 \otimes \varrho_0\, |\alpha\rangle\langle\alpha| + \frac{t}{N} \sum_{\alpha\beta} |\alpha\rangle\langle\beta|\, \varrho_0 \otimes \varrho_0\, |\beta\rangle\langle\alpha|\,.
\end{aligned} \tag{D.34}$$

Collecting all terms, and applying the purity functional, we get

$$A_I = \big(\, 2t^2 - \frac{t}{N}\,\big)\, \Big[\textstyle\sum_i (\,\mathrm{tr_e}\, \varrho_0\,)^2_{ii} - \sum_\alpha (\varrho_0)^2_{\alpha\alpha} + \sum_{ijk} |\langle ij|\varrho_0|kj\rangle|^2\Big] + \frac{t}{N}\, \big[n_\mathrm{e} - I_\mathrm{dual}(0) + n_\mathrm{c}\ \mathrm{tr}\, \varrho_0^2\big]\ . \tag{D.35}$$

If ϱ_0 is a pure initial state this simplifies to

$$A_I = \big(\, 2t^2 - \frac{t}{N}\,\big)\, \big[\mathrm{Ipr}\big(\,\mathrm{tr_e}\, \varrho_0\,\big) - \mathrm{Ipr}\, \varrho_0 + \mathrm{Ipr}\big(\,\mathrm{tr_c}\, \varrho_0\,\big)\big] + \frac{t}{N}\, \big[n_\mathrm{c} + n_\mathrm{e} - I(0)\big]\ , \tag{D.36}$$

where $\mathrm{Ipr}\, \varrho$ is the sum of the diagonal elements squared of ϱ. As such it is a certain generalization of the inverse participation ratio from pure to mixed states. For the purity, we obtain

$$\begin{aligned}
\langle I(t)\rangle &= 1 - 2\,(2\pi\varepsilon)^2\, \big[\, A_J - A_I\,\big] \\
&= 1 - 4\,(2\pi\varepsilon)^2\, \left\{ t^2\, \big[\, I(0) - \mathrm{Ipr}_2\, \varrho_0\,\big] + \frac{t}{2}\, \big[\, 1 - \frac{n_\mathrm{c} + n_\mathrm{e} - I(0) - \mathrm{Ipr}_2\, \varrho_0}{N}\big]\right\} + \mathcal{O}(\varepsilon^4)\,,
\end{aligned} \tag{D.37}$$

where $\mathrm{Ipr}_2\, \varrho = \mathrm{Ipr}(\,\mathrm{tr_e}\, \varrho\,) + \mathrm{Ipr}(\,\mathrm{tr_e}\, \varrho\,) - \mathrm{Ipr}\, \varrho$. If the initial state is a basis state of the product basis, this gives

$$I(t) = 1 - 4\,(2\pi\varepsilon)^2\, \frac{t}{2} \left(1 - \frac{n_\mathrm{c} + n_\mathrm{e} - 2}{N}\right) + \mathcal{O}(\varepsilon^4)\,. \tag{D.38}$$

If the initial state is a product state of two random states in $\mathcal{H}_c$ and $\mathcal{H}_e$, we find:

$$I(t) = 1 - 4\,(2\pi\varepsilon)^2 \left\{ t^2\, \big[\, 1 - \mathrm{Ipr}_2\, \varrho_0\,\big] + \frac{t}{2}\, \big[\, 1 - \frac{n_\mathrm{c} + n_\mathrm{e} - 1 - \mathrm{Ipr}_2\, \varrho_0}{N}\,\big]\right\} + \mathcal{O}(\varepsilon^4)\,, \tag{D.39}$$

where $\mathrm{Ipr}_2\, \varrho_0 = 3/(n_\mathrm{c}+2) + 3/(n_\mathrm{e}+2) - 9/((n_\mathrm{c}+2)(n_\mathrm{e}+2))$.

Appendix E. Higher order terms in the Born series

We will calculate averages of products of real symmetric matrices with zero diagonal and imaginary antisymmetric matrices with Gaussian independently distributed off-diagonal elements. Both ensembles have been used in the RMT formulation of the fidelity freeze in Section 4.3.

Nonzero matrix elements of the perturbation V are independent random numbers with Gaussian distribution, zero mean, and second moments equal to

$$\langle V_{ij}V_{kl}\rangle = \frac{1}{N}\begin{cases}\delta_{il}\delta_{jk}+\delta_{ik}\delta_{jl}-2\delta_{ij}\delta_{ik}\delta_{il} & ;\text{symmetric},\\ \delta_{il}\delta_{jk}-\delta_{ik}\delta_{jl} & ;\text{antisymmetric},\end{cases} \tag{E.1}$$

for the two cases considered. Equivalently, for $i\neq k$ the last equation can be stated as

$$\langle V_{ij}V_{ji}\rangle = \frac{1}{N}, \qquad \langle V_{ij}V_{ij}\rangle = \frac{1}{N}\begin{cases}1 & ;\text{symmetric},\\ -1 & ;\text{antisymmetric}.\end{cases} \tag{E.2}$$

The bracket $\langle\bullet\rangle$ denotes an average over a Gaussian distribution of matrix elements.

Using the Born expansion of the echo operator (11) the fidelity amplitude is expressed as a sum of integrals of m-time correlation functions, *i.e.*, terms of the form

$$\frac{1}{N}\operatorname{tr}\tilde{V}(t_1)\cdots\tilde{V}(t_m), \tag{E.3}$$

where we use a trace for the initial state average. What we would like to do is to get an estimate for the difference between both ensembles for the above average (E.3). Using the eigenbasis of the unperturbed evolution $U_0(t)$ and averaging over the ensemble of V's, the above correlation function is

$$\frac{1}{N}\langle V_{jk}V_{kl}\cdots V_{rj}\rangle\exp\{\mathrm{i}(E_j-E_k)t_1/\hbar+\cdots\}, \tag{E.4}$$

where a summation over indices $j,k,\ldots,r$ is implied and we did not write in full the exponential factor involving eigenvalues of U_0, as it is unimportant in the present context.

As far as the second order correlation function is concerned, we have already seen that it is the same for real symmetric and for complex antisymmetric ensembles. We shall show that the same holds also for the 4th order term. Forgetting about the exponential phase term, we would like to calculate

$$\langle V_{ik}V_{kl}V_{lp}V_{pi}\rangle. \tag{E.5}$$

Note that no summation is implied here. We use Wick contraction, giving three contribution,

$$\overbrace{V_{ik}V_{kl}}\overbrace{V_{lp}V_{pi}}, \qquad \overbrace{V_{ik}\overbrace{V_{kl}V_{lp}}V_{pi}}, \qquad \overbrace{V_{ik}\overbrace{V_{kl}}V_{lp}}^{}V_{pi}, \tag{E.6}$$

denoted terms (i), (ii) and (iii), respectively. By renaming indices as $i\to k$, $k\to l$, $l\to p$ and $p\to i$, we see that terms (iii) and (i) are equal. We are mainly interested whether there is a difference between the symmetric and the antisymmetric case. From Eq. (E.2) we see, that the difference could come only from the terms of form $\langle V_{ij}V_{ij}\rangle$, differing in sign between the two ensembles. Let us look if there are any such terms present in (i) or (ii) (E.6). In term (i) the presence of such contraction would immediately mean that we have also diagonal element, e.g. V_{ii}, which though are zero by construction for our perturbations. Similarly, in term (ii) we see that the nonzero term is $\langle V_{ij}V_{ij}\rangle\langle V_{ji}V_{ji}\rangle$. For the antisymmetric case the minus sign occurs twice. Thus the average is the same for both ensembles. Altogether there are no terms involving one minus sign, *i.e.* of the form $\langle V_{ij}V_{ij}\rangle\langle V_{kl}V_{lk}\rangle$, and therefore the 4th order average is the same for both ensembles. For the 4th order term (E.5) one can actually relatively quickly explicitly calculate the average by using (E.1). The result is

$$\begin{aligned}(\delta_{il}-\delta_{il}\delta_{ip}-\delta_{il}\delta_{ik}+\delta_{ik}\delta_{il}\delta_{ip})/N^2 \qquad &;\text{term (i)},\\ (\delta_{il}\delta_{kp}-\delta_{ik}\delta_{il}\delta_{ip})/N^2 \qquad &;\text{term (ii)},\end{aligned} \tag{E.7}$$

regardless of the ensemble.

For the higher order terms we suspect, that the two ensembles differ in terms of order $1/N$, because such is the case for $\operatorname{tr}V^6$.

References

[1] L. Boltzmann, Weitere Studien über das Wärmegleichgewicht unter Gasmolekülen, Sitzungsberichte der Akademie der Wissenschaften, Wien, II 66 (1872) 275–370, [for an English translation see [2]].

[2] S. Brush, Kinetic Theory, Vol. 2, Irreversible processes, Pergamon Press, Oxford, 1966.

[3] J. Loschmidt, Über den Zustand des Wärmegleichgewichtes eines Systems von Körpern mit Rücksicht auf die Schwerkraft, Sitzungsberichte der Akademie der Wissenschaften, Wien, II 73 (1876) 128–142.

[4] L. Boltzmann, Über die Beziehung eines allgemeine mechanischen Satzes zum zweiten Hauptsatze der Warmetheorie, Sitzungsberichte der Akademie der Wissenschaften, Wien, II 75 (1877) 67–73, [for an English translation see [2]].

[5] C. Cercignani, Ludwig Boltzmann: The Man Who Trusted Atoms, Oxford University Press, Oxford, 1998.

[6] W. Thompson, The kinetic theory of the dissipation of energy, Proceedings of the Royal Society of Edinburgh 8 (1874) 325–334, [reprinted in [2]].

[7] R. Jalabert, H. Pastawski, Environment-independent decoherence rate in classically chaotic systems, Phys. Rev. Lett. 86 (2001) 2490.

[8] E. Hahn, Spin echoes, Phys. Rev. 80 (1950) 580–594.

[9] W. Rhim, A. Pines, J. Waugh, Violation of the spin-temperature hypothesis, Phys. Rev. Lett. 25 (1970) 218–220.

[10] S. Zhang, B. Meier, R. Ernst, Polarization echoes in NMR, Phys. Rev. Lett 69 (1992) 2149–2151.

[11] P. Levstein, G. Usaj, H. Pastawski, Attenuation of polarization echoes in nuclear magnetic resonance: A study of the emergence of dynamical irreversibility in many-body quantum systems, J. Chem. Phys. 108 (1998) 2718–2724.

[12] A. Grêt, R. Snieder, Monitoring rapid temporal change in a volcano with coda wave interferometry, Geophys. Res. Lett. 32 (2005) L06304:1–4.

[13] M. Nielsen, I. Chuang, Quantum Computation and Quantum Information, Cambridge University Press, Cambridge, 2001.

[14] L. Viola, E. Knill, S. Lloyd, Dynamical decoupling of open quantum systems, Phys. Rev. Lett. 82 (1999) 2417.

[15] L. Viola, E. Knill, Random decoupling schemes for quantum dynamical control and error suppression, Phys. Rev. Lett. 94 (2005) 060502.

[16] T. Prosen, M. Žnidarič, Quantum freeze of fidelity decay for a class of integrable dynamics, New J. Phys. 5 (2003) 109.

[17] T. Prosen, M. Žnidarič, Quantum freeze of fidelity decay for chaotic dynamics, Phys. Rev. Lett. 94 (2005) 044101.

[18] T. Gorin, H. Kohler, T. Prosen, T. H. Seligman, H.-J. Stöckmann, M. Žnidarič, Anomalous slow fidelity decay for symmetry breaking perturbations, Phys. Rev. Lett. 96 (2006) 244105.

[19] F. Haake, Quantum Signatures of Chaos, Springer Verlag, Berlin, 1991, [2nd enlarged Edition 2000].

[20] H. Stöckmann, Quantum chaos: an introduction, Cambridge University Press, Cambridge, 1999.

[21] D. Shepelyansky, Some statistical properties of simple classically stochastic quantum systems, Physica D 8 (1983) 208–222.

[22] G. Casati, B. Chirikov, I. Guarneri, D. Shepelyansky, Dynamical stability of quantum "chaotic" motion in a hydrogen atom, Phys. Rev. Lett. 56 (1986) 2437–2440.

[23] S. Fishman, D. Grempel, R. Prange, Chaos, quantum recurrences, and Anderson localization, Phys. Rev. Lett. 49 (1982) 509–512.

[24] D. Grempel, R. Prange, S. Fishman, Quantum dynamics of a nonintegrable system, Phys. Rev. A 29 (1984) 1639–1647.

[25] L. Benet, T. H. Seligman, H. A. Weidenmüller, Quantum signatures of classical chaos: sensitivity of wave functions to perturbations, Phys. Rev. Lett. 71 (4) (1993) 529–532.

[26] D. Cohen, Chaos and energy spreading for time-dependent hamiltonians, and the various regimes in the theory of quantum dissipation, Ann. Phys. (NY) 283 (2000) 175–231.

[27] E. Heller, Wave packet dynamics and quantum chaology, in: A. Voros, J. Zinn-Justin, M. Giannoni (Eds.), Chaos and Quantum Physics, Proc. Les Houches Summer School, Session LII 1989, North-Holland, Amsterdam, 1991.

[28] D. Cohen, F. Izrailev, T. Kottos, Wave packet dynamics in energy space, random matrix theory, and the quantum-classical correspondence, Phys. Rev. Lett. 84 (2000) 2052.

[29] L. Kaplan, Quantization ambiguity, ergodicity and semiclassics, New J. Phys. 4 (2002) 90.

[30] A. Peres, Stability of quantum motion in chaotic and regular systems, Phys. Rev. A 30 (1984) 1610–1615, [see also book [31]].

[31] A. Peres, Quantum Theory: Concepts and methods, Kluwer, Dordrecht, 1995.

[32] L. Ballentine, J. Zibin, Classical state sensitivity from quantum mechanics, Phys. Rev. A 54 (1996) 3813–3819.

[33] S. A. Gardiner, J. I. Cirac, P. Zoller, Quantum chaos in an ion trap: The delta-kicked harmonic oscillator, Phys. Rev. Lett. 79 (24) (1997) 4790–4793.

[34] S. Gardiner, I. Cirac, P. Zoller, Erratum: Quantum chaos in an ion trap: The delta-kicked harmonic oscillator, Phys. Rev. Lett. 80 (1998) 2968.

[35] R. Schack, C. Caves, Information and entropy in the baker's map, Phys. Rev. Lett. 69 (1992) 3413.

[36] R. Schack, C. Caves, Hypersensitivity to perturbations in the quantum baker's map, Phys. Rev. Lett. 71 (1993) 525.

[37] R. Schack, C. Caves, Information-theoretic characterization of quantum chaos, Phys. Rev. E 53 (1996) 3257–3270.

[38] H. Pastawski, P. Levstein, G. Usaj, Quantum dynamical echoes in the spin diffusion in mesoscopic systems, Phys. Rev. Lett. 75 (1995) 4310–4313.

[39] G. Usaj, H. Pastawski, P. Levstein, Gaussian to exponential crossover in the attenuation of polarization echoes in NMR, Mol. Phys. 95 (1998) 1229.

[40] H. Pastawski, P. Levstein, G. Usaj, J. Raya, J. Hirschinger, A nuclear magnetic resonance answer to the Boltzmann-Loschmidt controversy?, Physica A 283 (2000) 166–170.

[41] F. Cucchietti, H. Pastawski, D. Wisniacki, Decoherence as decay of the Loschmidt echo in a Lorentz gas, Phys. Rev. E 65 (2002) 045206(R).

[42] T. Prosen, General relation between quantum ergodicity and fidelity of quantum dynamics, Phys. Rev. E 65 (2002) 036208.

[43] T. Prosen, M. Žnidarič, Can quantum chaos enhance the stability of quantum computation?, J. Phys. A 34 (2001) L681–L687.

[44] P. Jacquod, P. Silvestrov, C. Beenakker, Golden rule decay versus Lyapunov decay of the quantum Loschmidt echo, Phys. Rev. E 64 (2001) 055203(R).

[45] N. Cerruti, S. Tomsovic, Sensitivity of wave field evolution and manifold stability in chaotic systems, Phys. Rev. Lett. 88 (2002) 054103.

[46] T. Prosen, M. Žnidarič, Stability of quantum motion and correlation decay, J. Phys. A 35 (2002) 1455–1481.

[47] Z. Karkuszewski, C. Jarzynski, W. Zurek, Quantum chaotic environments, the butterfly effect, and decoherence, Phys. Rev. Lett. 89 (2002) 170405.

[48] T. Gorin, T. Prosen, T. H. Seligman, W. T. Strunz, Connection between decoherence and fidelity decay in echo dynamics, Phys. Rev. A 70 (2004) 042105:1–5.

[49] T. Prosen, T. Seligman, Decoherence of spin echoes, J. Phys. A 35 (2002) 4707–4727.

[50] M. Žnidarič, T. Prosen, Fidelity and purity decay in weakly coupled composite systems, J. Phys. A 36 (2003) 2463–2481.

[51] T. Prosen, T. Seligman, M. Žnidarič, Estimation of purity in terms of correlation functions, Phys. Rev. A 67 (2003) 062108.

[52] T. Gorin, T. Prosen, T. H. Seligman, A random matrix formulation of fidelity decay, New J. Phys. 6 (2004) 20:1–29.

[53] N. Cerruti, S. Tomsovic, A uniform approximation for the fidelity in chaotic systems, J. Phys. A 36 (2003) 3451–3465.

[54] N. Cerruti, S. Tomsovic, *Corrigendum:* A uniform approximation for the fidelity in chaotic systems, J. Phys. A 36 (2003) 11915–11916.

[55] H.-J. Stöckmann, R. Schäfer, Fidelity recovery in chaotic systems and the Debye-Waller factor, Phys. Rev. Lett. 94 (2005) 244101:1–4.

[56] H.-J. Stöckmann, R. Schäfer, Recovery of the fidelity amplitude for the gaussian ensembles, New J. Phys. 6 (2004) 199:1–18.

[57] J. Vaníček, Dephasing representation: Employing the shadowing theorem to calculate quantum correlation functions, Phys. Rev. E 70 (2004) 055201(R).

[58] J. Vaníček, Dephasing representation of quantum fidelity for general pure and mixed states, Phys. Rev. E 73 (2006) 046204.

[59] G. Benenti, G. Casati, Quantum-classical correspondence in perturbed chaotic systems, Phys. Rev. E 65 (2002) 066205.

[60] B. Eckhardt, Echoes in classical dynamical systems, J. Phys. A 36 (2003) 371–380.

[61] G. Benenti, G. Casati, G. Veble, Stability of classical chaotic motion under a system's perturbations, Phys. Rev. E 67 (2003) 055202(R).

[62] G. Veble, T. Prosen, Faster than Lyapunov decays of the classical Loschmidt echo, Phys. Rev. Lett. 92 (2004) 034101.

[63] G. Benenti, G. Casati, G. Veble, Decay of the classical Loschmidt echo in integrable systems, Phys. Rev. E 68 (2003) 036212.

[64] S. Montangero, A. Romito, G. Benenti, R. Fazio, Chaotic dynamics in superconducting nanocircuits, Europhys. Lett. 71 (2005) 893.

[65] V. Sokolov, G. Benenti, G. Casati, Quantum dephasing and decay of classical correlation functions in chaotic systems, preprint quant-ph/0504141 (2005).

[66] B. Misra, E. Sudarshan, The Zeno's paradox in quantum theory, J. Math. Phys. 18 (1977) 756–763.

[67] A. Peres, Zeno paradox in quantum theory, Am. J. Phys. 48 (1980) 913.

[68] O. I. Lobkis, R. L. Weaver, Coda-wave interferometry in finite solids: recovery of p-to-s conversion rates in an elastodynamic billiard, Phys. Rev. Lett. 90 (2003) 254302:1–4.

[69] R. Schäfer, T. Gorin, H.-J. Stöckmann, T. H. Seligman, Fidelity amplitude of the scattering matrix in microwave cavities, New J. Phys. 7 (2005) 152:1–14.

[70] R. Schäfer, H.-J. Stöckmann, T. Gorin, T. H. Seligman, Experimental verification of fidelity decay: from perturbative to Fermi golden rule regime, Phys. Rev. Lett. 95 (2005) 184102:1–4.

[71] W. Magnus, Commun. Pure Appl. Math. 7 (1954) 649.

[72] T. Prosen, T. Seligman, M. Žnidarič, Theory of quantum Loschmidt echoes, Prog. Theor. Phys. Suppl. 150 (2003) 200–228.

[73] P. Silvestrov, J. Tworzydło, C. Beenakker, Hypersensitivity to perturbations of quantum-chaotic wave-packet dynamics, Phys. Rev. E 67 (2003) 025204(R).

[74] W. Wang, B. Li, Crossover of quantum Loschmidt echo from golden-rule decay to perturbation-independent decay, Phys. Rev. E 66 (2002) 056208.

[75] C. Petitjean, P. Jacquod, Mesoscopic fluctuations of the loschmidt echo, Phys. Rev. E 71 (2005) 036223.

[76] L. Mandelstam, I. Tamm, The uncertainty relation between energy and time in nonrelativistic quantum mechanics, J. Phys. (USSR) 9 (1945) 245–254.

[77] G. Fleming, A unitary bound on the evolution of nonstationary states, Nuovo Cimento A 16 (1973) 232.

[78] J. Uffink, The rate of evolution of a quantum state, Am. J. Phys. 61 (1993) 935–936.

[79] L. Kaplan, Multiplicative semiclassical dynamics and the quantization time, Phys. Rev. E 58 (1998) 2383–2991.

[80] L. Kaplan, Semiclassical accuracy in phase space for regular and chaotic dynamics, Phys. Rev. E 70 (2003) 026223.

[81] L. Kaplan, Brownian motion model of quantization ambiguity and universality in chaotic systems, Phys. Rev. E 72 (2005) 036214.

[82] E. Bogomolny, Semiclassical quantization of multidimensional systems, Nonlinearity 5 (1992) 805–866.

[83] T. Gorin, T. H. Seligman, R. L. Weaver, Scattering fidelity in elastodynamics, Phys. Rev. E 73 (2006) 015202(R).

[84] J. R. Taylor, The quantum theory of nonrelativistiv collisions, Krieger, Malabar, 1972.

[85] C. Mahaux, H. A. Weidenmüller, Shell-Model Approach to Nuclear Reactions, North-Holland Publishing Company, 1969.

[86] T. Guhr, H. Weidenmüller, A. Müller-Groeling, Random-matrix theories in quantum physics: common concepts, Phys. Rep. 299 (1998) 189–425.

[87] R. Schäfer, T. Gorin, T. H. Seligman, H.-J. Stöckmann, Correlation functions of scattering matrix elements in microwave cavities with strong absorption, J. Phys. A: Math. Gen. 36 (2003) 3289–3302.

[88] C. A. Engelbrecht, H. A. Weidenmüller, Hauser-Feshbach theory and Ericson fluctuations in the presence of direct reactions, Phys. Rev. C 8 (3) (1973) 859–862.

[89] A. Uhlmann, The "transition probability" in the state space of a^*-algebra, Rep. Math. Phys. 9 (1976) 273–279.

[90] R. Jozsa, Fidelity for mixed quantum states, J. Mod. Opt. 41 (12) (1994) 2315–2323.

[91] W. Zurek, Decoherence and the transition from quantum to classical, Phys. Today 44 (10) (1991) 36–44.

[92] H. Araki, E. Lieb, Entropy inequalities, Commun. Math. Phys. 18 (1970) 160–170.

[93] O. Kübler, D. Zeh, Dynamics of quantum correlations, Ann. Phys. (N.Y.) 76 (1973) 405–418.

[94] J. Kim, M. Nemes, A. de Toledo Piza, H. Borges, Perturbative expansion for coherence loss, Phys. Rev. Lett. 77 (1996) 207.

[95] G. Berman, G. Zaslavsky, Condition of stochasticity in quantum nonlinear systems, Physica A 91 (1978) 450–460.

[96] V. Arnold, A. Avez, Ergodic problems of classical mechanics, Benjamin, New York, 1968.

[97] M. Feingold, A. Peres, Distribution of matrix elements of chaotic systems, Phys. Rev. A 34 (1986) 591–595.

[98] M. Wilkinson, A semiclassical sum-rule for matrix elements of classically chaotic systems, J. Phys. A 20 (1987) 2415–2423.

[99] M. Feingold, D. Leitner, O. Piro, Semiclassical structure of hamiltonians, Phys. Rev. A 39 (1989) 6507–6514.

[100] T. Prosen, M. Robnik, Distribution and fluctuation properties of transition probabilities in a system between integrability and chaos, J. Phys. A 26 (1993) L319–L326.

[101] T. Prosen, Statistical properties of matrix elements in a Hamilton system between integrability and chaos, Ann. Phys. 235 (1994) 115–164.

[102] D. Bevilaqua, E. Heller, Fidelity decay for phase space displacements, preprint nlin.CD/0409007 (2004).

[103] A. Tanaka, H. Fujisaki, T. Miyadera, Saturation of the production of quantum entanglement between weakly coupled mapping systems in a strongly chaotic region, Phys. Rev. E 66 (2002) 045201(R).

[104] H. Fujisaki, T. Miyadera, A. Tanaka, Dynamical aspects of quantum entanglement for weakly coupled kicked tops, Phys. Rev. E 67 (2003) 066201.

[105] W. Wang, G. Casati, B. Li, Stability of quantum motion: Beyond Fermi-golden-rule and Lyapunov decay, Phys. Rev. E 69 (2004) 025201(R).

[106] A. Scott, C. Caves, Entangling power of the quantum baker's map, J. Phys. A 36 (2003) 9553.

[107] S. Ghose, B. Sanders, Entanglement dynamics in chaotic systems, Phys. Rev. A 70 (2004) 062315.

[108] J. Bandyopadhyay, A. Lakshminarayan, Testing statistical bounds on entanglement using quantum chaos, Phys. Rev. Lett. 89 (2002) 060402.

[109] J. Bandyopadhyay, A. Lakshminarayan, Entanglement production in coupled chaotic systems: Case of the kicked tops, Phys. Rev. E 69 (2004) 016201.

[110] C. Pineda, T. Seligman, Evolution of pairwise entanglement in a coupled n-body system, Phys. Rev. A 73 (2006) 012305.

[111] C. Pineda, T. H. Seligman, A Bell pair in a generic random matrix environment, preprint quant-ph/0605169 (2006).

[112] T. Gorin, S. Mossmann, C. Pineda, T. H. Seligman, in preparation (2006).

[113] F. Izrailev, A. Castañeda-Mendoza, Entropy production and fidelity for quantum many-body systems with noise, Vol. 5472 of Proc. of SPIE : The International Society for Optical Engineering, 2004, pp. 252–265, also preprint `quant-ph/0403097`.

[114] X. Wang, S. Ghose, B. Sanders, B. Hu, Entanglement as a signature of quantum chaos, Phys. Rev. E 70 (2004) 016217.

[115] F. Cucchietti, D. Dalvit, J. Paz, W. Zurek, Decoherence and the Loschmidt echo, Phys. Rev. Lett. 91 (2003) 210403.

[116] F. Cucchietti, H. Pastawski, R. Jalabert, Universality of the Lyapunov regime for the Loschmidt echo, Phys. Rev. B 70 (2004) 035311.

[117] Y. Adamov, I. Gornyi, A. Mirlin, Loschmidt echo and Lyapunov exponent in a quantum disordered system, Phys. Rev. E 67 (2003) 056217.

[118] F. Cucchietti, C. Lewenkopf, E. Mucciolo, H. Pastawski, R. Vallejos, Measuring the Lyapunov exponent using quantum mechanics, Phys. Rev. E 65 (2002) 046209.

[119] D. Wisniacki, E. Vergini, H. Pastawski, F. Cucchietti, Sensitivity to perturbations in a quantum chaotic billiard, Phys. Rev. E 65 (2002) 055206(R).

[120] D. Wisniacki, Short time decay of the Loschmidt echo, Phys. Rev. E 67 (2003) 016205.

[121] J. Vaníček, E. Heller, Semiclassical evaluation of quantum fidelity, Phys. Rev. E 68 (2003) 056208.

[122] W. Wang, G. Casati, B. Li, T. Prosen, Uniform semiclassical approach to fidelity decay in the deep Lyapunov regime, Phys. Rev. E 71 (2005) 037202.

[123] W. Wang, B. Li, Uniform semiclassical approach to fidelity decay: from weak to strong perturbation, Phys. Rev. E 71 (2005) 066203.

[124] P. Jacquod, Semiclassical time evolution of the reduced density matrix and dynamically assisted generation of entanglement for bipartite quantum systems, Phys. Rev. Lett. 92 (2004) 150403.

[125] W. H. Zurek, S. Habib, J. P. Paz, Coherent states via decoherence, Phys. Rev. Lett. 70 (9) (1993) 1187–1190.

[126] A. Iomin, Loschmidt echo for a chaotic oscillator, Phys. Rev. E 70 (2004) 026206.

[127] J. Bolte, T. Schwaibold, Stability of wave packet dynamics under perturbations, Phys. Rev. E 73 (2006) 026223.

[128] M. Combescure, D. Robert, A phase-space study of the quantum Loschmidt Echo in the semiclassical limit, preprint quant-ph/0510151 (2005).

[129] J. van Vleck, Proc. Natl. Acad. Sci. 14 (1928) 178.

[130] M. Gutzwiller, Chaos in Classical and Quantum Mechanics, Springer-Verlag, Berlin, 1990.

[131] P. Cvitanović, R. Artuso, R. Mainieri, G. Tanner, G. Vattay, Chaos: Classical and Quantum, Niels Bohr Institute, Copenhagen, 2005, `http://ChaosBook.org`.

[132] A. Ozorio de Almeida, The Weyl representation in classical and quantum mechanics, Phys. Rep. 295 (1998) 265–342.

[133] J. Vaníček, private communication (2006).

[134] J. Vaníček, Dephasing representation: Unified semiclassical framework for fidelity decay, preprint quant-ph/0410205 (2004).

[135] T. A. Brody, J. Flores, J. B. French, P. A. Mello, A. Pandey, S. S. M. Wong, Random-matrix physics: spectrum and strength fluctuations, Rev. Mod. Phys. 53 (3) (1981) 385–479.

[136] K. Frahm, R. Fleckinger, D. Shepelyansky, Quantum chaos and random matrix theory for fidelity decay in quantum computations with static imperfections, Eur. Phys. J. D 29 (2004) 139.

[137] H. Stöckmann, H. Kohler, Fidelity freeze for a random matrix model with off–diagonal perturbation, Phys. Rev. E 73 (2006) 066212.

[138] G. Casati, F. Valz-Gris, I. Guarneri, Lett. Nuovo Cimento 28 (1980) 279.

[139] O. Bohigas, M. J. Giannoni, C. Schmit, Characterization of chaotic quantum spectra and universality of level fluctuation laws, Phys. Rev. Lett. 52 (1) (1984) 1–4.

[140] F. Leyvraz, T. H. Seligman, Structural invariance and the statistics of quasi-energies, Phys. Lett. A 168 (5-6) (1992) 348–352.

[141] B. D. Simons, B. L. Altshuler, Universalities in the spectra of disordered and chaotic systems, Phys. Rev. B 48 (8) (1993) 5422–5438.

[142] B. Dietz, M. Lombardi, T. H. Seligman, Universal parametric correlations of the eigenphases of the S-matrix, Physics Letters A 215 (1996) 181–186.

[143] E. Cartan, Domaines bornés homogènes de l'espace de n variables complexes, Abh. Math. Sem. Hamburg Univ. 11 (1935) 116–162.

[144] M. Mehta, Random Matrices and the Statistical Theory of Spectra, Academic Press, New York, 1991.

[145] M. Hiller, T. Kottos, D. Cohen, T. Geisel, Quantum reversibility: Is there an echo?, Phys. Rev. Lett. 92 (2004) 010402:1–4.

[146] D. Martinez, private communication (2005).

[147] J. Tworzydło, A. Tajic, H. Schomerus, C. W. J. Beenakker, Dynamical model for the quantum-to-classical crossover of shot noise, Phys. Rev. B 68 (2003) 115313:1–6.

[148] F. Haug, M. Bienert, W. Schleich, T. Seligman, M. Raizen, Motional stability of the quantum kicked rotor: A fidelity approach, Phys. Rev. A 71 (2005) 043803.

[149] J. J. M. Verbaarschot, H. A. Weidenmüller, M. R. Zirnbauer, Grassmann integration in stochastic quantum physics: the case of compound-nucleus scattering, Phys. Rep. 129 (1985) 367.

[150] C. Pineda, R. Schäfer, T. Prosen, T. H. Seligman, Verification of generic fidelity recovery in a dynamical system, Phys. Rev. E 73 (2006) 066120.

[151] S. Müller, S. Heusler, P. Braun, F. Haake, A. Altland, Semiclassical foundation of universality in quantum chaos, Phys. Rev. Lett. 93 (2004) 014103.

[152] S. Müller, S. Heusler, P. Braun, F. Haake, A. Altland, Periodic-orbit theory of universality in quantum chaos, Phys. Rev. E 72 (2005) 046207:1–10.

[153] S. Gnutzmann, A. Altland, Universal spectral statistics in quantum graphs, Phys. Rev. Lett. 93 (2004) 194101.

[154] F. Oppen, Exact distribution of eigenvalue curvatures of chaotic quantum systems, Phys. Rev. Lett. 73 (1994) 798.

[155] F. Oppen, Exact distributions of eigenvalue curvatures for time-reversal-invariant chaotic systems, Phys. Rev. E 51 (1995) 2647.

[156] Y. V. Fyodorov, H.-J. Sommers, Universality of "level curvature" distribution for large random matrices: systematic analytical approaches, Z. Phys. B 99 (1995) 123–135.

[157] M. Abramowitz, I. A. Stegun (Eds.), Handbook of mathematical functions, Dover publications, inc., New York, 1970.

[158] C. E. Porter, R. G. Thomas, Fluctuations of nuclear reaction widths, Phys. Rev. 104 (1956) 483.

[159] T. Gorin, Correlations in the scattering cross section of regular systems, J. Phys. A: Math. Gen. 32 (1999) 2315–2332.

[160] T. Gorin, T. H. Seligman, A random matrix approach to decoherence, J. Opt. B: Quantum Semiclass. Opt. 4 (2002) S386–S392.

[161] T. Gorin, T. H. Seligman, Decoherence in chaotic and integrable systems: a random matrix approach, Phys. Lett. A 309 (1-2) (2003) 61–67.

[162] T. Prosen, T. Seligman, M. Žnidarič, Evolution of entanglement under echo dynamics, Phys. Rev. A 67 (2003) 042112.

[163] J. Emerson, Y. Weinstein, S. Lloyd, D. Cory, Fidelity decay as an efficient indicator of quantum chaos, Phys. Rev. Lett. 89 (2002) 284102.

[164] D. Rossini, G. Benenti, G. Casati, Classical versus quantum errors in quantum computation of dynamical systems, Phys. Rev. E 70 (5) (2004) 056216.

[165] Y. Weinstein, C. Hellberg, Effect of symmetries on quantum fidelity decay, Phys. Rev. E 71 (2005) 035203(R).

[166] M. Berry, Semi-classical mechanics in phase space: a study of Wigner's function, Phil. Trans. R. Soc. A 287 (1977) 237–271.

[167] R. Sankaranarayanan, A. Lakshminarayan, Recurrence of fidelity in nearly integrable systems, Phys. Rev. E 68 (2003) 036216.

[168] R. Angelo, K. Furuya, M. Nemes, G. Pellegrino, Recoherence in the entanglement dynamics and classical orbits in the N-atom Jaynes-Cummings model, Phys. Rev. A 64 (2001) 043801.

[169] M. Combescure, The quantum fidelity for the time-dependent singular quantum oscillator, J. Math. Phys. 47 (2006) 032102.

[170] M. Žnidarič, Stability of Quantum Dynamics, Ph.D. thesis, University of Ljubljana, available as `quant-ph/0406124` (2004).

[171] Y. Weinstein, S. Helberg, Quantum fidelity decay in quasi-integrable systems, Phys. Rev. E 71 (2005) 016209.

[172] P. Braun, V. Savichev, The influence of higher-order anharmonic corrections to the energy spectrum on the evolution of quantum wavepackets, J. Phys. B 29 (1996) L329.

[173] C. Leichtle, I. Averbukh, W. Schleich, Multilevel quantum beats: An analytical approach, Phys. Rev. A 54 (1996) 5299.

[174] R. Robinett, Quantum wave packet revivals, Phys. Rep. 392 (2004) 1–119.

[175] S. Wimberger, A. Buchleitner, Saturation of fidelity in the atom-optics kicked rotor, J. Phys. B: At. Mol. Opt. Phys. 39 (2006) L145–L151.

[176] P. Jacquod, I. Adagideli, C. Beenakker, Anomalous power law of quantum reversibility for classically regular systems, Europhys. Lett. 61 (2003) 729–735.

[177] M. Žnidarič, T. Prosen, Generation of entanglement in regular systems, Phys. Rev. A 71 (2005) 032103.

[178] W. Zurek, Pointer basis of quantum apparatus: Into what mixture does the wave packet collapse?, Phys. Rev. D 24 (1981) 1516–1525.

[179] P. Jacquod, Erratum: Semiclassical time evolution of the reduced density matrix and dynamically assisted generation of entanglement for bipartite quantum systems [Phys. Rev. Lett. **92**, 150403 (2004)], Phys. Rev. Lett. 93 (2004) 219903(E).

[180] E. Schrödinger, Die gegenwartige situation in der quentenmechanik, Naturwissenschaften 23 (1935) 807–812.

[181] M. Žnidarič, T. Prosen, Decoherence in regular systems, J. Opt. B: Quantum Semiclass. Opt. 7 (2005) 306–311.

[182] D. Braun, F. Haake, W. Strunz, Universality of decoherence, Phys. Rev. Lett. 86 (2001) 2913.

[183] W. Strunz, F. Haake, D. Braun, Universality of decoherence for macroscopic quantum superpositions, Phys. Rev. A 67 (2003) 022101.

[184] W. Strunz, F. Haake, Decoherence scenarios from microscopic to macroscopic superpositions, Phys. Rev. A 67 (2003) 022102.

[185] R. Demkowicz-Dobrzański, M. Kuś, Global entangling properties of the coupled kicked tops, Phys. Rev. E 70 (2004) 066216.

[186] J. Lages, V. Dobrovitski, M. Katsnelson, H. De Raedt, B. Harmon, Decoherence by a chaotic many-spin bath, Phys. Rev. E 72 (2005) 026225.

[187] A. Wehrl, General properties of entropy, Rev. Mod. Phys. 50 (1978) 221–260.

[188] J. Gong, P. Brumer, When is quantum decoherence dynamics classical?, Phys. Rev. Lett. 90 (2003) 050420.

[189] J. Gong, P. Brumer, Intrinsic decoherence dynamics in smooth hamiltonian systems: Quantum-classical correspondence, Phys. Rev. A 68 (2003) 022101.

[190] J. Gong, P. Brumer, Chaos and quantum-classical correspondence via phase-space distribution functions, Phys. Rev. A 68 (2003) 062103.

[191] R. Angelo, S. Vitiello, M. de Aguiar, K. Furuya, Quantum linear mutual information and classical correlations in globally pure bipartite systems, Physica A 338 (2004) 458.

[192] C. Karney, Long time correlations in the stochastic regime, Physica D 8 (1983) 360–380.

[193] B. Chirikov, D. Shepelyansky, Correlation properties of dynamical chaos in hamiltonian systems, Physica D 13 (1984) 395–400.

[194] S. Ruffo, D. Shepelyansky, Universal diffusion near the golden chaos border 76 (1996) 3300.

[195] Y. Weinstein, S. Lloyd, C. Tsallis, Border between regular and chaotic quantum dynamics, Phys. Rev. Lett. 89 (2002) 214101.

[196] G. Veble, T. Prosen, Classical Loschmidt echo in chaotic many-body systems, Phys. Rev. E 72 (2005) 025202.

[197] M. Horvat, T. Prosen, M. D. Esposti, Quantum classical correspondence on compact phase space, Nonlinearity 19 (2006) 1471–1493.

[198] V. I. Oseledec, The multiplicative ergodic theorem. The Lyapunov characteristic numbers of dynamical systems, Trans. Mosc. Math. Soc. 19 (1968) 197.

[199] G. Casati, T. Prosen, Mixing property of triangular billiards, Phys. Rev. Lett. 83 (1999) 4729–4732.

[200] G. Casati, T. Prosen, Triangle map: A model of quantum chaos, Phys. Rev. Lett. 85 (2000) 4261–4264.

[201] G. Casati, T. Prosen, J. Lan, B. Li, Universal decay of the classical Loschmidt echo of neutrally stable but mixing dynamics, Phys. Rev. Lett. 94 (2005) 114101.

[202] D. Cohen, Quantum dissipation due to the interaction with chaotic degrees of freedom and the correspondence principle, Phys. Rev. Lett. 82 (1999) 4951.

[203] D. Cohen, T. Kottos, Quantum-mechanical nonperturbative response of driven chaotic mesoscopic systems, Phys. Rev. Lett. 85 (2000) 4839.

[204] D. Wisniacki, D. Cohen, Quantum irreversibility, perturbation independent decay, and the parametric theory of the local density of states, Phys. Rev. E 66 (2002) 046209.

[205] W. Wang, G. Casati, private communication, preprint (2006).

[206] R. Alicki, D. Makowiec, W. Miklaszewski, Quantum chaos in terms of entropy for a periodically kicked top, Phys. Rev. Lett. 77 (1996) 838–841.

[207] P. Miller, S. Sarkar, Signatures of chaos in the entanglement of two kicked tops, Phys. Rev. E 60 (1999) 1542–1550.

[208] W. Schleich, Quantum Optics in Phase Space, Wiley-VCH, Berlin, 2001.

[209] G. Agarwal, Relation between atomic coherent-state representation, state multipoles, and generalized phase-space distributions, Phys. Rev. A 24 (1981) 2889–2896.

[210] M. Horvat, T. Prosen, Wigner function statistics in classically chaotic systems, J. Phys. A 36 (2003) 4015–4034.

[211] M. Lombardi, T. Seligman, Universal and nonuniversal statistical properties of levels and intensities for chaotic Rydberg molecules, Phys. Rev. A 47 (1993) 3571–3586.

[212] E. Jaynes, F. Cummings, Comparison of quantum and semiclassical radiation theory with application to the beam maser, Proc. IEEE 51 (1963) 89–109.

[213] M. Tavis, F. Cummings, Exact solution for an n-molecule–radiation-field hamiltonian, Phys. Rev. 170 (1968) 379–384.

[214] W. H. Zurek, Sub-Planck structure in phase space and its relevance for quantum decoherence, Nature 412 (2001) 712–717.

[215] P. Jacquod, I. Adagideli, C. Beenakker, Decay of the Loschmidt echo for quantum states with sub-Planck-scale structures, Phys. Rev. Lett. 89 (2002) 154103.

[216] A. Jordan, M. Srednicki, Sub-Planck structure, decoherence, and many-body environments, preprint quant-ph/0112139 (2001).

[217] A. Ekert, R. Josza, Quantum computation and Shor's factoring algorithm, Rev. Mod. Phys. 68 (1996) 733–753.

[218] A. Steane, Quantum computing, Rep. Prog. Phys. 61 (1998) 117–173.

[219] D. B. A. Ekert, A. Zeilinger (Eds.), The Physics of Quantum Information, Springer Verlag, Berlin, 2000.

[220] C. Miquel, J. Paz, R. Perazzo, Factoring in a dissipative quantum computer, Phys. Rev. A 54 (1996) 2605–2613.

[221] C. Miquel, J. Paz, W. Zurek, Quantum computation with phase drift errors, Phys. Rev. Lett. 78 (1997) 3971.

[222] J. Gea-Banacloche, Qubit-qubit interaction in quantum computers, Phys. Rev. A 57 (1998) R1–R4.

[223] J. Gea-Banacloche, Qubit-qubit interaction in quantum computers. II. Adder algorithm with diagonal and off-diagonal interactions, Phys. Rev. A 60 (1999) 185–193.

[224] B. Georgeot, D. Shepelyansky, Quantum chaos border for quantum computing, Phys. Rev. E 62 (2000) 3504–3507.

[225] B. Georgeot, D. Shepelyansky, Emergence of quantum chaos in the quantum computer core and how to manage it, Phys. Rev. E 62 (2000) 6366–6375.

[226] G. Benenti, G. Casati, S. Montangero, D. Shepelyansky, Eigenstates of an operating quantum computer: hypersensitivity to static imperfection, Eur. Phys. J. D 20 (2002) 293–296.

[227] G. Benenti, G. Casati, S. Montangero, D. Shepelyansky, Statistical properties of eigenvalues for an operating quantum computer with static imperfections, Eur. Phys. J. D 22 (2003) 285–293.

[228] G. Benenti, G. Casati, S. Montangero, Stability of quantum computation in the presence of imperfections, Int. J. Mod. Phys. B 17 (2003) 3932–3946.

[229] V. Flambaum, Time dynamics in chaotic many-body systems: Can chaos destroy a quantum computer?, Aust. J. Phys. 53 (2000) 489–497.

[230] J. Flores, S. Kun, T. Seligman, Meltdown in quantum computers needs not occur: Nuclear experiments show a way out, preprint quant-ph/0502050 (2005).

[231] G. Benenti, G. Casati, S. Montangero, D. Shepelyansky, Efficient quantum computing of complex dynamics, Phys. Rev. Lett. 87 (2001) 227901.

[232] B. Levi, B. Georgeot, D. Shepelyansky, Quantum computing of quantum chaos in the kicked rotator model, Phys. Rev. E 67 (4) (2003) 046220.

[233] M. Terraneo, D. Shepelyansky, Imperfection effects for multiple application of the quantum wavelet transform, Phys. Rev. Lett. 90 (2003) 257902.

[234] O. Kern, G. Alber, D. Shepelyansky, Quantum error correction of coherent errors by randomization, Eur. Phys. J. D 32 (2005) 153.

[235] O. Kern, G. Alber, Controlling quantum systems by embedded dynamical decoupling schemes, Phys. Rev. Lett. 95 (2005) 250501.

[236] G. Berman, F. Borgonovi, F. Izrailev, V. Tsifrinovich, Delocalization border and onset of chaos in a model of quantum computation, Phys. Rev. E 64 (2001) 056226.

[237] G. Berman, F. Borgonovi, G. Celardo, F. Izrailev, D. Kamenev, Dynamical fidelity of a solid-state quantum computation, Phys. Rev. E 66 (2002) 056206.

[238] G. Berman, F. Borgonovi, F. Izrailev, V. Tsifrinovich, Avoiding quantum chaos in quantum computation, Phys. Rev. E 65 (2002) 015204(R).

[239] G. Celardo, C. Pineda, M. Žnidarič, Stability of the quantum Fourier transpormation on the Ising quantum computer, International Journal of Quantum Information 3 (2005) 441–462.

[240] D. Rossini, G. Benenti, G. Casati, Entanglement echoes in quantum computation, Phys. Rev. A 69 (2004) 052317.

[241] S. Bettelli, A quantitative model for the effective decoherence of a quantum computer with imperfect unitary operations, Phys. Rev. A 69 (2004) 042310.

[242] D. Shapira, S. Mozes, O. Biham, Effect of unitary noise on Grover's quantum search algorithm, Phys. Rev. E 67 (4) (2003) 042301.

[243] P. Facchi, D. Lidar, S. Pascazio, Unification of dynamical decoupling and the quantum Zeno effect, Phys. Rev. A 69 (2004) 032314.

[244] L. Viola, S. Lloyd, Dynamical suppression of decoherence in two-state quantum systems, Phys. Rev. A 58 (1998) 2733–2744.

[245] P. Facchi, S. Tasaki, S. Pascazio, H. Nakazato, A. Tokuse, D. Lidar, Control of decoherence: Analysis and comparison of three different strategies, Phys. Rev. A 71 (2005) 022302.

[246] P. Shor, Scheme for reducing decoherence in quantum computer memory, Phys. Rev. A 52 (1995) R2493.

[247] R. Calderbank, P. Shor, Good quantum error-correcting codes exist, Phys. Rev. A 54 (1996) 1098–1105.

[248] A. Steane, Error correcting codes in quantum theory, Phys. Rev. Lett. 77 (1996) 793–797.

[249] A. Steane, Multiple particle interference and quantum error correction, Phil. Trans. R. Soc. A 452 (1996) 2551.

[250] J. Clemens, S. Siddiqui, J. Gea-Banacloche, Quantum error correction against correlated noise, Phys. Rev. A 69 (6) (2004) 062313.

[251] P. Silvestrov, H. Schomerus, C. Beenakker, Limits to error correction in quantum chaos, Phys. Rev. Lett. 89 (2001) 5192.

[252] P. Zanardi, M. Rasetti, Noiseless quantum codes, Phys. Rev. Lett. 79 (1997) 3306.

[253] L. Duan, G. Guo, Reducing decoherence in quantum-computer memory with all quantum bits coupling to the same environmet, Phys. Rev. A 57 (1998) 737.

[254] D. Lidar, D. Bacon, J. Kempe, K. Whaley, Decoherence-free subspaces for multiple-qubit errors. I. Characterization, Phys. Rev. A 63 (2001) 022306.

[255] D. Lidar, D. Bacon, J. Kempe, K. Whaley, Decoherence-free subspaces for multiple-qubit errors. II. Universal, fault-tolerant quantum computation, Phys. Rev. A 63 (2001) 022307.

[256] E. Farhi, J. Goldstone, S. Gutmann, M. Sipser, Quantum computation by adiabatic evolution, preprint quant-ph/0001106 (2000).

[257] E. Farhi, J. Goldstone, S. Gutmann, J. Lapan, A. Lundgren, D. Preda, A quantum adiabatic evolution algorithm aplied to random instances of an NP-complete problem, Science 292 (2001) 472–476.

[258] P. Zanardi, M. Rasetti, Holonomic quantum computation, Phys.Lett. A 264 (1999) 94–99.

[259] V. Kuvshinov, A. Kuzmin, Stability of holonomic quantum computations, Phys. Lett. A 316 (2003) 391–394.

[260] P. V. Buividovich, V. I. Kuvshinov, Fidelity of holonomic quantum computations in the case of random errors in the values of control parameters, Phys. Rev. A 73 (2006) 022336.

[261] V. Kuvshinov, A. Kuzmin, Decoherence induced by squeezing control errors in optical and ion trap holonomic quantum computations, Phys. Rev. A 73 (2006) 052305.

[262] P. Shor, Algorithms for quantum computation: discrete logarithms and factoring, in: Proc. 35th Symp. on Foundations of Computer Science, 1994, pp. 124–134.

[263] D. Coppersmith, An approximate Fourier transform useful in quantum factoring, IBM Research Report RC 19642 (1994).

[264] L. Benet, H. Weidenmüller, Review of the k-body embedded ensembles of Gaussian random matrices, J. Phys. A 36 (2003) 3569–3594.

[265] L. Viola, E. Knill, Robust dynamical decoupling of quantum systems with bounded controls, Phys. Rev. Lett. 90 (2003) 037901.

[266] L. Santos, L. Viola, Dynamical control of qubit coherence: Random versus deterministic schemes, Phys. Rev. A 72 (2005) 062303.

[267] G. Berman, D. Kamenev, R. Kassman, C. Pineda, V. Tsifrinovich, Method for implementation of universal quantum logic gates in a scalable Ising spin quantum computer, Int. J. Quant. Inf. 1 (2003) 51.

[268] W. Zhang, D. G. Cory, First direct measurement of the spin diffusion rate in a homogenous solid, Phys. Rev. Lett. 80 (9) (1998) 1324–1327.

[269] P. Levstein, A. Chattah, H. Pastawski, J. Raya, J. Hirschinger, NMR polarization echoes in a nematic liquid crystal, J. Chem. Phys. 121 (2004) 7313–7319.

[270] Y. Weinstein, S. Lloyd, J. Emerson, D. Cory, Experimental implementation of the quantum Baker's map, Phys. Rev. Lett. 89 (2002) 157902.

[271] C. Ryan, J. Emerson, D. Poulin, C. Negrevergne, R. Laflamme, Characterization of complex quantum dynamics with a scalable NMR information processor, Phys. Rev. Lett. 95 (2005) 250502.

[272] K. Schaadt, A. P. B. Tufaile, C. Ellegaard, Chaotic sound waves in a regular billiard, Phys. Rev. E 67 (2003) 026213:1–7.

[273] D. Giulini, E. Joos, C. Kiefer, J. Kupsch, I.-O. Stamatescu, H.-D. Zeh, Decoherence and the appearence of a classical world in quantum theory, Springer, Berlin, 1996.

[274] M. Brune, E. Hagley, J. Dreyer, X. Maître, A. Maali, C. Wunderlich, J. M. Raimond, S. Haroche, Observing the progressive decoherence of the "meter" in a quantum measurement, Phys. Rev. Lett. 77 (24) (1996) 4887–4890.

[275] F. L. Moore, J. C. Robinson, C. F. Bharucha, B. Sundaram, M. G. Raizen, Atom optics realization of the quantum delta-kicked rotor, Phys. Rev. Lett. 75 (25) (1995) 4598–5601.

[276] J. M. Raimond, M. Brune, S. Haroche, Adv. At., Mol., Opt. Phys. 41 (1999) 43.

[277] M. B. d'Arcy, R. M. Godun, M. K. Oberthaler, D. Cassettari, G. S. Summy, Quantum enhancement of momentum diffusion in the delta-kicked rotor, Phys. Rev. Lett. 87 (7) (2001) 074102:1–4.

[278] M. Bienert, F. Haug, W. P. Schleich, M. G. Raizen, State reconstruction of the kicked rotor, Phys. Rev. Lett. 89 (5) (2002) 050403:1–4.

[279] M. B. d'Arcy, R. M. Godun, D. Cassettari, G. S. Summy, Accelerator-mode-based technique for studying quantum chaos, Phys. Rev. A 67 (2003) 023605:1–4.

[280] M. Andersen, A. Kaplan, N. Davidson, Echo spectroscopy and quantum stability of trapped atoms, Phys. Rev. Lett. 90 (2003) 023001.

[281] S. Kuhr, W. Alt, D. Schrader, I. Dotsenko, Y. Miroshnychenko, W. Rosenfeld, M. Khudaverdyan, V. Gomer, A. Rauschenbeutel, D. Meschede, Coherence properties and quantum state transportation in an optical conveyor belt, Phys. Rev. Lett. 91 (21) (2003) 213002:1–4.

[282] Y. S. Weinstein, J. V. Emerson, S. Lloyd, D. G. Cory, Fidelity decay saturation level for initial eigenstates, Quantum Information Processing 1 (2003) 439.

[283] J. R. Cary, J. D. Meiss, Phys. Rev. A 24 (1981) 2664.

[284] B. Chirikov, Investigations on the theory of nonlinear resonances and stochasticity, preprint 267, Institute of Nuclear Physics SOAN SSSR, Novosibirsk, [see also [295]] (1969).

[285] P. Meystre, M. Sargent III, Elements of Quantum Optics, Springer, Berlin, 1990.

[286] F. Haake, M. Kuś, R. Scharf, Classical and quantum chaos for a kicked top, Z. Phys. B 65 (1987) 381.

[287] R. Schack, M. D'Ariano, C. Caves, Hypersensitivity to perturbations in the quantum kicked top, Phys. Rev. E 50 (1994) 972–987.

[288] R. Fox, T. Elston, Chaos and a quantum-classical correspondence in the kicked top, Phys. Rev. E 50 (1994) 2553–2563.

[289] J. Breslin, G. Milburn, Sensitivity to measurement errors in quantum kicked top, Phys. Rev. A 59 (1999) 1781–1787.

[290] F. Haake, Can the kicked top be realized?, J. Mod. Opt. 47 (2000) 2883–2890.

[291] T. Niemeijer, Physica 36 (1967) 377.

[292] H. W. Capel, J. H. H. Perk, Physica A 87 (1977) 211.

[293] T. Prosen, Prog. Theor. Phys. Suppl. 139 (2000) 191.

[294] T. Gorin, T. H. Seligman, Signatures of the correlation hole in total and partial cross sections, Phys. Rev. E 65 (2002) 026214:1–18.

[295] B. Chirikov, A universal instability of many-dimensional oscillator systems, Phys. Rep. 52 (1979) 263–379.